6th International Meeting on Induced Polarization WIP2022

June 27th – 30th, Annecy, France

Version 26.06.2022

Abstract booklet

https://sites.google.com/view/ipworkshop6

6th International Meeting on Induced Polarization WIP2022

The 6th international meeting on induced polarization will be organized at Annecy (Haute-Savoie) in France on the 27nd -30th June 2022. It will take place at the Imperial Palace on the banks of Lake of Annecy. The charming city of Annecy is located 30 minutes away from the international airport of Geneva in Switzerland (https://www.gva.ch/en/). The meeting will be organized in honor of Conrad Schlumberger, celebrating the 100th anniversary of his seminal book on electrical methods published in 1920 in both French and English (l'Etude sur la Prospection électrique du Sous-sol, Study regarding electrical prospection of the underground). This book contains the first quantitative description of induced polarization.

Conrad Schlumberger

Conrad Schlumberger (2 October 1878 in Alsace, German Empire– 9 May 1936 in Stockholm, Sweden) and Emile Henry Marcel Schlumberger (21 June 1884 in Guebwiller – 9 May 1953 in Val-Richer, France) were two brothers who developed geophysical methods that impacted the entire well logging industry and beyond.

Salle de l'Europe

https://www.hotel-imperial-palace.com/en

60 attendees registered. 20 Posters and 25 oral presentations.
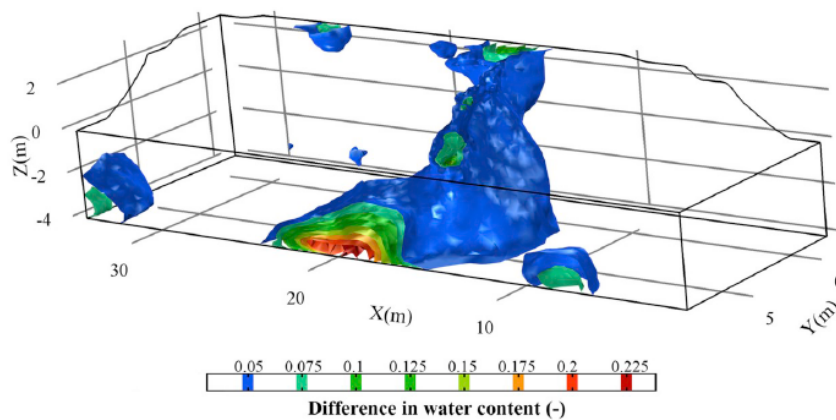
Leak in a dam obtained from induced polarization tomography.

Organization committee: A. Revil (CNRS, EDYTEM, andre.revil@univ-smb.fr) D. Jougnot (CNRS, UPMC, damien.jougnot@upmc.fr), Jacques Deparis (BRGM, j.deparis@brgm.fr) and Matthias Halisch Matthias.Halisch@leibniz-liag.de).

Conrad Schlumberger (2 October 1878 in Alsace, German Empire– 9 May 1936 in Stockholm, Sweden) was a pioneer in the area of geophysic. He was the first to highlight the phenomena of induced polarization (IP) and explain its physics. He devoted an entire chapter in his famous book "Undergroung Electrical Prospecting" published in 1920 both in French and in English. He introduced this new concept while speaking "of a subject very different from those already considered, namely of differences of potential existing temporarily in the earth following the passage of an electric current". He presented the objective of this new method to locate deposits of metallic conductors, such as pyrite (…) or galena, by observing the phenomena of polarisation caused on their surfaces by the passage of a direct current through the ground. According to C. Schlumberger, the origin of the IP is due to the presence of metallic mass buried in the saturated ground. The electric current decompose the water and has for consequence a hydrogen deposit where the current enters into the mass, and an oxygen deposit where the current leave the ore bodies. The analogy of "a veritable storage electric battery" is then used. The entire work is done with the usual apparatus already described (movable line, non-polarizing electrodes, galvanometer and voltmeter). Schlumberger concluded his chapter by the difficulties of measuring this phenomenon by saying that "I have not as yet obtained really satisfying result in the field, but the difficulties which I encountered, on the other hand, enabled me to make two interesting observations". The first one is the influence of self-potential on the measurement and the second one is the electrode polarisation. A new exciting area of geophysics was born. Our conference will honour Conrad Schlumberger for his contribution.

General Agenda

Day 1 - Monday 27th of June, 2022

8H00-8H30 Welcoming of the participants
8H30-8H40 André Revil – Introduction to the meeting
08H40 – 10H00 Session O1 – Petrophysics of Induced Polarization. Part 1
09H20 – 09H55 A.Weller, KEYNOTE
10H05 – 10H20 Coffee Break
10H20 – 12H20 Session O1 – Petrophysics of Induced Polarization. Part 2.
12H20 – 14H00 Lunch
14H00 – 15H00 Poster Pitch Presentations
15H00 – 15H20 K. Titov, KEYNOTE
15H20 – 15H40 F. Magnin, Introduction to the field Trip
15H40 – 16H00 Coffee Break
16H00 – 18H00 Poster Session P1 - Petrophysics

Day 2 – Tuesday 28th of June, 2022

08H00 – 09H00 Poster Pitch Presentations
09H00 – 10H00 Session O2 – Case Studies and sponsors
10H00 – 10H40 Coffee Break & sponsors
10H40 – 12H00 Session O3 – Applications to mineral deposits, permafrost and volcanoes
12H00 – 14H00 Lunch
14H00 – 15H30 Session Applications to mineral deposits, permafrost and volcanoes
14H00 - 14H45 R. Chen, KEYNOTE
14H45 - 15H35 A. Kemna, KEYNOTE
15H45 - 16H00 Coffee break
16H00 – 18H00 Poster Session P2 – Field Cases

Day 3 - Wednesday 29th of June, 2022

08H30 – 09H45 Session O4 - IP and biogeophysics, soil physics and agriculture
09H45 – 10H20 Coffee Break
10H20 – 12H00 Open Discussion
13H50 – 16H10 Session O5 –Metrology, capacitive and electromagnetic effects
16H10 – 16H30 Coffee Break
16H30 – 17H30 Session O6 – Closing Discussion, Open Topics

Day 4 - Thursday 30th of June, 2022

Field Trip to Aiguille du Midi, close to the Mont-Blanc, see p. 166
Timing will be providing later

Preliminary detailed Agenda

Room Europe - Imperial Palace

8H00-8H30 Welcoming of the participants

8H30-8H40 André Revil – Introduction to the meeting

8H40 **Session O1 – Petrophysics of Induced polarization**
            Chair: Matthias HALISCH (Leibniz Institute of Applied Geophysics)

8H40-9H00 V. Iván, B. Mary, N. Schwartz, M. Ghinassi, and G. Cassiani
     O29 - Experimental study on the Spectral Induced Polarization response of artificial soils with varying water saturation, salinity and clay content, p. 86.

9H00-9H20   T. Martin, T. Günther, A. Weller, and K. Kuhn.
     O1 - Classification of IP spectra considering their magnitude and shape, p. 14.

9H20-9H55   A. Weller - KEYNOTE
     O21 - Induced polarization signals and petrophysical relationships, p. 70.

10H00 Coffee Break

10H20-10H40 E. Zibulski, and N. Klitzsch
     O2 - SIP response of grains with rough surfaces – a numerical study, p. 15.

10H40-11H00   C. L. Bérubé, and F. Baron
     O3 - Data-driven sensitivity analysis of mechanistic induced polarization models, p. 17.

11H00-11H20   A. Mendieta, D. Jougnot, P. Leroy, and A. Maineult
     O6 - Spectral induced polarization of non-consolidated clays, p. 27.

11H20-11H40   A. Maineult, G. Gurin, and K.Titov
     O7 - Impedance network modelling to simulate the chargeability of sand-pyrite mixtures, p. 29.

11H40-12H00   D. Kreith, and M. Bücker
     O15 - A new semi-analytic model for Stern-layer polarization in pore throats, p. 49.

12H00-12H20   P. Leroy, A. Maineult, A. Mendieta, and D. Jougnot
     O27 - A petrophysical model for the spectral induced polarization of clays, p. 83.

Lunch

14H00-15H00 Poster pitch presentations (5 minutes max. each, 3 slides max.)
Posters P1, P4, P6, P7, P11, P15, P9, P14, P16, P18, P22, P13

15H00-15H20 K. Titov, KEYNOTE
O20 - Complex conductivity of kimberlite, p. 65.

15H20 -15H40 F. Magnin
Geophysics at the Aiguille du Midi (introduction to the field trip), p. 166.

15H40-16H00 Poster pitch presentations (5 minutes max. each, 3 slides max.)

15H50-16H Coffee break

16H00-18H00. **Poster session 1 – P1 Petrophysics** (poster format A0, vertical, portrait)
Chair: Damien JOUGNOT (CNRS)

P1 - Proxies for surface conductivity and formation factor in permeability prediction of sandstones by Z. Zhang, and A. Weller, p. 92.

P4 - Ice content Estimation with High-Frequency Induced polarization by J. Mudler, D. Kreith, M. Sugand, and A. Hördt, p. 103.

P6 - New hardware for measurement of fast and slow temporal changes of spectral resistivity by T. Radić, p. 109.

P7 - Anisotropy of induced polarization response- sulfide ore samples by S. Ahmadi, A. Coperey, A. Ghorbani, and A. Revil, p. 112.

P9 - On a new method for the determination of Relaxation Time Distributions by A. Maineult, and N. Florsch, p. 120.

P11 - Analysis on fitting time domain decaying curves from time domain induced polarization inversion for NAPL synthetic models by J. Jeong, B. Kim, D. Caesary, Y. S. Mun, and M. J. Nam, p. 123.

P14 - Characterization of surface conductivity of clays by V. Emelianov, Z. Zhang, K. Titov, M. Halisch, and A. Weller, p. 131.

P15 - Temperature dependence of SIP ice signatures of partially frozen rocks based on Cole-Cole model parameterization by J. K. Limbrock, and A. Kemna**,** p. 132.

P16 - Complex conductivity response of diffusion driven calcite precipitation in sandstone by A. M. Mansfeld, and A. Kemna, p. 137.

P18 - Estimating spectra of embedded ore samples by M. Lührs, and A. Hördt**,** p. 144.

P22 - Numerical modelling of Stern-layer polarization in dense packings by J. Wentzki, and D. Bücker, p. 154.

P13 - Spectral induced polarization response of lake-bottom sediments by R.Glebe, J. Hoppenbrock, J. Buckel, A. Hördt, L. Pérez, P. Hoelzmann, and M.Bücker, p. 128.

Day 2 - Tuesday 28th of June, 2022

Room Europe - Imperial Palace

8H00-9H00 Poster pitch presentations (5 minutes max. each, 3 slides max.)
   Posters P2, P3, P5, P8, P10, P12, P17
   Posters P19, P20, P21, P23, P24, P25

9H00 **Session O2 Case studies**
Chair: Jacques DEPARIS (BRGM)

9H00-9H20   A. Signora, S. Spagna, N.A. Sullivan, B. Burkey, and M. Lonardi
   O9 - Characterization of geological heterogeneity through time-domain induced polarization at contaminated sites: the case of a former gravel pit filled with waste, p. 33

9H20-9H40 G. Fiandaca, L.M. Madsen, T. Martin, M. Olmo, and P.K. Maurya
   O10 - Direct inversion of hydraulic conductivity from Induced Polarization field data, p. 35.

9H40-10H00 T. Xia, J. Meng, S. Liu, and D. Mao
   O17 - Integration of Hydrochemical and Induced Polarization Analysis for Leachate Localization in a Municipal Landfill, p. 54.

10H00-10H40- Coffee Break and companies

10H40
Session O3 - Applications to mineral deposits, permafrost and volcanoes
Chair: Damien JOUGNOT (CNRS)

10H40-11H00   A. Revil, P. Vaudelet, Z. Su, and R. Chen.
   O24 - Induced polarization as a tool to assess mineral deposits: a review, p. 75.

11H00-10H20 H.L. Luo, D. Jougnot, and A. Jost
   O19 - A novel model for describing the electrical conductivity of saturated frozen porous media, p. 62.

11H20-11H40 P-A. Duvillard, A. Revil, F. Magnin, L. Ravanel, and P. Vaudelet.
   O22 - Overview of using conductivity and induced polarization tomography to detect mountain permafrost, p. 71.

11H40-12H00 A.Revil, P-A. Duvillard, P. Vaudelet, and M. Gresse
   O18 - Ice and Fire: IP-based temperature imaging in extreme environments, p. 58.

Lunch

14H00-14H45   R. Chen, KEYNOTE. R. Chen, H. Yao, R. Shen, W. Liu, and S. Chen
   O25 - Spread spectrum induced polarization: from concepts to instruments and applications, p. 79.

14H45 -15H35 A. Kemna, KEYNOTE
   O28 - Towards functional root imaging using SIP: Recent advances and current challenges, p. 85.

15H45-16H Coffee break

16H00-18H00   **Poster session P2 – Field cases** (poster format A0, vertical, portrait)
                  Chair: Matthias HALISCH (Leibniz Institute of Applied Geophysics)

   P2 - SIP-based monitoring of denitrification in aquifer sediments by C. Strobel, O. A. Cirpka, C. Leven, J. A. Huisman, and A. Mellage, p. 96.

   P3 - NFDI4Earth Pilot at LIAG: Improving interoperability and reusability of SIP data by S. Nordsiek, and M. Halisch, p. 99.

   P5 - Multi-Frequency excitation speeds up SIP measurement by T. Radić, p. 107.

   P8 - Electromagnetic coupling in time and frequency domains induced polarization- a review by A. Ghorbani, and P. Vaudelet, p. 116.

   P10 - Comparative analysis on IP data obtained in LNAPL contamination sites of different concentrations by B. Kim, H. Yu, S. Y. Song, I. S. Joung, A. Cho, J. Jeong, J. S. Son, and M. J. Nam, p. 122.

   P12 - Geophysical mapping of aquifer properties in infrastructure projects using DCIP and MRS by T. Martin, M. A. Kass, D. Grombacher, G. Fiandaca, C. Butron, M. Griffiths, M. Østbjerg Vang, S. Rejkjaer, A. Mendoza, and T. Dahlin, p. 124.

   P17 - Measurement of dried seafloor massive sulphides by M. Lührs, and A. Hördt, p. 141.

   P19 - Sensing of winter wheat root systems at the field scale using spectral electrical impedance tomography by V. Michels, M. Weigand, and A. Kemna, p. 148.

   P20 - 3D Cole Cole Inversion of time domain induced polarization data by H. Langenbach, and B. Tezkan, p. 152.

   P21 - The evaluation of HIRIP data to investigate a large scale graphite anomaly in the Bavarian Forest/Germany by S. Schiebel, W. Mörbe, P. Yogeshwar, B. Tezkan, T. Günther, and M. Tauchnitz, p. 153.

   P23 - Multi-geophysical approach to characterize fracturation and characterize the transport properties of carbonate rocks by A. N. Yacouba, C. Mallet, J. Deparis, and D. Jougnot, p. 156.

P24 - Past metallurgic sites and deposits characterization using complex conductivity measurements by P. Kessouri, C. Ryckebusch, J. Deparis, A. Fernandez Visentini, J. Gance, D. Caterina, I. Isunza Manrique, and F. Nguyen, p. 158.

P 25- Understanding landslide triggering processes with induced polarization - Case studies in New Caledonia by S. Barde Cabusson, P. Vaudelet, A. Revil, and P.-A. Duvillard, p. 162.

Day 3 - Wednesday 29ᵗʰ of June, 2022

Room Europe - Imperial Palace

8H30
Session O4 –Induced polarization and biogeophysics, soil physics and agriculture
Chair: André REVIL (CNRS)

8H30-8H55 Y. Wu, C. Downs, C. Chou, L. Peruzzo, J. Wang, S. Uhlemann, and K. Kuhlman
   O16 - Extremely large induced polarization phenomenon p. 52.

8H55-9H20 K. Tsukanov, and N. Schwartz
   O4 - Electrical signature of roots and rhizosphere, p. 19.

9H20-9H45 A. Mellage, G. Zakai, B. Efrati, H. Pagel, and N. Schwartz
   O5 - Spectral induced polarization (SIP)-based detection of paraquat sorption in mineral and organic-rich soils, p. 23.

9H45-10H20- Coffee Break and companies

10H20-12H00   **Open discussion on the following subjects**

Chair : Matthias HALISCH (Leibniz Institute of Applied Geophysics) / A. REVIL (CNRS)

1) Petrophysics, where are we? Can we critically test petrophysical models?
2) Induced polarization imaging: How to provide the community better tools?
3) Metrology in the laboratory
4) ?

Lunch

13H50
Session O5 –Metrology, capacitive and electromagnetic effects
Chair : Vincent DEPARIS (BRGM)

13H50-14H10 D. Domenzain, L. Liu, I. Y. Vela, and A.V. Christiansen
   O12 - Enhancing DC data quality using the full IP response, p. 41.

14H10-14H30 T. Dahlin, and P. Hedblom
   O13 - Fast DCIP data acquisition with full-range gradient array, p. 43.

14H30-14H50 H. Wang, J.A. Huisman, E. Zimmermann, and H. Vereecken
   O8 - Reduction of capacitive coupling in spectral electrical impedance tomography (sEIT) measurements, p. 31.

14H50-15H10   D.R. Glaser, B.E. Barrowes, F. Shubitidze, and L.D. Slater
   O26-Investigating Spectral EMI for IP Relaxation Signatures, p. 80.

15H10-15H30 G. Fiandaca, F. Dauti, and A. Signora
   O11 - Effect of induced polarization on galvanic and inductive data: where does it matter most? p. 38.

15H30-15H50 F. Dauti, A. Viezzoli, and G. Fiandaca
   O23 - Induced Polarization Effects in Electromagnetic data: the Loupe case study, p. 73

15H50-16H10 D. Cong-Thi, L. Pham Dieu, D. Caterina, X. De Pauw, H. Dang Thi, H.H.. et al.
   O14 - Determining lab and field petrophysical relationships of unconsolidated sediments in the Luy River coastal aquifer though SIP and co-located geophysical well logs, p. 47.

16H10-16H30 Coffee break

16H30 **Session O6** –**What's next ?**

Discussion of the next meeting
Special issue?

Day 4 - Thursday 30th of June, 2022

Field trip organized in the Valley of Chamonix. We will go at the Aiguille du Midi (Chamonix Valley), which is equipped with electrodes for time lapse conductivity and induced polarization tomography. More information will be provided later (See Section 3 at the end of the booklet). Bring appropriate clothing (we will be at 3700 m). **Lunch will not be provided.**

Leaving the **Imperial Palace at 8:00** and **coming back at the Imperial around 18:00** (depending on the traffic)

Part 1. Oral presentations

O1 - Classification of IP spectra considering their magnitude and shape by T. Martin, T. Günther, A. Weller, and K. Kuhn.

O2 - SIP response of grains with rough surfaces – a numerical study by E. Zibulski and N. Klitzsch

O3 - Data-driven sensitivity analysis of mechanistic induced polarization models by C. L. Bérubé, F. Baron

O4 - Electrical signature of roots and rhizosphere by K. Tsukanov and N. Schwartz

O5 - Spectral induced polarization (SIP)-based detection of paraquat sorption in mineral and organic-rich soil by A. Mellage, G. Zakai, B. Efrati, H. Pagel, and N. Schwartz

O6 - Spectral induced polarization of non-consolidated clays by A. Mendieta, D. Jougnot, P. Leroy, and A. Maineult

O7 - Impedance network modelling to simulate the chargeability of sand-pyrite mixtures by A. Maineult, G. Gurin, K.Titov

O8 - Reduction of capacitive coupling in spectral electrical impedance tomography (sEIT) measurements by H. Wang, J.A. Huisman, E. Zimmermann,, and H. Vereecken

O9 - Characterization of geological heterogeneity through time-domain induced polarization at contaminated sites: the case of a former gravel pit filled with waste by A. Signora, S. Spagna, N.A. Sullivan, B. Burkey, M. Lonardi[1], F. Dauti, A. Lucchelli, M. Gisolo, G. Fiandaca

O10 - Direct inversion of hydraulic conductivity from Induced Polarization field data by G. Fiandaca, L.M. Madsen, T. Martin, M. Olmo, P.K. Maurya

O11 - Effect of induced polarization on galvanic and inductive data: where does it matter most? by G. Fiandaca, F. Dauti, A. Signora

O12 - Enhancing DC data quality using the full IP response by D. Domenzain, L. Liu, I. Y. Vela, A.V. Christiansen

O13 - Fast DCIP data acquisition with full-range gradient array by T. Dahlin and P. Hedblom

O14 - Determining lab and field petrophysical relationship of unconsolidated sediments in the Luy River coastal aquifer though SIP and co-located geophysical well logs by D. Cong-Thi, L. Pham Dieu, D. Caterina, X. De Pauw, H. Dang Thi, H.H.. Ho, T. Hermans, and F. Nguyen

O15 - A New Semi-Analytic Model for Stern-Layer Polarization in Pore Throats by D. Kreith and M. Bücker

O16 - Extremely large induced polarization phenomenon by Y. Wu, C. Downs, C. Chou, L. Peruzzo, J. Wang, S. Uhlemann, K. Kuhlman

O17 - Integration of Hydrochemical and Induced Polarization Analysis for Leachate Localization in a Municipal Landfill by T. Xia, J. Meng, S. Liu, and D. Mao

O18 - Ice and Fire: IP-based temperature imaging in extreme environments by A.Revil, P-A. Duvillard, P. Vaudelet, and M. Gresse

O19 - A novel model for describing the electrical conductivity of saturated frozen porous media H.L. Luo, D. Jougnot, and A. Jost

O20 - Complex conductivity of kimberlite by K. Titov, V. Abramov, V. Emelianov, A. Revil,

O21 - Induced polarization signals and petrophysical relationships by A. Weller

O22 - Overview of using conductivity and induced polarization tomography to detect mountain permafrost by P-A. Duvillard, A. Revil, F. Magnin, L. Ravanel, and P. Vaudelet.

O23 - Induced Polarization Effects in Electromagnetic data: the Loupe case study by F. Dauti, A. Viezzoli, and G. Fiandaca

O24 - Induced polarization as a tool to assess mineral deposits: a review by A.Revil, P. Vaudelet, Z. Su, and R. Chen.

O25 - Spread spectrum induced polarization: from concepts to instruments and applications by R. Chen, H. Yao, R. Shen, W. Liu, and S. Chen

O26-Investigating Spectral EMI for IP Relaxation Signatures by D.R. Glaser, B.E. Barrowes, F. Shubitidze, and L.D. Slater

O27 - A petrophysical model for the spectral induced polarization of clays by P. Leroy, A. Maineult, A. Mendieta, and D. Jougnot

O28 - Towards functional root imaging using SIP: Recent advances and current challenges by A. Kemna

O29 - Experimental study on the Spectral Induced Polarization response of artificial soils with varying water saturation, salinity and clay content by V. Iván, B. Mary, N. Schwartz, M. Ghinassi, G. Cassiani

O1 - Classification of IP spectra considering their magnitude and shape

T. Martin[1], T. Günther[2], A. Weller[3], K. Kuhn[4]

(1) Engineering Geology, Lund University (LU), Lund, Sweden
(2) Leibniz Institute for Applied Geophysics (LIAG), Hannover, Germany
(3) Clausthal University of Technology, Institute of Geophysics, Clausthal-Zellerfeld, Germany
(4) Federal Institute for Geosciences and Natural Resources (BGR), Hannover, Germany

Presenter: T. Martin (tina.martin@tg.lth.se) **Student y/n:** No
Web page: NA   **Preferred presentation oral/poster:** Oral

Abstract. Historical slag dumps are of increasing interest due to economic, environmental or archaeological reasons. Geophysical investigations can help accessing the potential reuse of slag material to recover metallic raw material or the estimation of the hazard potential of the buried slag material due to dissolution occurrence. We have investigated various slag material in the laboratory with the spectral induced polarization (SIP) method, obtained from different historical slag dumps, located in the Harz Mountains, Germany. We also conducted SIP field measurements at a historical slag dump. Based on our laboratory and field results we found a discrimination between three different slag grades (low, medium, high) by using the imaginary conductivity at a medium frequency in both laboratory and field. Furthermore, additional information was obtained by a classification based on the spectral polarization behavior of the slag material and considering the field frequency range (0.1 Hz – 100 Hz). Five different types of spectra (ascending, descending, constant, maximum and minimum type) can be discriminated and recognized in the laboratory and in distinct areas of the slag dump. Even though a direct comparison between the laboratory and field results still needs to be proven, the buried slag material can be differentiated from the surrounding material by the polarization magnitude. This classification can be also applied to other scientific questions and application areas.

O2 - SIP response of grains with rough surfaces – a numerical study

E. Zibulski and N. Klitzsch

Computational Geoscience and Reservoir Engineering, RWTH Aachen, Germany

Presenter: E. Zibulski (ezibulski@eonerc.rwth-aachen.de)   Student: Yes
Preferred presentation oral/poster: Oral

SIP (spectral induced polarization) laboratory measurements on water-saturated rocks show a strong correlation between the electrical polarization strength and the inner surface area of rocks. This is reasonable since the electrical double layer at the inner solid-water interface causes the polarization in the low frequency range. So far published mechanistic SIP models consider this correlation based on grain or pore sizes but neglect the influence of the inner surface roughness. We study the influence of the inner surface roughness on the SIP response by simulating the frequency dependent complex conductivity of simple micro-scale rock models using Comsol Multiphysics®. Starting from smooth grain models, we introduce surface roughness using a fractal approach (Fig. 1) and randomly generated surface structures. Subsequently, we compare the SIP parameter obtained by Debye decomposition of the simulated spectra with analytical and empirical SIP models.
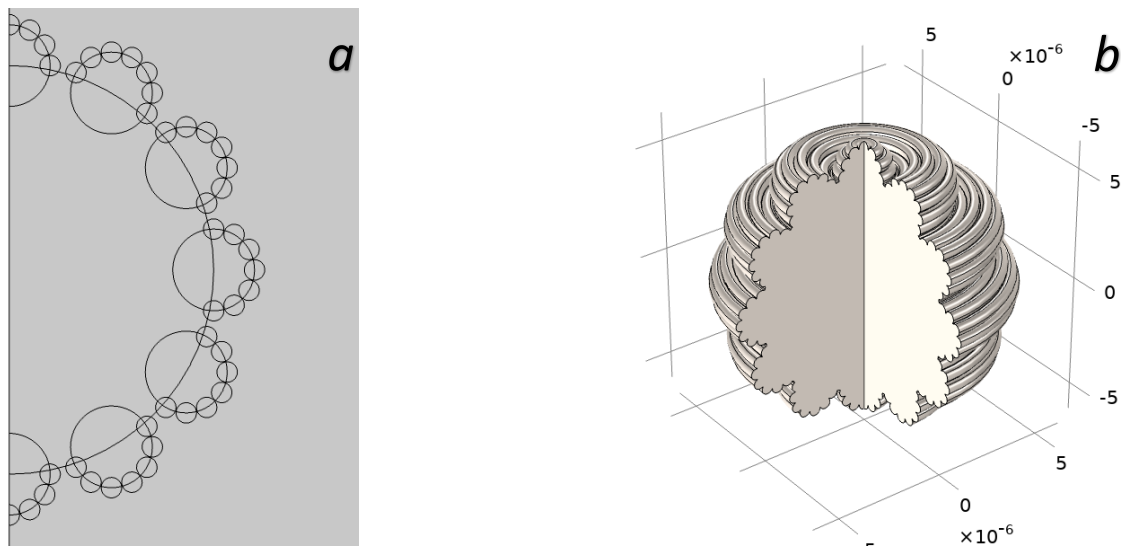
Figure 1: Fractal grain model. **a.** 2D model domain in Comsol® showing a grain with two self-similar daughter generations on the surface of a half-circle. **b.** 3D representation of the 2D geometry in a.

We observe a strong influence of inner surface roughness on the SIP response. Compared to smooth grains of equal size, surface roughness causes additional polarization at higher frequencies and decreases the primary relaxation frequency (Fig. 2). We attribute the latter to the larger circumference, i.e., a larger polarization length of the rough grain and the former to the polarization of the small structures on the rough surface.
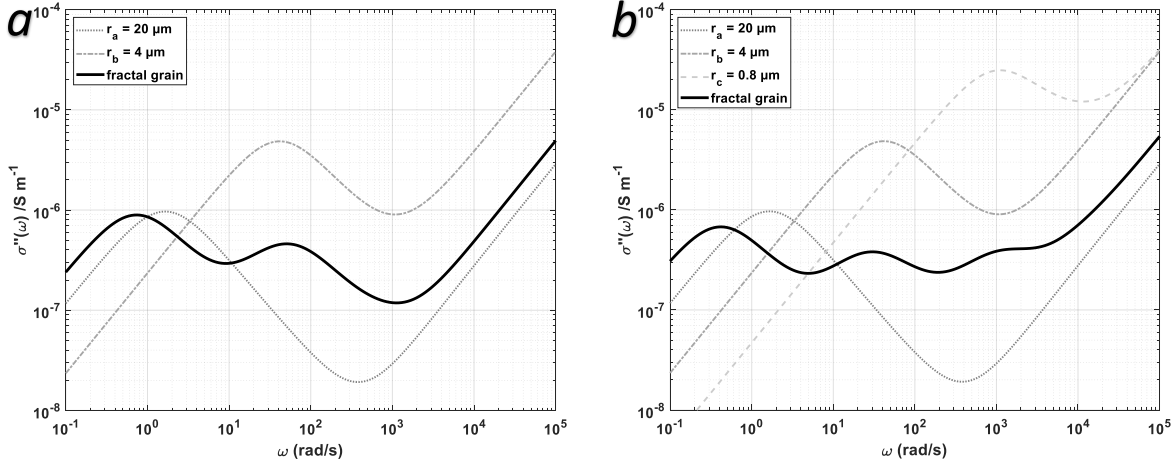
Figure 2. Imaginary conductivity of fractal grain models with (a) two and (b) three different radii. The black lines represent the fractal model and the grey lines the smooth spheres used to construct the fractal model.

The comparison of all grain simulations with empirical results obtained from laboratory measurements reveals the same linear trend between normalized chargeability and inner surface area even though the simulations show considerably lower chargeabilities (Fig. 3a). The empirical relation between imaginary conductivity at 1 Hz and inner surface area, however, is not confirmed by the simulation results obtained for tiny single grains (Fig. 3b). Thus, we conclude that the polarization lengths in rocks are larger than those of single grains, i.e., possibly extend over several grains.
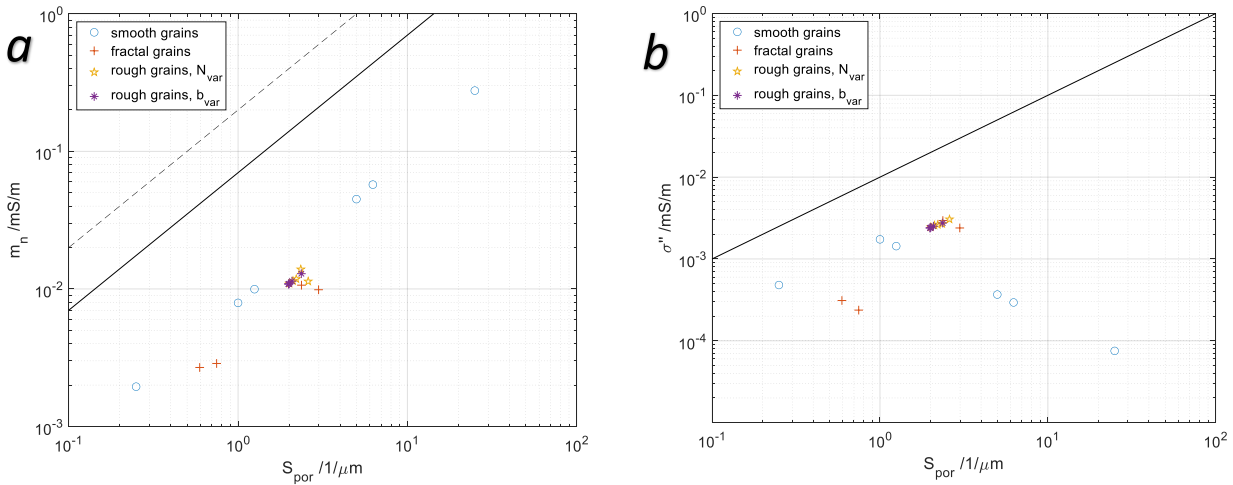
Figure 3a. $S_{por} - m_n$-relation plot of grain-based and cylindrical pore-based simulations. The lines show empirical behavior of sandstone (solid line) and unconsolidated sand-clay mixtures (dashed line) from Weller et al., 2010. **b.** $S_{por} - \sigma''$-relation of grain-based and cylindrical pore-based simulations. The line shows an empirical relation from various sandstone samples and unconsolidated sand-clay mixtures (Weller et al., 2010).

O3 - Data-driven sensitivity analysis of mechanistic induced polarization models

C. L. Bérubé[1], F. Baron[2]

(1) Civil, geological and mining engineering department, Polytechnique Montréal, C.P. 6079 Centre-ville, Montréal, Canada H3C 3A7
(2) Institute for research on exoplanets, Physics department, Université de Montréal, C.P. 6128 Centre-ville, Montréal, Canada H3C 3J7

Presenter: C. L. Bérubé (charles.berube@polymtl.ca)   **Student y/n:** No
Web page: https://clberube.org   **Preferred presentation oral/poster:** Oral

Abstract. We present a quantitative sensitivity analysis of the in-phase, quadrature, and effective components of the "perfectly polarized interfacial polarization" (PPIP) complex conductivity model. The effective conductivity of a simple mixture of spherical metallic inclusions in a conductive host medium is governed by the host's conductivity (62 % sensitivity), followed by the inclusions' volumetric fraction (23 %), conductivity (8 %), and length (6 %). The diffusion coefficient and relative permittivity of both phases have a negligible impact. The error on the estimated size of the inclusions is reduced by 41 % if their electrochemical properties are known. Conversely, the error on the estimated conductivity of the inclusions is reduced by 31 % if their volumetric content and size are constrained.

Introduction. Induced polarization (IP) data can be modelled with mechanistic (Jin et al., 2019), empirical (e.g., Warburg impedance) or data-driven methods (Bérubé & Bérubé, 2022). IP practitioners rarely use mechanistic models to interpret data, partly because the uncertainty with which the intrinsic properties of geomaterials can be estimated from their complex conductivity spectra is poorly understood. This study aims to quantify the sensitivity and parameter estimation limitations of the PPIP model in the 10^2 to 10^8 Hz frequency range (Misra et al., 2016; Jin et al., 2019). The following sections describe the data generation process, sensitivity analysis results, and parameter estimation recommendations.

Complex conductivity data. The complex conductivity spectrum of a mixture of spherical metallic inclusions in an electrolyte host depends on the radius of the inclusions (a_i), their volumetric content in the mixture (ϕ_i), their diffusion coefficient (D_i), their conductivity (σ_i), their relative permittivity ($\epsilon_{r,i}$), the diffusion coefficient of the host (D_h), its conductivity (σ_h), and its relative permittivity ($\epsilon_{r,h}$). Data for this study is generated by drawing 81 920 parameter sets with Saltelli's sampling scheme. Table 1 provides the parameter bounds.

Parameter	a_i (m)	ϕ_i (-)	D_i (m²/s)	σ_i (S/m)	$\epsilon_{r,i}$ (-)	D_h (m²/s)	σ_h (S/m)	$\epsilon_{r,h}$ (-)
Minimum	10^{-5}	10^{-3}	10^{-5}	10^0	10	10^{-10}	10^{-3}	70
Maximum	10^{-3}	2×10^{-1}	10^{-3}	10^5	20	10^{-8}	10^0	90

Table 1. Parameter bounds used to generate complex conductivity spectra with the PPIP model.

Model sensitivity and parameter estimation. We use a conditional variational autoencoder (CVAE) framework (Sohn et al., 2015) to perform sensitivity analysis and parameter estimation. CVAE are Bayesian neural networks with an encoder module that compresses input data to a latent statistical distribution, while a decoder module reconstructs data by sampling the latent distribution. The encoder and decoder modules comprise three fully connected layers (32 connections) with leaky rectified linear activation functions. While training the CVAE with stochastic gradient descent, descriptive data labels (i.e., PPIP parameters) condition the latent distribution. The PPIP sensitivity measures thus correspond to the CVAE's Jacobian matrix (Molamohammadi, 2021). Figure 1 shows that σ_h is responsible for 99 % of the PPIP model's in-phase component sensitivity. The quadrature

component is most sensitive to ϕ_i (42 %), followed by σ_h (29 %), σ_i (15 %), a_i (11 %), and D_i (2 %). Overall, D_i, D_h, $\epsilon_{r,i}$ and $\epsilon_{r,h}$ have negligible impact on the effective conductivity. Sobol' sensitivity indices validate the CVAE sensitivity analysis (Figure 1). An auxiliary network predicts PPIP model parameters from the conditioned latent distribution. The mean absolute percentage errors for eight parameter estimation scenarios are reported in Figure 2. With no prior knowledge of the inclusions' properties, only ϕ_i and σ_h are estimated within less than 14 % error (Figure 2A–B). Prior knowledge of the inclusions' electrochemical properties improves a_i estimations by up to 41 % (Figure 2C–D). On the other hand, prior knowledge of the inclusions' geometry (Figure 2E–G) improves σ_i estimations by up to 31 %. Figure 2H shows the trivial case.

Figure 1 (Relative sensitivity in %)

	a_i	ϕ_i	D_i	σ_i	$\epsilon_{r,i}$	D_h	σ_h	$\epsilon_{r,h}$
σ' Sobol'	0.0	0.7	0.0	0.1	0.0	0.0	99.1	0.0
σ' CVAE	0.0	0.4	0.0	0.0	0.0	0.0	99.6	0.0
σ'' Sobol'	11.1	42.1	2.3	14.9	0.1	0.2	29.3	0.1
σ'' CVAE	9.9	44.2	2.3	12.9	0.1	0.1	30.4	0.1
σ_{eff} Sobol'	5.9	22.7	1.2	8.0	0.0	0.1	62.0	0.0
σ_{eff} CVAE	5.2	23.4	1.2	6.8	0.0	0.1	63.2	0.0

Figure 1. Relative sensitivity (in %) of the PPIP model in-phase (σ'), quadrature (σ''), and effective (σ_{eff}) conductivity components.

Figure 2 (Relative parameter estimation errors in %)

	a_i	ϕ_i	D_i	σ_i	$\epsilon_{r,i}$	D_h	σ_h	$\epsilon_{r,h}$
A	68	14	96	70	100	99	2	99
B	66	14	95	68	100	2*	1*	2*
C	27	14	1*	3*	1*	98	6	99
D	17	12	1*	2*	2*	3*	2*	1*
E	1*	2*	90	39	100	93	4	100
F	1*	1*	1*	1*	2*	100	6	100
G	3*	1*	89	38	99	3*	1*	1*
H	0*	0*	1*	0*	0*	0*	1*	0*
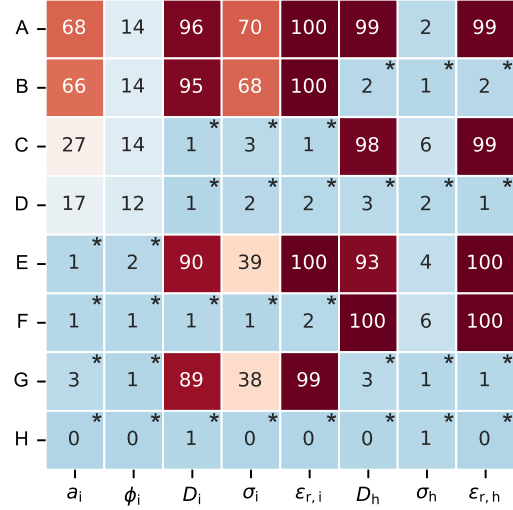
Figure 2. Relative parameter estimation errors (in %) for eight conditioning scenarios (A–H). Asterisks (*) mark the conditioned parameters.

Conclusion. In order of importance, the effective complex conductivity of a simple mixture of metallic spheres in a conductive host medium is governed by σ_h, ϕ_i, σ_i, and a_i. It is impossible to estimate D_i, D_h, $\epsilon_{r,i}$, or $\epsilon_{r,h}$ from complex conductivity spectra because these parameters have no sensitivity. Moreover, prior knowledge of the inclusions' electrochemical properties improves the estimation of their geometrical properties and vice versa. The method is data-driven and thus extensible to more complex mixtures.

References

Bérubé, C. L., & Bérubé, P. (2022). Data-driven modeling of time-domain induced polarization. *Geophysics*, *87*(3), E135–E146.

Jin, Y., Misra, S., Homan, D., Rasmus, J., & Revil, A. (2019). Mechanistic model of multi-frequency complex conductivity of porous media containing water-wet nonconductive and conductive particles at various water saturations. *Advances in Water Resources*, *130*, 244–257.

Molamohammadi, M. (2021). *Generative Modeling and Sensitivity Analysis of Gallium arsenide-based Solar Cell Device Processes*. [M.Eng. thesis, McGill University]. eScholarship@McGill.

Misra, S., Torres-Verdín, C., Revil, A., Rasmus, J., & Homan, D. (2016). Interfacial polarization of disseminated conductive minerals in absence of redox-active species — Part 1: Mechanistic model and validation. *Geophysics*, *81*(2), E139–E157.

Sohn, K., Lee, H., & Yan, X. (2015). Learning Structured Output Representation using Deep Conditional Generative Models. *Advances in Neural Information Processing Systems*, *28*.

O4 - Electrical signature of roots and rhizosphere

K. Tsukanov and N. Schwartz

The Hebrew University of Jerusalem, Institute of Environmental Sciences, Rehovot, Israel.

Presenter: N. Schwartz (nimrod.schwartz@mail.huji.ac.il) **Student y/n:** No

Web page: https://openscholar.huji.ac.il/soilhydrology. **Preferred presentation oral/poster:** Oral

Abstract. In situ monitoring of plant roots and their activity is essential for agriculture production. Geoelectrical methods, especially the spectral induced polarization (SIP), hold a great promise for that aim, as it is sensitive to surface charge, such as at the root cell's membrane. In a series of experiments conducted in hydroponic solution, we demonstrate a linear relationship between root surface area and polarization. In addition, by reducing the cell membrane potential (using cyanide), we verify that the magnitude of polarization is related to the cell's membrane potential. We used a numerical simulation to confirm the experimental data's interpretation and show that the relaxation time relates to the root diameter. An inverse relationship between the quadrature conductivity and the root biomass was observed in the soil. This is probably because the SIP signature of the soil masks that of the root and since soil-root processes such as water and nutrient uptake and root exudation alter the SIP signature of the rhizosphere.

Introduction

The root system and the interactions between roots and their immediate environment (the rhizosphere) are central to optimal yield. However, compared to the above-ground part of the plant, roots and rhizosphere are less studied and understood, mainly because of the technical challenges. For example, most root measurements are performed in a hydroponic solution, and translation of the results to soil media is not trivial. High-resolution imaging of root architecture, e.g., by μCT, can be obtained only with small sample sizes and applied primarily to seedlings. Lastly, many rhizosphere methods are destructive, limiting our ability to study the system dynamics. Geoelectrical methods are increasingly used to study roots and rhizosphere as they can map the subsurface in a noninvasive fashion, on various spatial and temporal scales, and at a relatively low cost. However, to effectively use geoelectrical methods for root and rhizosphere research, the relationships between the electrical signature of roots/ rhizosphere and the roots/rhizosphere properties and processes of interest (e.g., root biomass, root water uptake) need to be established. Here we report results from a series of experiments and a numerical model that enhance our understanding of such a relationship.

Roots in Hydroponic

We coupled SIP measurements of wheat roots in hydroponic solution with root biomass, root surface area, and root diameter measurements. In addition, we monitored the SIP response of roots after poisoning them with cyanide (known to reduce the root cell membrane potential). We found a linear correlation between root surface area and polarization (Fig 1a). In addition, we demonstrate a relationship between root cell membrane potential and root polarization. Based on the results, we suggest that polarization occurs at the external surface area of the root. Consequently, the relaxation

time is related to the roots` outer structures, such as root diameter and hair (Tsukanov & Schwartz 2020).

To examine this hypothesis, we developed a mechanistic model for root polarization which is based on the solution of the Poisson-Nernst-Planck equations. Based on this model and available experimental data, we argue that when the current is directly injected into the plant stem (as in Ozier-Lafontaine & Bajazet, 2005), the polarization is relatively high and related to the total surface area of the root's EDL. In this case, the polarization length scale is associated with the root's cells. When the current is injected into the rooting medium (Weigand & Kemna, 2019; Tsukanov & Schwartz 2020), the relatively high resistive root prevents the low-frequency current from penetrating the root, and polarization occurs at the external surface area of the root (Fig 1b-d, see Tsukanov & Schwartz 2021).
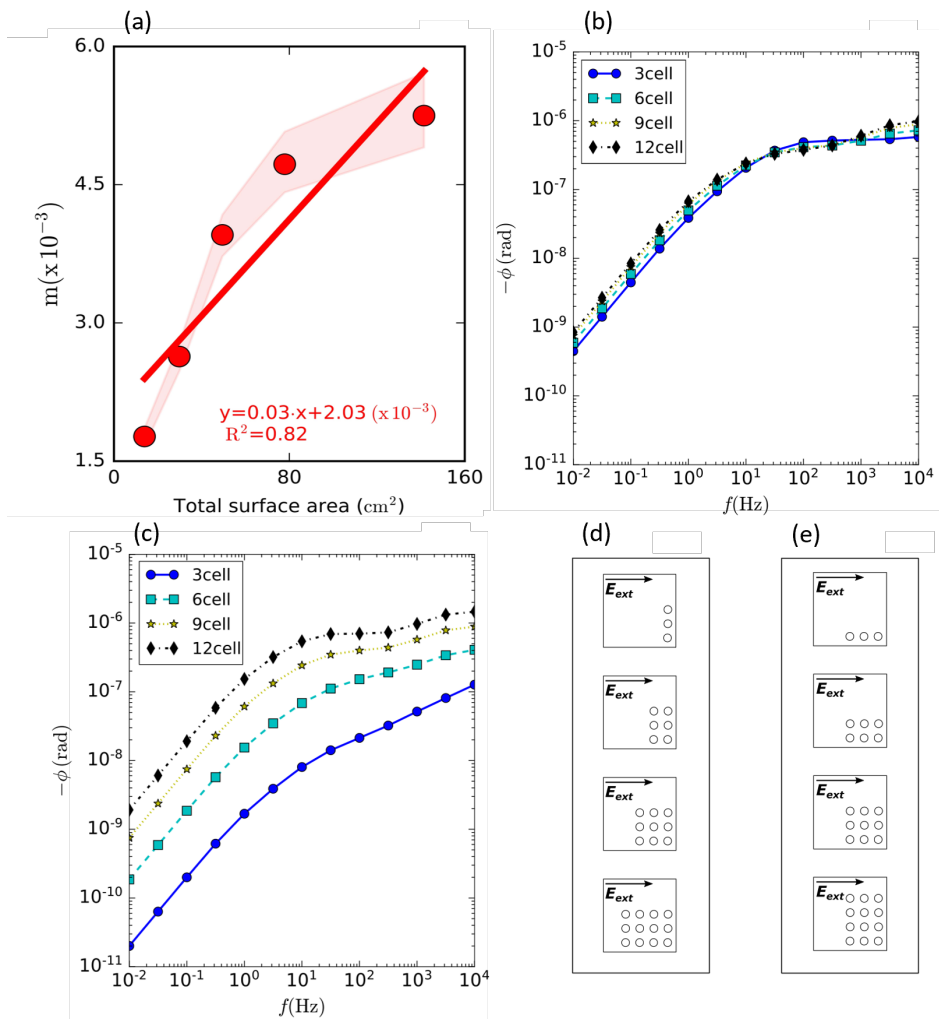
Figure 1. Experimental results from the hydroponic solution (**a**) and results from the numerical simulations (**b-d**). Electrical chargeability as a function of the total root surface area (**a**). Small changes in the polarization with an increase in the number of cells, where the cells are added perpendicular to the external electric field (see panel **d**). When the cells are added parallel to the electric field and the outer surface area of the root grows (**e**), a significant increase in polarization is observed (**c**).

Roots in Soil

The studies mentioned above attempt to isolate and relate the SIP signature of roots to the root's architectural properties (biomass, surface area, etc.). However, they neglect the impact of soil and soil-root interactions on the measured SIP signature. In a series of experiments, we measured the SIP signature of soil in which wheat roots are growing. We found a decrease in polarization with plant age (Fig. 2). These results contradict the results obtained for the case of roots in hydroponic, where a positive correlation between root biomass and polarization was obtained (Fig. 1a). Several rhizosphere processes can explain this discrepancy. For example, roots deplete water and nutrients from the soil, compact the rhizosphere, and exude various organic substances. The influence of water depletion and salinity was accounted for by measuring the SIP response of the experimental soil at different water content and salinity. Based on these results, we calculated an adjusted quadrature conductivity that normalized the plant quadrature conductivity according to the water content of the control samples.

Comparing $\sigma''_{control}$, σ''_{plant} and σ''_{adj} (Fig. 2) demonstrates that most of the decreases in the quadrature conductivity during the root system's development are associated with the decline in the soil water content due to root water uptake. The increase in the rhizosphere salinity doesn't impact the quadrature conductivity. However, changes in the rhizospheres` ions composition (e.g., due to active uptake by the plant) may influence the quadrature conductivity. For example, plants' nutrients consumed in the largest amount are nitrogen, phosphorous, and potassium. The depletion of these nutrients from the rhizosphere increases the divalent to the monovalent ratio in the soil solution, explaining the decrease in polarization. Another possible explanation for the decline in the σ''_{adj} is the secretion of root exudates composed of various organic compounds (mostly mucilage). In most cases, adding organic compounds (especially polar or charged organic compounds) to soil decreases the soil quadrature conductivity (as observed here). Much further research is needed to understand how soil-root interactions impact the SIP signature of the soil.
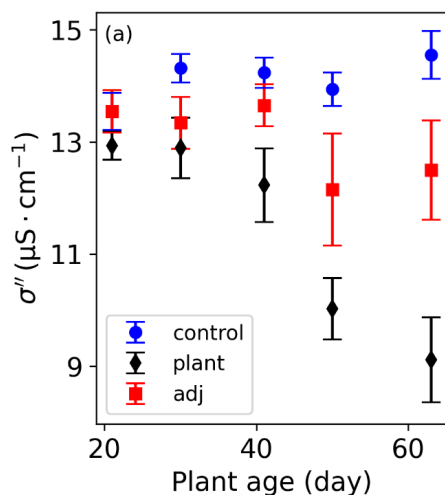
Figure 2. Quadrature conductivity as a function of time from planting. $\sigma''_{control}$ stand for the case of soil without plants, σ''_{plant} show data for the soil with plants, and σ''_{adj} stand for σ''_{plant} at the same water content as the control.

Conclusions. A linear relationship between root surface area and the quadrature conductivity was established in hydroponic solution. The source for the polarization is the root cells` membrane potential at the outer surface area of the root, and the relaxation time is related to the root diameter

and the root hair. The numerical model further supports these conclusions. We found an inverse relationship between root biomass and quadrature conductivity in soil. Most of the decline in polarization was associated with the decrease in soil water content due to root water uptake. Still, part of the decline in polarization is probably related to processes at the soil-root interface (e.g., divalent to monovalent ion ratio and root exudation). It seems that the background signature of the soil masks the polarization of the root and that rhizosphere processes mainly influence the SIP signature.

References

Ozier-Lafontaine, H., & Bajazet, T. (2005). Analysis of root growth by impedance spectroscopy (EIS). Plant and Soil, 277(1–2), 299–313.

Tsukanov, K., & Schwartz, N. (2020). Relationship between wheat root properties and its electrical signature using the spectral induced polarization method. Vadose Zone Journal, 19(1), e20014. https://doi.org/10.1002/vzj2.20014.

Tsukanov, K., & Schwartz, N. (2021). Modeling plant roots spectral induced polarization signature. Geophysical Research Letters, 48, e2020GL090184. https://doi.org/10.1029/2020GL090184.

Weigand, M., & Kemna, A. (2019). Imaging and functional characterization of crop root systems using spectroscopic electrical impedance measurements. Plant and Soil, 435(1–2), 201–224. https://doi.org/10.1007/s11104-018-3867-3.

O5 - Spectral induced polarization (SIP)-based detection of paraquat sorption in mineral and organic-rich soil

A. Mellage[1], G. Zakai[2], B. Efrati[2], H. Pagel[3] and N. Schwartz[2]

(1) University of Kassel, Kurt-Wolters-Str. 3, 34125 Kassel, Germany
(2) The Hebrew University of Jerusalem, Rehovot 76100 Israel
(3) University of Hohenheim, Emil-Wolff-Str. 27, 70599 Stuttgart, Germany

Presenter: A. Mellage (adrian.mellage@uni-kassel.de) **Student y/n:** No
Web page: NA   **Preferred presentation oral/poster:** Oral

Abstract. The retention, via sorption, of solutes in soil and sediment matrices is dominated by charge interactions at charged solid surfaces that modify the ion density and composition of the electrical double layer (EDL). Spectral induced polarization (SIP)'s sensitivity to the properties of the EDL of solid matrixes makes it a suitable proxy for monitoring sorption-driven changes in EDL composition, offering a non-invasive alternative to monitor the retention of relevant ionic or ionizable (organic) contaminants of concern. Herein, we present SIP signals obtained from a series of column experiments packed with mineral soil and a mineral soil amended with solid organic matter (SOM), both contaminated with increasing concentrations of the model herbicide paraquat. Our measurements highlight that the polarization of the mineral soil drops proportional to increasing amounts of sorbed paraquat, exhibiting the expected saturation-type (Langmuir) dependence. The addition of 8%-SOM, however, shifted the dependence between σ'' and sorbed paraquat, yielding a continuous drop in σ'' even after the maximum sorption capacity was reached. The contrasting behavior in Cole-Cole derived time constants (τ) between mineral and SOM treatments highlights the presence of additional, poorly understood, polarization mechanism within polydisperse SOM that complicate the interpretation of sorption driven SIP responses.

Introduction

Experiments that quantify equilibrium sorption of solutes onto soils and sediments typically rely on a series of solid-liquid suspensions amended with a known amount of solute. Such experiments are standard practice in soil science, geochemistry and contaminant hydrogeology. The traditional approach, however, suffers from a reliance on skewed solid-to-liquid rations that favor large liquid volume fractions enabling the straight-forward quantification of aqueous concentrations (Kaiser and Guggenberger, 2007). The presence of a very small solid phase, the actual binding matrix, can mask the sorption of weekly sorbing compounds whose retention is non-negligible under in situ solid-to-liquid ratios, that is, the pore space structure of soils and sediments.

Sorption-driven electrostatic interactions and complexation reactions modify the charge density of soils, the mobility of charged species within the electrical double layer (EDL) and the effective charged surface area that remains exposed for ion-exchange with the bulk solution. Thus, geo-electrical methods, spectral induced polarization (SIP), in particular, offer powerful monitoring alternatives, sensitive to the conductive and charged properties of mineral particles and colloids in porous media. Moreover, SIP measurement can be conducted on soils or sediments packed in their natural configuration.

Here, we performed sorption experiments with the herbicide paraquat (PQ^{2+}), a model divalent organic contaminant, in columns packed either with a natural mineral soil or the same soil amended with increasing fractions of (solid) organic matter (SOM). By monitoring SIP real and imaginary conductivity signals over a range of PQ^{2+} concentrations we aim to link electrical signal changes to PQ^{2+} sorption. Our findings shed light on the effect sorption has on the electrical properties of mineral-dominated and organic matter-containing soils, and highlight the suitability of SIP as a non-invasive sorption monitoring proxy.

Experimental Methods

We packed a series of flow-through (PVC-)columns (inner diameter = 3.0 cm, length = 30 cm) with an organic matter-poor red sandy loam prevalent across agricultural landscapes in Israel, prone to pesticide contamination (referred to as Hamra soil). Experiments were conducted either with pure Hamra soil (mineral soil, < 0.2% SOM content) or with a Hamra soil-SOM mixture. The SOM-rich treatment was prepared by amending the Hamra soil with a commercial humus. The solid matrices were packed into triplicate columns via mixing with a $CaCl_2$ solution (3.5 mM, electrical conductivity (EC)=700 µS cm^{-1}) at varying concentrations of PQ^{2+} and incubated for 24 hours. Following the initial equilibration time, three pore volumes of the $CaCl_2$ solution were injected through the columns to ensure that the inlet and outlet EC were equal. The sorption of PQ^{2+} onto the Hamra soil is poorly reversible, thus the pore water flushing enabled the comparison of treatments with different degrees of sorption but identical pore water ECs.

All columns were equipped with ports for current and potential electrodes. The current electrodes, placed 2.5 cm from the top and bottom of each column, were 8 cm long (made of brass) and crossed the entire sample diameter. Retracted, non-polarizing Ag-AgCl potential electrodes were emplaced at 12.5 cm from the top and bottom of the sample. The potential Ag-AgCl electrodes were encased in tensiometers (T5 tensiometers, METER GmbH, Germany). Phase shift (φ) and impedance magnitude (|Z|) were recorded at 52 log-spaced frequency intervals between 0.01 and 1000 Hz, using a Portable Spectral Induced Polarization (PSIP) Unit (Ontash & Ermac Inc., USA).

Overview of results

SIP phase shift and imaginary conductivity signals for batches of increasing PQ^{2+} concentration in Hamra soil and Hamra soil plus 8% SOM are shown in Figure 1. In both cases the PQ^{2+} adsorption led to a drop in polarization. In the SOM-free pure Hamra soil the sequential addition of PQ^{2+} reduced the magnitude of σ'' across all measured frequencies, and suppressed the frequency peak, slightly shifting it to higher frequencies. Above a concentration of 822 mg kg^{-1}, 86% of the maximum sorption capacity, the decrease in σ'' was no longer apparent yielding a plateau in σ''. The drop in σ'' with increasing PQ^{2+} concentration is driven by the complexation of PQ^{2+} onto the clay (montmorillonite) fraction of the Hamra soil, which neutralizes negatively charged sites yielding a drop in the density of mobile, easily polarizable counterions in the EDL. Thus, the drop in charge storage agrees well with the saturation-type sorption behavior of PQ^{2+} expected for the Hamra soil.

In contrast to the pure Hamra soil, in the 8% SOM treatment, increasing PQ^{2+} concentrations yielded a continued drop in σ'', past the maximum sorption capacity (for the 8%-SOM treatment =

1569 mg kg^{-1}) and σ'' did not level off. Despite PQ^{2+} exhibiting similar Langmuir sorption behavior in both mineral and SOM-containing soils, in the presence of SOM, its sorption does not yield the expected inverse saturation-type drop in charge storage. We attribute this to not yet fully understood polarization mechanisms in organic matter rich sediments (Katona et al., 2021). We speculate that the addition of PQ^{2+} at concentrations above the maximum sorption capacity led to a small amount of complexation within the polydisperse organic matter only, that disproportionately affects charge storage (σ''). The latter was substantiated by the contrasting behavior in the Cole-Cole model derived time constants (τ) for spectra collected in pure Hamra soil versus in SOM-rich soil.
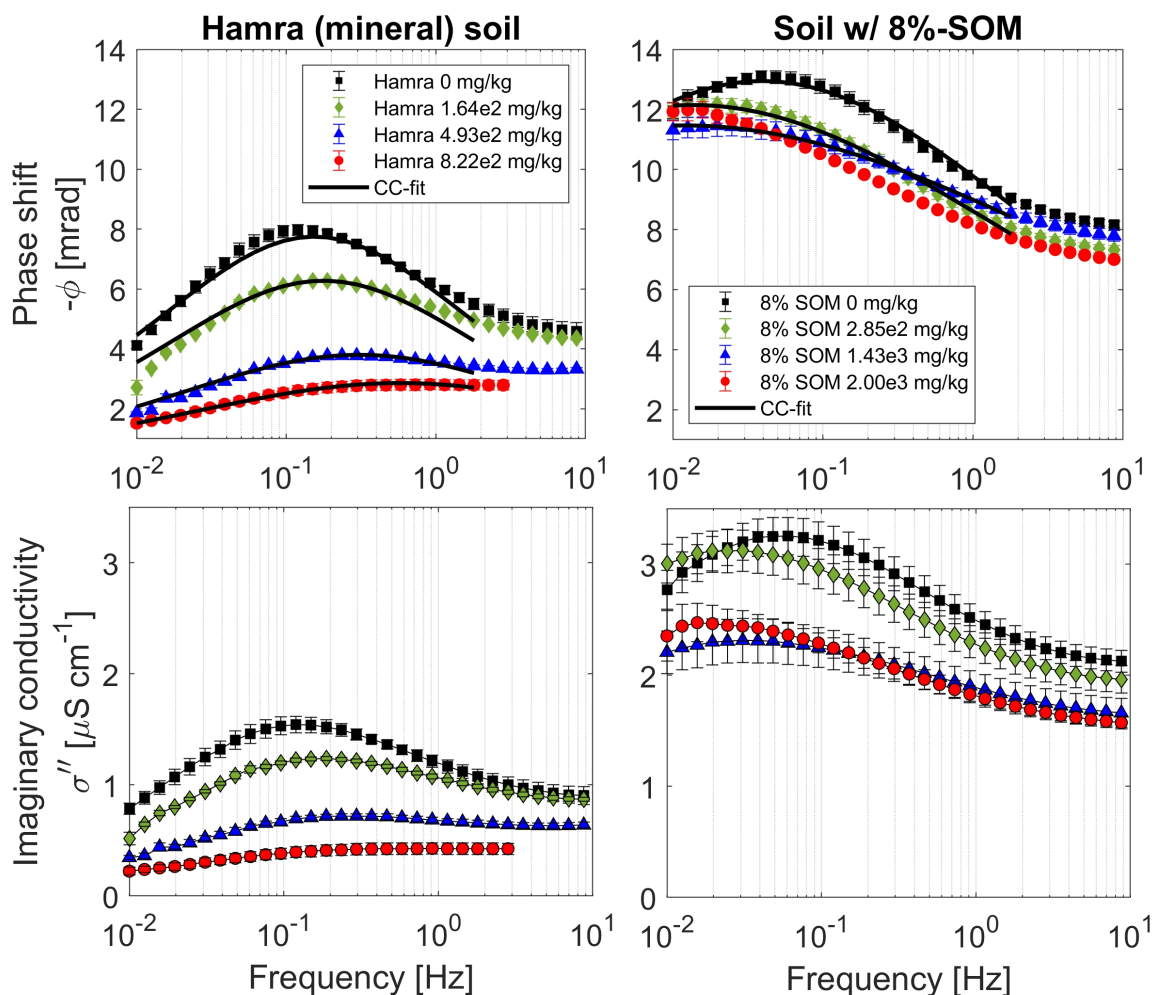
Figure 1. Phase shift ($-\phi$) and imaginary conductivity (σ'') spectral responses for a mineral (Hamra) and organic matter containing soils (Hamra soil plus 8% solid organic matter, SOM) amended with increasing concentrations of the herbicide paraquat. The solid black lines in the $-\phi$ plots illustrate the fit of Cole-Cole relaxation. (Modified from: Mellage et al., 2022).

Conclusions

In mineral soils SIP is directly applicable as a non-invasive monitoring proxy to measure the adsorption of PQ^{2+} and likely other organic cations, without the need for sample collection, that is, in undisturbed samples and under natural solid-to-liquid ratios. The measured drop in σ'' in our experiments was proportional to the expected sorbed concentration of PQ^{2+}.

While PQ^{2+} sorption in the 8%-SOM containing treatment also yielded a reduced charge storage (σ''), the drop in σ'' did not exhibit the characteristic (and expected) Langmuir-type saturation behavior. The signals' continued drop with increasing PQ^{2+} above the maximum sorption capacity, suggest a potentially disproportionate contribution of additional polarization mechanisms related to a small amount of continued complexation of PQ^{2+} into the polydisperse volume of the SOM. These complex polarization and conduction mechanisms in SOM-containing soils can hinder the quantitative information gained from SIP signals, and must be taken into account in SIP-based investigations.

Our findings highlight the suitability of SIP as a monitoring tool for contaminant sorption in laboratory experiments with natural soils. In addition, our results provide a foundation for the interpretation of sorption-driven SIP signal changes in systems containing a non-negligible SOM fraction.

References

Kaiser, K. & Guggenberger, G., 2007. Sorptive stabilization of organic matter by microporous goethite: sorption into small pores vs. surface complexation, European Journal of Soil Science, 58, 45-59. https://doi.org/10.1111/j.1365-2389.2006.00799.x.

Katona, T., Gilfedder, B.S., Frei, S., Bücker, M. & Flores-Orozco, A., 2021. High-resolution induced polarization imaging of biogeochemical carbon-turnover hot spots in a peatland, Biogeosciences, 18(13), 4039-4058. https://doi.org/10.5194/bg-18-4039-2021.

Mellage, A., Zakai, G., Efrati, B., Pagel, H., & Schwartz, N. (2022). Paraquat sorption-and organic matter-induced modifications of soil spectral induced polarization (SIP) signals. Geophysical Journal International, 229, 1422-1433. https://doi.org/10.1093/gji/ggab531.

O6 - Spectral induced polarization of non-consolidated clays

A. Mendieta[1], D. Jougnot[1], P. Leroy[2], and A. Maineult[1]

(1) Sorbonne Université, CNRS, EPHE, UMR 7619 METIS, 75005 Paris, France
(2) BRGM, Department of Water, Environment, Processes and Analysis, 45100 Orléans, France

Presenter: A. Mendieta (aida.mendieta_tenorio@sorbonne-universite.fr) **Student y/n:** No
Web page: NA   **Preferred presentation oral/poster:** Oral

Abstract. Spectral induced polarization measurements were carried out on a variety of non-consolidated clay samples. One experiment was done with 4 different clay types (illite, red and green montmorillonite, and kaolinite) at varying salinities (initially de-ionized water, 10^{-3}, 10^{-2}, 10^{-1} and 1 mol L^{-1} of NaCl). The second experiment was done with different geometrical arrangements (series and parallel arrangements) with illite and red montmorillonite at initially 10^{-2} L^{-1} of NaCl. For the second experiment we tested mixing models and complex conductance network models with the data. The first experiment strongly suggests coagulation with increasing salinity. The second experiment proves the predicting capacity of both modeling approaches.

Introduction

Clays are ubiquitously present in the Earth's near surface and they have a high impact on the permeability of a system. Due to this property, clay formations are used in a variety of geology related applications (oil and gas, geothermal, nuclear waste storage, critical zone research, among others). Clays have a high surface charge and a high specific surface area, this property gives clays a particularly strong electrical double layer (EDL). Spectral induced polarization (SIP) is an active geo-electrical method that measures in a non-invasive manner the frequency-dependent complex conductivity of a geo-material from the mHz to the kHz. The complex conductivity informs about the ability the probed material has to conduct an electrical current and the ability to polarize (to reversibly store electrical charges).

SIP of clays at varying salinity

Using a detailed laboratory protocol to obtain SIP measurements of different types of clay at varying salinities (see Mendieta et al., 2021), as well as an artificial heterogeneous mixture of illite and red montmorillonite with a salinity of around 10^{-2} mol L^{-1} (see Fig. 1). The results of the first study show that the real part of the electrical conductivity increases with salinity, but the imaginary part increases until a maxima and then decreases. An interpretation of the decrease can come from the fact that clays coagulate at high salinities. The potential coagulation of clays would alter the pore space and then alter the polarization mechanisms in play. Furthermore, when comparing the ratio of the surface conductivity (imaginary versus real) of these results with other data in the literature, we notice that this ratio decreases with clay content.

SIP of heterogeneous clay samples

For the second study, we observe that red montmorillonite dominates the polarization with respect to illite. However, both clays effect the conduction of the mixtures. Mixing laws are an effective approach to model the complex conductivity of these heterogeneous mixtures. Complex conductance

network models are better at predicting the shape of the polarization spectra. Our results open new opportunities for clay characterization using SIP.

Conclusions

SIP is a powerful tool to better understand the pore-scale polarization phenomena in non-consolidated clays. Furthermore, for increasing salinities non-consolidated clays coagulate and thus its polarization evolves. Additionally, mixing models and complex conductance network models are able to correctly predict the spectra of two heterogeneous mixes of clays in parallel and series arrangements.

References

Mendieta, A., D. Jougnot, P. Leroy, and A. Maineult (2021). Spectral induced polarization characterization of non-consolidated clays for varying salinities - an experimental study. Journal of Geophysical Research: Solid Earth 126(4). doi: 10.1029/2020jb021125.
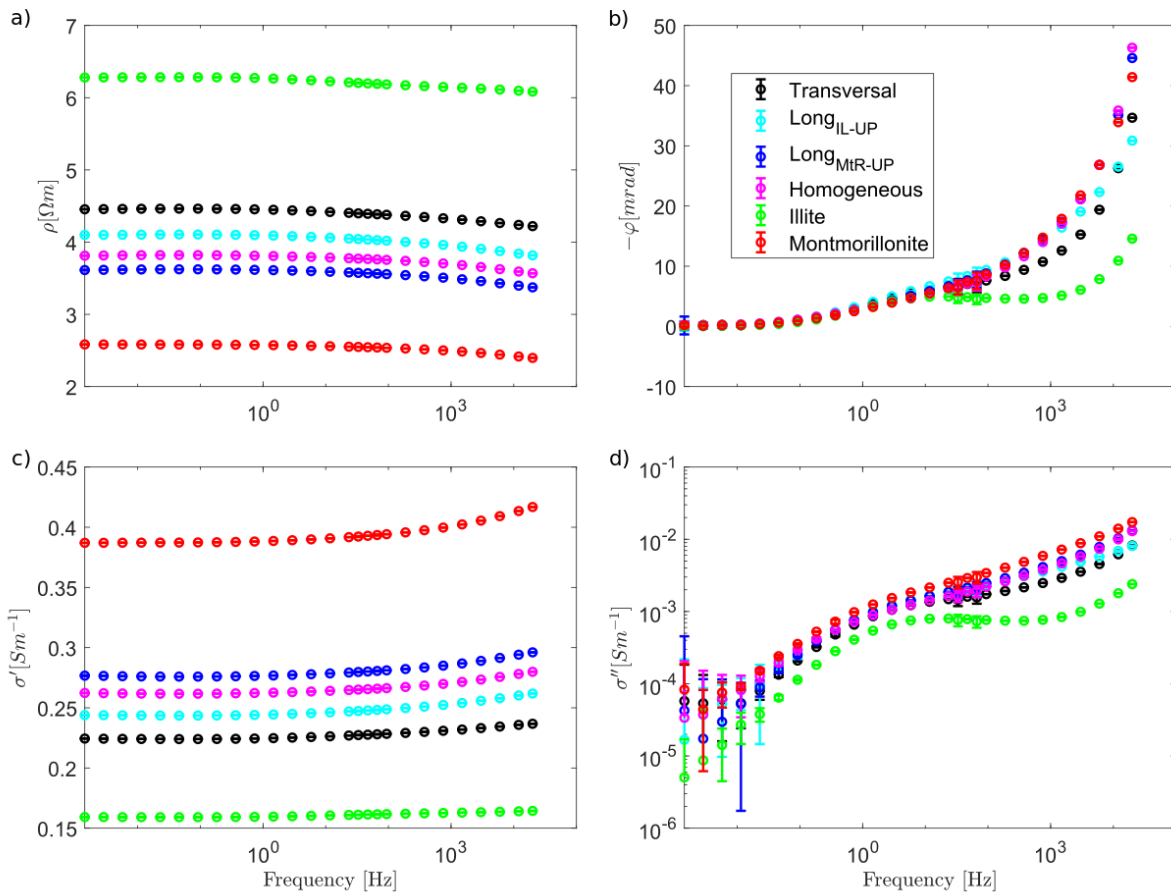
Figure 1. SIP data, as **a)** amplitude, **b)** phase, and **c)** real component and **d)** imaginary components of the complex conductivity. The illite and red montmorillonite clay samples have been taken from Mendieta et al. (2021). The rest of the datasets here presented are a homogeneous mixture of illite and red montmorillonite, as well as three heterogeneous mixtures: a transversal mixture (series), and two longitudinal mixtures (parallel), one with illite in contact with the measuring electrodes (Long$_{IL-UP}$), and with red montmorillonite (Long$_{MtR-UP}$).

O7 - Impedance network modelling to simulate the chargeability of sand-pyrite mixtures

A. Maineult[1], G. Gurin[2], K.Titov[2]

(1) Sorbonne Université, CNRS, EPHE UMR 7619 METIS, France
(2) Saint-Petersburg State University Institute of Earth Sciences, Russia

Presenter: A. Maineult (alexis.maineult@sorbonne-universite.fr) **Student y/n:** No
Web page: NA   **Preferred presentation oral/poster:** Oral

Abstract. In this work, we apply the Complex Impedance Network Modelling (CINM) to simulate the evolution of the total chargeability of sand-pyrite mixtures with different pyrite content. The results of the simulations are in very good agreement with experimental data.

Introduction

The induced polarization (IP) method is highly sensitive to the presence of disseminated ores. But for the interpretation of field data, it is important to rely the measured total chargeability to the ore content. This can be done using theoretical models, or experimental measurements in the laboratory. Here we propose a numerical approach based on the use of networks of complex impedances to calculate such relationships.

Networks of complex impedances

We consider finite 2D networks of complex impedances (hexagonal, square, inclined square and triangular), on which we solved the electrical problem obtained by the combination of Kirchhoff's and Ohm's laws and appropriate boundary conditions (Maineult et al., 2017, Maineult, 2018). From the computed values of the electrical potential at each node for all the considered frequencies, the resulting IP spectra can be deduced, and therefore the total chargeability.

We simulate a mixture made of saturated sand and pyrite grains. Considering that quartz grains are insulating, the embedding medium is made of pores saturated with water, whose impedance is a simple resistance R_0. To model the response of pyrite grains, we use a resistance R_1 in series with a capacitance C.

Results and discussion

We used 50x50 networks, with the impedances associated to pyrite randomly distributed. We tried to reproduce the experimental data obtained by Gurin et al. (2013). The computed total chargeability as a function of the volumetric pyrite content is shown in Figure 1, for R_0=100 ohm, R_1=10 ohm and C=0.001 F. We can observe a good agreement between the simulated and the measured values.

We also remark that the connectivity of the network (i.e., 3 for the hexagonal mesh, 4 for the square mesh and 6 for the triangular mesh) has a very limited influence on the values of the total chargeability, even though the computed IP spectra present some differences (not shown here).

Conclusions

We successfully reproduced the experimental results obtained by Gurin et al. (2013) for the SIP response of sand-pyrite mixtures using the CINM method. The use of such a rapid approach could be a way to reduce the number of required experimental measurements to calibrate the evolution of the total chargeability with ore content.
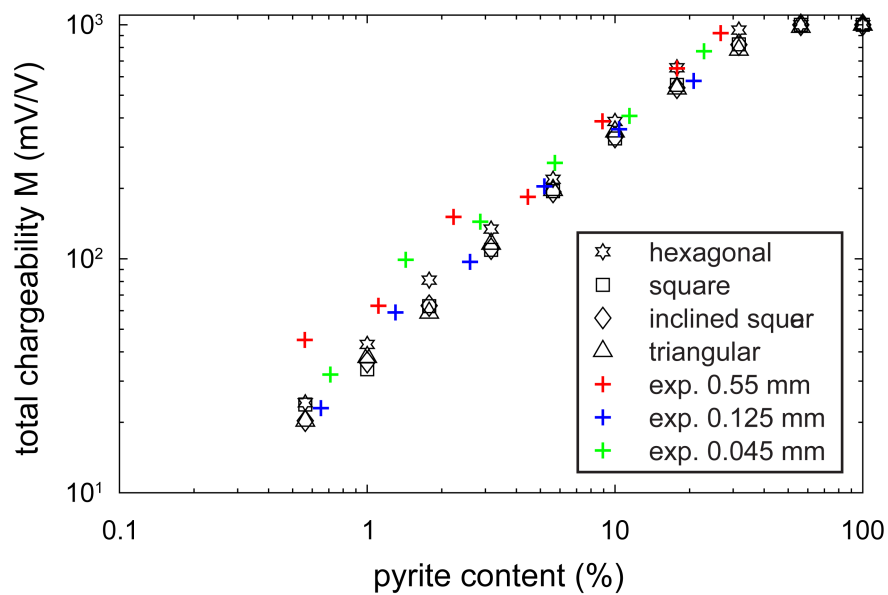
Figure 1. Total chargeability in function of the pyrite content, for the simulations (open symbols) and for the experimental data acquired by Gurin et al. (2013) (crosses).

References

Gurin, G., Tarasov, A., Ilyin, Yu. & Titov, K. (2013). Time domain spectral induced polarization of disseminated electronic conductors: laboratory data analysis through the Debye decomposition approach. Journal of Applied Geophysics, 98, 44¬53.

Maineult, A., Revil, A., Camerlynck, C., Florsch, N. & Titov, K. (2017). Upscaling of spectral induced polarization response using random tube networks. Geophysical Journal International, 209(2), 948¬960.

Maineult, A. (2018). Corrigendum to "Upscaling of spectral induced polarization response using random tube networks", by Maineult et al. (2017, Geophysical Journal International, 209, pp.948–960). Geophysical Journal International, 213(2), 1296.

O8 - Reduction of capacitive coupling in spectral electrical impedance tomography (sEIT) measurements

Haoran Wang[1], Johan Alexander Huisman[1], Egon Zimmermann[2] and Harry Vereecken[1]

(1) Institute of Bio- and Geoscience (Agrosphere IBG-3), Forschungszentrum Jülich GmbH, Jülich, Germany.
(2) Central Institute of Engineering Electronics and Analytics (Electronic systems ZEA-2), Forschungszentrum Jülich GmbH, Jülich, Germany.

Presenter: H. Wang (h.wang@fz-juelich.de) **Student y/n:** Yes
Web page: NA   **Preferred presentation oral/poster:** Oral

Abstract. Spectral electrical impedance tomography (sEIT) is a promising method to image the complex resistivity distribution of subsurface materials. However, electromagnetic (EM) coupling effects can be problematic at higher frequencies. In resistive environments, avoiding capacitive coupling becomes particularly challenging. In this study, we present a method to evaluate the capacitive coupling strength (CCS) of all possible measurement configurations to identify configurations with low CCS for inversion. With the proposed selection method, we achieved plausible and consistent inversion results over a broad frequency range up to the kHz range even for resistive environments.

Introduction. Electromagnetic (EM) coupling is an essential problem in spectral electrical impedance tomography (sEIT) measurements, especially at high frequency. To address this issue, advanced measurement systems have been developed (Zimmermann et al., 2008) and correction methods have been proposed (Zhao et al., 2015). It has been shown that inductive coupling can be corrected using a combination of calibration measurements and numerical calculations (Zhao et al., 2015; Zimmermann et al., 2019) or by proper selection of measurement configurations (Wang et al., 2021). However, correcting capacitive coupling is still challenging, especially in resistive environments, even though methods have been proposed to consider capacitances and leakage currents in sEIT forward modelling (Zimmermann et al., 2019). The aim of this study is to propose an index called capacitive coupling strength (CCS) based on sEIT modelling with capacitances and leakage currents to quantify the influence of capacitive coupling on each individual measurement configuration. In a next step, configurations with low CCS are used to obtain plausible inversion results over a broad frequency range.

Methodology. The field sEIT data was acquired in Senna Lodigiana, Italy using a customized sEIT system (Zimmermann et al., 2008) which measures the potential at one electrode reference to the system ground. The system also measures the true injected current at both positive and negative current electrodes which can be used to calculate the leakage current. The complex impedance of four-pole measurements can then be constructed in the post-processing. The inversion for sEIT data was conducted using the two-step real-valued inversion method (Martin and Günther, 2013) in which the real part of complex apparent resistivity is inverted first and then the imaginary part is linearly inverted using the Jacobian from the first step. All the measurements with large modelling error, large geometric factor and large normalized leakage current were removed. The remaining measurements were considered to obtain the inverted 2D distribution of the real part of the resistivity. Instead of additional calibration measurements to obtain the total capacitance between the cable shields and the ground (Zimmermann et al., 2019), we derived the total capacitance directly from the field sEIT measurements using the measured voltages relative to the system ground and the leakage current. The 2D resistivity section was then mapped to 3D grids and the capacitances were distributed on the nodes along the positions of cables. The leakage currents were also considered in the 3D modelling. By assuming that the subsurface is not polarizable, this 3D model is then used to obtain the imaginary

part of the impedance Z_c'' induced by capacitive coupling. The measured imaginary part impedance Z_m'' can then be corrected for capacitive coupling using $Z_0'' = Z_m'' - Z_c''$. The CCS is defined as the ratio of Z_c'' and the corrected imaginary part impedance Z_0''. A threshold CCS value of 5% was adopted to select configurations for the final sEIT inversion, which resulted in 410 data points (CCS) compared to 363 data points (EZ) for the configurations used in Zimmermann et al. (2019).

Results. The inversion results for the imaginary part of the resistivity are shown in Fig.1. It is clear that the inversion results obtained with the EZ configurations were improved after correction of capacitive coupling. However, the improvement is limited to a small range of frequencies. At higher frequencies, the inversion results with the corrected EZ configurations still showed artifacts. The inversion results with the configurations obtained using CCS filtering showed reasonable and consistent images even without considering capacitive coupling during the inversion.
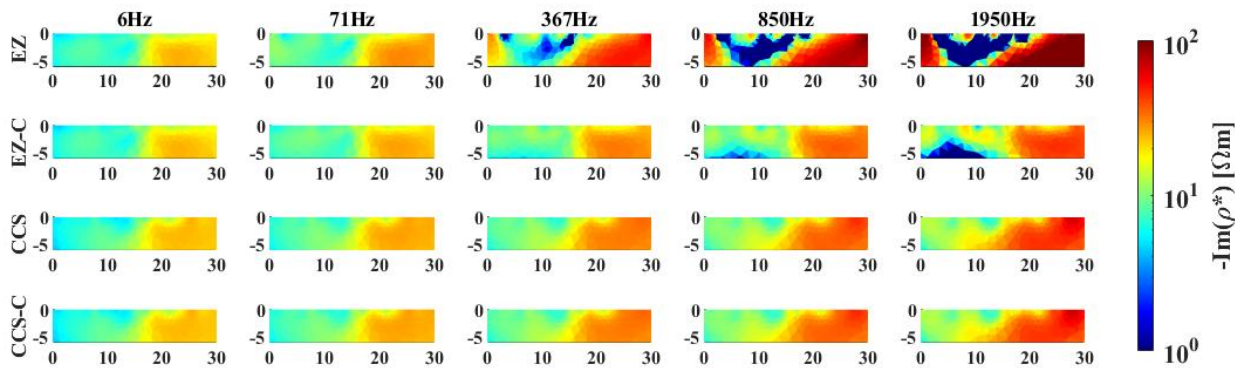
Figure 1. Inversion results for the imaginary part of the resistivity for different configurations: EZ (Raw data), EZ-C (Corrected data), CCS (Raw data), and CCS-C (Corrected data).

Conclusions. We proposed a novel index called capacitive coupling strength (CCS) to quantify capacitive coupling for all possible measurement configurations. Next, configurations with low CCS were selected for inversion. The inversion results showed that the configurations obtained used CCS filtering provide plausible and consistent inversion results for a broad frequency range up to kHz. Further studies should be carried out to transfer the method developed in this study to commercial sEIT systems.

References

Martin, T., and Günther, T. (2013). Complex resistivity tomography (crt) for fungus detection on standing oak trees. *European Journal of Forest Research, 132*(5-6), 765-776.

Wang, H., Huisman, J. A., Zimmermann, E., and Vereecken, H. (2021). Experimental design to reduce inductive coupling in spectral electrical impedance tomography (seit) measurements. *Geophysical Journal International, 225*(1), 222-235.

Zhao, Y., Zimmermann, E., Huisman, J. A., Treichel, A., Wolters, B., van Waasen, S., and Kemna, A. (2015). Phase correction of electromagnetic coupling effects in cross-borehole eit measurements. *Measurement Science and Technology, 26*(1).

Zimmermann, E., Huisman, J. A., Mester, A., and van Waasen, S. (2019). Correction of phase errors due to leakage currents in wideband field measurements on soil and sediments. *Measurement Science and Technology, 30*(8).

Zimmermann, E., Kemna, A., Berwix, J., Glaas, W., and Vereecken, H. (2008). Eit measurement system with high phase accuracy for the imaging of spectral induced polarization properties of soils and sediments. *Measurement Science and Technology, 19*(9).

O9 - Characterization of geological heterogeneity through time-domain induced polarization at contaminated sites: the case of a former gravel pit filled with waste

A. Signora[1], S. Spagna[1], N.A. Sullivan[1], B. Burkey[1], M. Lonardi[1], F. Dauti[1], A. Lucchelli[1], M. Gisolo[2], G. Fiandaca[1]

(1) The EEM Team for Hydro & eXploration, Department on Earth Sciences "Ardito Desio", University of Milano, Milano, Italy
(2) A2A Ciclo Idrico, Brescia, Italy

Presenter: A. Signora (alessandro.signora@unimi.it) **Student y/n:** Yes
Web page: NA   **Preferred presentation oral/poster:** Oral

Abstract. In the recent years, time-domain induced-polarization (TCIP) surveys have been successfully employed in a wide range of environmental applications. Soil and groundwater contaminated sites represent challenges that require the contamination extent definition and a detailed description of geological heterogeneity, to predict the contaminant flows accurately. In this study 9.8 kilometers of 2D DCIP profiles, 400 to 1000 meters long, have been performed in the surroundings of a former gravel pit filled with municipal and industrial wastes after its depletion. Data have been inverted via traditional resistivity inversion and with full-decay spectral IP inversion, directly in terms of hydraulic conductivity (K), using petrophysical relation to re-parameterize the Cole-Cole model in terms in hydraulic properties. Reasonable K models, in accordance with log-wells information are retrieved. Furthermore, the resistivity models improve significantly when inverted along with IP data, in terms of coherence among profiles acquired with different acquisition length.

Introduction. In recent years TCIP surveys have been implemented in a wide range of environmental applications showing accurate results in depicting geological settings (e.g. Rossi et al., 2017; Maurya et al., 2018). With specific regard to soil and groundwater contamination studies, accurate knowledge about the stratigraphical setting and the distribution of hydraulic properties is crucial to forecast the contamination spreading via groundwater flow and transport modeling. This study aims at depicting geological heterogeneity through TDIP surveying at a contaminated site, with the acquisition of 9.8 km of TDIP data.

Survey layout and data processing

In this study, 9.8 km of 2D TCIP data have been acquired in the surrounding area of the former gravel pit "La Vallosa", in the province of Brescia (Italy). After its depletion the gravel pit has been filled with municipal and industrial wastes, contaminating the surrounding aquifers. Profiles with length ranging from 400 to 1000 meters have been acquired, with electrode spacing of 5 or 10 meters (Figure 1a). All data have been collected recording full-waveform data with a 100% duty cycle protocol and on-time of 12.3 seconds. The IP decays have been processed following Olsson et al. (2016), allowing increases in the usable range of IP decays to almost four decades in time.

Results and conclusions. The gathered data have been inverted i) via traditional resistivity inversion process, ii) implementing hydraulic conductivity (K) as model space inversion parameter (Fiandaca et al., 2022). Figure 1b shows the hydraulic conductivity K estimated from TDIP inversion on a selection of the acquired profiles, with depth range up to 60 m, where unconsolidated formations are present (i.e. where the petrophysical relations for K estimation are valid). Good coherence is

evidenced among the profiles, and the K estimates agree with the borehole information at the site. Furthermore, the resistivity models improve significantly when inverted along with IP data, in terms of coherence among profiles acquired with different acquisition length. These findings are being incorporated in the flow and transport model at the site, in order to study the vulnerability of the groundwater resources of the towns downstream of the contaminated site.
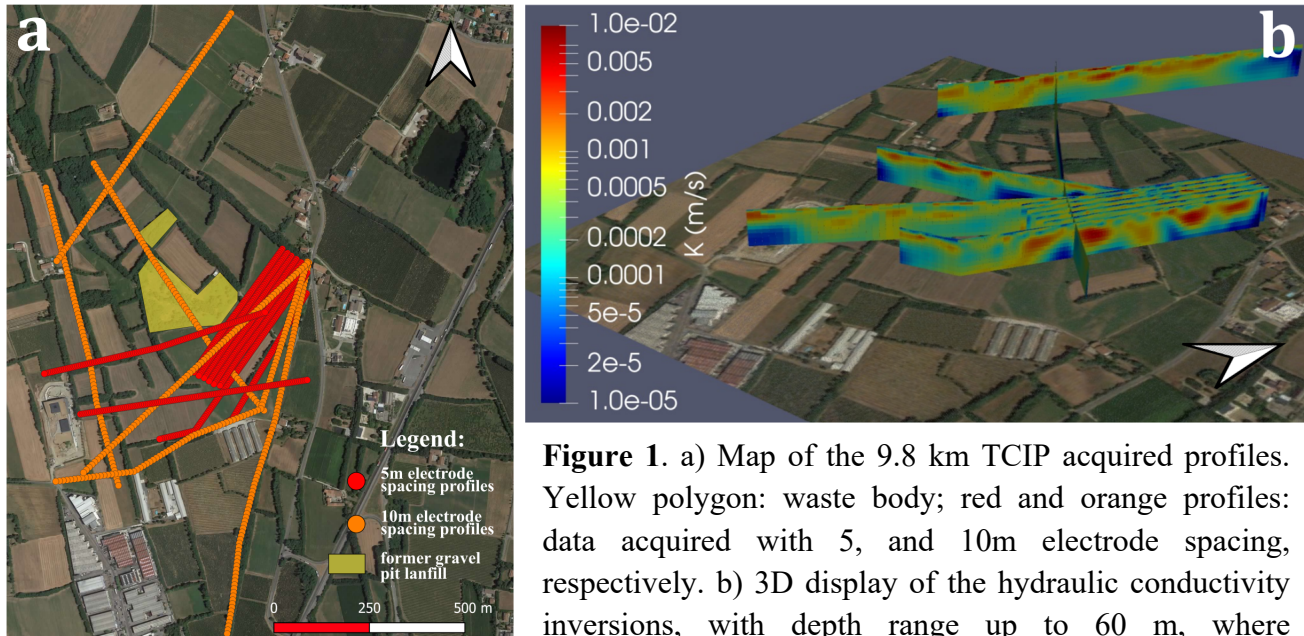
Figure 1. a) Map of the 9.8 km TCIP acquired profiles. Yellow polygon: waste body; red and orange profiles: data acquired with 5, and 10m electrode spacing, respectively. b) 3D display of the hydraulic conductivity inversions, with depth range up to 60 m, where unconsolidated formations are present.

References

Fiandaca, G., Auken, E., Christiansen, A.V., Gazoty, A., 2012. Time-domain-induced polarization: Full-decay forward modeling and 1D laterally constrained inversion of Cole-Cole parameters. GEOPHYSICS 77, E213–E225.

Fiandaca G., Madsen L.M., Martin T., Olmo M., Maurya P.K., 2022. Direct inversion of hydraulic conductivity from Induced Polarization field data. 6th IP workshop, June 2022, Annecy, France.

Maurya P.K., Balbarini N., Møller I., Rønde V., Christiansen A.V., Bjerg P.L., Auken E., Fiandaca G., 2018. Subsurface imaging of water electrical conductivity, hydraulic permeability and lithology at contaminated sites by induced polarization, Geophys. J. Int, 213, 770-785.

Olsson, P.-I., Fiandaca, G., Larsen, J.J., Dahlin, T., Auken, E., 2016. Doubling the spectrum of time-domain induced polarization by harmonic de-noising, drift correction, spike removal, tapered gating and data uncertainty estimation. Geophysical Journal International 207, 774–784.

Rossi, M., Olsson, P.-I., Johanson, S., Fiandaca, G., Preis Bergdahl, D., Dahlin, T., 2017. Mapping geological structures in bedrock via large-scale direct current resistivity and time-domain induced polarization tomography. Near Surface Geophysics.

O10 - Direct inversion of hydraulic conductivity from Induced Polarization field data

G. Fiandaca[1], L.M. Madsen[2], T. Martin[3], M. Olmo[1], P.K. Maurya[2]

(1) The EEM Team for Hydro & eXploration, Department on Earth Sciences "Ardito Desio", University of Milano, Milano, Italy
(2) Hydrogeophysics Group, Geoscience Department, Aarhus University, Aarhus, Denmark
(3) Engineering Geology, Lund University, Lund, Sweden

Presenter: G. Fiandaca (gianluaca.fiandaca@unimi.it) **Student y/n:** No
Web page: NA **Preferred presentation oral/poster:** Oral

Abstract. In the laboratory, the Induced Polarization (IP) method has a long story of successful hydraulic conductivity (K) estimation, with two main approaches: i) the approach based on the link between K and imaginary conductivity σ'' and ii) the approach based on the link between K and relaxation time τ. In this work, we re-parameterize the Cole-Cole model using both σ'' and τ approaches, to obtain a model space described directly in terms of hydraulic conductivity K, together with electrical conductivity σ_0, diffusion coefficient in the Stern layer D_+ and Cole-Cole exponent C. We studied parameter correlations and resolution with the Markov chain Monte Carlo method, and we evaluated the quality of K estimation on field data, against K estimates from grain size analyses and slug tests. The proposed re-parameterization is well suited for inversion, because weak correlations exist among parameters. More important, the direct inversions of field data retrieve very good K estimates. We believe that this new inversion approach might open the way for reliable, cost-effective geophysical estimation of hydraulic conductivity in the field.

Introduction

The estimation of hydraulic conductivity (K) from geophysical measurements is a key research topic in hydrogeophysics, because K is a key parameter for modelling of groundwater flow. In the laboratory, the Induced Polarisation (IP) geophysical method has a long story of successful estimation of K, with two main approaches debated in the literature: i) the approach based on the link between K and the imaginary conductivity σ'' (e.g. Weller et al., 2015) and ii) the approach based on the link between K and the relaxation time τ of the IP phenomenon (e.g. Revil et al., 2012). Recently, field studies of K estimation from time-domain IP (TDIP) have been presented, converting the inverted electrical properties into permeability using the empiric formulae presented in Weller et al. (2015), for borehole acquisitions (Fiandaca et al., 2018) and surface 2D acquisitions (Maurya et al., 2018). In this work, we study more in detail the estimation of hydraulic conductivity from TDIP data from the inversion point of view, defining the inversion model space directly in terms of hydraulic properties, and we benchmark the quality of K estimation on data acquired on several field survey, both in boreholes and along 2D profiles.

Method

The proposed method consists in the re-parameterization of the Cole-Cole model (Fiandaca et al., 2018B) through petrophysical equations, for the direct estimation of hydraulic conductivity as inversion parameters. In particular, two equations are used: i) the link between permeability k, imaginary conductivity σ'' and formation factor F for unconsolidated formations presented by Weller et al. (2015) (equation 1); ii) the link between permeability k, diffusion coefficient in the Stern layer D_+ and formation factor presented by Revil et al (2012) (equation 2):

$$k = \frac{\alpha}{F^\beta {\sigma''}_{ref}^\gamma} \qquad (1) \qquad\qquad k = \frac{\tau_\sigma \cdot D_+}{4F} \qquad (2)$$

In equation (1) α, β and γ represent empirical constants derived from the inversion of laboratory data, while τ_σ in equation (2) is the time constant of the conductivity Cole-Cole formula. We use these equations for obtaining as inversion parameters the total electrical conductivity σ_0, the hydraulic conductivity K, the diffusion coefficient in the Stern layer D_+ and the frequency exponent of the Cole-Cole formula C. The MCMC and 1D/2D deterministic inversions of full-decay TDIP data are carried out following Fiandaca et al. (2018B).

Results

The MCMC modelling was performed on halfspace models, with one full-decay TDIP quadrupole, with acquisition times ranging from 0.003 s to 12 s and uniform 5% STD. Two models, one representing sand and one representing clay were analysed. Overall, the correlations between parameters in the re-parameterisation in terms of hydraulic properties are weaker than the correlations between classic Cole-Cole parameters. In particular, K il less correlated than m0, making the re-parameterisation a good candidate for inversion. The new inversion method was tested on the TDIP data acquired in boreholes presented in Fiandaca et al., (2018), and on 2D profiles acquired in five European countries (Martin et al., 2021). Standard estimates of hydraulic conductivity through grain size analyses and slug tests are available at the sites for comparison, as shown in Figure 1. Overall, a very good agreement exists between KIP and Kmeasured, over four decades. The values of diffusion coefficient in the Stern layer compatible with literature

Conclusions

We re-parameterized the Cole-Cole formula in terms of hydraulic conductivity and diffusion coefficient in the Stern layer, for direct estimation of hydraulic properties from inversion of time-domain induced polarization data. This re-parameterization is better suited for inversion than the classic Cole-Cole model, as shown through Markov chain Monte Carlo inversions. More important, the direct inversions of field data acquired in boreholes and 2D profiles retrieve very good estimates of hydraulic conductivity. We believe that this new inversion approach might open the way for reliable, cost-effective geophysical estimation of hydraulic conductivity in the field.
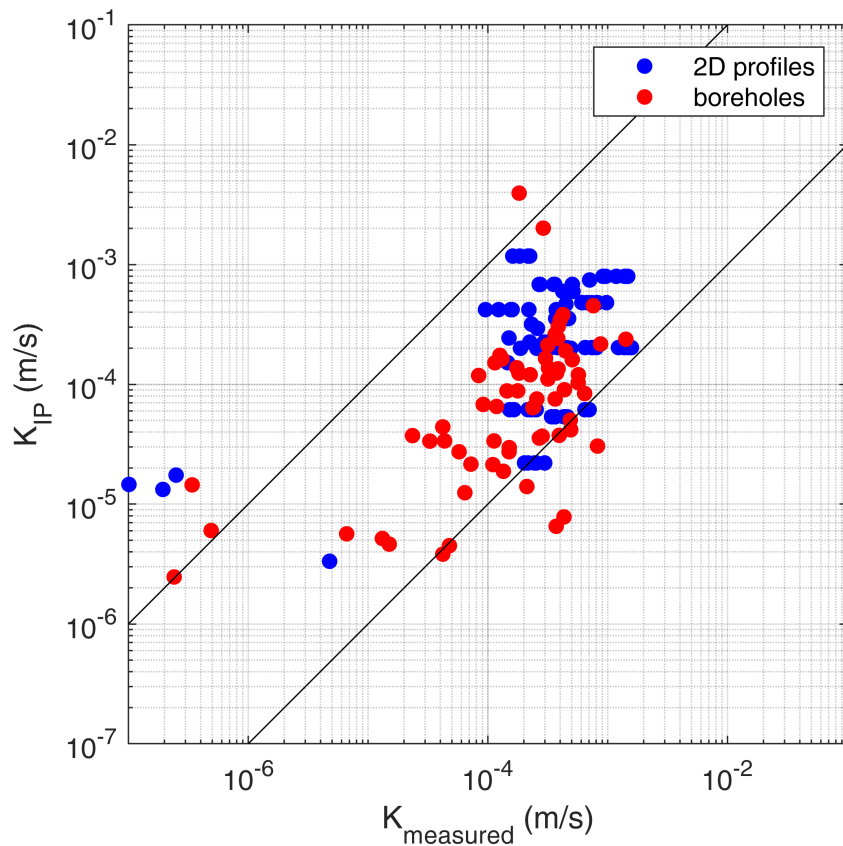
Figure 1. Comparison of hydraulic conductivity estimated from TDIP (K_{IP}) and hydraulic conductivity $K_{measured}$, estimated with grain size analyses and slug tests, in the three boreholes described in Fiandaca et al. (2018) and the 2D profiles described in Martin et al. (2021). The continuous black lines represent a deviation of one order of magnitude.

References

Fiandaca G., Maurya P.K., Balbarini N., Hördt A., Christiansen A.V., Foged N., Bjerg P.L., Auken E., 2018. Permeability estimation directly from logging-while-drilling Induced Polarization data, Water Resources Research, 54 (4), 2851-2870.

Fiandaca G., Meldgaard Madsen L., Maurya P.K., 2018B. Re-parameterisations of the Cole-Cole model for improved spectral inversion of induced polarization data, Near Surface Geophysics, 16 (4), 385-399.

Martin T., Pauw P.S., Karoulis M., Medoza A., Günter T., Madsen L.M., Maurya P.K., Doetsch J., Reijkær S., Dahlin T., Fiandaca G.. Inversion of hydraulic conductivity from Induced Polarisation, Part B: field examples from five countries. Near Surface Geoscience 2021-27th European Meeting of Environmental and Engineering Geophysics, 1-4.

Maurya P.K., Balbarini N., Møller I., Rønde V., Christiansen A.V., Bjerg P.L., Auken E., Fiandaca G., 2018. Subsurface imaging of water electrical conductivity, hydraulic permeability and lithology at contaminated sites by induced polarization, Geophys. J. Int, 213, 770-785.

Revil, A., Koch, K., & Holliger, K. (2012). Is it the grain size or the characteristic pore size that controls the induced polarization relaxation time of clean sands and sandstones? Water Resources Research, 48(5).

Weller, A., Slater, L., Binley, A., Nordsiek, S., & Xu, S. (2015). Permeability prediction based on induced polarization: Insights from measurements on sandstone and unconsolidated samples spanning a wide permeability range. Geophysics, 80(2), D161–D173.

O11 - Effect of induced polarization on galvanic and inductive data: where does it matter most?

G. Fiandaca[1], F. Dauti[1], A. Signora[1]

(1) The EEM Team for Hydro & eXploration, Department on Earth Sciences "Ardito Desio", University of Milano, Milano, Italy

Abstract. The phenomenon of Induced Polarization (IP) is commonly studied with galvanic methods, both in the field and in the laboratory. IP effects on inductive electromagnetic (EM) data have been reported since the early '80s, but the attention of the EM community in IP focuses mainly on exploration purposes, because strong chargeable anomalies trigger negative EM responses.
In this study we show that the IP effect strongly affects EM data also in sand/clay environments, with a variety of acquisition systems, ranging from airborne EM, classic ground-based and portable systems for continuous ground acquisitions (the tTem system, towed by an ATV, and the Loupe system, mounted on backpacks). The effect on EM data simulated with these systems is much stronger than on data acquired with the galvanic method. This triggers bias in resistivity-only inversions, and makes data acquired with different systems incompatible with each other: data simulated with different systems cannot be fitted jointly. These findings highlight the importance of induced polarization on EM data, and open the way for new approaches for joint inversion of galvanic and inductive data, as well as for joint inversion of EM data acquired with different systems.

Introduction

The phenomenon of Induced Polarization (IP) is commonly studied with galvanic methods, both in the field and in the laboratory. IP effects on inductive electromagnetic (EM) data have been reported since the early '80s (e.g. Spies, 1980; Lee, 1981), but the attention of the EM community in IP focuses mainly on exploration purposes (e.g. Viezzoli et al., 2017; Lin et al, 2019; Couto et al., 2020), because strong chargeable anomalies trigger negative EM responses. In this study we show that the IP effect strongly affects EM data also in sand/clay environments, with a variety of acquisition systems, ranging from airborne EM, classic ground-based equipment, and portable systems for continuous ground acquisition (the tTem system, towed by an ATV, and the Loupe system, mounted on backpacks). The electrical values of the sand/clay layers are set up using petrophysical relations developed from laboratory experiments on the link between IP properties and hydraulic conductivity (Weller et al., 2015; Revil et al., 2012). Forward modelling and inversions are carried out in 1D, following the approach described in Auken et al. (2015).

Method

Forward modelling and inversion have been carried out in 1D, following Auken et al. (2015), on a variety of 1D models simulating sand and clays layers. Data have been modelled for galvanic vertical electrical sounding (VES) with IP modelling, as well as on four different EM systems:

- the airborne EM time-domain XCite system, from New Resolution Geophysics (https://www.nrgex.co.za/)
- a classic ground-based system with 40m x 40m transmitter loop, in dual moment acquisition
- the recent tTem system (Auken et al., 2019), which acquires continuously towed by an ATV in offset configuration
- the recent Loupe system (Street et al., 2018), with transmitter and receiver mounted on two backpacks in offset configuration for continuous acquisition while walking.

Results

Figure 1 shows an example of comparison of forward modelling for a 3-layer model, simulating a 3m thick clay layer at 10m depth. Data have been simulated taking into account IP (blue lines), and neglecting the IP effect (red lines), using the DC resistivity for computations. Overall, a great difference exists between EM data computed with and without considering the IP effect, on all systems; much stronger than on galvanic data. This difference makes the data incompatible with each other, when interpreted in terms of resistivity-only inversion.

Conclusions

The effect on EM data is much stronger than on data acquired with the galvanic method. This triggers bias in resistivity-only inversions, and makes data acquired with different systems incompatible with each other: data simulated with different systems cannot be fitted jointly. These findings highlight the importance of induced polarization on EM data, and open the way for new approaches for joint inversion of galvanic and inductive data, as well as for joint inversion of EM data acquired with different systems.
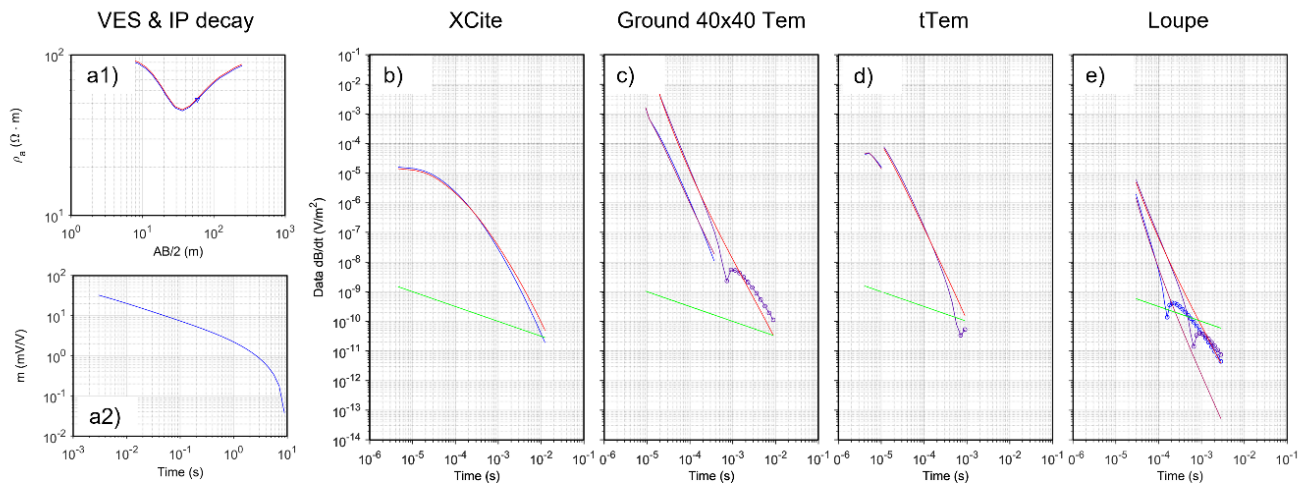
Figure 1. Forward responses of galvanic and inductive data on a three-layer synthetic model consisting of a 3 m-thick clay layer embedded in sand at depths comprised between 10 m and 13 m. Blue lines: forward computations that take into account induced polarization. Red lines: forward computations that neglect induced polarization. Green lines: typical EM noise level. Circled data: negative data. a1) comparison of VES galvanic data. a2) Induced polarization decay of the VES sounding with highest signal level (AB/2 indicated by triangle in a1)). b) Airborne EM sounding with XCite system. c) Ground-based EM sounding with 40x40 transmitter area, dual moment. d) tTem souding, dual moment. e) Loupe sounding, X and Z components.

Acknowledgements

References

Auken E., Christiansen A.V., Kirkegaard C., Fiandaca G., Schamper C., Behroozmand A.A., Binley A., Nielsen E., Efferso F., Christensen N.B., Sorensen K., Foged N. & Vignoli G., 2015. An overview of a highly versatile forward and stable inverse algorithm for airborne, ground-based and borehole electromagnetic and electric data, *Exploration Geophysics,* 46**,** 223-235.

Auken, E., Foged, N., Larsen, J. J., Lassen, K. V. T., Maurya, P. K., Dath, S. M., & Eiskjær, T. T., 2019. tTEM—A towed transient electromagnetic system for detailed 3D imaging of the top 70 m of the subsurface. *Geophysics*, *84*(1), E13-E22.

Couto Junior, M. A., Fiandaca, G., Maurya, P. K., Christiansen, A. V., Porsani, J. L., & Auken, E., 2020. AEMIP robust inversion using maximum phase angle Cole–Cole model re-parameterisation applied for HTEM survey over Lamego gold mine, Quadrilátero Ferrífero, MG, Brazil. *Exploration Geophysics*, *51*(1), 170-183.

Lee, T., 1981. Transient electromagnetic response of a polarizable ground. *Geophysics*, 46,7, 1037-1041.

Lin, C., Fiandaca, G., Auken, E., Couto, M. A., & Christiansen, A. V., 2019. A discussion of 2D induced polarization effects in airborne electromagnetic and inversion with a robust 1D laterally constrained inversion scheme. *Geophysics*, *84*(2), E75-E88.

Revil, A., Koch, K., & Holliger, K., 2012. Is it the grain size or the characteristic pore size that controls the induced polarization relaxation time of clean sands and sandstones? Water Resources Research, 48(5).

Spies, B.R., 1980. A field occurrence of sign reversals with the transient electromagnetic method. *Geophysical Prospecting*, 28, 620-632.

Street, G., Duncan, A., Fullagar, P., Tresidder, R., 2018. LOUPE – A Portable EM Profiling System. System, ASEG Extended Abstracts, 2018:1, 1-3, DOI: 10.1071/ASEG2018abW10_3G.

Viezzoli, A., Kaminski, V., Fiandaca, G., 2017. Modeling induced polarization effects in helicopter TEM data: Synthetic case studies. *Geophysics*, (82-2) E31-E50.

Weller, A., Slater, L., Binley, A., Nordsiek, S., & Xu, S., 2015. Permeability prediction based on induced polarization: Insights from measurements on sandstone and unconsolidated samples spanning a wide permeability range. Geophysics, 80(2), D161–D173.

O12 - Enhancing DC data quality using the full IP response

D. Domenzain[1], L. Liu[1], I. Y. Vela[2], A.V. Christiansen[1]

(1) Department of Geoscience, Aarhus University, Denmark
(2) Ejlskov A/S, Denmark

Presenter: D. Domenzain (diego.domenzain@geo.au.dk) **Student y/n:** No
Web page: NA   **Preferred presentation oral/poster:** Oral

Abstract. We present a numerical and computationally fast processing routine for direct current (DC) voltage data using the full induced polarization (IP) response in time. Often DC data quality control is based on apparent resistivity, geometrical factor, and statistical cut-offs of the observed DC data without using the full IP record in time. These approaches may fail to identify unstable voltage noise that damage the quality of the recovered conductivity. We present cross-borehole field data results measured with the novel multi-channel Adapt instrument. Our proposed method significantly improves the 3D DC inversion results and points forward to improved IP inversions as well.

Introduction

Direct current (DC) voltage measurements of the subsurface require for the injected electric current to reach steady state. Since this steady state is not instantaneously achieved, the instrument must inject current over a period of time. The induced polarization response is therefore the entire time record until steady state is reached. We use this time-domain information to quickly assess quality in the observed DC data. Specifically, we identify unstable voltage noise which is automatically removed in data processing by adding a fraction of computation cost. Figure 1 shows an example of the type of noise we target with our method: voltage decay where voltage build-up is expected.

Our approach requires for the full IP response to be recorded. However, conventional IP processing (drift removal, harmonic denoising, and time-gating (Olsson et al. 2016), in that order) is not needed. We only require up to drift removal, followed by an average of the time derivative of the signal: the sign of this average determines whether the voltage experienced a decay (noise) or a build-up (signal). This last step adds 1% more computation time. Processing efficiency is particularly important since the novel multi-channel Adapt instrument can measure up to a million IP quadrupoles in a one-day survey.

Field data

We test our scheme on cross-borehole IP data collected in central Denmark. The site is dominated by layered clay deposits. We follow a similar approach as Domenzain et al. (2021) to invert the data. Figure 2 shows slices in depth of the recovered 3D DC conductivity using the fully conventionally processed data, and with our added scheme.

Conclusion. We present an efficient way of detecting unstable voltage noise in the IP response. Our scheme significantly improves the quality of the 3D DC inversion results. Moreover, it cuts computation costs for the full IP processing by enabling an early criterion to skip the harmonic denoising and gating of the data.
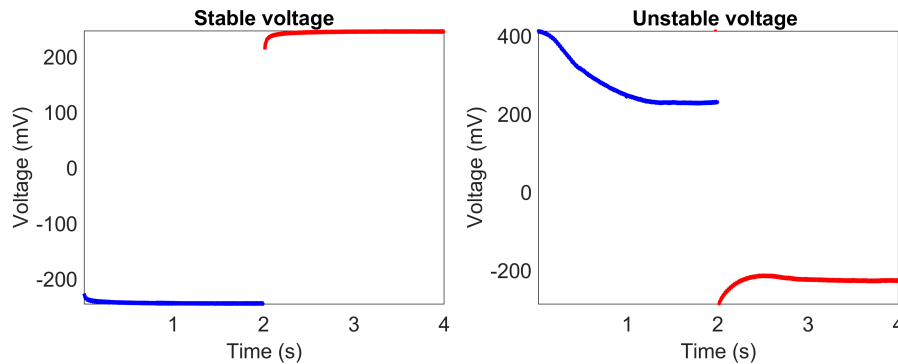
Figure 1. Example of a stable and unstable voltage quadrupole in a cross-borehole configuration. The data were measured with a 100% duty-cycle current injection of 4 seconds in total. This type of unstable voltage is automatically removed with our scheme.
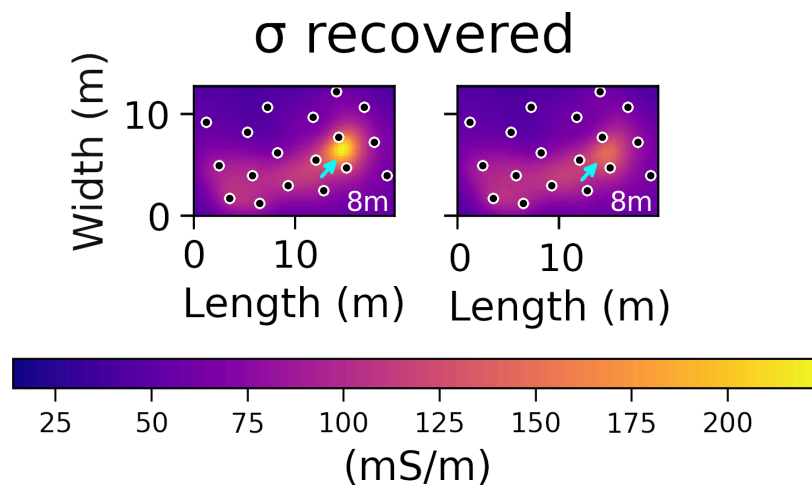
Figure 1. Slice at 8m depth of the recovered 3D DC conductivity without (left) and with (right) our proposed IP processing routine. The black dots denote borehole locations. The annotated region on the left is an artifact. The artifact is removed on the right.

References

Olsson, P. I., Fiandaca, G., Larsen, J. J., Dahlin, T., & Auken, E. (2016). Doubling the spectrum of time-domain induced polarization by harmonic denoising, drift correction, spike removal, tapered gating and data uncertainty estimation. Geophysical Supplements to the Monthly Notices of the Royal Astronomical Society, 207(2), 774-784.

Domenzain, D., Bradford, J., & Mead, J. (2021). Efficient inversion of 2.5 D electrical resistivity data using the discrete adjoint method. Geophysics, 86(3), E225-E237.

O13 - Fast DCIP data acquisition with full-range gradient array

T. Dahlin and P. Hedblom

Engineering Geology, Lund University, Lund, Sweden

Presenter: T. Dahlin (torleif.dahlin@tg.lth.se) **Student y/n:** No
Web page: NA **Preferred presentation oral/poster:** Oral

Abstract. Direct current resistivity and time-domain induced polarization (DCIP) with long measurement pulses, that are required for spectral information, can become too time-consuming to be practical in some applications. We tested a full-range gradient array in combination with simultaneous measurement of 32 potential electrodes in a separated spreads setup with 64 electrodes. The results show that it is a promising approach and that continued tests are well motivated.

Introduction

Spectral induced polarization (SIP) information can be extracted from direct current resistivity and time-domain induce polarization (DCIP) data under certain circumstances and with suitable data processing algorithms (Olsson et al. 2016). It is however important to measure with sufficiently long pulses for the low frequency end of the spectral content, which makes the time required for the data acquisition grow accordingly so that it becomes a major limitation in practical application. This applies to 2D surveys with current pulses of several seconds or more and becomes severe in 3D surveys. It is possible to speed up the data acquisition process by close to a factor 2 with 100 % duty cycle (Olsson et al. 2015), but that is not sufficient and the only conceivable way to handle this while retaining the number of data points is to measure with more parallel channels.

To speed up the data acquisition process we tested an extended version of the commonly used multiple gradient array (MG) (Dahlin and Zhou 2006), which may be referred to as full-range gradient array (FRG) or expanded gradient array (Zhou et al. 2020).

Numerical simulation

We simulated different variations of FRG and MG against different models of subsurface structures with forward modelling using Res2dmod, followed by inversion with Res2dinv. The results show, as illustrated by the example in Figure 1, that more data and similar or better resolution of the modelled structures could be achieved with FRG in half the time or less compared to MG depending on the number of current transmissions and associated data.
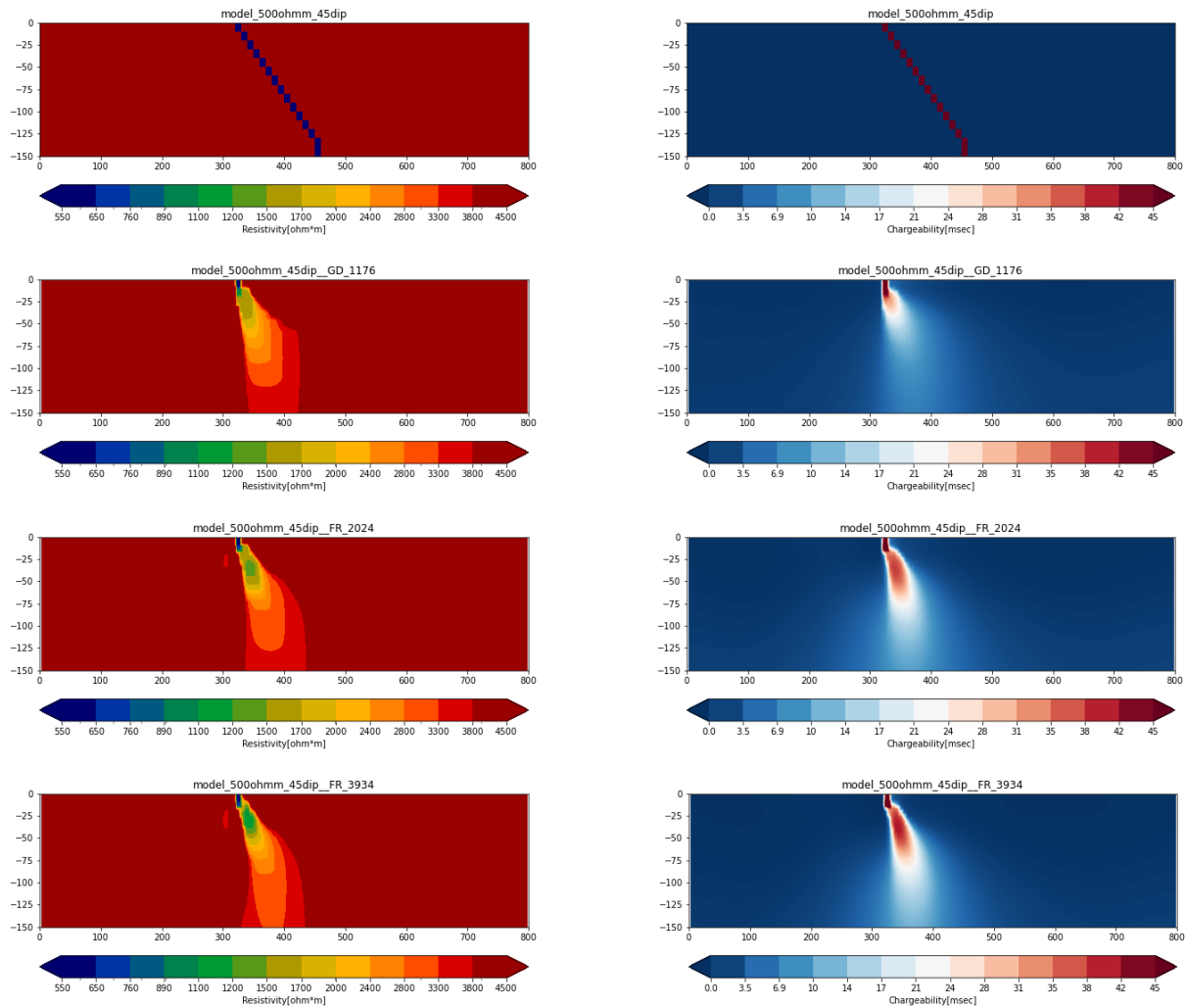
Figure 1. Synthetic modelling results example with resistivity and integral chargeability. From top to bottom: a) Forward model sections, b) Multiple gradient array inverted sections (1176 data), c) Full-range gradient array inverted sections (2024 data), d) Full-range gradient array inverted sections (3934 data).

Small scale field test

A small-scale field test measurement test with a 32-channel receiver was made on a lawn on Lund University campus, where an ABEM Terrameter LS2 was used as transmitter. Separated electrode spreads were used for current transmission and potential measurements (Dahlin and Leroux 2012), consisting of 32 electrodes each. Odd numbered electrodes were connected to transmitter (TX) spread and the even ones to the receiver (RX), resulting in an electrode separation of 0.5 m. A measurement sequence with 42 current electrode combinations was used on the TX spread with measurement of 31 gradients on the RX spread, whereafter the role of the cables was reversed, and the procedure repeated to generate a mirrored sequence. This should give 2 x 1302 data points, but due to a glitch in the data acquisition software around 6% of the data were lost. A 100 % IP duty cycle (Olsson et al. 2015) with 1 s long pulses was used, with 20 mA transmitted current and 2 stacks (+-+-). Due to an error in the wiring to the receiver, different gradients than those intended were measured, resulting in 24 % alpha, 32 % beta and 44 % gamma arrays, but the results still illustrate

the applicability. The actual measurement time, not counting time required for setting up the electrode spreads and the instrumentation, was 10 minutes out of which 5.6 minutes were actual time used for the current pulses and measurement. The remaining time was used by the instrument for relay switching, setting up the current transmitter, saving data, etc. Using the same setup, transmitter and relay switching etc. it would take 27 minutes with 4 s pulses and 49 minutes with 8 s pulses.

The data were inverted for resistivity and integral chargeability which resulted in model sections (Figure 2) that are well in line with those measured with other electrode arrays over the same area. The mean residuals below 1% reflect excellent data quality.
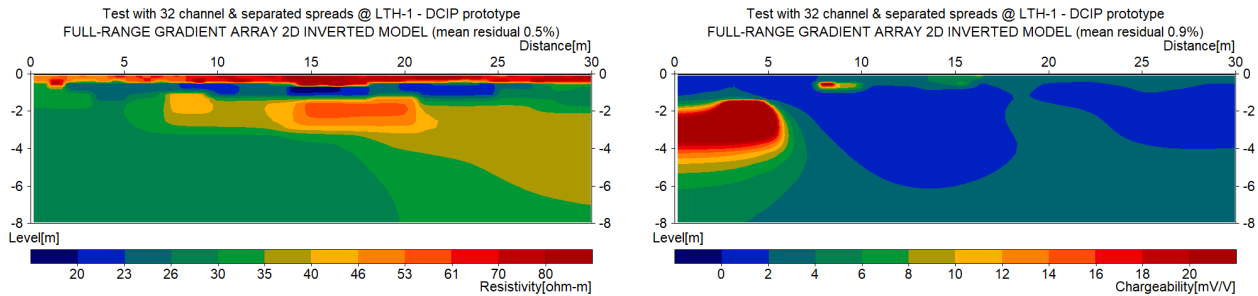
Figure 2. Inverted sections from 32 channel test: a) resistivity, b) integral chargeability.

Discussion and conclusions

Full-range gradient array was tested for DCIP measurement as a means of speeding up the data acquisition process, in addition to the faster measurement process of 100% IP duty cycle. Synthetic modelling and a small-scale field test shows that it is a promising approach. In full scale applications in various environments there are however some measurement technical questions that need to be considered. The measured signal will vary over magnitudes, depending on if it is a nested configuration or dipole-dipole type, and depending on the distance between the receiver dipole and a current electrode. This means that different measurement ranges may most likely be required for the different measurement channels to maximise resolution for those with small signal levels while avoiding overrange for those with high signal levels. Furthermore, the total voltage difference between all measurement channels will most likely often fall outside the measurement range, which can lead to large errors unless the measurement channels are galvanically separated. Future work should include modelling with simulated voltage dependent noise. Furthermore, the measuring device needs to be adapted according to the measurement technical considerations above, and field tests be carried out in different scales and environments.

References

Dahlin T. & Leroux V. (2012) Improvement in time-domain induced polarisation data quality with multi-electrode systems by separating current and potential cables, *Near Surface Geophysics*, **10**, 545-565.

Dahlin T. & Zhou B. (2006) Multiple-gradient array measurements for multichannel 2D resistivity imaging, *Near Surface Geophysics*, **4**, 113-123.

Olsson P.-I., Fiandaca G., Juul Larsen J., Dahlin T. & Auken E. (2016) Doubling the spectrum of time-domain induced polarization by harmonic de-noising, drift correction, spike removal, tapered gating and data uncertainty estimation, *Geophysical Journal International*, 207(2): 774-784.

Olsson P.-I., Dahlin T., Fiandaca G. and Auken E. (2015) Measuring time domain spectral induced polarization in the on-time – decreasing the acquisition time and increasing the signal levels, *Journal of Applied Geophysics*, 123, 316-321

Zhou B., Bouzidi Y., Ullah S. & Asim M. (2020) A full-range gradient survey for 2D electrical resistivity tomography, *Near Surface Geophysics,* **18**, 609–626.

O14 - Determining lab and field petrophysical relationship of unconsolidated sediments in the Luy River coastal aquifer though SIP and co-located geophysical well logs

D. Cong-Thi[1,2], L. Pham Dieu[1,2], D. Caterina[3], X. De Pauw[1], H. Dang Thi[2], HH. Ho[2], T. Hermans[1], F. Nguyen[3,4]

(1) Department of Geology, Ghent University, 9000-Gent, Belgium.
(2) Department of Marine Geology, Vietnam Institute of Geosciences and Mineral Resources (VIGMR), 100000 Hanoi, Vietnam.
(3) Department of Urban and Environmental Engineering, Liege University, B52- 4000 Liège, Belgium.
(4) Department of Civil Engineering, KU Leuven, 3000 Leuven, Belgium.

Presenter: D. Cong-Thi (diep.congthi@ugent.be) **Student y/n:** Yes
Web page: NA   **Preferred presentation oral/poster:** Oral

Abstract. The lithological and stratigraphical heterogeneity of coastal aquifers has a great influence on saltwater intrusion (SI). This makes it difficult to predict SI pathways and their persistence in time and to quantify salinities based on petrophysics. In this context, electrical resistivity tomography (ERT) and induced polarization (IP) methods are receiving increased attention regarding the discrimination between saltwater-bearing and clayey sediments. To simplify the interpretation of ERT data, it is commonly assumed that the bulk conductivity mostly depends on the conductivity of pore fluid, while surface conductivity is generally disregarded in the spatial and temporal variability of the aquifers, particularly, once the aquifer is affected by the presence of saltwater. However, this can lead to misinterpretation for aquifers constituted by clay-bearing sand layers or alternating sand and clay layers. In this study, we rely on co-located data from drilled boreholes coinciding with the geophysical measurements to formulate petrophysical relationships between bulk and fluid conductivity in both presence and absence of clay content in the porous sediments. We investigate both the laboratory scale through spectral induced polarization (SIP, Figure 1) and field scale through the comparison of ERT and time-domain IP with electromagnetic logging and lithologs. First, the sedimentary samples from the drilled wells were classified according to their grained size distribution, and then analyzed in the lab using a SIP system using the four-point measurement method in controlled salinity conditions. Second, logging results were compared with the field data extracted from inversion imaging. We found that the formation factors of the different unconsolidated sedimentary classification are varying from 2.0 to 4.5 for coarse-grained sand and clay-bearing mixtures, respectively. The clay bearing sediments were revealed to be distributed in small lenses and discontinuously distributed along the Luy River Catchment. In addition, they are occasionally locally present around the saline part of the aquifers. In these circumstances, ERT/IP inversions do not have the resolution to unequivocally discriminate clay-rich zones from saline zones. The comparison with logging data shows that ERT and to a lesser extent IP are able to image the main trend observed in wells, but that sharp transition and thin layer are missed. The latter seem to have a huge influence on the salinity distribution, making ERT and IP data inappropriate to characterize small-scale variations. The assumption of homogenous geological media is therefore leading to overestimate SI in heterogeneous clay-bearing aquifers.
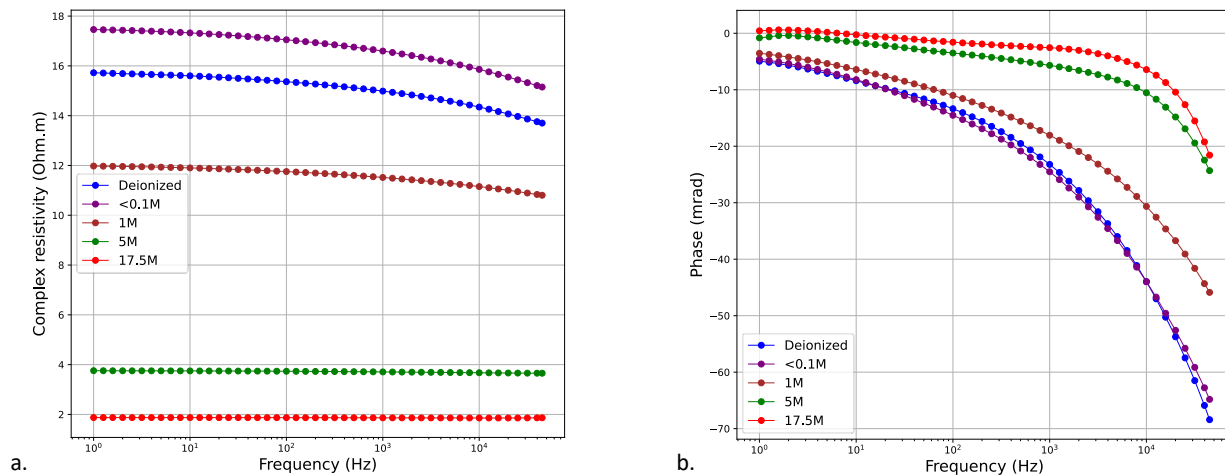
Figure 1. Spectra (a) and phase shift (b) made on saturated clay-bearing mixture (30% clay) in different salinity solutions using SIP measurements.

References

Archie, G.E. (1942). The electrical resistivity log as an aid in determining some reservoir characteristics. Trans. AIME 1942, 146, 54–62.

Cong-Thi, D., Dieu, L.P., Thibaut, R., Paepen, M., Huu, H.H., Nguyen, F., Hermans, T. (2021). Imaging the structure and the saltwater intrusion extent of the Luy River coastal aquifer (Binh Thuan, Vietnam) using electrical resistivity tomography. Water 2021, 13, 1743. https://doi.org/10.3390/w13131743.

Waxman, W.H., Smits L.J.M. (1968). Electrical conductivities in oil-bearing sands. Social Petroleum Engineering Journal, 8, 107-122

Wentworth, C. K. (1922). A scale of grade and class terms for clastic sediments. Journal of Geology, v. 30, p. 377.

Zimmermann, E., Kemna, A., Berwix, J., Glaas, W., Münch, H.M., Huismann, J.A. (2008). A high-accuracy impedance spectrometer for measuring sediments with low polarizability. Measurement Science and Technology, 19, 105603. doi:10.1088/0957-0233/19/10/105603

Zimmermann, E., Huisman, J.A., Kemna, A., Berwix, J., Glaas, W., Meier, H., Wolters, B., Esser, O. (2010). Advanced electrical impedance tomography system with high phase accuracy. Presented at the 6th World Congress on Industrial Process Tomography, pp. 583–591.

O15 - A new semi-analytic model for Stern-layer polarization in pore throats

D. Kreith and M. Bücker

TU Braunschweig, Institute of Geophysics and Extraterrestrial Physics, Mendelssohnstr. 3, 38106 Braunschweig, Germany

Presenter: Dennis Kreith (d.kreith@tu-braunschweig.de), **Student**: y
Web page: https://www.tu-braunschweig.de/igep, **Preferred presentation oral/poster**: Oral

Abstract. We present a new semi-analytic model to describe the polarization of the Stern layer in pore throats. Our geometrical model is a pore system consisting of two cylindrical pores, which is usually used to model membrane polarization. We solve a one-dimensional Nernst-Planck-Poisson equation system for a total of three ion species, i.e., the anions and cations in the electrolyte solution and the diffuse layer as well as the cations in the Stern layer. In our model, the latter are treated as an individual ion species and, thus, are allowed to present an own polarization. To investigate the influence of this Stern-layer polarization and to compare it to the "classical" membrane polarization of the diffuse layer, we carry out various parameter studies. In general, the relative contributions of Stern-layer and membrane polarization to the overall polarization response strongly depend on the specific configuration of the electrical double layer, i.e., the Zeta-potential and the Stern-layer surface charge, as well as on pore radii and lengths.

Introduction. In metal-free geologic materials, the electrical double layer (EDL) causes the frequency-dependent behavior of the electric conductivity. It consists of two layers: The Stern layer that only contains cations adsorbed to the negatively-charged surface and the diffuse layer that contains both cations and anions, the concentrations of which increase or decrease with the distance from the surface. Under the influence of an external electric field, the Stern layer in the pore-constriction geometry polarizes due to the different net Stern-layer conductances in the two pores. So far, Stern-layer polarization has mostly been treated theoretically around spherical particles (e.g., Lyklema et al., 1973), where the simultaneous polarization of the diffuse layer usually plays a secondary role. In a pore channel, membrane polarization may gain importance – especially in narrow pore throats. Our new semi-analytic model describes both the polarization of the Stern layer and the membrane polarization in a simple pore-constriction geometry.

Model . We consider a system of two cylindrical pores (Fig. 1) filled with a monovalent, symmetrical electrolyte. Therefore, we only have one anion (denoted by n) and one cation (denoted by p) species, each. The respective current densities are described by a Nernst-Planck equation:

$$j_{p,n} = -FD_{p,n}\frac{\partial c_{p,n}}{\partial x} \pm F\mu_{p,n}c_0 E \qquad (1)$$

with Faraday's constant F, the ion diffusivities $D_{p,n}$, the mobilities $\mu_{p,n}$, the equilibrium concentration c_0, the perturbation ion concentrations $c_{p,n}$, and the perturbing electric field E. Effective mobilities of

the ions in the electrolyte and the diffuse layer are calculated using the model of Bücker and Hördt (2013) to describe the unequal transport rates in the diffuse layer.

Since we want the Stern layer to polarize individually, we treat the Stern-layer cations as a separate ion species. As common for Stern-layer polarization models, we assume the Stern layer to be thin compared to the pore radius. Thus, we can describe the concentration of Stern-layer cations as a surface charge density Σ_S, which is transformed into an effective ion concentration

$$c_{S,1} = \frac{2\Sigma_S}{FR_1}, \quad c_{S,2} = \frac{2\Sigma_S}{FR_2} \tag{2}$$

depending on the respective pore radius $R_{1,2}$. Using these effective concentrations, we can set up a Nernst-Planck equation for the Stern-layer cations:

$$j_S = -FMD_S\frac{\partial c_S}{\partial x} + F\mu_S c_S^{(0)} E, \tag{3}$$

where D_S and μ_S are the Stern-layer cation diffusivity and mobility, respectively, c_S is the perturbation concentration of Stern-layer cations with the equilibrium value $c_S^{(0)}$, that can be calculated by using eq. (2). The parameter M is a correction factor suggested by Lyklema et al. (1973), which describes the interaction of the polarized Stern layer with the charges of the diffuse layer and the electrolyte.
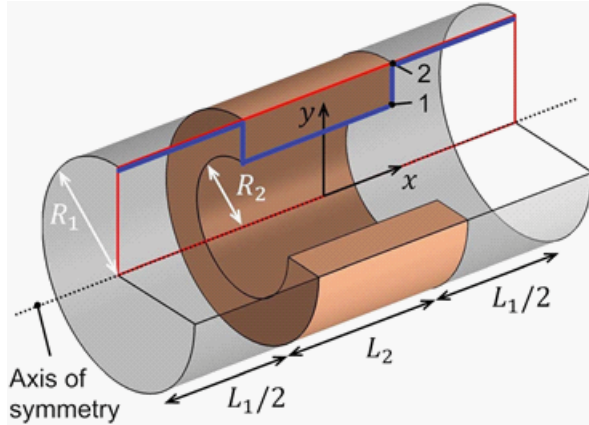
Figure 1: Sketch of the pore system consisting of two cylindrical pores. The blue line indicates the Stern layer. The gray area represents the electrolyte, the brown area is the matrix material narrowing the pore channel (modified from Bücker et al., 2019).

We can describe the influence of the perturbation concentration of all three ion species on the electric field by Poisson's equation

$$\frac{\partial E}{\partial x} = \frac{F}{\epsilon}(c_p - c_n + c_S) \tag{4}$$

with the electric permittivity ε. Equations (1) (for cations and anions), (2), and (4) represent a system of four coupled partial differential equations. We solve these equations under suitable boundary conditions semi-analytically to yield the perturbation concentrations, the electric field, and finally the effective conductivity of the pore system.

Results. Fig. 2 shows the maximum imaginary conductivity and the relaxation time as a function of the Zeta potential and the Stern-layer surface charge. We can identify two regimes: For Zeta

potentials below 120 mV, both the maximum imaginary conductivity and the relaxation time strongly depend on the surface-charge density in the Stern layer, while above that threshold, they become almost independent of the Stern-layer charge and are controlled by the Zeta potential, only. This behavior can be explained by the presence of both the Stern-layer polarization and the membrane polarization. Below the threshold of 120 mV, the overall polarization response is dominated by the polarization of the Stern layer. Above that value, membrane polarization becomes the dominant process. Similar results can be obtained by varying the geometry of the pore system, particularly the pore radius (not shown here).
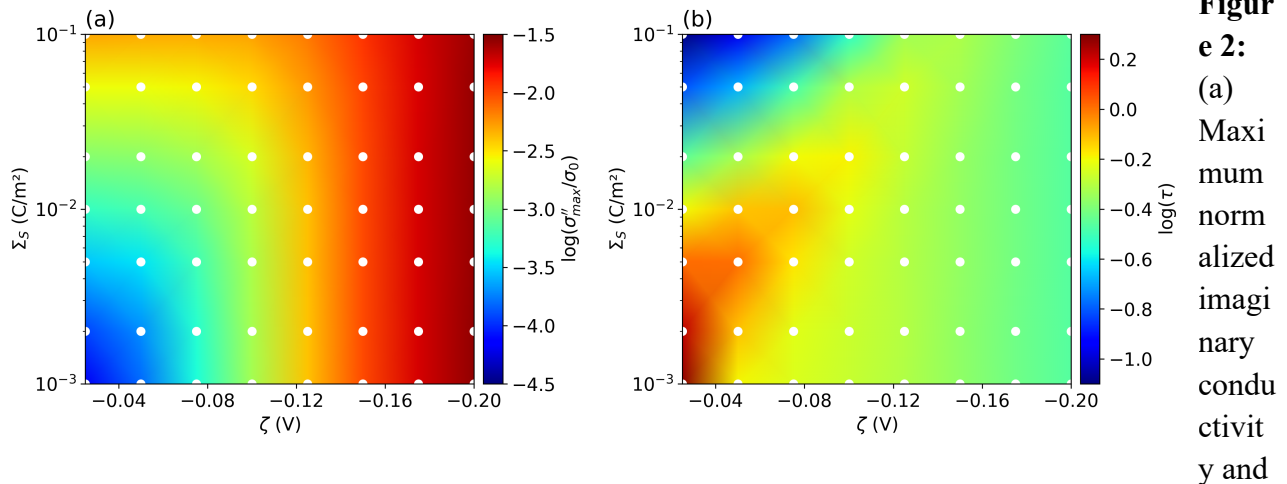
Figure 2: (a) Maximum normalized imaginary conductivity and (b) relaxation time of the new model for varying Zeta potential (ζ) and surface-charge density in the Stern layer (Σ_S)different parameter of the E. Spectra are calculated and evaluated at the white dots, values in between are interpolated.

Conclusions. We have developed and tested a new semi-analytical model for the Stern-layer polarization in a pore throat. Parameter studies to investigate the influence of the EDL structure and the pore geometry on the polarization response show that the resulting conductivity spectra contain and are controlled by both Stern-layer and membrane polarization. Each polarization process dominates for specific parameter combinations.

References

Bücker, M., and Hördt, A., 2013. Analytic modeling of membrane polarization with explicit parametrization of pore radii and the electrical double layer. Geophysical Journal International, 194, 804–813.

Bücker, M., Flores-Orozco, A., Undorf, S., and Kemna, A., 2019. On the Role of Stern- and Diffuse-Layer Polarization Mechanisms in Porous Media. Journal of Geophysical Research: Solid Earth, 124, 5656-5677.

Lyklema, J., Dukhin, S. S., and Shilov, V. N., 1983. The relaxation of the double layer around colloidal particles and the low-frequency dielectric dispersion: Part I. Theoretical considerations. Journal of Electroanalytical Chemistry and Interfacial Electrochemistry, 143, 1-21.

O16 - Extremely large induced polarization phenomenon

Y. Wu[1], C. Downs[2], C. Chou[1], L. Peruzzo[1], J. Wang[1], S. Uhlemann[1], K. Kuhlman[2]

(1) Lawrence Berkeley National Laboratory, Berkeley CA U.S. 94720
(2) Sandia National Laboratories, Albuquerque. New Mexico, U.S. 87123

Presenter: Y. Wu (YWu3@lbl.gov) **Student y/n:** No
Web page: NA   **Preferred presentation oral/poster:** Oral

Abstract. While most geological materials exhibit small to modest spectral induced polarization (SIP) signals, typically within tens of milliradians (mrads) phase shift, extremely large induced polarization signals, with phase shifts in the range of a few hundred milliradians or higher, are observed in multiple types of materials in both biotic and abiotic systems. These large IP signals are repeatedly observed across many samples while the underlying mechanism driving such large signals is not well explored. We present two examples of such materials with measurements at both lab and field scales, demonstrating the consistency of such large signals. We will also explore quantitatively the underlying mechanisms driving such large signals and discuss their practical applications.

The first example of such materials is geologically deposited rock salt, which is considered an ideal storage formation for nuclear waste disposal due to its low permeability and ability to creep close fractures or permeabilities over time, among other desirable properties. There have been several studies on the geoelectrical properties of rock salt, with most these studies focused on the electrical conductivity behavior of rock salt and very limited examination of its induced polarization behaviors (Yaramanci, 2000). Our recent SIP measurements of rock salt were conducted using polyhalite rock salt samples from the WIPP (Waste Isolation Pilot Plant) site in New Mexico, U.S., the world-only licensed underground storage site for nuclear waste. Experiments were conducted using different experimental setup and measurement devices and the effect of temperature on the SIP behaviors were explored. All measurements showed large polarization signals with phase values on the order of a few hundred milliradians or higher. In addition, temperature experiments demonstrated strong temperature dependent behaviors of the SIP signals for multiple rock salt samples (Figure 1).
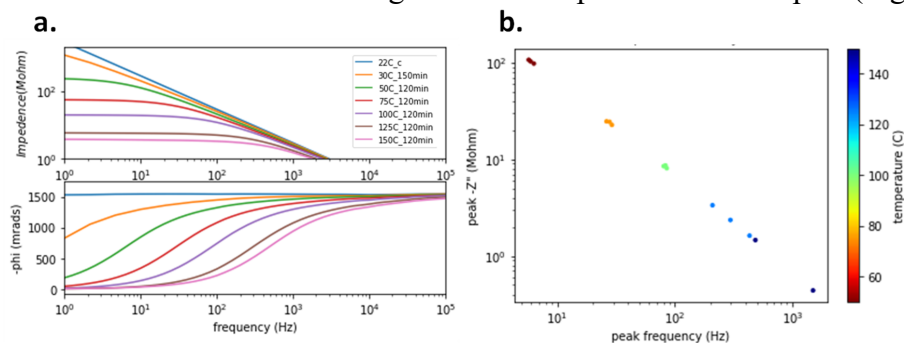
Figure 1: (a) The impedance magnitude and phase values for a rock salt sample during heating experiments indicating extremely large phase shift values that decrease with temperature, especially at low frequencies. (b) The correlation between imaginary impedance and peak frequency with changing temperature, indicating temperature dependent behaviors. These responses have been validated on multiple samples.

A second example exhibiting large IP signals is plant tissues, such as roots. Previous studies suggest that plant roots exhibit large IP signals due to the polarization of charges near the cell membranes, which primarily occur at high frequencies when apoplastic, in addition to symplastic, pathways dominant (Ozier-Lafontaine and Bajazet, 2005). Such electrical behaviors of roots have been used to explore its potential use for root characterization, yet most of these results were based on laboratory studies conducted in controlled conditions, such as hydroponics. We conducted extensive

measurements of SIP signals under both lab and field conditions for multiple plant species, including wheat, corn, soybean, carrots, all of which exhibit large IP signals at high frequencies. Quantitative correlations between SIP signals and root traits of interests, such as total root mass and length, are explored which have been used for noninvasive phenotyping of crop roots (Figure 2).
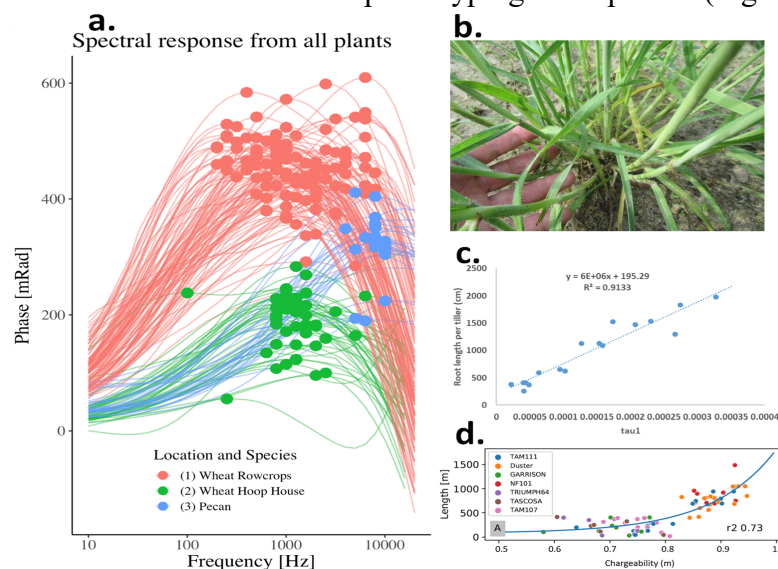
Figure 2: (a) examples of SIP signals from wheat and pecan roots grown in both field and greenhouse conditions; (b) above ground shoot of winter wheat; (c) correlations between SIP parameter, tau, and root length; (d) correlation between SIP parameters, chargeability, and root length of multiple wheat cultivars grown in both greenhouse and field conditions. Figure modified from Peruzzo et al, 2021

While rock salt and plant roots are two completely different types of materials, they both display large polarization signals, primarily at high frequencies. While the underlying mechanism of polarization is still under investigation, the SIP signals from roots are thought to be associated with the EDL polarization of the cell walls (Ehosioke et al, 2020; Tsukanov and Schwartz, 2021). The extremely large SIP signals from rock salt is likely not associated with EDL polarization, but rather Maxwell Wegner type of effects from the dielectric contrast at interfaces between brine inclusions and salt matrix. While these mechanisms are under further investigation, these characteristically large SIP signals could lead to new applications, such as new methods for root phenotyping and geoelectrical monitoring of brine movement in rock salt under unclear waste disposal conditions.

References

Ehosioke, S., Nguyen, F., Rao, S., Kremer, T., Placencia-Gomez, E., Huisman, J. A., Kemna, A., Javaux, M., & Garre, S. (2020). Sensing the electrical properties of roots: A review. Vadose Zone Journal, 19(1). 1‑29. https://doi.org/10.1002/vzj2.20082

Ozier-Lafontaine, H., & Bajazet, T. (2005). Analysis of root growth by impedance spectroscopy (EIS). Plant and Soil, 277(1-2), 299‑313. https://doi.org/10.1007/s11104-005-7531-3

Peruzzo, L., Liu, X., Chou, C., Blancaflor, E. B., Zhao, H., Ma, X.-F., Mary, B., Ivan, V., Weigand, M., & Wu, Y. (2021). Three-channel electrical impedance spectroscopy for field-scale root phenotyping. Plant Phenome J. 2021;4:e20021. https://doi.org/10.1002/ppj2.20021

Tsukanov, K., & Schwartz, N. (2021). Modeling plant roots spectral induced polarization signature. Geophysical Research Letters, 48, e2020GL090184. https://doi.org/10.1029/2020GL090184

Yaramanci, U., (2000), Geoelectric exploration and monitoring in rock salt for the safety assessment of underground waste disposal sites, Journal of Applied Geophysics, 44, 181–196.

O17 - Integration of hydrochemical and induced polarization analysis for leachate localization in a municipal landfill

Teng Xia[1], Jian Meng[1], Shiliang Liu[1], Deqiang Mao[1]

(1) School of Civil Engineering, Shandong University, Jinan 250061, China

Presenter: Teng Xia (Tengxiasdu@163.com) **Student y/n:** Yes
Web page: NA   **Preferred presentation oral/poster:** Poster

Abstract. Landfills have been identified as a significant concern to the surrounding surface and groundwater ecosystem because of the leachate discharge. To tackle the uncertain localization of the contamination plume due to low sampling densities, a combination of hydrochemical analysis and induced polarization survey (IP) is employed to characterize the leachate in a municipal landfill. The polarization effect in the contaminated area is significantly higher than expected for landfill sites, but relatively low chargeability zones (< 100 mV/V) indicating the distribution of leachate are observed inside high conductivity (> 600mS/m) areas. With reliable geophysical results confirmed by similar formation factors from both field and laboratory data, the abnormal high polarization effect is attributed to installed steel sheet piles next to the survey cable. In addition, we successfully identify linear relationship between the geophysical responses and dominant inorganic conservative compounds (Cl- and Na+) from the leachate plume. The gentle variations of borehole chemical parameters show that the plume is not affected by a continuous contamination source any more, indicating that the steel sheet pile effectively cut off the continuous contamination from the leachate tanks. In conclusion, the integration of IP and hydrochemical data is an excellent way to locate contaminated zones and monitor the behaviors of leachate plume in the landfill.

Introduction. Leachate plumes that migrate into surface waters can potentially pose a long-term threat to public health and environment. For plumes with organic and inorganic constituents, the concentration of ionic species originated from contaminant sources is a widely applied method for assessing the ecological effect of landfills. To overcome the limitation of the direct sampling methods, less costly and non-invasive geophysical techniques have been adopted to depict contaminated plume. Induced polarization (IP) method is an extension of direct current resistivity method. It can help in distinguishing salinity changes from those caused by lithology or the effects of metals in geological formations (Mao and Revil, 2016). Consequently, IP method has a greater potential to detect landfill plume compared to resistivity alone. However, field data is often complex and challenging because of different field circumstances such as geological settings and contaminant compositions. Immovable facilities in the landfill can affect the measured IP results as well, especially existing metallic infrastructures.

This study aimed to develop a method for leachate localization by integrating hydrochemical and geophysical data. Specifically, we investigate the usefulness of IP method for improved landfill leachate characterization, in particular to discriminate between metallic structures and leachate seepage. To better understand abnormal the geophysical response from the leachate plume, we further validate the formation factors through soil column experiments. Additionally, a link between inorganic conservative compounds and electrical conductivity is derived. Finally, we conclude the benefit of integrating of hydrochemical and geophysical information to obtain a high resolution spatio-temporal distribution of leaked landfill plume.

Materials and methods

The landfill is located in southwest of Shandong province, China. The groundwater levels of all boreholes suggest that the overall groundwater flow is in north direction (Fig. 1). In December 2020, the chemical oxygen demand (COD) and ammonia nitrogen content in the water samples from the wetland were higher than the standard values. Considering that there were no other factories around the wetlands, the leachate from landfill were judged to be the contaminant source. In March 2021, as a quick response, steel sheet piles (~15 m bgs) were installed on the north and east sides of the landfill to prevent further seepage and stabilize the landfill.
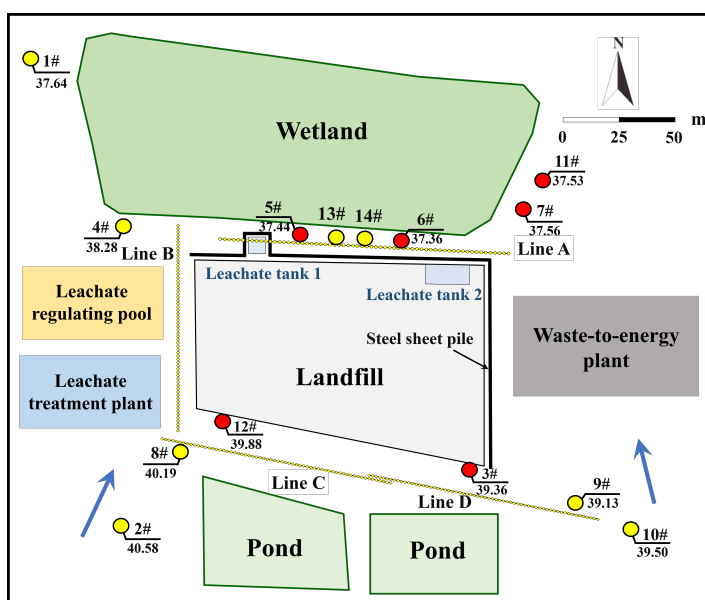
Figure 1. Deployment of field survey. Geophysical survey (four yellow lines) was designed to intersect with groundwater monitoring boreholes. The red dots show the contaminated sampling boreholes, while the yellow dots represent non-contaminated sampling boreholes. The number marked next to each borehole is the groundwater level and the blue arrow indicates the groundwater flow direction.

There were in total 14 boreholes and four geophysical survey lines in and around the study area. In addition, soil samples for laboratory measurement were collected at the depth of 7-8.5 m from boreholes 13# and 14#. Ontash PSIP instrument and ABEM Terrameter LS2 was used for laboratory FDIP and field TDIP measurement, respectively. The laboratory column and saturation pattern used for IP measurements were reported by Joyce et al. (2012). For field TDIP measurements, separation distance between two parallel cable spreads was around 1 m. Each cable consisted of 64 electrodes with a 2 m inter-electrode spacing. The injected current waveform had a duty cycle of 100% with 2 s on-time of current injection and 2 full stacks. The 2D inversion algorithm was adopted to invert TDIP data (Fiandaca et al. 2013).

Results and discussion

Inorganic compounds and ionic strength: In terms of COD (>10.6 mg/L), ammonia nitrogen (>0.761 mg/L), ionic strength (> 60 meq/L) and TDS (> 4000 mg/L), the extension of the plume is confirmed in the six boreholes, 3#, 5#, 6#, 7#, 11# and 12# (Fig. 1). The results reveal that the contamination plume transport away from the source mainly under the effect of hydraulic gradient. In addition, Cl^- and Na^+ are more dominant in the contaminated areas, SO_4^{2-} and Ca^{2+} have more influence in the uncontaminated areas. The linear regression analysis indicates that Cl^- and Na^+

have a statistically significant link with groundwater conductivity. For this site, if the electrical conductivity is above 500 mS/m, it means leachate plume has arrived into borehole locations.

Validation with formation factors: The range of formation factors (4.16-4.40) and surface conductivity (11.59-14.93 mS/m) obtained in laboratory are narrow, which indicates the near homogenous texture of soil samples. The result indicates that not only the field geophysical results are reliable, but the high polarization is not caused by the metal content in the soil.

Abnormal high chargeability in the contaminated area: The polarization effect in the leachate seepage area presented in Fig. 2b is much higher than the ones usually observed in landfill studies. We think that the steel sheet pile near Line A controls the increased polarization response. Whereas two distinguishable anomalies with relatively low chargeability zones can be seen, which coincide and further refine the high conductivity zones in Fig. 2a.
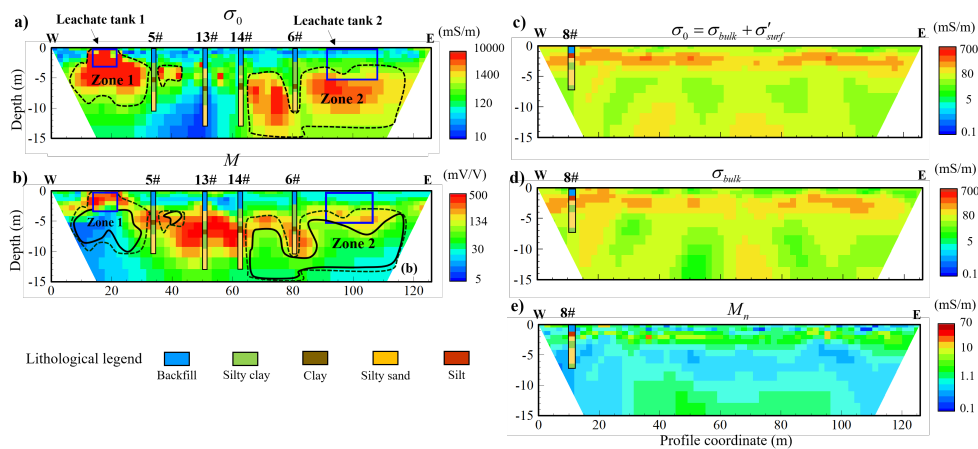
Figure 2. Inverted profiles of Lines A and C with superposed geological reference data. Line A: (a) Conductivity. (b) Chargeability. The dashed lines and black solid lines represent the conductivity above 600 mS/m and chargeability below 100 mV/V at the same time. Line C: (c)-(e) is the DC conductivity, bulk conductivity and normalized chargeability sections, respectively.

Note that the distance between Line A and the steel sheet pile was about 2 m. The measured data can be affected by the 3D spatial formation surrounding the inverted profile. The results illustrate that the general high IP response in the landfill is due to the presence of steel sheet pile, but the high salinity of leachate seepage decreases the polarization effect.
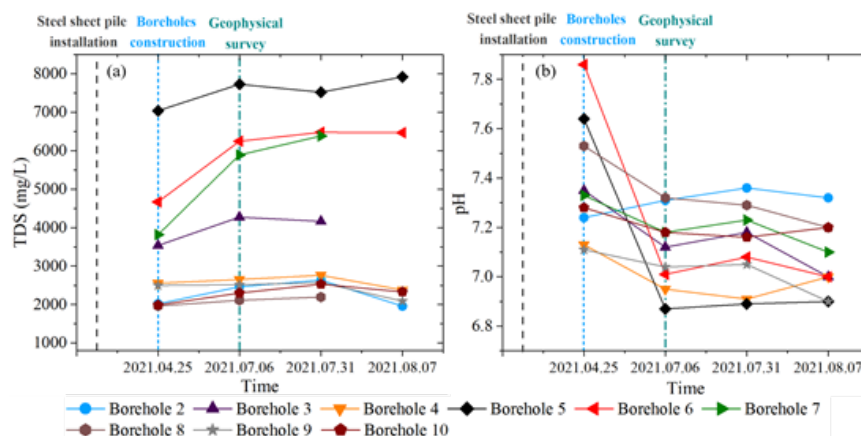
Figure 3. The temporal variation of TDS (a) and pH (b) in borehole water samples. It is suggested that the source of leachate plume may have been caused by leachate tanks spill.

Variations of chemical parameters from leachate plume: As shown in Fig. 3, the gentle variation after July illustrate that the steel sheet piles block the local groundwater flow, which reduces the rate of ionic advection.

Source location of leachate seepage: IP images provide a more accurate spatial delineation of leachate geometry than investigations performed by borehole drilling and chemical sampling, while hydrochemical analysis illustrates that the variations of leachate plume and validates geophysical results.
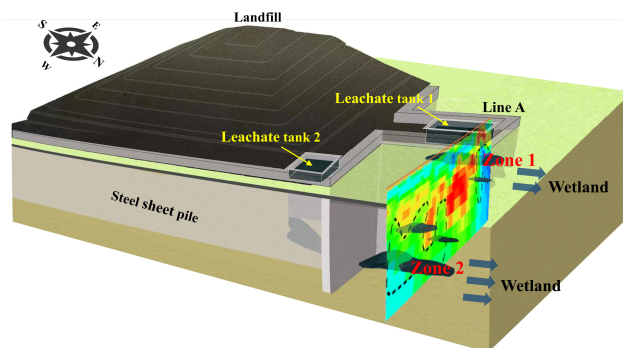
Figure. 4 Illustration of the inferred leachate seepage source. The leachate tanks 1 and 2 are the potential source of contamination.

Conclusions. The integration of hydrochemical and IP analysis for leachate localization in this study was designed to accurately capture the contaminant distribution at a municipal landfill, where the number of water-sample points is often limited compared to the extension of the control plane. The abnormal high polarization background was controlled by the presence of steel sheet pile. The leachate plume was depicted as high conductivity and low chargeability zones. Relatively low chargeability values (below 100 mV/V) were observed in the high conductivity (above 600mS/m) areas under the effect of high salinity leachate plume. The combination of chemical and geophysical parameters successfully identified similarities between the distribution of the geophysical imaging and inorganic constituents in groundwater. The gentle variation of major chemical parameters in the groundwater samples indicated that the continuous plume was cut off by the presence of the steel sheet pile. The source location of the leachate was identified from these two leachate tanks by a combination of these two survey methods. Results presented in this study suggest that the integration of induced polarization images and hydrochemical analysis can help to characterize contaminant sources zones in high resolution and thus optimize the formulation of contamination assessment and remediation strategies.

References

Mao, D., Revil, A. & Hinton, J. (2016). Induced polarization response of porous media with metallic particles — Part 4: Detection of metallic and nonmetallic targets in time-domain induced polarization tomography. Geophysics, 81(4), D359-D375. http://doi.org/10.1190/geo2015-0480.1.

Joyce, R.A., Danney, R.G., Werkema, D.D., Atekwana, E.A. (2012). Spectral induced polarization response to nanoparticles in a saturated sand matrix. Journal of Applied Geophysics, 77, 63-71. https://doi.org/10.1016/j.jappgeo.2011.11.009.

Fiandaca, G., Ramm, J., Binley, A., Gazoty, A., Christiansen, A. & Auken, E. (2013). Resolving spectral information from time domain induced polarization data through 2-D inversion. Geophysical Journal International, 192(2), 631-646. http://doi.org/10.1093/gji/ggs060.

O18 - Ice and Fire: IP-based temperature imaging in extreme environments

A.Revil[1], P-A. Duvillard[2,3], P. Vaudelet[3], and M. Gresse[4]

(1) Univ. Grenoble Alpes, Univ. Savoie Mont-Blanc, CNRS, UMR CNRS 5204, EDYTEM, 73370 Le Bourget du Lac, France
(2) STYX 4D, Le Bourget-du-Lac, France
(3) NAGA Geophysics, Le Bourget-du-Lac, France
(4) Earthquake Research Institute, The University of Tokyo, Tokyo, Japan

Presenter: André Revil (andre.revil@univ-smb.fr) **Student y/n:** No
Web page: NA   **Preferred presentation oral/poster:** Oral

Abstract. Induced polarization is a non-intrusive geophysical method that can be used to image both the electrical conductivity .of rocks and sediments. In volcanoes and geothermal systems, induced polarization derived parameters (electrical conductivity and normalized chargeability) are very sensitive to the presence of clays minerals (especially smectite) resulting from the alteration of the rocks. The production of smectite (the clay mineral with the highest cation exchange capacity) dominates both the conductivity of the rock and the normalized chargeability (in absence of magnetite and pyrite). We show how induced polarization can be used to image temperature in the smectite stability zone (up to 220°C). Similarly, we show that induced polarization can be used to estimate temperature in permafrost. A case study is used to show that temperature can be imaged in a perlmafrost-affected ridge. The reason is that the production of ice in a rock or a sediment is a temperature-affected process depending on the pore size distribution of the material. Temperature can be imaged from the freezing temperature (typically between -2°C to 0°C) down to -20°C.

Introduction

Induced polarization is a geophysical technique developed initially by Conrad Schlumberger a bit more than one hundred years ago (Schlumberger, 1920). In addition to conduct electricity, the Earth materials can store reversibly electrical charges under a low-frequency electrical field. The underlying physics of induced polarization is nowadays well-established and mechanistic models can be used to determine the induced polarization properties of Earth-materials in presence of absence of metallic particles (Revil et al., 2021). In absence of metallic particles, the dynamic Stern layer (DSL) model has been able to explain the vast amount of available data in a very simple way (Revil et al., 2021). This model is simple enough to be application to interpret field data. The DSL model is here used to decipher the role of smectite in controlling the induced polarization properties in volcanic rocks. Similarly, the DSL model can be applied to understand the effect of freeze and thaw on the electrical conductivity and normalized chargeability of a porous material. Field cases are investigated in this presentation.

Research work

Revil et al. (2021), we have recently demonstrated that induced polarization provides an unique opportunity ti image the temperature field of volcanoes. Kilauea is used as a test site. It is an active shield volcano located in Hawai'i (USA). An induced polarization survey was performed in 2015 at the scale of the caldera with a 2.5 km cable with 64 electrodes and a spacing of 40 m between the electrodes. A total of 6210 measurements were performed. The apparent chargeability data were inverted using a least square technique to obtain a chargeability tomogram. The normalized chargeability tomogram is obtained by multiplying cell-by-cell the chargeability by the conductivity. Once the conductivity and normalized chargeability tomograms are obtained, they are jointly

48

interpreted using a dynamic Stern layer conduction/polarization model, which explains the low-frequency polarization spectra of volcanic rocks. This conductivity/polarization model is tested here on new laboratory experiments performed on 24 samples from a drill-hole located on the Kilauea East Rift Zone (Hole SOH-2). We show that for Kilauea, the ratio between the normalized chargeability and the conductivity is equal to a dimensionless number $R = 0.10\pm0.02$ proving that the conductivity and the normalized chargeability are both controlled by the alteration products of the volcanic rocks with a minor role of magnetite except close to the ground surface. In turn, the degree of alteration is controlled by temperature and therefore normalized chargeability and electrical conductivity can both be used as a non-intrusive temperature sensor. This approach is then applied to the field data and temperature tomograms can be produced from the electrical conductivity and normalized chargeability tomograms (Figure 1).
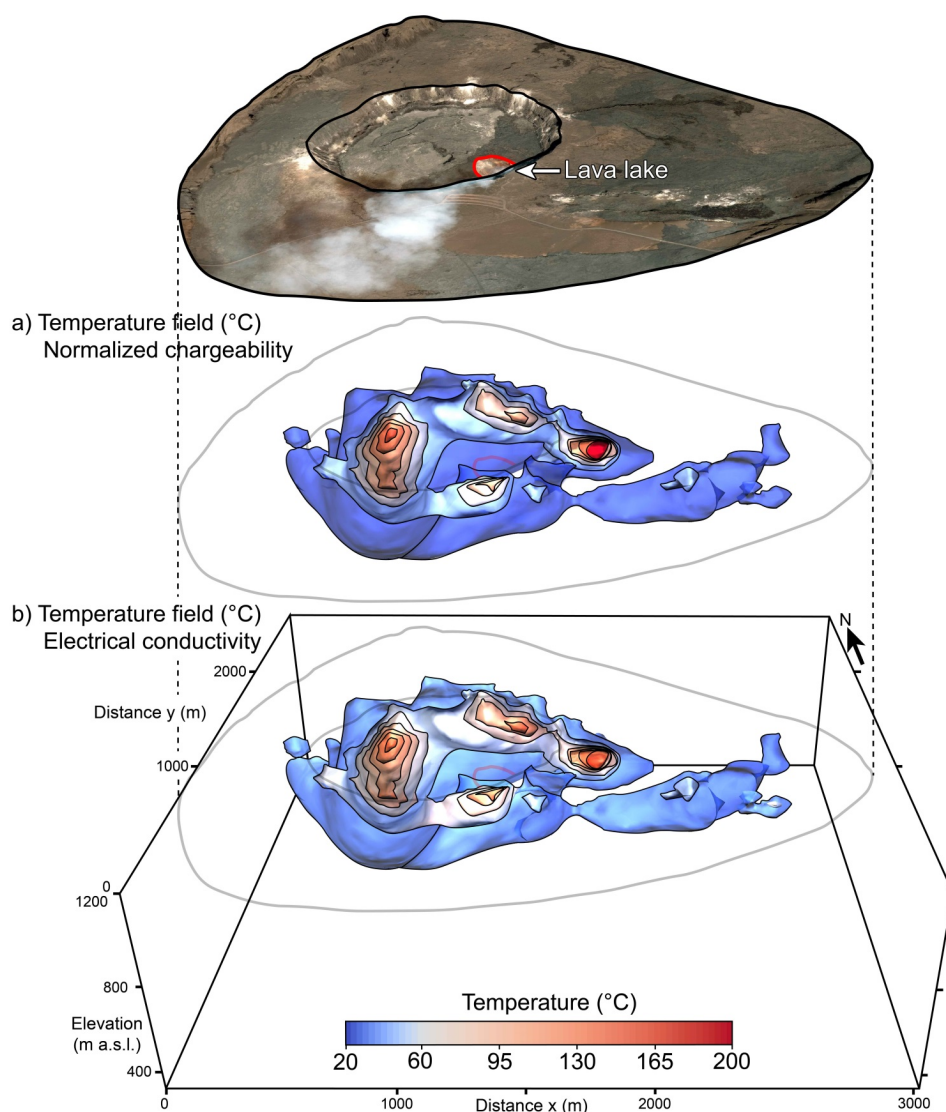
Figure 1. Temperature distribution from the conductivity and induced polarization methods. **a.** Result from the conductivity distribution. **b.** Result from the normalized chargeability distribution (from Revil et al. 2021).

In a similar way, we have demonstrated in Duvillard et al. (2021) that induced polarization can be used to track temperature in permafrost. Since, the knowledge of the thermal state of steep alpine rock faces is crucial to assess potential geohazards associated with the degradation of

permafrost, this approach is highly welcome for risk assessment. Temperature measurements at the rock surface or in boreholes are however expensive, invasive, and provide spatially-limited information. Electrical conductivity and induced polarization tomography can detect permafrost. We test here a recently developed petrophysical model based on the use of an exponential freezing curve applied to both electrical conductivity and normalized chargeability to infer the distribution of temperature below the freezing temperature. We then apply this approach to obtain the temperature distribution from electrical conductivity and normalized chargeability field data obtained across a profile extending from the SE to NW faces of the lower Cosmiques ridge (Mont Blanc massif, Western European Alps, 3613 m a.s.l., France). The geophysical datasets were acquired both in 2016 and 2019. The results indicate that the only NW face of the rock ridge is frozen. To evaluate our results, we model the bedrock temperature across this rock ridge using CryoGRID2, a 1D MATLAB diffusive transient thermal model and surface temperature time series. The modelled temperature profile confirms the presence of permafrost in a way that is consistent with that obtained from the geophysical data. Our study offers a promising low-cost approach to monitor temperature distribution in Alpine rock walls and ridges in response to climate change.
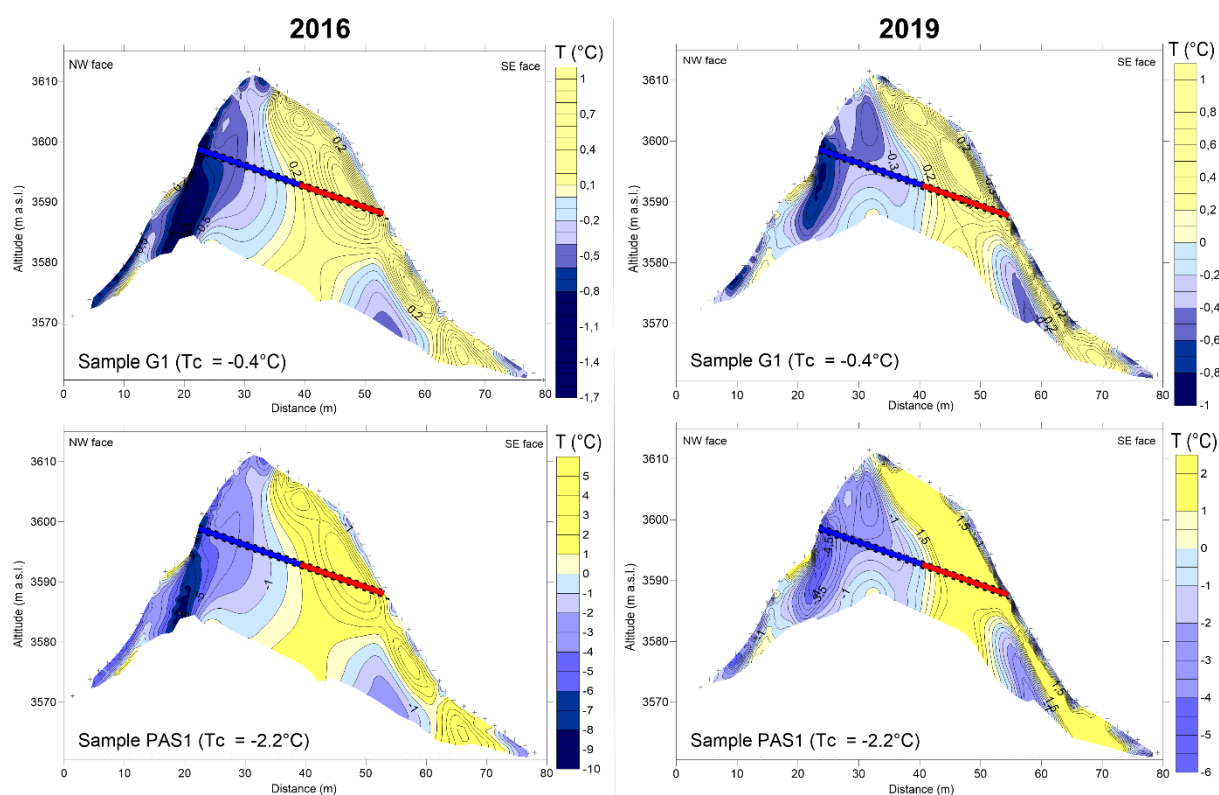
Figure 2. Distribution of the temperature for the 2016 and 2019 tomograms. The blue portion of the profiles denotes the frozen section while the red portion indicates the zone above the freezing temperature. Geophysical predictions agree with numerical modeling (from Duvillard et al., 2021).

Conclusions

In both volcanoes and permafrost, induced polarization can be used to obtain temperature tomograms. In active volcanoes, the effect of the temperature on the conductivity and normalized chargeability depends on the degree of alteration and the production of smectite, which is characterized by high cation exchange capacity. In permafrost, the effect of temperature is related to the change in water content below the freezing temperature. Data fusion will be the next step in

creating temperature tomograms that are meaningful in terms of underlying physics in the context of Bayesian Model averaging.

References

Duvillard, P.A., F. Magnin, A. Revil, A. Legay, L. Ravanel, F. Abdulsamad, and A. Coperey, 2021. Determining 2D temperature distribution in a permafrost-affected rock ridge from electrical conductivity tomography, Geophysical Journal. International, 225, 1207–1221, doi: 10.1093/gji/ggaa597.

Revil A., Y. Qi, A. Ghorbani, M. Gresse, and D.M. Thomas, 2021, Induced polarization of volcanic rocks. 5. Imaging the temperature field of shield volcanoes, Geophys. J. Int., 225, 1492–1509, doi: 10.1093/gji/ggab039.

Schlumberger, C. Etude sur la Prospection Electrique du Sous-Sol, Gauthier-Villars, Paris. The Second Edition without Modification Is Available at https://gallica.bnf.fr/ark:/12148/bpt6k64569898.texteImage. English Version, Translated by Sherwin F. Kelly: "Study of Underground Electrical Prospection". Available online: https://archive.org/details/studyofundergrou00schlrich/page/n37 (accessed on 24 April 2022).

O19 - A novel model for describing the electrical conductivity of saturated frozen porous media

H.L. Luo, D. Jougnot, and A. Jost

Sorbonne Université, CNRS, EPHE, METIS, F-75005 Paris, France

Presenter: H.L. Luo (haoliang.luo@sorbonne-universite.fr) Student **y/n:** y.

Web page: **Preferred presentation oral/poster:** oral

Abstract. Liquid water is a key component in frozen porous media that controls the moisture and solution migration, thus accurate determination and monitoring of the unfrozen water content are crucial in studying the frost-heave and thaw-weakening problems in cold regions. Electrical and electromagnetic methods are increasingly used to cover a larger range of application in cold regions and electrical conductivity is a physical properties that is not only related to the bulk characteristics such as the water content, the types and the concentration of the electrolytes, but also is linked with the surface characteristics of solid surface-water and bulk ice-water interfaces. In this study, we derive a novel physically-based model for electrical conductivity of saturated frozen porous media with different pore size distribution (lognormal and fractal PSDs) by upscaling a microstructural description and considering Gibbs-Thomson effect. Then, we analyze the model sensitivity with various model parameters and compare the lognormal and fractal pore size distribution models by calculating the values of the electrical conductivity of the pore water and the specific surface conductance of the solid surface-water and the bulk ice-water interfaces based on the surface complexation models (figure 1). In addition, we measure the electrical conductivity and unfrozen water saturation for different types of soils and different salt concentration based on laboratory LCR digital bridge and nuclear magnetic resonance (NMR), and accuracy of the proposed model is verified based on experimental data (figure 2). We observe that the proposed model successfully predicts the experimental data of electrical conductivity versus temperature for different samples from experiments that part of this work and published data. Furthermore, we consider the effect of bulk and surface conductivities in the proposed model. The surface conductivity decreases when the grain diameter increases and it is also sensitive to the cation exchange capacity (CEC). Finally, from the proposed model, we obtain an expression for the effective formation factor that is explicitly linked with porosity, tortuosity and unfrozen water saturation, and this expression for effective formation factor is then well validated by published data. The new physically-based model for electrical conductivity opens up new possibilities to characterize the distribution and dynamic of liquid water with geoelectrical and electromagnetic techniques in frozen environments. Among the future developments of this physically-based approach, we plan to investigate the complex conductivity of frozen porous media.
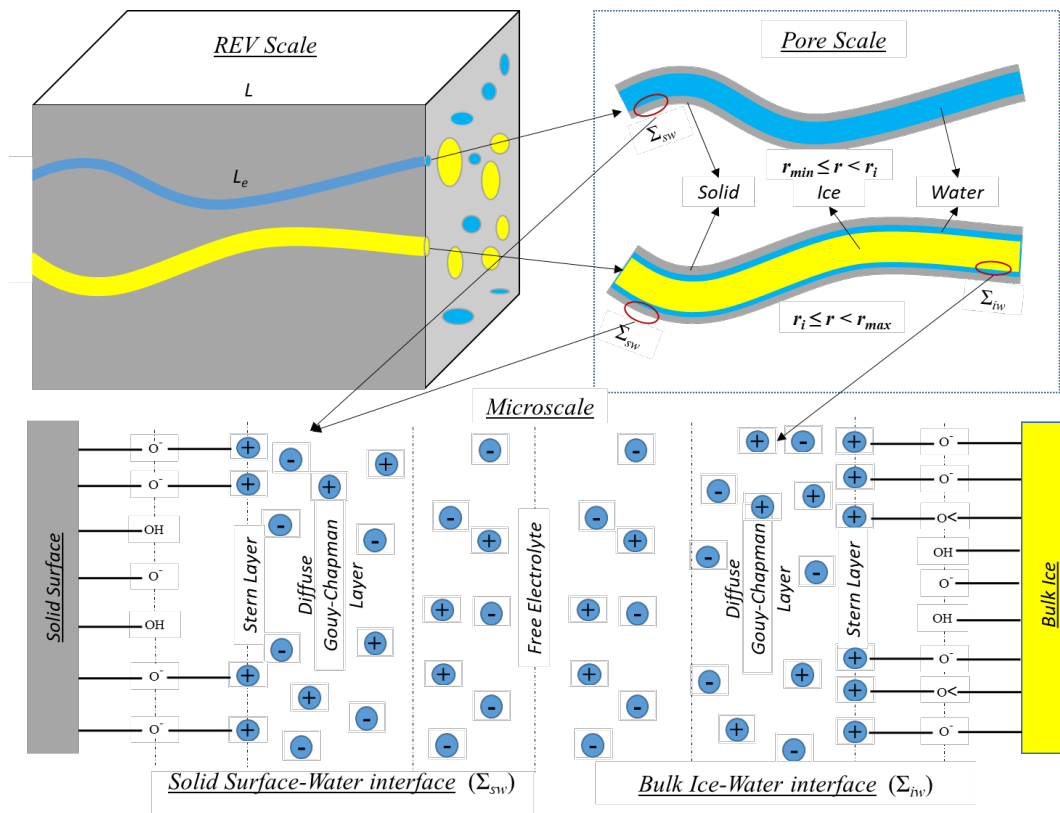
Figure 1. The electrical conductivity model is composed of a large number of capillary tubes at the cylindrical REV scale. All the capillaries have the same tortuous length L_e (m) and their radii follow a lognormal distribution or a fractal distribution. In accordance with the Gibbs-Thomson effect, at a given temperature, the capillary is either filled by water or by ice-water film depending on its radius (pore scale). Scheme of the electrical double layer at the solid surface in contact with water or at the bulk ice-water interface (microscale) for a given capillary radius -r.

References

Coperey, A., Revil, A., Abdulsamad, F., Stutz, B., Duvillard, P. A., Ravanel, L. (2019). Low-frequency induced polarization of porous media undergoing freezing: Preliminary observations and modeling. Journal of Geophysical Research: Solid Earth, 124(5), 4523–4544.

Thanh, L. D., Jougnot, D., Van Do, P., A, N. V. N., Tuyen, V. P., Ca, N. X., Hien, N. T. (2020). A physically based model for the electrical conductivity of partially saturated porous media. Geophysical Journal International, 223(2), 993–1006. https://doi.org/10.1093/gji/ggaa307.

Jougnot, D., Mendieta, A., Leroy, P., Maineult, A. (2019). Exploring the effect of the pore size distribution on the streaming potential generation in saturated porous media, insight from pore network simulations. Journal of Geophysical Research: Solid Earth, 124(6), 5315–5335.
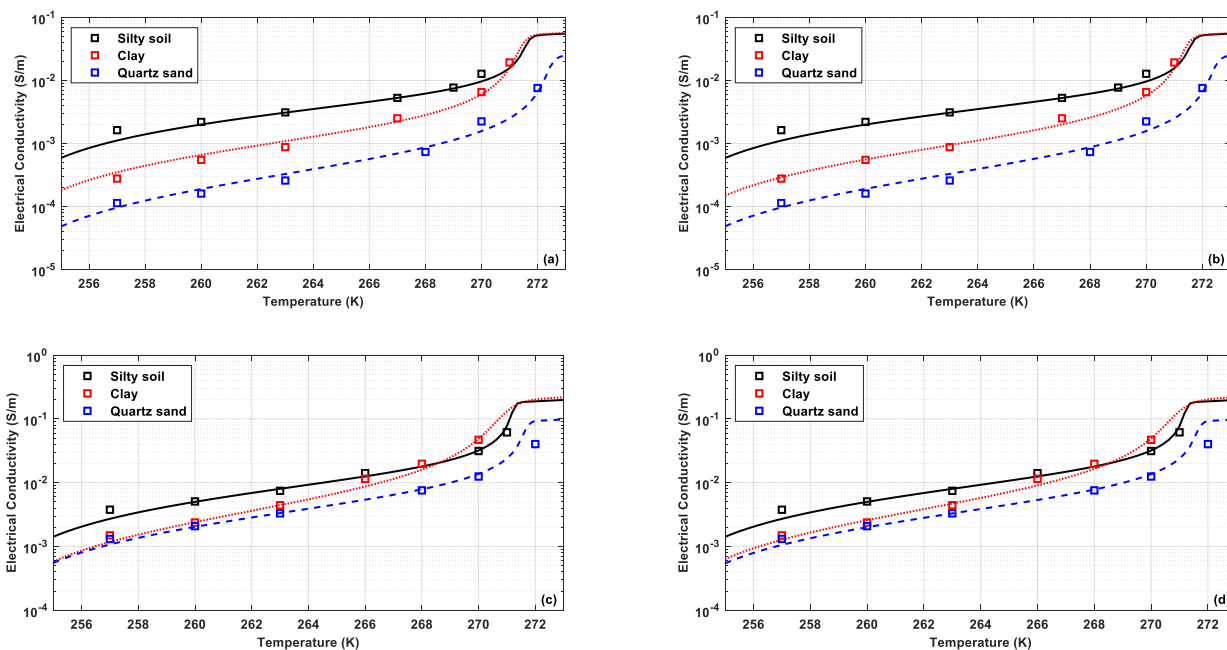
Figure 2. Electrical conductivity σ as a function of temperature for three soil samples, as measured in our experiments (symbols) and predicted by the lognormal and fractal PSDs models (solid lines). (a) Lognormal distribution, initial concentration 0.046 mol/L; (b) Fractal distribution, initial concentration 0.046 mol/ L; (c) Lognormal distribution, initial concentration 0.180 mol/L; (d) Fractal distribution, initial concentration 0.180 mol/ L.

O20 - Complex conductivity of kimberlite

K. Titov[1], V. Abramov[1], V. Emelianov[1], A. Revil[2],

(1) Saint-Petersburg State University, Institute of Earth Sciences, 7-9 Universitetskaya naberezhnaya, 199034 St. Petersburg, Russia
(2) Univ. Grenoble Alpes, Univ. Savoie Mont-Blanc, CNRS, UMR CNRS 5204, EDYTEM, 73370 Le Bourget du Lac, France

Presenter: K. Titov (k.titov@spbu.ru) **Student y/n:** No
Web page: NA   **Preferred presentation oral/poster:** Oral

Abstract. In this paper, we study the complex conductivity and surface conductivity of kimberlite. Six samples of different facies were taken within Alto Cuilo field in Angola: two hard (porphyric) kimberlites, three kimberlite breccia and one tuff-sandstone with kimberlite material. We also measured the specific surface area and the cation exchange capacity. Based on multi-salinity complex electrical conductivity measurements we obtained the formation factor and the real part of the surface conductivity. We found medium – to – high values of the imaginary conductivity (Induced Polarization, IP) especially for the breccia samples. All studied samples contain ore minerals in minor quantity, so the IP effect can be attributed to both ore mineral or clayey matrix. We found a good correlation between the cation exchange capacity and both the quadrature conductivity and the real surface conductivity, which proves that the IP effect is related to the clayey matrix. We also found a satisfactory correlation between the imaginary conductivity and the surface conductivity. The respective slope (0.015) is typical of clayey sandstones. Considering also the surface conductivity values in the range from 0.013 to 0.16 S/m, we state that the values of electrical properties of the kimberlite are typical rater of soils or clayey sandstones than of ingenious rocks.

Introduction. Magnetic method is commonly used for kimberlite exploration. However, some pipes exhibit no magnetic response. Moreover magnetic anomalies of the same shape and magnitude are produced by both kimberlite and non-kimberlite bodies. This is why, last decades, electrical methods are increasingly applied for kimberlite exploration (e.g., Macnae, 1995; Cunion, 2009; Kaminski and Viezzoli, 2016). In particular, relatively high DC electrical conductivity values as well as elevated Induced Polarization (IP) chargeability values were detected *in situ*. However only scarce factual base concerning electrical properties of kimberlite is available to date (Zinchuk et. al., 2002; Titov et al., 2021). In this paper, for the first time, we present the complex electrical conductivity of six intact kimberlite samples of different types. We collected the samples of early cretaceous age within Alto-Cuilo deposit (Angola, Cassai shield). We saturated the samples with NaCl solutions with the electrical conductivity ranged from 0.11 to 2.4 S/m, which allowed us to carry out the multi-salinity experiments. In addition, we characterized the samples by the cation exchange capacity (CEC), and specific surface area (SSA, BET method) measurements as well as the optical microscopy study.

Materials and methods. The samples were cylindrical in shape with 4.7 cm in diameter and 3.0-4.9 cm in length. Before measurements, the samples were triple weighted and saturated with NaCl water solution (σ_w = 2.4 S/m) under vacuum. We left the samples in a tank filled with the same brine, which we used for the saturation for several days to achieve an equilibrium between the matrix, the pore water and the water outside the sample. Then we performed the first series of the complex electrical conductivity measurements. Next, we put the samples in the tank containing fresher ambient water and we waited for a next equilibrium state for several weeks. We monitor the water conductivity in the tank upon a moment when it stabilized. From this criterion, we consider that the equilibrium was

achiever. This procedure of a sample "desalinization" takes enormous time, and can be a source of some experimental errors if the equilibrium between the pore water and the tank water was not actually achieved. We measured the amplitude $Z(\omega)$ and phase $\varphi(\omega)$ of the complex impedance with SIP FUCHS III equipment by Radic Research. With the predefined geometrical factor k, we obtained the complex resistivity, $\rho(\omega) = kZ(\omega)$ and the complex conductivity $\sigma(\omega) = 1/\rho(\omega)$. We calculated the real and imaginary parts of the complex conductivity based on the electrical conductivity magnitude and phase: $\sigma' = |\sigma| \cos \varphi$, (1); $\sigma'' = |\sigma| \sin \varphi$. (2). More details about the complex conductivity measurements can be found in e.g., Weller and Slater, (2012) and Revil et al. (2017). In addition, we carried out, the cation exchange capacity (CEC), and specific surface area (SSA, BET method) measurements as well as optical microscopy studies to obtain the mineral composition. We should note that a small amount of ore minerals (magnetite, hematite) which can polarize by metallic particle mechanism was detected in optical microscopy images.

Results. Figure 1 shows the real conductivity of the samples as a function of the pore water conductivity. The linear fit corresponds to Archie's (1942) law taking into account an effect of the surface conductivity, σ_s (see e.g., (Binley and Slater, 2021): $\sigma' = \sigma_w/F + \sigma_s$, (3) where $F = \phi^{-m}$ is the formation factor, ϕ is the porosity, m is the first Archie (cementation) exponent, σ_w is the pore water conductivity, and σ_s is the surface conductivity. Based on Eq. (3), and using the best fit to data, we determined the formation factor and the surface conductivity (Table 1). With known values of the porosity, we also obtained the first Archie exponent.
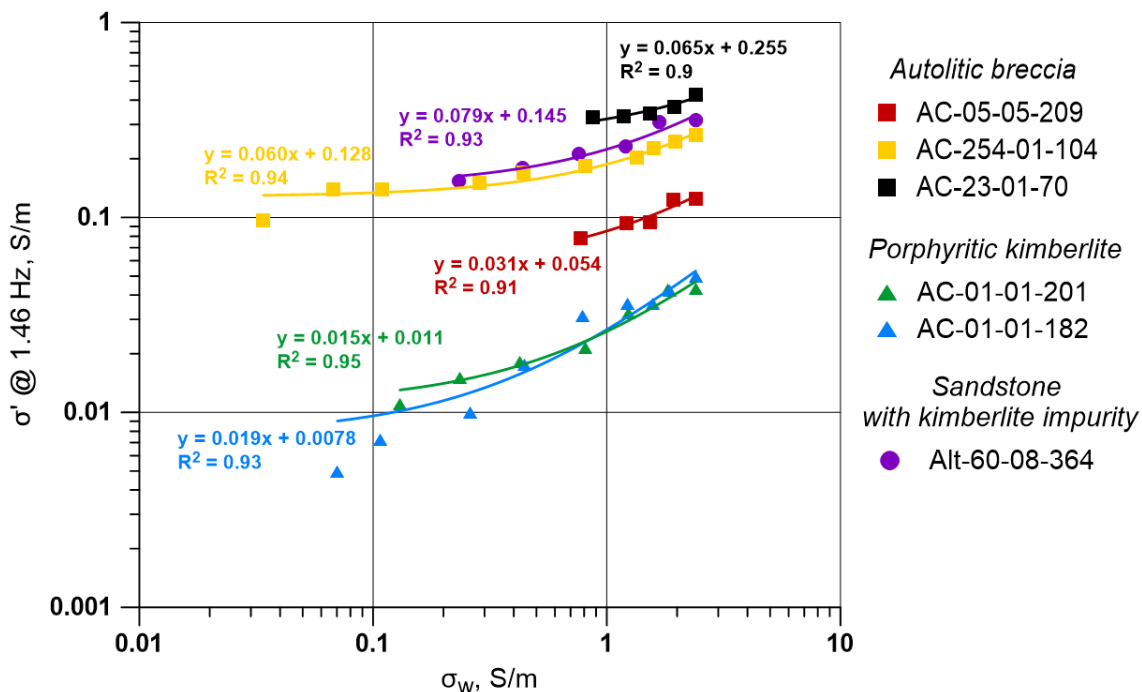
Figure 1 *Real part of the complex conductivity versus pore water conductivity.*

Table 1. Physical properties of the samples.

Sample	Description	ϕ	F	m	σ_s, S/m	σ'', S/m	CEC, meq/100 g	SSA, m^2/g
AC-05-05-209	Autolitic breccia	0.23	15.4	1.85	0.054	5.69E-04	15.41	40.3
AC-254-01-104	Autolitic breccia	0.25	16.8	2.01	0.128	1.11E-03	18.53	17.7
AC-23-01-70	Autolitic breccia	0.18	32.3	2.04	0.255	3.69E-03	66.22	41.7
AC-01-01-182	Porthyritic kimb.	0.22	55.6	2.63	0.008	1.68E-04	7.41	11.7
AC-01-01-201	Porthyritic kimb.	0.13	69.9	2.04	0.011	1.36E-04	6.73	12.9
Alt-60-08-364	Tuffisitic sandstone	0.19	12.6	1.52	0.145	3.57E-03	32.6	25.5

ϕ, F, m are the porosity, formation factor and cementation exponent, respectively; σ_s is the surface conductivity, σ'' is the imaginary part of the complex conductivity (at 1.46 Hz, $\sigma_w \sim 1$ S/m).

Figure 2 illustrates relationships between SSA, σ_s and CEC for the studied samples. Except for one point, the data can be well approximated by linear fits (Fig. 2 a) and linear fits forced to go through the origin (Fig. 2 b). Figure 3a shows a relationship between the imaginary part of the complex conductivity (at 1.46 Hz, $\sigma_w \sim 1$ S/m) and the surface conductivity. This relationship is fairly well approximated by a linear fit forced to go through the origin. Figure 3 b shows imaginary conductivity spectra for the six studied samples. For the autolitic breccias two types of spectra were detected: (i) with monotonous increased values with frequency increase; and (ii) with a more or less pronounced maximum in the frequency range 0.01 to 1 Hz. For the porthyritic kimberlite, we detected a monotonous increase of σ'' with increased frequency. For the tuff-sandstone with kimberlite material, we detected a pronounced maximum.
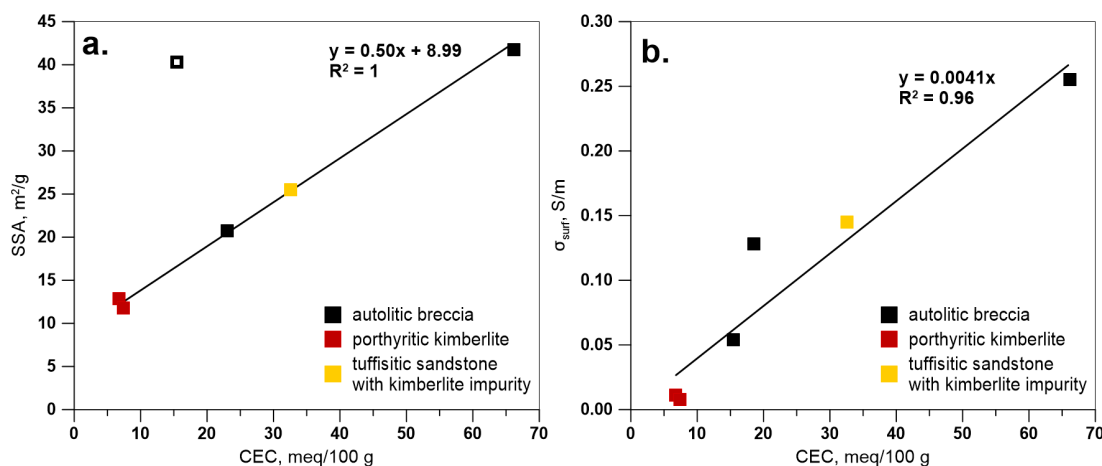
Figure 2 *Specific surface area vs. cation exchange capacity (a), and surface conductivity vs. cation exchange capacity (b). One outliner point was not considered to the data fit in Fig. a.*

Discussion. The origin of so high values of the imaginary conductivity (which expresses the intensity of the IP effect) may be (i) presence of conductive ore minerals (like magnetite) or (ii) some "optimal" content of "sand" and clay material within the rock texture. All samples contain a certain small amount of conductive minerals. Therefore, first, we should identify the nature of the IP mechanism: metallic particles vs. ion-conducting rocks. For the case of the metallic particles, a strong relationship between the relaxation time (and the peak position in the phase spectra) and the water salinity is typical (see e.g., Gurin et al., 2015). Because we did not detect such behavior (not seen for the sake of brevity), we believe that the IP effect in the studied kimberlites is produced by the polarization of the Stern layer (e.g., Leroy et al., 2008) or the membrane (e.g., Titov et al., 2002) polarization. In addition, we found that the strong variations of the surface conductivity are

determined by the variations of both the cation exchange capacity and the specific surface (Fig. 2b), which also confirms our hypothesis. Electrical behavior of the studied samples (the values of the surface conductivity and of the formation factor (Table 1)) is typical of sandstones rather than of igneous rocks. For sandstone with different clay content a theoretical parameter, $l = \sigma''/\sigma'_s$, was defined to obtain a link between the polarization and the surface conduction (Revil et al. 2017; Weller et al. 2013). By plotting σ'' vs. σ'_s (Fig. 3 a) we obtained the slope of $1.5 \cdot 10^{-2}$, which is of the same order of magnitude than that obtained with a sandstone collection ($1.5 \cdot 10^{-2}$ (Weller et al., 2013)). This relationship presents another proof about an anomalous behavior of the studied kimberlites comparing common ingenious rocks and the proximity of their electrical properties to those of clayey sandstones.
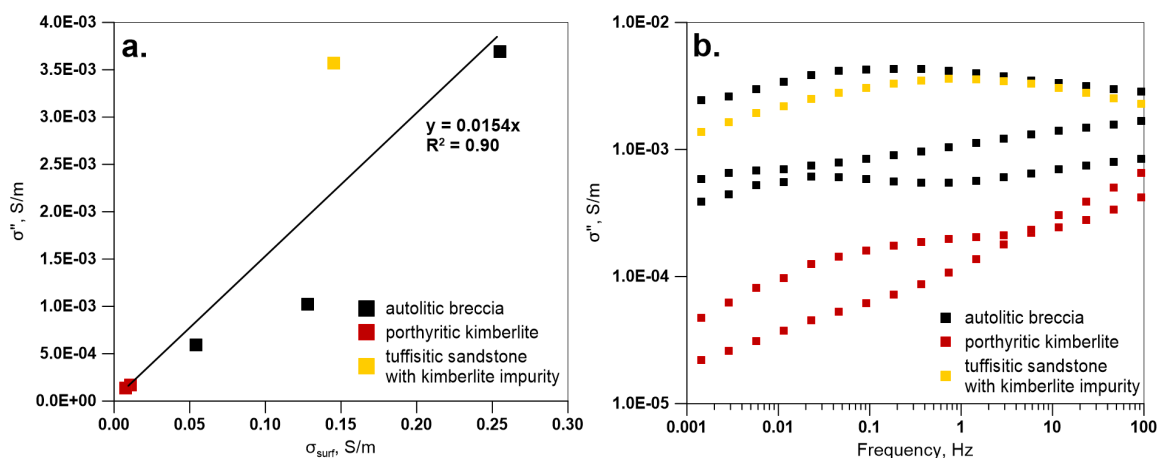
Figure 3 *Imaginary conductivity (at the water conductivity of about 1 S/m) vs. surface conductivity from multi-salinity measurements (a); Imaginary conductivity spectra at water conductivity about 1 S/m (b).*

Conclusions. Significantly different electrical properties characterize different types of kimberlites. The highest values of the formation factor and the lowest values of the surface conductivity correspond to porphyritic kimberlites. Other samples of our collection present large surface conductivity and IP effects. We hope this fact can attract practitioners dealing with kimberlite exploration. Regarding our collection, the nature of IP is not associated with inclusions of conductive ore minerals. The intensity of surface conductivity and polarization are determined by the specific surface area and cation exchange capacity, which is typical of sandstones with various clay content.

References

Binley A. and Slater L. [2021]. *Resistivity and Induced Polarization: Theory and Applications to the Near-Surface Earth*. Cambridge: Cambridge University Press. doi:10.1017/9781108685955

Cunion E. [2009]. Comparison of ground TEM and VTEM responses over kimberlites in the Kalahari of Botswana. *Exploration Geophysics*, **40**(4), 308-319.

Kaminski V. and Viezzoli A. [2016]. Airborne IP: examples from the Mount Milligan deposit, Canada, and the Amakinskaya kimberlite pipe, Russia. *Exploration Geophysics*. **47**(4), 269-278.

Leroy P, Revul A., Kemna A., Cosenza P., and Ghorbani A. [2008] Complex conductivity of water-saturated packs of glass beads. *Journal of Colloid and Interface Science* **321** 103–117.

Macnae J. [1995] Applications of geophysics for the detection and exploration of kimberlites and lamproites. *J. Geochemical Explor.*, 53, 213-243.

Revil A., et al. [2017] Complex conductivity of soils. *Water Resour. Res.*, 53, 7121-7147.

Titov K., Emelianov V., Abramov V., and Revil A. [2021] Complex electrical conductivity of kimberlite. Conference Proceedings, Near Surface Geophysics 2021, 27th European Meeting of Environmental and Engineering Geophysics, Aug 2021, Volume 2021, p.1 - 5.

Titov K., Komarov V., Tarasov V., and Levitski A. [2002] Theoretical and experimental study of time domain-induced polarization in water-saturated sands. *Journal of Applied Geophysics*, 2002, 50(4), 417–433. doi:10.1016/s0926-9851(02)00168-4

Weller A. and Slater L. [2012]. Salinity dependence of complex conductivity of unconsolidated and consolidated materials: comparisons with electrical double layer models. *Geophysics* 77, 185-198.

Weller A., Slater L. and Nordsiek S. [2013]. On the relationship between induced polarization and surface conductivity: implications for petrophysical interpretation of electrical measurements. *Geophysics* 78, 315-325.

Zinchuk N., Bondarenko A. and Garat M. [2002]. *Petrophysics of kimberlites and host rocks*. Moscow: OOO «Nedra-Biznescenter» (In Russian)

O21 - Induced polarization signals and petrophysical relationships

A. Weller

Technische Universität Clausthal, Institut für Geophysik, 38678 Clausthal-Zellerfeld, Germany

Presenter: A. Weller (andreas.weller@tu-clausthal.de) **Student y/n:** No

Web Page: NA **Preferred presentation oral/poster:** oral

Abstract. The talk summarizes the results of more than five decades of petrophysical research work related to the electrical properties of rocks. Starting in the 1970s, the Clausthal petrophysics group has proposed valuable relationships that link electrical properties to the permeability of reservoir rocks. Permeability is a geometric quantity that is related to porosity and effective pore radius or the specific surface area per unit pore volume (S_{por}). The fractal nature of the latter quantity has been integrated into petrophysical models. The geometric quantities, which are not easily accessible, should be replaced by measurable parameters. The electrical parameters formation factor (F) and the surface conductivity (σ_{surf}^*), which is a complex quantity, have proved to be the key parameters in models of permeability prediction. The imaginary part (σ'') of σ_{surf}^* is readily determined by a measurement of induced polarization (IP). It can be used as a proxy for S_{por} in models of permeability prediction. Assuming a constant ratio $l = \sigma''/|\sigma_{surf}^*|$, the measured complex conductivity is separated into volume conductivity, which is related to porosity, and surface conductivity that is controlled by the pore size. Following this approach, the ratio l is a valuable quantity for the estimation of F. Considering the comprehensive databases with an increasing number of experimental data, some of the earlier assumptions and models have to be verified. Recent experiments have shown that the ratio l decreases with increasing clay content. Therefore, the assumption of a constant value of l is problematic. The formation factor seems to be the most critical parameter in models of permeability prediction for consolidated rocks. Empirical models suggest higher power law exponents that are not fully explained by theoretical models. The retrospection shows the progress in the understanding of the origin of IP signals and the challenges for further research to establish reliable petrophysical relationships.

O22 - Overview of using conductivity and induced polarization tomography to detect mountain permafrost

P-A. Duvillard[13], A. Revil[2], F. Magnin[2], L. Ravanel[2] and P. Vaudelet[3]

(1) STYX 4D, Le Bourget-du-Lac, France
(2) Univ. Grenoble Alpes, Univ. Savoie Mont-Blanc, CNRS, UMR CNRS 5204, EDYTEM, 73370 Le Bourget du Lac, France
(3) NAGA Geophysics, Le Bourget-du-Lac, France

Presenter: P-A. Duvillard (pierre-allain.duvillard@styx4d.com) **Student y/n:** Yes
Web page: NA   **Preferred presentation oral/poster:** Oral

Abstract. Geoelectric prospecting is a widely used method for detecting and studying permafrost on steep rock wall, rock glaciers and superficial deposit. The electrical resistivity has been recently combined with induced polarization measurements both in the laboratory and in the field. The use of a recently developed petrophysical model allows the conversion of conductivity and normalized chargeability into temperature and water content. This combines method will help to characterise the thermal state and distribution of permafrost. The presentation will be focused on three site (1) detection of permafrost below an infrastructure in high mountain in steep rock wall and (2) superficial deposit (3) and (2) the estimation of ice content in rock glacier.

Research

Knowledge about the thermal state of steep alpine rock faces and of rock glaciers and the ice distribution is crucial to assess potential geohazards associated with the permafrost warming. Temperature measurements at the rock surface or in boreholes are however expensive, invasive, and provide spatially-limited information. Electrical conductivity tomography has been broadly used to detect and monitor mountain permafrost since 30 years on rock walls and rock glaciers (e.g. Mollaret et al., 2019). Recent studies showed the interest of coupling, at several time and scales, methods of electrical conductivity tomography, induced polarization tomography in the field, in parallel with petrophysical characterization of core samples (Figure 1). The aim of the latter is to develop petrophysical transforms between geophysical observables and parameters of interest such as temperature or water content. The advantages of these geophysical methods are their low cost and their non-invasive character. They provide 2D, 3D, and 4D tomograms/images of the subsurface (Duvillard et al., 2018, 2020; Coperey et al., 2019; Revil et al., 2020).

References

Coperey A., Revil A., Abdulsamad F., Stutz B., Duvillard P.A, Ravanel L. (2019) Low frequency induced polarization of porous media undergoing freezing: preliminary observations and modelling. Journal of Geophysical Research, 124. https://doi.org/10.1029/2018JB017015

Duvillard P.A., Revil A., Qi Y., Soueid Ahmed A., Coperey A., Ravanel L. (2018) Three-dimensional electrical conductivity and induced polarization tomography of a rock glacier, Journal of Geophysical Research, 123. https://doi.org/10.1029/2018JB015965

Duvillard P. A., Magnin F., Revil A., Legay A., Ravanel L., Abdulsamad F., & Coperey A., (2020) Temperature distribution in a permafrost-affected rock ridge from conductivity and induced polarization tomography. Geophysical Journal International. https://doi.org/10.1093/gji/ggaa597

Mollaret C., Hilbich C., Pellet C., Flores-Orozco A., Delaloye R., Hauck C. (2019) Mountain permafrost degradation documented through a network of permanent electrical resistivity tomography sites, The Cryosphere, 13, 2557–2578. https://doi.org/10.5194/tc-13-2557-2019

Revil A., Soueid Ahmed A., Coperey A., Ravanel L., Sharma R., Panwar N. (2020) Induced polarization as a tool to characterize shallow landslides. Journal of Hydrology, 589, 125369. https://doi.org/10.1016/j.jhydrol.2020.125369
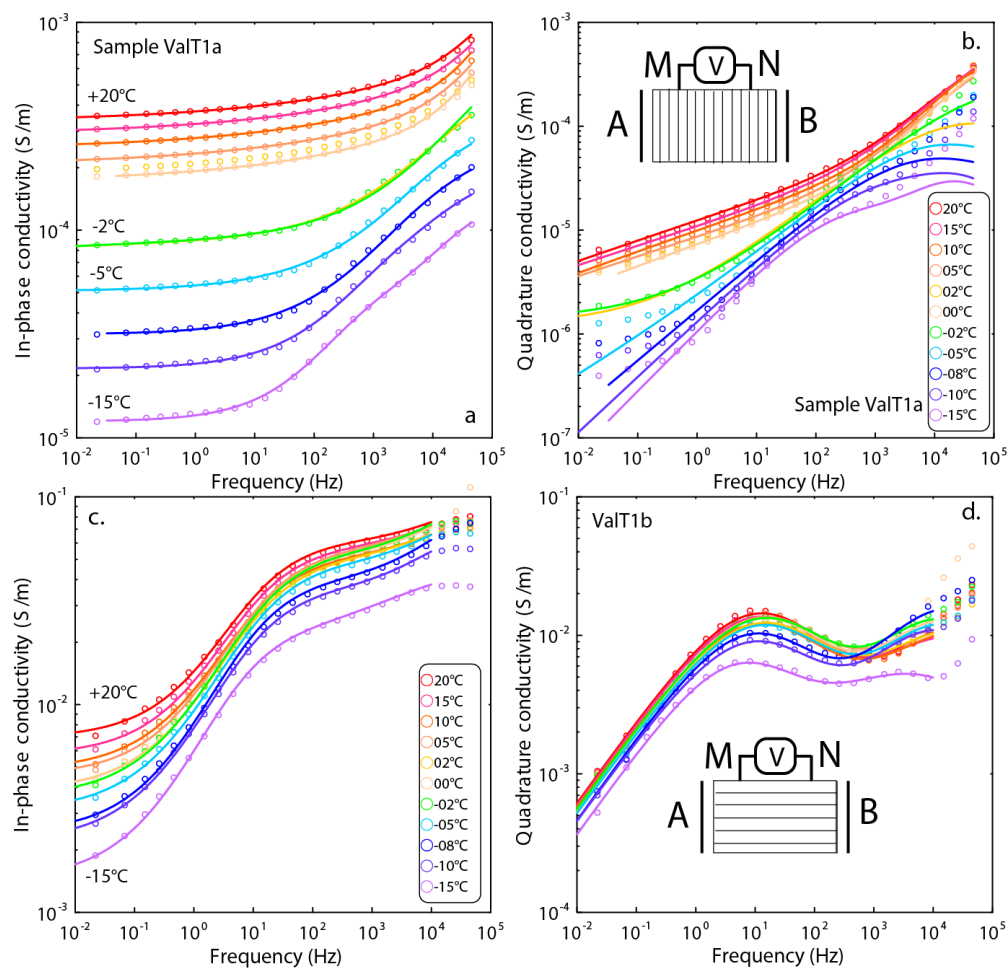
Figure 1. Complex conductivity spectra of sample ValT1. **a.** In-phase conductivity (transverse component). **b.** Quadrature conductivity (transverse component). The phase reaches ~400 mrad at its peak frequency. **c.** In-phase conductivity (in-plane component). **d.** Quadrature conductivity (in-plane component). The phase reaches ~600 mrad at the peak frequency. Only the data with an uncertainty smaller than 1% were considered in the Cole Cole fit of the data.

O23 - Induced Polarization Effects in Electromagnetic data: the Loupe case study

F. Dauti[1], A. Viezzoli[2], and G. Fiandaca[1]

(1) The EEM Team for Hydro & eXploration, Department on Earth Sciences "Ardito Desio", University of Milano, Milano, Italy
(2) EMergo srl, Vicopisano, Italy

Presenter: F. Dauti (francesco.dauti@unimi.it) **Student y/n:** Yes
Web page: NA   **Preferred presentation oral/poster:** Oral

Abstract. It is nowadays accepted, both in industry and in academy, that Induced Polarization (IP) affects electromagnetic (EM) data, when these are collected over a medium characterized by strong IP properties. With this study we want to verify if and how IP effects are detectable also by the new ground-EM system Loupe. The Loupe system is a two-operator walkable transient EM (TEM) profiling system designed to image the electrical properties of the ground with a high lateral and vertical resolution. In order to map the IP effects, we set up a large data space and model space analysis, parametrizing a two-layer synthetic model and calculating thousands of forward responses varying the model's parameters. We thus compare the forward responses affected by IP with the equivalent purely-resistive ones. We find that significant IP effects are present on most models, also with moderate polarization properties.

Introduction

We aim to assess how the new Loupe time-domain electromagnetic system (Street et al., 2018) is sensitive to Induced Polarization (IP) effects. The IP effects on EM data have been studied since the early '80s (e.g. Smith, 1981), and have re-gained attention in recent years thanks to the ability to invert for IP effects on EM data in terms of Cole-Cole models (e.g. Viezzoli et al., 2017). However, the importance of IP modelling in EM data is still often overlooked, and false structures (incorrect conductivity-thickness parameters) may be recovered when IP is not properly modelled (Viezzoli et al. 2017).

Method & results

In order to study the IP effect on the Loupe system, we focused on a simple but representative case: a two-layer model with a chargeable cover over a resistive bedrock. This case may represent targets suitable for the Loupe system: mine wastes; permafrost; weathered covers over bedrock on mountainous areas. The study is performed varying the Cole and Cole parametrization of the cover layer, and its thickness, in order to highlight quantitatively the significance of the IP effect, while the second layer is considered purely resistive. The amount of distortion produced by IP for each forward response is computed as the mean absolute percentage difference over the entire response, as follows:

$$Distortion = \sum_{j=1}^{n} \frac{100}{n} \left\| \frac{fwr_{NOIP_j} - fwr_{IP_j}}{fwr_{NOIP_j}} \right\| \tag{1}$$

Where n represents the number of gates above the noise floor, set to 1e-12 V/Am4 at 1 ms, in order to quantify only detectable IP effects; $fwrNOIPj$ represents the jth gate of the forward response computed disregarding IP; $fwrIPj$ is the jth forward response computed with IP. This difference, expressed as a percentage, is interpreted as the magnitude of the IP effects on a modelled Loupe transient. The metric is calculated only above the noise level, set to 1e-12 V/Am4 at 1 ms, in order to quantify only detectable capacitive effects. After its computation, the metric is displayed in a multi-dimensional plot in order to map the distortion as a function of the values of the model Cole & Cole parameters (Figure 1).
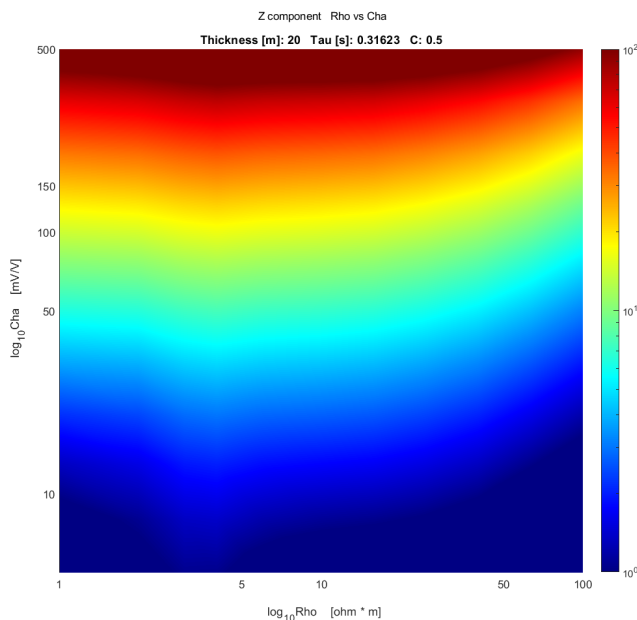
Figure. 1. Representation of the IP distortion (equation 1) for the Loupe Z component for two-layer models. The first layer thickness, Tau and C parameters are kept fixed (values in the title), while Resistivity and Chargeability vary along the axis. The second layer is a purely resistive one. The color-scale represents the distortion, computed following equation 1.

Conclusions. The results presented in this study are surprising: in a two-layer environment with a chargeable cover over a resistive bedrock, even small chargeability values (e.g. 10 mV/V) creates significant effect in the responses measurable with the portable Loupe System, also with detectable data change of sign. Furthermore, these effects are not confined to low values of the time constant of the Cole-Cole model (e.g. below 1 ms), but persist also for tau values in the range of seconds. These results imply that the IP effect cannot be overlooked when operating with the Loupe system, for instance in surveys involving mine wastes, permafrost and weathered covers over bedrock on mountainous areas.

References

Smith R. and West G., 1989, TEM Coincident Loop Negatives and the Loop Effect: Exploration Geophysics, 19, 1235-1251.
Street, G., Duncan, A., Fullagar, P., Tresidder, R., 2018. LOUPE – A Portable EM Profiling System. ASEG Extended Abstracts, 2018:1, 1-3, DOI: 10.1071/ASEG2018abW10_3G.
Viezzoli, A., Kaminski, V., Fiandaca, G., 2017. Modeling induced polarization effects in helicopter TEM data: Synthetic case studies. (82-2) E31-E50 Geophysics.

O24 - Induced polarization as a tool to assess mineral deposits: a review

A.Revil[1], P. Vaudelet[2], Z. Su[3, 4], and R. Chen[5]

(1) Univ. Grenoble Alpes, Univ. Savoie Mont-Blanc, CNRS, UMR CNRS 5204, EDYTEM, 73370 Le Bourget du Lac, France
(2) NAGA Geophysics, Le Bourget-du-Lac, France
(3) State Key Laboratory of Petroleum Resources and Prospecting, China University of Petroleum (Beijing), Beijing, China
(4) Key Laboratory of Submarine Geosciences, Second Institute of Oceanography, MNR, Hangzhou, China
(5) School of Geoscience and Info-Physics, Central South University, Changsha City, Hunan Province, China

Presenter: André Revil (andre.revil@univ-smb.fr) **Student y/n:** No
Web page: NA   **Preferred presentation oral/poster:** Oral

Abstract. Disseminated ores in porous or fractured media can be polarized under the application of an external low frequency electrical field. This polarization is characterized by a dimensionless property called the chargeability. Induced polarization is a non-intrusive geophysical sensing technique that be used in the field to image both the electrical conductivity and the chargeability of porous rocks together with a characteristic relaxation time. A petrophysical model of induced polarization of metallic ores immersed in a porous conductive and polarizable material is reviewed and its predictions are compared to a large dataset of experimental data. The model shows that the chargeability of the material is linearly dependent on the volume fraction of ore and the chargeability of the background material, which can be in turn related to the conductivity of the pore water and the cation exchange capacity of the clay fraction. The relaxation time depends on the grain sizes of the ores and the conductivity of the background material, which is close to the conductivity of the porous rock itself. Five applications of the induced polarization method to ore and metallic bodies are discussed in order to show the usefulness of this technique. These applications include (i) a sandbox experiment in which cubes of pyrite are located in a specific area of the tank, (ii) the tomography of an iron slag at an archeological site in France, (iii) a study of partially frozen graphitic schists in the French Alps, (iv) the detection of a metallic tank through the tomography of the relaxation times, and (v) the detection and localization of a deep ore body associated with a tectonic fault. We also discuss the possibility to combine self-potential and induced polarization tomography to better characterize ore bodies below the seafloor.

Introduction

In this presentation, we will review a simple physics-based model to account for the presence of disseminated metallic particles in a porous material, which can be polarizable (Revil et al., 2018a, b). Numerical simulations performed with the finite element method are used to validate the theory and to get better insights into the underlying physical mechanisms at play and especially to decipher the observed dependence of the relaxation time with the conductivity of the background material (i.e., the material around the metallic grains, see Abdulsamad et al., 2017; 2020). This petrophysical model is compared to experimental data from the literature. Then, we discuss various approaches used to invert the electrical conductivity, the chargeability, and the relaxation time. We briefly discuss five applications of the method to the detection of ores and metallic bodies. Finally, we discuss how induced polarization could complement the self-potential technique recently used to explore sulfide deposits at the seafloor using deep-towed geophysical instruments.

Research work

We will review a physics-based model describing the complex conductivity of porous materials containing disseminated metallic particles embedded in a complex background made of pore water, insulating grains coated by an electrical double layer and bacteria (Figure 1). This model is based on the intrinsic polarization of the metallic grains in which charge carriers accumulate at the boundary of the grains (Figure 2). This model can be applied to characterize metallic deposits using a geophysical technique called induced polarization. The chargeability depends on the volumetric content of metallic particles plus the chargeability of the background material. The relaxation time depends on the square of the radius of the metallic grains and is inversely proportional with respect to the conductivity of the background material, which is weakly dependent on the volume fraction of the metallic particles. The DC conductivity decreases with the increase of the concentration of the metallic particles while the high frequency conductivity increases with the concentration of metallic particles. This statement may appear obvious from the fact that the grains act as conductors at high frequency (absence of polarization) and insulators at low frequency (grains totally polarizes). That said, this point is often forgotten by practitioners of electromagnetic methods when dealing with the dependence of the electrical conductivity with the fraction of metallic particles. In other words, conduction is not just an electromigration problem and cannot be fully understood without its counterpart corresponding to grain polarization. We have not discussed the potential effect of redox reactions at the grain/water interface but such effect would make the metallic grains are leaking capacitors rather than perfect capacitors as described in this presentation.
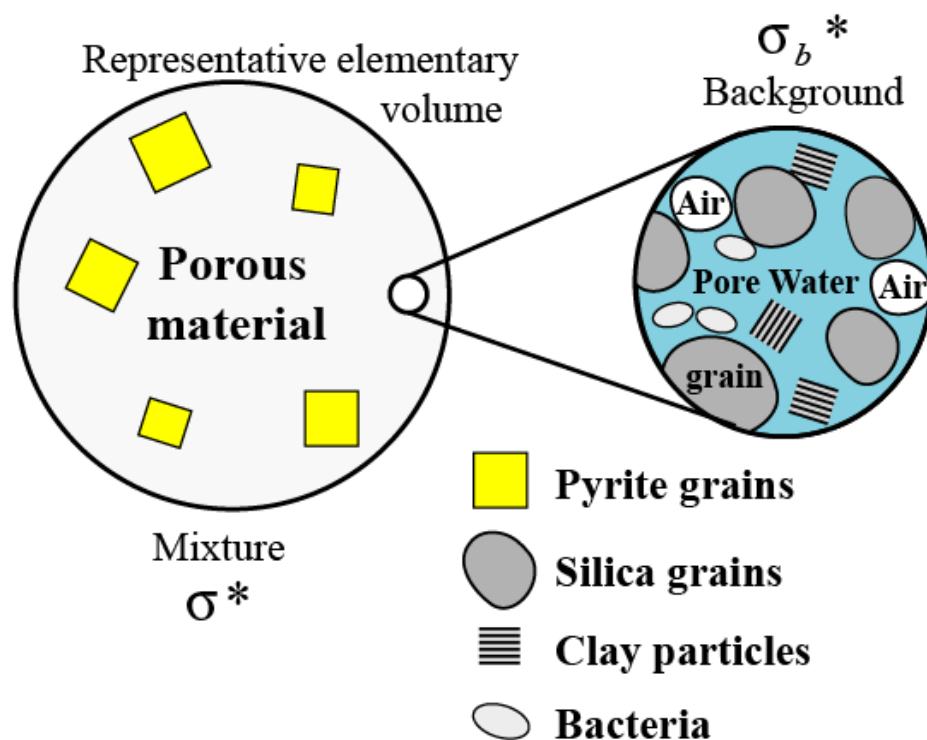
Figure 1. Sketch of the complex background and the mixture between the background and the metallic particles (with metallic grains, for instance pyrite). The background material can be partially saturated (with air as a non-wetting immiscible fluid) at a partial saturation. It can comprise various types of grains. Polarizable bacteria can be present in the pore space. The quantity σ^* and σ_b^* denote the complex conductivity of the mixture and the complex conductivity of the background material around the metallic particles, respectively.

We will discuss 5 applications and tests of the petrophysical model using induced polarization tomography including conductivity, chargeability and relaxation time tomography. Our tests demonstrate that electrical conductivity tomography is not efficient to image disseminated ores. In time-domain induced polarization, the secondary voltage decay can be understood as a transient self-potential problem. The relaxation time tomography is efficient to image massive metallic structures. We also show that the effect of temperature including the effect of permafrost is well-understood (Figure 3) and can used to interpret field data. An exploration case shows that, based on the spread spectrum communication idea and the array SSIP signal acquisition based on ZigBee and GPS timing, high-resolution induced polarization exploration at depths of ~1000 meters even in presence of strong electromagnetic interferences can be realized. Further works will need to be done to perform joint inversion of induced polarization data with self-potential data to further image and localize SMS deposits below the seafloor.
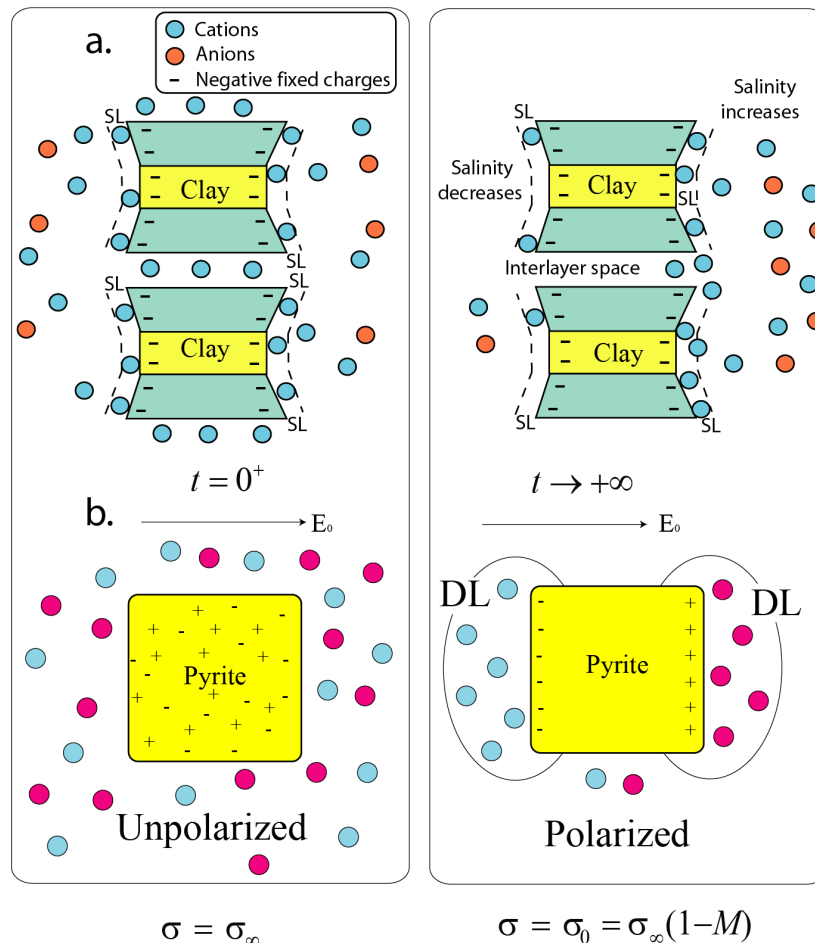
Figure 2. Induced polarization of metallic and non-metallic grains. **a.** Non-metallic grains like clays are characterized by an electrical double layer coating their surface. Under the influence of an external electrical field **E**$_0$, the polarization of this electrical double layer provides a dipole moment to the grain. The main mechanism of polarization is the polarization of the Stern layer (SL), which is the inner part of the electrical double layer. **b.** Polarization of a pyrite cube. The electro-diffusion of the charges carriers inside the grain (electrons and p-holes) polarize the grain providing a dipole moment to the grain. A second polarization component is associated with field induced diffuse layers (DL) in the electrolyte at the solid-liquid interface. The left-hand side figures define the instantaneous (high-frequency) conductivity for the non-metallic and metallic grains while the right-hand side figures

define the DC (Direct Current, low-frequency) conductivity corresponding to a long application of the electrical field.
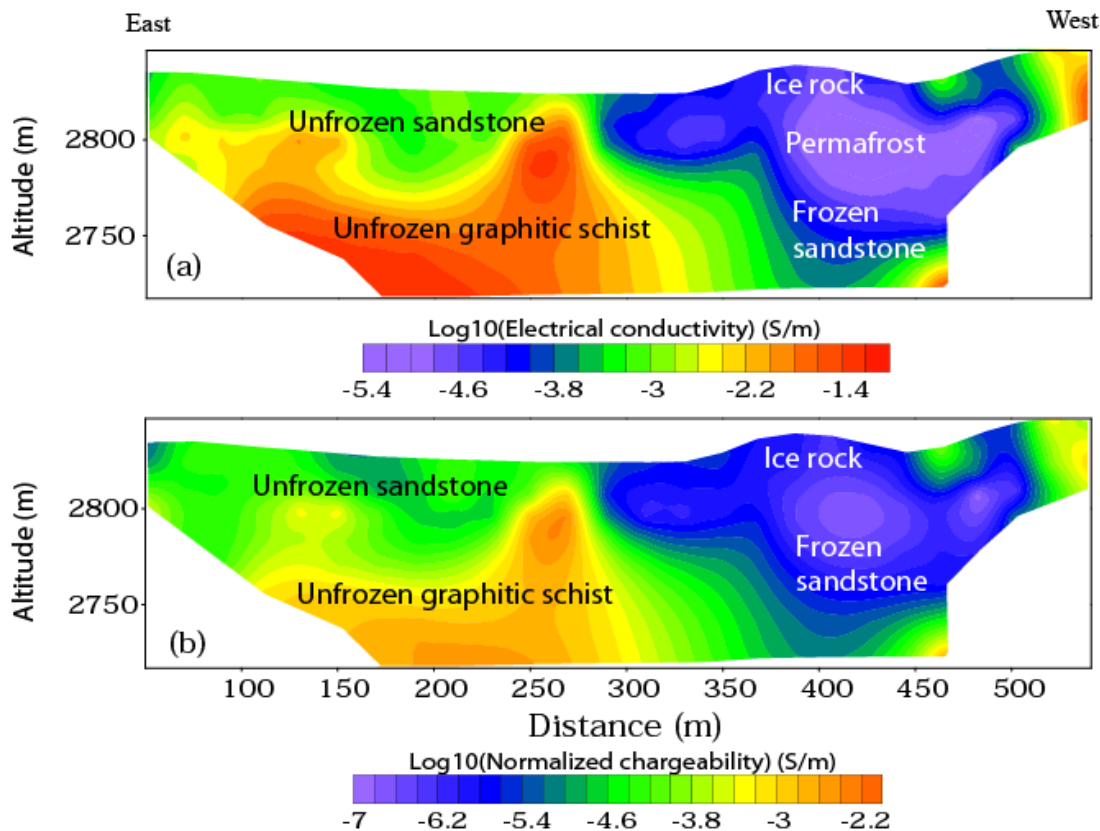
Figure 3. Large-scale electrical conductivity and normalized chargeability tomograms crossing an area associated with a rock glacier and permafrost below it. **a.** Electrical conductivity tomogram showing position and depth of the permafrost (about 70 m). **b.** Normalized chargeability tomogram high normalized chargeability zones correlated with graphitic schist formation. The frozen area is in blue. Modified from Abdulsamad et al. (2020).

References

Abdulsamad, F., N. Florsch, and C. Camerlynck, 2017, Spectral induced polarization in a sandy medium containing semiconductor materials: experimental results and numerical modelling of the polarization mechanism: Near Surface Geophysics, **15**, 669-683, , http://dx.doi.org/10.3997/1873-0604.2017052. Abdulsamad F., A. Revil, A. Ghorbani, V. Toy, M. Kirilova, A. Coperey, P.A. Duvillard, G. Ménard, and L. Ravanel, 2020, Complex conductivity of graphitic schists and sandstones, Journal of Geophysical Research-Solid Earth, **124**, 8223–8249. , http://dx.doi.org/10.1029/2019JB017628.

Revil, A., A. Coperey, D. Mao, F. Abdulsamad, A. Ghorbani, M. Rossi, and D. Gasquet, 2018a, Induced polarization response of porous media with metallic particles – Part 8. Influence of temperature and salinity, Geophysics, **83**, no. 6, 1-22. doi: 10.1190/geo2018-0089.1.Revil A., T. Tartrat, F. Abdulsamad, A. Ghorbani, and A. Coperey, 2018b, Chargeability of porous rocks with or without metallic particles, Petrophysics, **59**, 4, 544-553. https://doi-org.insu.bib.cnrs.fr/10.30632/PJV59V4-2018a8.

O25 - Spread spectrum induced polarization: from concepts to instruments and applications

R. Chen[1], H. Yao[1], R. Shen[1], W. Liu[2], S. Chen[1]

(1) School of Geoscience and Info-Physics, Central South University, Changsha 410083, China
(2) Chinese Academy of Geological Sciences, Beijing, 100037, China

Presenter: R. Chen (chen.rujun@foxmail.com) **Student y/n:** No
Web page: NA   **Preferred presentation oral/poster:** Oral

Abstract. Spectral induced polarization (SIP) may be used to discriminate minerals in ore deposit exploration. However, traditional SIP method is suffered by low efficiency, small depth of exploration, and poor data quality. We developed the spread spectrum induced polarization (SSIP) to attack above problems, and achieved 1000 -1500 m depth of exploration using 5 – 10 kW transmitter. The idea of spread spectrum is widely used in modern communication. We adopted the same idea in spectral induced polarization to realize large depth of exploration. At first, we developed a receiver array which support 1200+ channels in parallel data acquisition. Then, we can receive and transmit m-sequence pseudo-random waveform at the same time. At last, a series of data processing is used to get induced polarization information in several frequencies. Above SSIP instrument is used in China for more than 10 years, and significant ore prospecting breakthroughs including mineral discrimination have been achieved many times.

O26-Investigating Spectral EMI for IP Relaxation Signatures

D.R. Glaser[1,2], B.E. Barrowes[3], F. Shubitidze[2], and L.D. Slater[1]

(1) Earth & Environmental Sciences Department, Rutgers University Newark, 101 Warren St., Newark, NJ 07102 USA
(2) Thayer School of Engineering, Dartmouth College, 15 Thayer Drive, Hanover, NH 03755 USA
(3) US Army ERDC Cold Regions Research & Engineering Laboratory, 72 Lyme Rd., Hanover, NH 03755 USA

Presenter: D.R. Glaser (dan.glaser@rutgers.edu) **Student y/n:** Yes and No
Web page: NA   **Preferred presentation oral/poster:** Oral or Poster

Abstract. Frequency-domain electromagnetic induction (FDEMI) techniques have advanced such that continuous, non-contact spectra can be obtained over the traditional direct contact induced polarization relaxation frequencies. Yet, spectral induced polarization (SIP) signatures of porous media within the FDEMI response remain elusive, likely due to the translation between electrical and magnetic signal in the quasistatic regime. Engineered samples of unconsolidated materials known to have SIP relaxation signatures, including sand-pyrite mixtures were measured using high and low frequency spectral electromagnetic instrumentation. Here we present the preliminary results from the original high-frequency EMI system (HFEMI) and the evolution of the low-frequency system development, as well as, our attempts to obtain SIP results from this new low-frequency EMI instrumentation (LFEMI). Initial results demonstrate reduction in 1/f noise. Effects of electrical conductivity and sample volume and placement relative to the sensing coils are also discussed. Further, we show forward modeled responses of conductive spheres in both the quasi-electrostatic frequency range and the coincident magneto-quasistatic results. Results demonstrate an inverse relationship for frequency dependent conductivity signatures in the electrical and magneto quasi-static responses.

Introduction.

A high-frequency electromagnetic induction system (HFEMI), designed for detection of improvised explosive device (IED) constituent parts was evaluated for detection of spectral relaxation signatures associated with induced polarization mechanisms in soils (Tabbagh et al, 2021; Glaser et. al., 2022). A variety of engineered unconsolidated soil samples known to exhibit induced polarization responses were tested using both the traditional direct contact laboratory systems and this non-contact HFEMI system operating over a range of 1kHz through 20MHz (Placencia-Gómez and Slater, 2016; Revil et al 2017). The HFEMI system was designed to provide reliable signatures above 100kHz, but system settings allowed for lower frequency measurements.

LFEMI System Development

Through our initial experiments with the HFEMI system we identified three improvements to be made to optimize the system for IP relaxation measurements, resulting in our low frequency electromagnetic induction system (LFEMI): 1) frequency range; 2) sample placement; and 3) volume. The measurements obtained below the HFEMI systems design specifications of 100kHz through 20 MHz worked well for high electrical conductivity metallic samples, but the SNR is too low to detect soils which tend to be relatively low conductivity. This low frequency range of 1kHz to 100kHz was primarily comprised of pink noise (1/f), with some white noise. The 1/f noise was instrument specific.

To improve signal to noise (SNR) at lower frequencies, we enlarged the coil diameters and increased the number of wire turns, allowing for a lower frequency range (3 Hz - 1 kHz).

The second consideration was the sample placement relative to the receiver and transmitter coils. As designed the HFEMI system uses a transmitter loop and a receiver loop, with a precise overlap that allows for bucking of the primary field. We found that when samples were placed within the overlap area, the sensitivity of the system was increased by multiple orders of magnitude. As such, the increased diameter of the coils allowed for a greater area within the overlap for optimum placement. Finally, the sample volume also contributed to the frequency dependent response. Larger samples placed within the coil overlap area should result in the greatest signal. Thus, relatively larger samples of higher conductivity give the greatest response, conversely smaller samples of lower conductivity are not sufficient SNR to be detected.

EMI Polarizability Forward Modeling

Forward modeling of a metal sphere response in both the electric field and magnetic field was completed. The responses within the electric field demonstrated a frequency dependent response where increasing conductivity correlated with increasing frequency; however, in the magnetic data, the frequency dependence was inverse, i.e. increased conductivity was observed at lower frequencies.
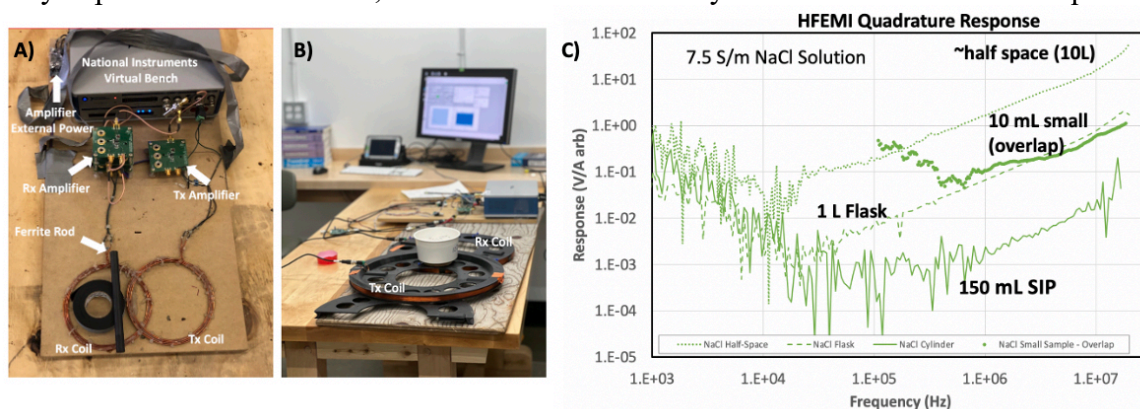
Figure 1. a. HFEMI system, **b.** LFEMI system, and **c.** effects of volume and placement.
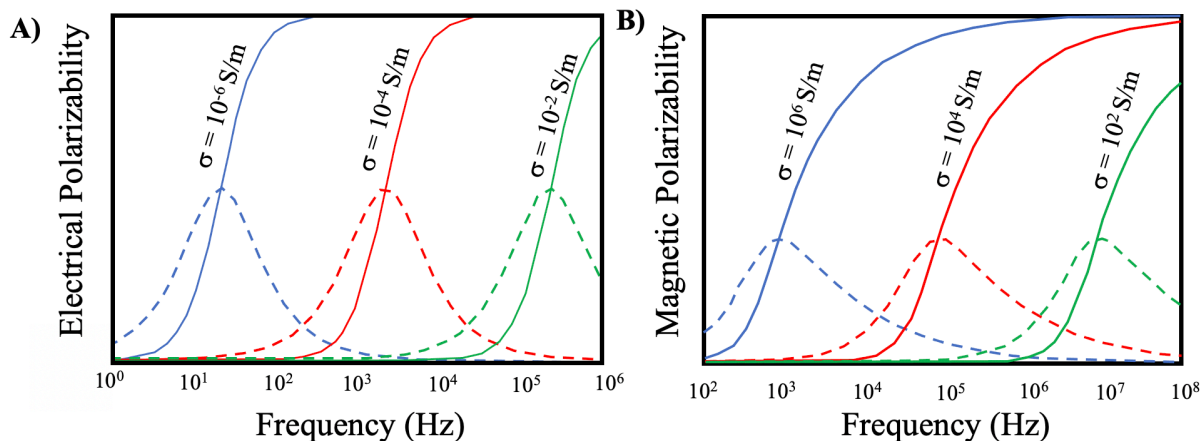
Figure 2. a. Electrical polarizability; and **b.** magnetic polarizability for a 10 cm metal sphere.

Conclusions

At the lab scale, volume and sample placement have a significant effect on the EMI response. Additionally, based on the forward modeling, the electromagnetic measured conductivity demonstrates an inverse dependency on frequency.

References

Glaser, D.R., Shubitidze, F., & Barrowes, B.E. (2022). Standoff high-frequency electromagnetic induction response of unsaturated sands: a tank-scale feasibility study. Journal of Environmental and Engineering Geophysics, 27(1), 1-8.

Placencia-Gómez, E., & Slater, L.D. (2016). On the pore water chemistry effect on spectral induced polarization measurements in the presence of pyrite. Journal of Applied Geophysics, 135, 474-485.

Qi, Y., El-Kaliouby, H., Revil, A., Ahmed, A.S., Ghorbani, A., & Li, J. (2019). Three-dimensional modeling of frequency- and time-domain electromagnetic methods with induced polarization effects. Computers and Geosciences, 124, 85-92.

Revil, A., Mao, D., Shao, Z., Sleevi, M.F., & Wang, D. (2017). Induced polarization response of porous media with metallic particles – Part 6: the case of metals and semimetals. Geophysics 82(2), E97-E110.

Tabbagh, A., Rejiba, F., Finco, C., Schamer, C., Souffaché, B., Camerlynk, C., Theisson, J., Jougnot, D., & Maineult A. (2021). The case for considering polarization in the interpretation of electrical and electromagnetic measurements in the 3 kHz to 3 MHz frequency range. Surveys in Geophysics, 42(2), 377-397.

O27 - A petrophysical model for the spectral induced polarization of clays

Philippe Leroy[1], Alexis Maineult[2], Aida Mendieta[2], and Damien Jougnot[2]

(1) BRGM, French Geological Survey, 45060 Orléans, France.
(2) Sorbonne Université, CNRS, EPHE, UMR 7619 METIS, 75005 Paris, France.

Presenter: P. Leroy (p.leroy@brgm.fr) **Student y/n:** No
Web page: NA   **Preferred presentation oral/poster:** Oral

Abstract. Clays are sedimentary minerals that are ubiquitous in the Earth's crust. They have remarkable adsorption, catalytic and containment properties due to their high surface charge and very large specific surface area. However, their electrochemical and microstructural properties are not completely understood. In this study, we have developed a new petrophysical model to interpret spectral induced polarization (SIP) measurements on illite and montmorillonite muds when salinity increases, from around 0.01 mol L^{-1} to 1 mol L^{-1} NaCl. Our model considers surface conduction in the interlayer space, Stern layer as well as Maxwell-Wagner polarization. By fitting predicted to measured SIP spectra, we found that the interlayer space of Na-montmorillonite muds may be conducting, which was not considered in the modelling as far as we know.

Introduction

Clay minerals are fine-grained materials (particle size below 2 μm) that are very common in geologic deposits, terrestrial weathering environments (e.g., regolith), and marine sediments [Sposito, 1989]. They are the main constituent of soils and make up about 40% of the minerals in sedimentary rocks. For instance, illite and smectite alone constitute about 30% of all sedimentary rocks on Earth and smectite was even observed by the Curiosity rover on Mars. Clay-rich (argillaceous) rocks, including marls, shale, mudstone, argillite and claystone (herein referred to as clay rocks), are sedimentary formations with a very low permeability. The low permeability of clay rock is a consequence of the nanoscale porosity of consolidated fine-grained sediments and may also result from the loss of pore connectivity during diagenetic or metamorphic rock reactions. Because of their confining properties, clay geological formations act as cap rocks above oil, gas and geothermal energy reservoirs and are frequently used for the geological storage of H$_2$, CO$_2$ and nuclear waste underground [Jougnot et al., 2010]. In this study, we propose a new petrophysical model considering electrical double layer (EDL) and Maxwell-Wagner polarization to interpret SIP measurements on clay muds, here illite and montmorillonite muds [Mendieta et al., 2021] as a function of salinity (NaCl concentration) in terms of EDL, petrophysical (e.g, porosity) properties and aggregate size distribution.

Complex conductivity modelling

The conductivity of Na-Mt dispersions was modelled by considering that Na-Mt particles form aggregates containing both neutral and diffuse layer water. We consider thick diffuse layers, that is, diffuse layers larger than the thickness of a Na-Mt particle, and the effect of electro-osmosis on their electrical conductivity. The diffuse layer is assumed to contribute to the volume conductivity and not to fully polarize because the volume of neutral water controlling the diffuse layer polarization is restricted. We consider that most of the counter-charge is located in the Stern layer and that the Stern layer polarizes. We also consider the Maxwell-Wagner polarization due to the charge build-up

at the boundary between clay and water and interlayer conduction. The fitting procedure was undertaken according to Maineult (2016) (Figure 1).
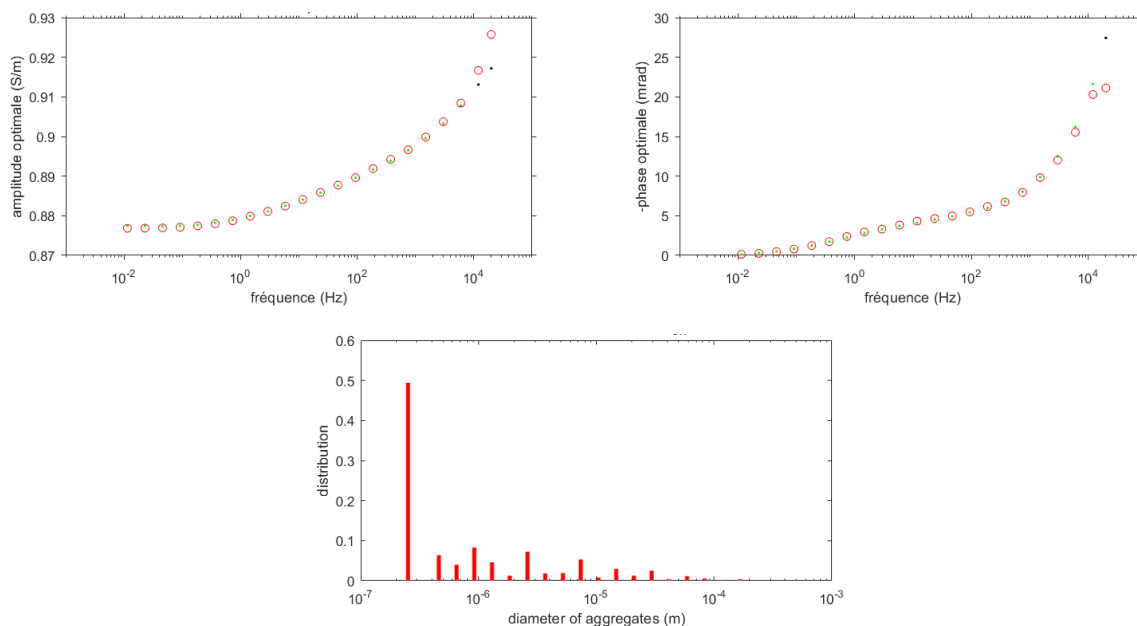
Figure 1. Complex conductivity spectra of Na-montmorillonite muds. Measurements: red circles, model predictions: points, distribution of the aggregate diameters inferred from the fitting procedure (NaCl concentration equal to around 0.1 M).

Conclusions. We have developed a new petrophysical model to understand laboratory SIP measurements on pure montmorillonite and illite muds at varying NaCl concentrations. Apart from the porosity and microstructural changes inferred from the fitting procedure, we found that the only way to reproduce the conductivity of clays was to consider conduction of the interlayer space of Na-Montmorillonite particles.

References

Jougnot, D., A. Ghorbani, A. Revil, P. Leroy, and P. Cosenza (2010a), Spectral induced polarization of partially saturated clay-rocks: a mechanistic approach, Geophys. J. Int., 180(1), 210-224, https://doi.org/10.1111/j.1365-246X.2009.04426.x.

Maineult, A. (2016), Estimation of the electrical potential distribution along metallic casing from surface self-potential profile, J. Appl. Geophys., 129, 66-78, https://doi.org/10.1016/j.jappgeo.2016.03.038.

Mendieta, A., D. Jougnot, P. Leroy, and A. Maineult (2021), Spectral Induced Polarization Characterization of Non-Consolidated Clays for Varying Salinities—An Experimental Study, Journal of Geophysical Research: Solid Earth, 126(4), https://doi.org/10.1029/2020jb021125.

Okay, G., P. Leroy, A. Ghorbani, P. Cosenza, C. Camerlynck, J. Cabrera, N. Florsch, and A. Revil (2014), Spectral induced polarization of clay-sand mixtures: Experiments and modeling, Geophysics, 79(6), E353-E375, https://doi.org/10.1190/Geo2013-0347.1.

Sposito, G. (1989), The Chemistry of Soils 344 pp., Oxford University Press, New York.

O28 - Towards functional root imaging using SIP: Recent advances and current challenges

A. Kemna

Institute of Geosciences, Geophysics Section, University of Bonn, Meckenheimer Allee 176, Bonn, 53115, Germany

Presenter: A. Kemna (kemna@geo.uni-bonn.de)   **Student y/n:** No
Web page: www.geo.uni-bonn.de   **Preferred presentation oral/poster:** Oral

Abstract. Over the past decade, electrical imaging methods have been increasingly applied to the investigation of root systems of plants. This development has been driven by, first, the lack of non-invasive measurement techniques for agricultural purposes providing subsurface spatial resolution and, second, the sensitivity of electrical impedance measurements to structure, state and function of the soil-root continuum. While root zone monitoring with time-lapse electrical resistivity tomography is mainly based on imaging patterns and changes in soil water content, from which conclusions on the distribution and activity (water/nutrient uptake) of roots can be drawn, the imaging of the spectral induced polarization (SIP) properties of roots offers potential for a direct characterization of root system structure and function. The latter approach combines the diagnostic capabilities of electrical spectroscopy, which, for roots, have been recognized for decades, with the spatial resolution benefits of a modern tomographic framework. While results of first applications of this method are promising, with demonstrated potential to delineate root system extension and thus to monitor root growth, as well as to capture information on the root physiological state, interpretation is still limited due to a lack of understanding of the root SIP response in terms of the underlying polarization mechanisms, involving different spatial length scales, and how this response scales up to an effective response of the soil-root continuum at the imaging scale. Simple mixing-model analyses show that disentangling the root response from the superimposed soil-root response is a non-trivial task, in particular for varying water content. Moreover, the generally made assumption of isotropic electrical properties in imaging algorithms is likely violated given the directional characteristics of both individual root segments as well as root system architecture, prompting the need for a consequent consideration of anisotropy at the effective (imaging) scale. Imaged anisotropy, however, may open the way to an improved characterization of root architecture and thus, in conjunction with the physiological sensitivity of the SIP response, enhanced plant phenotyping capabilities of SIP imaging.

O29 – Experimental study on the Spectral Induced Polarization response of artificial soils with varying water saturation, salinity and clay content

V. Iván[1], B. Mary[1,2], N. Schwartz[3], M. Ghinassi[1], G. Cassiani[1]

(1) Department of Geosciences, University of Padua, Padova, Italy
(2) Earth and Environmental Sciences Area, Lawrence Berkeley National Laboratory, Berkeley, CA, United States
(3) Department of Soil and Water Sciences, The Hebrew University of Jerusalem, Rehovot 7610001, Israel

Presenter: V. Iván (veronika.ivan@unipd.it) **Student y/n:** No
Web page: NA   **Preferred presentation oral/poster:** Oral

Abstract. A critical challenge of the application of geoelectrical methods in arid and semi-arid environments is to be able to discriminate between the effects of water content and pore water salinity on soil resistivity, since they are both inversely related to it. The heterogeneity of soils, the varying clay content makes the interpretation even more complex. In the frames of a small-scale laboratory experiment series, the combined effect of water saturation, pore water salinity and clay content was studied with the Spectral Induced Polarization (SIP) method. In our experimental setup these three parameters were gradually varied under controlled conditions. Ca-montmorillonite and very fine-coarse sand were mixed during multiple dry-wet mixing cycles in order to create artificial soil samples that are mimicking natural soils. In total, 4 samples were used with clay content varying from 2 to 8 m/m% of clay. The other two variables were manipulated on these 4 samples: the water saturation ranging from 100% to 10 % in 9-15 steps, and the salinity of the pore water ranging from 0.05 to 0.7 S/m in 4 steps. The obtained data was fitted with a double Cole-Cole model. The analysis of the Cole-Cole parameters along the three variables is promising for the separation between pore water salinity and water content.

Introduction

Geoelectrical methods provide diverse toolsets to image the subsurface and monitor its water dynamics. These observations might be crucial in arid areas, where the structure and function of agricultural and natural ecosystems are dramatically determined by water availability. Dryland ecosystems can be characterized by heterogeneous soil cover, high salt content in upper soil layers and low levels of soil moisture. However, understanding the combined effect of soil water content, salinity and soil composition on the electrical signal remains a challenging issue. Recent studies demonstrated the sensitivity of the IP method to water content (Breede et al. 2012; Kremer et al. 2016), clay content (Osterman et al. 2019) and salinity (Grunat 2013; Mendieta et al. 2021). Grunat (2013) noted that the quadrature conductivity is weakly dependent on the pore fluid salinity, thus, it might be used to separate between pore water salinity and water content.

Here, in a laboratory experiment series, we conducted Spectral Induced Polarization (SIP) measurements on artificial soils samples to observe under controlled conditions how the SIP response is affected by water saturation and salinity. This laboratory setup with manipulated gradients of water content and salinity levels allowed to perform measurements with high accuracy, and establish relationships between the electrical and hydrological properties of unconsolidated deposits or soils.

Methods and Materials

The artificial soil samples consist very fine-coarse sand (d= 0.1-0.6 mm, SiO_2 > 99.6%) and clay powder (Ca-montmorillonite) which were mixed during multiple dry-wet mixing cycles (Figure 1). The mixing protocol was tested by X-ray microCT scan on a small sample, which validated that the artificial mixture imitates sufficiently well the natural soils. In total, 4 samples were created with gradually growing clay content (2-4-6-8 %). The samples were packed into 170.1 cm^3 cylindrical plexiglass cells under dry conditions. Afterwards they were submerged into de-aerated tapwater and flushed with it (with a volume 2-3 times larger than the cell body volume) by applying vacuum. The gradually decreasing water saturation was obtained by air injection with gradually growing pressure (0.05-2.5 bar) in 9-15 steps. The saturation level was determined by measuring the weight of the samples at each phase. SIP measurements were conducted at each de-saturation steps in the 0.01 Hz to 1 kHz range at 21 (±0.3) °C using a ZEL-SIP04-V02 impedance meter developed at the Forschungszentrum Juelich. The whole cycle of measurements from 100% to 10-20% saturation level was repeated 3 further times for each sample, with increased pore water salinity. The salinity was increased by dissolving NaCl in the de-aerated tapwater, reaching the following levels of electrical conductivity of the solution: 0.1-0.35-0.7 S/m.
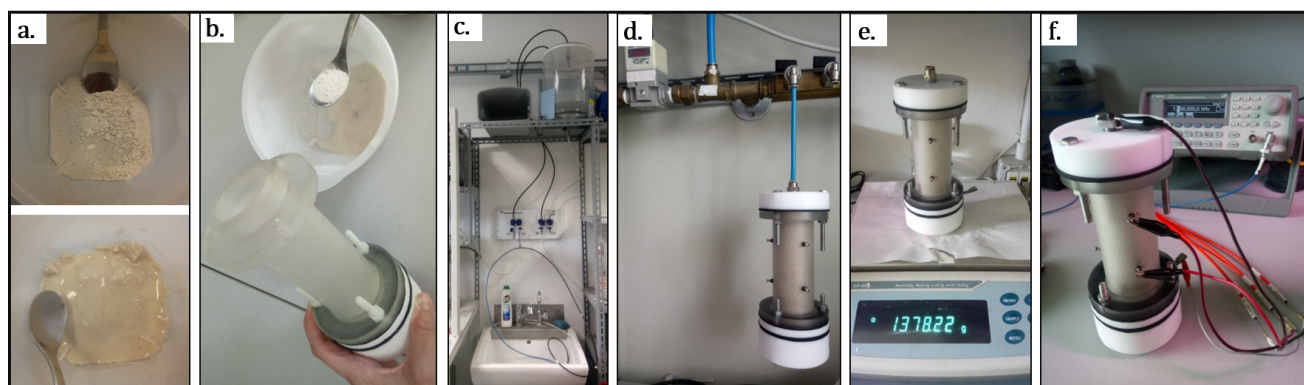
Figure 1. Experimental setup: **a.** creation the artificial soil samples. **b.** sample packing under dry conditions. **c.** saturation of samples. **d.** desaturation by air injection. **e.** weighing of samples. **f.** SIP measurement.

Results

As a result, a massive dataset was obtained with around 180 measurements. On Figure 2 an example of the raw SIP data is represented. The spectral induced polarization phase curves show a peak at low frequency (in the 0.1–10 Hz range), with the peak frequency and intensity varying according to the water saturation.
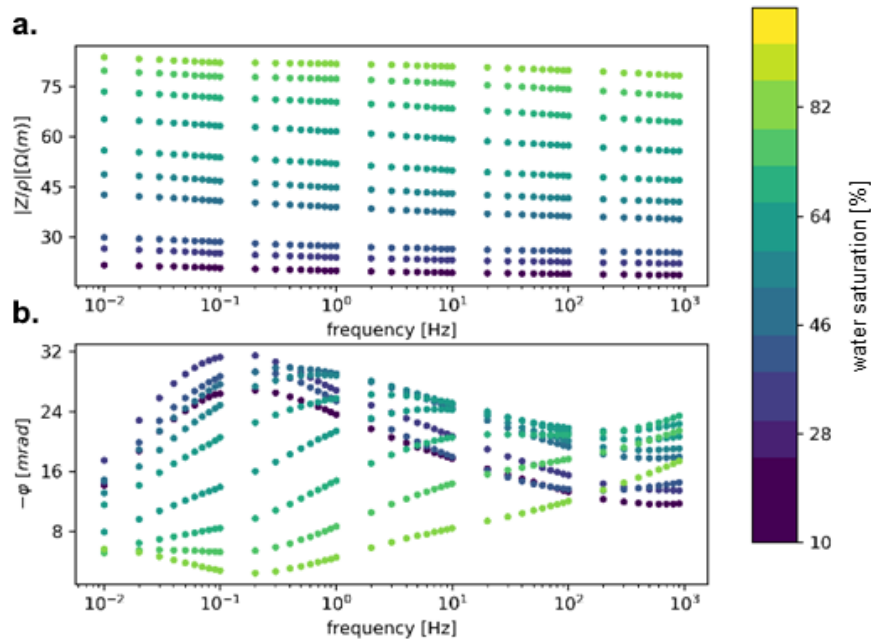
Figure 2. Example of raw SIP data for the sample with clay content: 6 %, salinity: 0.1 S/m, water saturation: 10-100%: **a.** resistivity spectra. **b.** phase spectra.

The interpretation of the SIP data was carried out by means of the widely used macroscopic relaxation model, the Cole-Cole model (Pelton et al. 1978). In order to remove the high-frequency electromagnetic noise, a double Cole-Cole model was fitted to the data. The removal of the high-frequency Cole-Cole component allowed to analyze separately the component linked to the SIP response. The fitting procedure was conducted according to the routine of Weigand (2017). From the Cole-Cole model four key parametrs can be identified: the DC resistivity (ρ_0), the relaxation time (τ), the chargeability (m) and the Cole-Cole exponent (c). Figure 3 is representing an example of the dependence of each Cole-Cole parameter from water saturation and clay content at the salinity level of 0.1 S/m. The further investigation of the quadrature conductivities and the statistical analysis of the Cole-Cole parameters is currently under development.
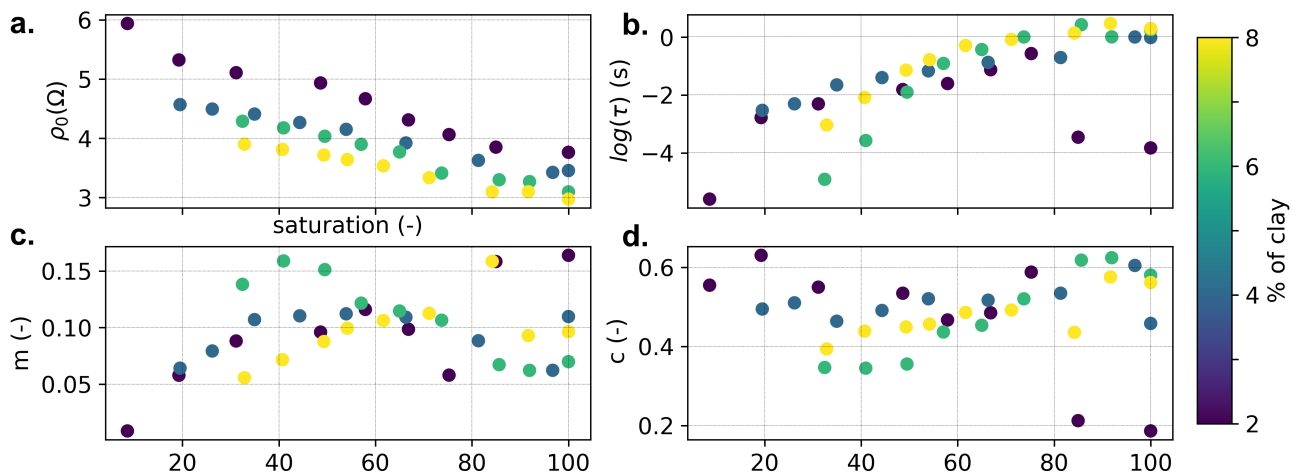
Figure 3. Example of fitted Cole-Cole parameters plotted against the water saturation levels for the salinity level of 0.1 S/m: **a.** DC resistivity. **b.** relaxation time. **c.** chargeability. **d.** Cole-Cole exponent.

Conclusions

The laboratory experiment demonstrated the sensitivity of the SIP method to water content, clay content and salinity. The results are perspectivic for the separation between pore water salinity and water content. A rigorous method for the discrimination through statistical analysis is currently under development. Further steps will test the performance of the model in field sites representing different ecological conditions.

References

Breede, K., Kemna, A., Esser, O., Zimmermann, E., Vereecken, H., & Huisman, J. A. (2012). Spectral induced polarization measurements on variably saturated sand-clay mixtures. Near Surface Geophysics, 10(6), 479-489.

Grunat, D.A. (2013). Effects of soil saturation and pore fluid salinity on complex conductivity. PhD Thesis. Rutgers University-Graduate School-Newark.

Kremer, T., Schmutz, M., Leroy, P., Agrinier, P., & Maineult, A. (2016). Modelling the spectral induced polarization response of water-saturated sands in the intermediate frequency range (10^2–10^5 Hz) using mechanistic and empirical approaches. Geophysical Supplements to the Monthly Notices of the Royal Astronomical Society, 207(2), 1303-1312.

Mendieta, A., Jougnot, D., Leroy, P., & Maineult, A. (2021). Spectral Induced Polarization Characterization of Non-Consolidated Clays for Varying Salinities—An Experimental Study. Journal of Geophysical Research: Solid Earth, 126(4), e2020JB021125.

Osterman, G., Sugand, M., Keating, K., Binley, A., & Slater, L. (2019). Effect of clay content and distribution on hydraulic and geophysical properties of synthetic sand-clay mixtures. Geophysics, 84(4), E239-E253.

Pelton W.H., Ward S.H., Hallof P.G., Sill W.R. and Nelson P.H. (1978). Mineral discrimination and removal of inductive coupling with multifrequency IP. Geophysics 43, 588–609.

Weigand, M. (2017). Time-lapse Cole-Cole decomposition routines. https://m-weigand.github.io/ccd_tools/doc_ccd/index.html.

Part 2. Poster presentations

P1 - Proxies for surface conductivity and formation factor in permeability prediction of sandstones by Z. Zhang and A. Weller

P2 - SIP-based monitoring of denitrification in aquifer sediments by C. Strobel, O. A. Cirpka, C. Leven, J. A. Huisman, and A. Mellage

P3 - NFDI4Earth Pilot at LIAG: Improving interoperability and reusability of SIP data by S. Nordsiek and M. Halisch

P4 - Ice content Estimation with High-Frequency Induced polarization by J. Mudler, D. Kreith, M. Sugand, and A. Hördt

P5 - Multi-Frequency excitation speeds up SIP measurement by T. Radić

P6 - New hardware for measurement of fast and slow temporal changes of spectral resistivity by T. Radić

P7 - Anisotropy of induced polarization response- sulfide ore samples by S. Ahmadi, A. Coperey, A. Ghorbani and A. Revil

P8 - Electromagnetic coupling in time and frequency domains induced polarization- a review by A. Ghorbani and P. Vaudelet

P9 - On a new method for the determination of Relaxation Time Distributions by A. Maineult and N. Florsch

P10 - Comparative analysis on IP data obtained in LNAPL contamination sites of different concentrations by B. Kim, H. Yu, S. Y. Song, I. S. Joung, A. Cho, J. Jeong, J. S. Son, and M. J. Nam

P11 - Analysis on fitting time domain decaying curves from time domain induced polarization inversion for NAPL synthetic models by J. Jeong, B. Kim, D. Caesary, Y. S. Mun, and M. J. Nam

P12 - Geophysical mapping of aquifer properties in infrastructure projects using DCIP and MRS by T. Martin, M. A. Kass, D. Grombacher, G. Fiandaca, C. Butron, M. Griffiths, M. Østbjerg Vang, S. Rejkjaer, A. Mendoza and T. Dahlin

P13 - Spectral induced polarization response of lake-bottom sediments by R.Glebe, J. Hoppenbrock, J. Buckel, A. Hördt, L. Pérez, P. Hoelzmann, and M.Bücker

P14 - Characterization of surface conductivity of clays by V. Emelianov, Z. Zhang, K. Titov, M. Halisch, and A. Weller

P15 - Temperature dependence of SIP ice signatures of partially frozen rocks based on Cole-Cole model parameterization by J. K. Limbrock and A. Kemna

P16 - Complex conductivity response of diffusion driven calcite precipitation in sandstone by A. M. Mansfeld and A. Kemna

P17 - Measurement of dried seafloor massive sulphides by M. Lührs and A. Hördt

P18 - Estimating spectra of embedded ore samples by M. Lührs and A. Hördt

P19 - Sensing of winter wheat root systems at the field scale using spectral electrical impedance tomography by V. Michels, M. Weigand, and A. Kemna

P20 - 3D Cole Cole Inversion of time domain induced polarization data by H. Langenbach and B. Tezkan

P21 - The evaluation of HIRIP data to investigate a large scale graphite anomaly in the Bavarian Forest/Germany by S. Schiebel, W. Mörbe, P. Yogeshwar, B. Tezkan, T. Günther, and M. Tauchnitz

P22 - Numerical modelling of Stern-layer polarization in dense packings by J. Wentzki and D. Bücker

P23 - Multi-geophysical approach to characterize fracturation and characterize the transport properties of carbonate rocks by A. N. Yacouba, C. Mallet, J. Deparis, and D. Jougnot

P24 - Past metallurgic sites and deposits characterization using complex conductivity measurements by P. Kessouri[1], C. Ryckebusch, J. Deparis, A. Fernandez Visentini, J. Gance, D. Caterina, I. Isunza Manrique, and F. Nguyen

P 25- Understanding landslide triggering processes with induced polarization - Case studies in New Caledonia by S. Barde Cabusson, P. Vaudelet, A. Revil, and P-A. Duvillard

P1 - Proxies for surface conductivity and formation factor in permeability prediction of sandstones

Z. Zhang and A. Weller

Technische Universität Clausthal, Institut für Geophysik, 38678 Clausthal-Zellerfeld, Germany

Presenter: Z. Zhang (zeyu.zhang.1@tu-clausthal.de) **Student y/n:** Yes

Web Page: NA **Preferred presentation oral/poster:** poster

Abstract. Using the surface conductivity of sandstones measured in laboratory to predict permeability yields reliable results. The surface conductivity is proportional to the imaginary part of complex conductivity as well as the normalized chargeability. Using these two parameters as proxies of the surface conductivity and the specific internal surface, permeability prediction will be easily carried out without multi-salinity measurements. The formation factor can be further replaced by the conductivity of sandstones fully saturated by formation fluid. The validity of an in situ permeability prediction model with parameters derived from SIP is checked.

Introduction and Theory

The Kozeny-Carman equation for permeability prediction requires the knowledge of formation factor F and the specific surface area per unit pore volume S_{por}:

$$k^* = \frac{a}{F S_{por}^2}. \tag{1}$$

Rink and Schopper (1974) proposed an alternative permeability prediction model using the surface conductivity and formation factor with the following exponents:

$$k^* = \frac{a_1}{F^5 \sigma_{surf}^2}. \tag{2}$$

The surface conductivity σ_{surf}, which is regarded as a proxy of S_{por}, is determined by laborious multi-salinity measurements. Assuming the validity of the proportionalities between surface conductivity and the imaginary part of conductivity (at a frequency of 1 Hz) $\sigma_{surf} \sim \sigma''$ or between surface conductivity and the normalized chargeability $\sigma_{surf} \sim m_n$, the surface conductivity can be replaced by parameters that are provided by measurements of induced polarization. Equation 2 can by formulated as:

$$k^* = \frac{a_2}{F^5 \sigma''^2} \tag{3}$$

$$k^* = \frac{a_3}{F^5 m_n^2}. \tag{4}$$

The normalized chargeability is the product of conductivity and total chargeability, which are determined by Debye decomposition (e.g., Nordsiek and Weller, 2008).

For clean sandstones, the formation factor F describes the ratio between water conductivity σ_w and the conductivity of the fully saturated rock σ_0: $F = \frac{\sigma_w}{\sigma_0}$. Assuming a constant water conductivity, the formation factor can be replaced by $1/\sigma_0$ in equations 3 and 4:

$$k^* = \frac{a_4 \sigma_0^5}{\sigma''^2} \qquad (5)$$

$$k^* = \frac{a_5 \sigma_0^5}{m_n^2}. \qquad (6)$$

We use equations 2 to 6 for permeability prediction of 24 sandstone samples from Shahejie Formation, China (Zhang and Weller, 2014, 2021). In order to evaluate the predictive quality of different equations, we determine the average absolute deviation (in log space) between predicted permeability k^* and measured permeability k (e.g., Weller et al., 2015)

$$d = \frac{1}{n} \sum_{j=1}^{n} \left| \log_{10}(k_j) - \log_{10}(k_j^*) \right|. \qquad (7)$$

A value of $d = 1$ denotes an average absolute deviation of one order of magnitude (or a factor 10). Robinson et al. (2018) rate one order of magnitude above or below the measured value as an acceptable estimation if samples of varying lithology are regarded. Considering samples of a single formation, a value of $d \approx 0.5$ should be achieved for a good predictive quality. The prefactors a_1 to a_5 in equations 2 to 6 have to be adjusted to get the minimum of d.

Results. The result of equation 2 is shown in Figure 1. In spite of one outlier, the resulting deviation $d = 0.548$ indicates a good predicting quality. If the parameter σ_{surf} is substituted by σ'' (Figure 2a, equation 3), we get a slightly higher deviation with $d = 0.624$. The deviation decreases at $d = 0.594$ when m_n replaces σ_{surf} (Figure 2b, equation 4). In the next step, we consider equations 5 and 6 that replace the formation factor by $1/\sigma_0$. We get a deviation $d = 0.626$ for equation 5 (Figure 2c) and $d = 0.596$ for equation 6 (Figure 2d).
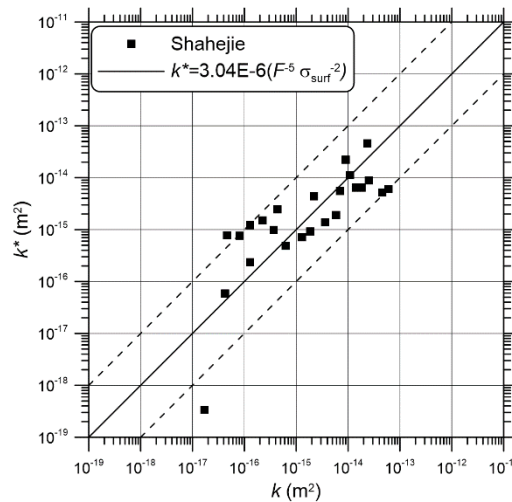
Figure 1. Comparison of measured permeability with predicted permeability using formation factor F and surface conductivity σ_{surf} (equation 2). The two dashed lines on either side of the diagonal indicate a deviation of one order of magnitude from the measured permeability value.

Conclusions. The permeability of sandstones of the Shahehjie Formation can be well predicted from the surface conductivity and formation factor using the Rink & Schopper model, which has been published nearly 40 years ago. The imaginary part of complex conductivity and the normalized chargeability are two proxies for the surface conductivity. The permeability prediction with normalized chargeability results in a slightly better predictive quality. The most crucial parameter in

the permeability prediction of sandstones is the formation factor. The proposed exponent of five for the formation factor is higher than the exponent used in the Kozeny-Carman model. We find that the formation factor can be replaced by the conductivity of the fully saturated rock without any significant loss of predictive quality. The resulting equations consider parameters that can be determined in an induced polarization field survey. Further tests with sandstones from other formations should verify whether the results acquired with the sample set of the Shahejie Formation can be generalized.
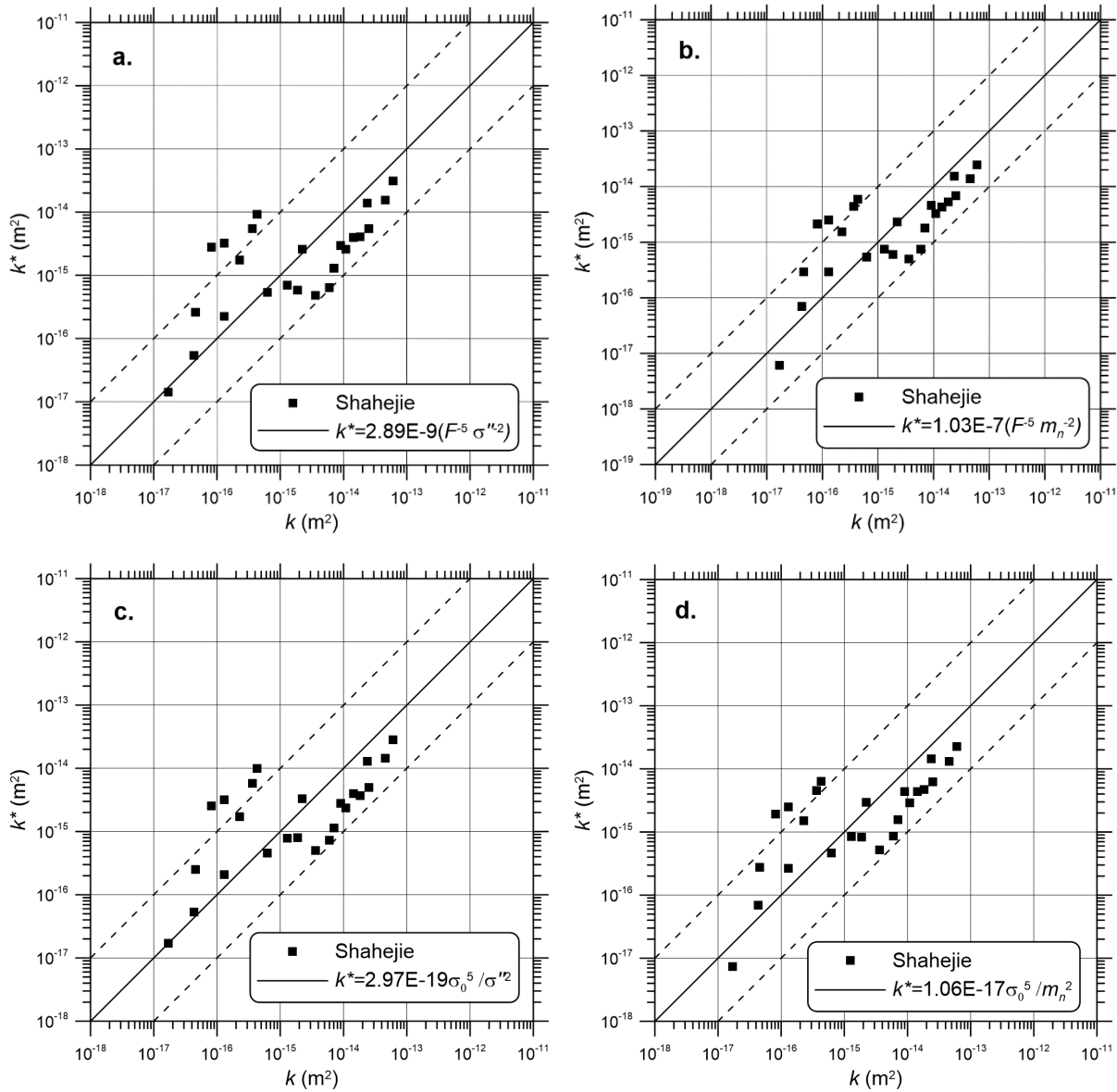
Figure 2. Comparison of measured permeability with predicted permeability using **a.** formation factor F and imaginary part of conductivity σ'' (equation 3), **b.** formation factor F and normalized chargeability m_n (equation 4), **c.** the conductivity of the fully saturated rock σ_0 and imaginary part of conductivity σ'' (equation 5), **d.** the conductivity of the fully saturated rock σ_0 and normalized chargeability m_n (equation 6).

References

Nordsiek, S., & Weller, A. (2008). A new approach to fitting induced-polarization spectra. Geophysics, 73(6), F235-F245. doi: 10.1190/1.2987412.

Rink, M., & Schopper, J. R. (1974). Interface conductivity and its implication to electric logging. Presented at SPWLA 15th Annual Logging Symposium, Paper J.

Robinson, J., Slater, L., Weller, A., Keating, K., Robinson, T., Rose, C., & Parker, B. (2018). On permeability prediction from complex conductivity measurements using polarization magnitude and relaxation time. Water Resources Research, 54, 3436-3452. doi: 10.1002/2017WR022034.

Weller, A., Slater, L., Binley, A., Nordsiek, S., & Xu, S. (2015). Permeability prediction based on induced polarization: Insights from measurements on sandstone and unconsolidated samples spanning a wide permeability range. Geophysics, 80(2), D161-D173. doi:10.1190/GEO2014-0368.1.

Zhang, Z., & Weller, A. (2014). Fractal dimension of pore space geometry of an Eocene sandstone formation. Geophysics, 79(6), D377-387. doi: 10.1190/GEO2014-0143.1.

Zhang, Z., & Weller, A. (2021). A comparative study of permeability prediction for Eocene sandstones - Part 1: Application of modified Swanson models to mercury injection capillary pressure and nuclear magnetic resonance data. Geophysics, 86(6), M233-243. doi: 10.1190/GEO2014-0143.1.

P2 - SIP-based monitoring of denitrification in aquifer sediments

C. Strobel[1,2], O. A. Cirpka[1], C. Leven[1], J. A. Huisman[3], A. Mellage[2]

(1) Center of Applied Geoscience, University of Tübingen, Tübingen, Germany
(2) Institute of Water, Waste and the Environment, University of Kassel, Kassel, Germany
(3) Institute of Bio- and Geosciences, Agrosphere (IBG-3), Forschungszentrum Jülich GmbH, Jülich, Germany

Presenter: C. Strobel (cora.strobel@uni-tuebingen.de) **Student y/n:** Yes
Web page: NA   **Preferred presentation oral/poster:** Poster

Abstract. The sensitivity of spectral induced polarization (SIP) to the (bio)geochemical properties of porous media has opened promising avenues for monitoring microbial abundance and activity linked to solute turnover and solute/solid-matrix interactions. However, SIP is an indirect method and its application to biogeochemistry requires a profound understanding of how different and often parallel reactive processes modulate the integrated signals that we measure. In natural soils and sediments, containing a heterogeneous distribution of mineral and organic colloids, a key first step is to separate 'background' polarization signals related to the solid matrix from target abiotic and / or biotic reactive processes. Here, we present results from a well-controlled flow-through experiment in calcareous alluvial aquifer sediment, rich in organic carbon, where SIP was applied to monitor microbial activity during denitrification. Insights gained from these experiments will guide the deployment of a SIP-probe array in the field and the interpretation of SIP signals obtained in field stimulations. We biostimulated the sediment pack via a continuous injection of nitrate and lactate, followed by a static incubation, while continuously monitoring pore-water composition and SIP signal changes. During the denitrification phase, SIP responses exhibited a distinct σ'' peak at roughly 10 Hz that was otherwise absent during the injection of bromide, a conservative tracer. We quantified this additional contribution to subsurface charge storage via a double Cole-Cole model. The increase in the secondary polarization response during biostimulation and subsequent decrease during the static phase, matched the expected timing of increasing and decreasing microbial activity based on the geochemical data. Our findings provide a framework for the decoupling of parallel geophysical signal contributions during reactive transport in natural porous media, enabling the non-invasive detection of the location and timing of elevated microbial activity. Our recently developed and deployed SIP-probes will monitor a similar biostimulation experiment across the depth profile of an aquifer under forced gradient flow and yield a direct comparison of frequency resolved measurements between lab and field scales for the same reactive system.

Introduction

Monitoring microbially active zones in porous media with spectral induced polarization (SIP) has the potential to improve both our understanding of dynamic reactive processes and the monitoring of natural attenuation and bioremediation (Kessouri et al. 2019). In particular, the natural attenuation of nitrate, a ubiquitous contaminant of concern, remains a process of great interest due to the risk posed to groundwater quality. Denitrification, the reduction of nitrate to N_2, requires the co-occurrence of nitrate (electron acceptor), degrading microbes, and suitable electron donors. Whether and where the microbes experience the necessary conditions to reduce nitrate is governed by the physico-chemical heterogeneity of aquifers, highlighting the need for non-invasive monitoring techniques. To take advantage of the non-invasive monitoring capabilities of SIP, it is important to

discriminate between parallel signal contributions stemming from different processes. In natural soils and sediments, the separation of polarization processes brought on by microbial activity and those modulated by parallel geochemical reactions at the mineral-water interface are of particular interest. Moreover, investigating the transferability of relationships derived under well-controlled laboratory conditions to field sites is a prerequisite to delineating the method's applicability.

Methods

We conducted a column-scale biostimulation experiment with natural calcareous Tufa aquifer sediment from the Ammer Valley (Tübingen, Germany), followed by the development of an in-situ SIP-probe for permanent field installation for monitoring a reactive transport experiment in the Tufa aquifer. Sediment collected from the aquifer was packed into triplicate columns (l = 17.3 cm, d = 3.5 cm) fitted with brass electrodes (d = 0.5 cm) at the column inlet and outlet for current injection and two potential electrode pairs with midpoints at 4.5 cm and 10.5 cm from the inlet. Potential electrodes (d = 0.5 cm) were retracted from the current flow path and encased in an agar gel electrolyte. The experiment was conducted at 12°C, the mean groundwater temperature of the Tufa aquifer, and columns were subjected to three injection phases. Initially, bromide (as NaBr, 8.6 mM) was injected as a conservative tracer. The tracer injection was followed by a biostimulation phase in which nitrate (as $NaNO_3$, 2 mM – 5 mM) and lactate (0.5 mM) were injected continuously at varying flow rates and concentrations, until nitrate was detected in outflow samples. Two columns were biostimulated while the third served as a control (i.e. no nitrate or lactate was injected). Lactate was added to enhance and accelerate denitrification and shorten potential lag times of microbial activity. By fine-tuning the boundary conditions, denitrification activity was successfully stimulated along the entire column length. Following nitrate injection, flow was stopped, yielding a static phase, in which the columns were sealed and incubated with the nitrate remaining from the previous biostimulation phase. Geochemical analyses of the pore water were conducted on samples collected at the outflow and at two locations (4.5 cm and 10.5 cm from the inlet) within the column. SIP measurements were conducted every 4 h over a frequency range of 0.01 Hz – 1000 Hz.

The field SIP-probe consists of copper point electrodes (d = 1 cm) attached to a 2'' PVC-pipe with 15 cm electrode spacing. To reduce inductive coupling between the cables, RG58 coaxial cables were used. Prior to probe deployment, measurements were conducted in a water-filled cylinder and by short circuiting the electrodes to quantify inductive coupling effects. Two SIP probes were installed at 6 m depth into the same calcareous Tufa aquifer sediment that was packed into the laboratory experiments. We plan to follow a similar injection regime in our field experiment as outlined above for the lab experiments, with a biostimulation phase following a tracer injection. Currently, the field investigation is ongoing and results are forthcoming.

Results of the flow-through column experiments

During the biostimulation flow phase, NO_3^- was reduced throughout the column, with the strongest concentration drop occurring close to the inlet (Figure 1 (a)). During the static phase, the NO_3^- that remained in the columns was reduced within 225 h at 4.5 cm from the inlet. The phase of denitrification activity, i.e. during the biostimulation flow phase and the first 225 h of the static phase, coincided with the formation of a distinct σ'' peak with a maximum at around 10 Hz followed by a steady decrease of σ'' to background levels and spectral shape at the end of the static phase. In contrast, while the σ'' also increased during the conservative tracer injection, the shape and peak frequency remained constant. The σ'' dynamics during the breakthrough of NaBr were attributed to cation exchange of Ca^{2+} with Na^+. A double Cole-Cole model was used to differentiate between

abiotic charge storage and microbial activity. The model accounts for the superposition of a background contribution from the sediment and a secondary microbial contribution. The background contribution was described with a fixed time constant τ_{mtx} and Cole-Cole exponent c, similar to the Cole-Cole parameters of the sediment prior to biostimulation. The parameter range of the time constant, τ_{bac}, of the secondary contribution was constrained within the range of previously reported microbially-driven polarization signals (e.g. Joo et al. 2021; Mellage et al. 2018; Rosier et al. 2018). An example fit for a spectrum at the end of the flow phase is shown in Figure 1 (d). The double Cole-Cole model successfully differentiated between the abiotic tracer injection and biostimulation. Moreover, the temporal evolution of the secondary contribution (Figure 1 (b) and (c)) matched the expected development of microbial activity. A comparison with signals recorded in the control column, experiencing an identical flow regime but with no added nitrate, highlighted a clear absence of the secondary signal, thus providing further evidence for a microbial contribution.

Conclusions

The column experiment provides evidence that the denitrification activity of a natural microbial community modifies the SIP signal to an extent that can be resolved even within a polarizing matrix like the calcareous peat rich sediment investigated here. In agreement with previously reported spectral responses during microbial growth experiments, our experiments yielded spectra with a peak frequency peak at roughly 10 Hz, exclusively detected during the biostimulation phase. Moreover, we showed that a superposition of Cole-Cole terms is a useful approach for successfully decoupling the parallel contributions of abiotic cation exchange process and microbial activity from σ'' signals. The results from the laboratory and the deployment of the SIP-probe provide a platform for field experiments in which we plan to monitor microbial activity under conditions that are comparable to those in the laboratory experiments. We expect to shed light on the transferability of laboratory-derived results for the interpretation and validation of SIP monitoring in the field.

References

Joo, H.-W., Kwon, T.-H., Lee, S.-R., and Wu, Y. (2021). Relaxation behavior in low frequency complex conductivity of sands caused by bacterial growth and biofilm formation by Shewanella oneidensis under a high-salinity condition. Geophysics, 86(6):B389–B400. https://doi.org/10.1190/geo2020-0213.1

Kessouri, P., Furman, A., Huisman, J. A., Martin, T., Mellage, A., Ntarlagiannis, D., Bücker, M., Ehosioke, S., Fernandez, P., Flores-Orozco, A., Kemna, A., Nguyen, F., Pilawski, T., Saneiyan, S., Schmutz, M., Schwartz, N., Weigand, M., Wu, Y., Zhang, C., and Placencia-Gomez, E. (2019). Induced polarization applied to biogeophysics: recent advances and future prospects. Near Surface Geophysics, 17(6): 595–621. https://doi.org/10.1002/nsg.12072

Mellage A, Smeaton CM, Furman A, Atekwana EA, Rezanezhad F, Van Cappellen P. (2018). Linking Spectral Induced Polarization (SIP) and Subsurface Microbial Processes: Results from Sand Column Incubation Experiments. Environment Science & Technology, 52(4):2081-2090. https://doi.org/10.1021/acs.est.7b04420

Rosier, C. L., Atekwana, E. A., Aal, G. A., and Patrauchan, M. A. (2019). Cell concentrations and metabolites enhance the SIP response to biofilm matrix components. Journal of Applied Geophysics, 160:183–194. https://doi.org/10.1016/j.jappgeo.2018.10.023

P3 - NFDI4Earth Pilot at LIAG: Improving interoperability and reusability of SIP data

S. Nordsiek and M. Halisch

Leibniz Institute of Applied Geophysics, Stilleweg 2, 30655 Hannover, Germany

Presenter: M. Halisch (Matthias.Halisch@leibniz-liag.de)   **Student y/n:** No
Web page: NA   **Preferred presentation oral/poster:** Poster

Abstract. Within the framework of the Association German National Research Data Infrastructure (NFDI) and the Consortium "NFDI4Earth" of German research institutes within the Earth System Sciences, we develop a strategy to store data of laboratory spectral induced polarization (SIP) measurements in a way that follows the FAIR data principles. As a first step, we analyze the workflow of SIP data from sample preparation, measurement, and publication to archiving of the data and suggest a modular system to gather relevant metadata, so that the resulting data can be considered as interoperable and reusable. However, due to complexity, legal issues concerning data reusability are not considered in this first study.

Introduction

Spectral induced polarization (SIP) laboratory studies normally cover a limited number of samples investigated under defined ambient conditions. Usually, these measurements focus on one or more parameters varied on purpose, for instance fluid conductivity (e.g., Weller et al., 2011) or ambient temperature (e.g., Bairlein et al., 2016). Such systematic investigations on the impact of single parameters on the observed SIP spectra are essential for verification of analytical models that describe the IP effect (e.g., Hördt et al., 2016). Laboratory studies may also incorporate additional data, such as petrophysical (e.g., Weller et al., 2010; Weller and Slater, 2019) or soil hydraulic parameters (e.g., Breede et al., 2011; Nordsiek et al., 2016). Investigating SIP spectra in terms of empirical relationships to such parameters, which often result from elaborate measurements, can help to find an approach for an easier applicable estimation. In both cases, a large database is beneficial to strengthen the validity of the laboratory study. Besides increasing the number of investigated samples, consideration of data resulting from comparable studies published by other researchers can help to support the significance.

Accurate sample preparation, repeated SIP measurements, and careful evaluation of the measured SIP spectra are required to get representative and reliable results. Producing high quality SIP data is laborious and time-consuming. Thus, data resulting from laboratory SIP studies are highly valuable. Despite these strong efforts, a plan how to use the measured spectra and associated data sustainably is often missing. A first approach to increase the visibility and reusability of SIP data is the so-called "SIP-Archiv" (Halisch et al., 2016), a repository for SIP spectra and metadata, developed and maintained by Leibniz Institute of Applied Geophysics (LIAG) and the "Working Group Induced Polarisation" within the German Geophysical Society.

Generally, to improve the accessibility and reusability of scientific data, the Association German National Research Data Infrastructure (NFDI) was founded in 2020. NFDI comprises several

discipline-specific consortia, such as NFDI4Earth. This group of research institutes from Earth System Sciences in Germany, including LIAG, is aiming to develop and establish commonly accepted standards for managing geoscientific research data (NFDI4Earth, 2022). Within the NFDI4Earth pilot project at LIAG, we develop a data map for petrophysical measurements, where we compile all instruments, processing methods as well as all measured and processed parameters within a typical petrophysical workflow. Our aim is to establish the basis for a database providing petrophysical data and metadata according to the so-called "FAIR data principles" (Wilkinson et al., 2016), i.e. **F**indable, **A**ccessible, **I**nteroperable, and **R**eusable data. Clarity about captured and processed data and definition of consistent metadata are required to facilitate a petrophysical database according to the FAIR data principles.

In this study, we confine to the workflow of laboratory SIP measurements, which mark an important node within the network of petrophysical measurements, as several parameters derived from SIP spectra exhibit distinct relationships to other rock / soil properties. The workflow of SIP measurements is complex, covering different types and sizes of samples, various experimental setups, and several approaches to evaluate the spectra. Therefore, we separate the workflow into two parts, starting with sample preparation and SIP measurements. Afterwards, we refer to evaluation of the measured spectra as well as to publication and archiving of the data.

An analysis of the SIP workflow from sample preparation to measurement

Before starting with the SIP measurements, we have to prepare thoroughly the associated metadata. For the sake of clarity, we can organize the metadata into three categories. Firstly, we collect metadata related to the *sample* (e.g., type of sample, type and numerical values of sample geometry etc.). Then, we consider metadata about the instrument and the cell, i.e. the *hardware* metadata (e.g., manufacturer, name of the product, output data format etc.). Finally, we refer to metadata about the settings of the current *measurement* (e.g., type of fluid, conductivity, temperature, distances between electrodes etc.). All metadata should be captured in advance or during the setup of the SIP measurement. Two of the three categories, i.e., *sample* and *hardware* metadata, are not restricted to a certain measurement. Thus, it seems beneficial to store these metadata into separate files that are linked with the third metadata file describing the current *measurement*. As result of the SIP measurement, we get a raw data file according to the format described in the *hardware* metadata. In the next section, we will continue with processing of the measured spectra.

Working with SIP data from evaluation to archive

Occasionally, the measured data are prepared in advance to further analysis. For instance, it might be desirable to rearrange the order of columns, to add columns containing derived parameters, and to confine to a certain range of frequencies, respectively. To prevent confusion with *raw data*, we have to store *prepared data* separately. Generally, a detailed documentation of all modifications applied to the *raw data* is mandatory to allow reconstruction of the experiment. Usually, the same processing steps apply to all measurements of a defined dataset. Therefore, it can be favorable to describe the *data preparation* in detail in one file, e.g., as a Matlab or Python code. After the preparation of the SIP spectra, *data evaluation* can be performed in multiple ways. Fitting empirical models, e.g., the Cole-Cole model (Cole & Cole, 1941; Pelton et al., 1978) to the measured spectra is

a straightforward approach (e.g., Hupfer et al., 2016). Alternatively, algorithms using a superposition of multiple terms can be applied to the data, e.g., a Debye decomposition (Nordsiek & Weller, 2008). However, due to the diversity of models, the evaluation process of SIP spectra needs to be documented thoroughly. The *resulting data* are stored in a separate file.

For archiving SIP data, a modular strategy seems to be advantageous. First, we consider the acquisition of data, where the *raw data* provided by the SIP instrument are connected with the *measurement* metadata. This represents the main metadata file of this section, where all information relevant to the SIP measurement is available, including connections to the *hardware* and *sample* metadata. The latter needs to be connected in both directions, as we want to store references to previous SIP measurements within the *sample* metadata. Considering the interpretation of data, the *processing* metadata is the main element, connected to the *resulting data* and to both algorithms, *data preparation* and *data evaluation*, that have been applied to the original data. SIP measurements are usually published as parts of a study that includes a number of samples or even involves different methods applied to these samples. To be able to find all publications related to a certain measurement, we suggest to link the *processing* metadata to the publications by storing the according DOIs. A link between *measurement* metadata and *processing* metadata is necessary for completion. For the sake of clarity, the modular strategy for archiving SIP data is displayed schematically (Fig. 1).

Conclusions. SIP measurements under controlled laboratory conditions are very important, as they can support or falsify theoretical models, enable estimation of petrophysical parameters by empirical approaches, and provide reference data for field surveys. Treatment of laboratory SIP data does not reflect the importance. A well-organized, commonly accepted data storage and publication strategy obeying the FAIR data principles is missing up to now. Several sources of metadata essential to describe the measured SIP spectra and their evaluation appear during the whole lifecycle of a sample, from preparation to archiving of the data. We identify different groups of data and metadata that can be organized in a modular system.
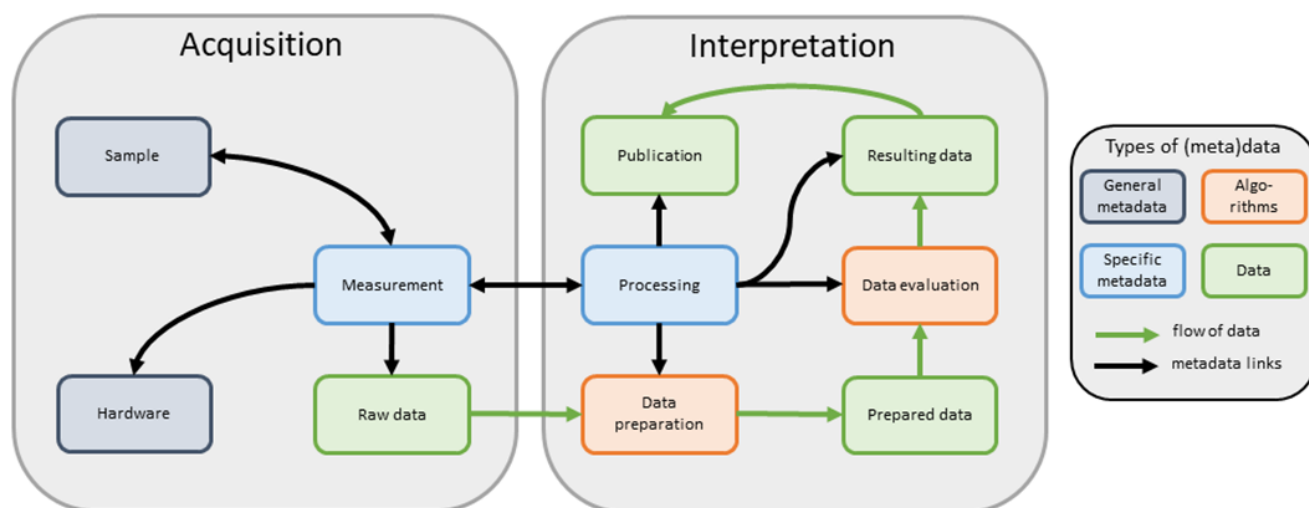
Figure 1. Scheme of data flow and metadata links for an SIP measurement.

References

Bairlein, K., Bücker, M., Hördt, A. & Hinze, B. (2016). Temperature dependence of spectral induced polarization data: experimental results and membrane polarization theory. Geophysical Journal International, 205, 440–453. DOI: 10.1093/gji/ggw027.

Breede, K., Kemna, A., Esser, O., Vereecken, H. & Huisman, J. A. (2011). Joint measurement setup for determining spectral induced polarization and soil hydraulic properties. Vadose Zone Journal, 10(2), 716–726.

Cole, K.S. & Cole, R.H. (1941). Dispersion and Absorption in Dielectrics: I. Alternating Current Characteristics. Journal of Chemical Physics, 9, 341–351.

Halisch M., Gramenz J., Gorling L., Krause K. & Bolotovski I. (2016). www.sip-archiv.de - an internet based, interactive archive and database for SIP data. 4th International Workshop on Induced Polarization, Aarhus, Denmark.

Hördt, A., Bairlein, K. Bielefeld, A., Bücker, M., Kuhn, E., Nordsiek, S. & Stebner, H. (2016). The dependence of induced polarization on fluid salinity and pH, studied with an extended model of membrane polarization. Journal of Applied Geophysics, 135, 408–417. DOI: 10.1016/j.jappgeo.2016.02.007.

Hupfer, S., Martin, T., Weller, A., Günther, T., Kuhn, K., Djotsa, V. & Noell, U. (2016). Polarization effects of unconsolidated sulphide-sand-mixtures. Journal of Applied Geophysics, 135, 456–465.

NFDI4Earth (2022), https://www.nfdi4earth.de, last accessed: 2022-05-18.

Nordsiek, S. & Weller, A. (2008). A new approach to fitting induced-polarization spectra. Geophysics, 73(6), F235-F245. DOI: 10.1190/1.2987412.

Pelton, W., Ward, S., Hallof, P., Sill, W. & Nelson, P. (1978). Mineral discrimination and removal of inductive coupling with multifrequency IP. Geophysics, 43, 588–609.

Weller, A., Breede, K., Slater, L. & Nordsiek, S. (2011). Effect of changing water salinity on complex conductivity spectra of sandstones. Geophysics, 76(5), F315–F327.

Weller, A. & Slater, L. (2019). Permeability estimation from induced polarization: an evaluation of geophysical length scales using an effective hydraulic radius concept. Near Surface Geophysics, 17, 581–594. DOI: 10.1002/nsg.12071.

Weller, A., Slater, L., Nordsiek, S. & Ntarlagiannis, D. (2010). On the estimation of specific surface per unit pore volume from induced polarization: a robust empirical relation fits multiple data sets. Geophysics, 75(4), WA105–WA112.

Wilkinson, M. D. et al. (2016). The FAIR Guiding Principles for scientific data management and stewardship. Scientific Data, 3, 160018. DOI:10.1038/sdata.2016.18.

P4 - Ice content Estimation with High-Frequency Induced polarisation

J. Mudler, D. Kreith, M. Sugand, and A. Hördt

TU Braunschweig, Institute of Geophysics and Extraterrestrial Physics, Mendelssohnstr. 3, 38106 Braunschweig, Germany

Presenter: Dennis Kreith (d.kreith@tu-braunschweig.de) **Student**: y
Web page: NA   **Preferred presentation oral/poster:** Poster

Abstract. We suggest a method to estimate ice content of the frozen subsurface based on high-frequeny induced polarization measurements. The method uses a 2-D inversion algorithm to obtain the spatial distribution of five parameters which define the frequency-dependent electrical permittivity with a Cole-Cole type relaxation model. We fit a two-phase model that describes the complex electrical conductivity of a mixture of ice and matrix material to the spectral behaviour of the Cole-Cole model. Ice content is one of the parameters determined during the inversion.

Introduction. Ice content is one essential parameter in permafrost research. It controls the sensitivity of permafrost to climate change (e.g. Pellet et al., 2016) and the change of the landscape due to permafrost degradation (Martin et al., 2019). The estimation of ice content with geophysics normally relies on a combination of different methods, typically DC resistivity and seismic refraction tomography (e.g. Mollaret et al., 2020). However, the necessity of using two methods, which can be logistically difficult, might be overcome by using spectral induced polarization (SIP). This idea exploits the electrical permittivity of ice, which exhibits a characteristic behaviour in the frequency range around 10 kHz. Therefore, by measuring SIP in the frequency range up to 100 kHz, in which case we call the method high-frequency SIP (HFIP), ice content of the frozen subsurface may be estimated with a single method.

Method . Due to electromagnetic (EM) coupling effects, which encompasses all types of coupling between transmitter and receiver cables and the ground, measuring SIP up to 100 kHz or even larger requires special hardware. We use the Chameleon II equipment by Radic Research, which was designed specifically for HFIP measurements. The main features are active probes at the receiver electrodes to minimize any coupling to the receiver, and fibre optic cables connecting transmitter and receiver with each other. Furthermore, Chameleon II uses two transmitters, making sure that the same current flows through each electrode. The transmitter voltage (400 V each) and the imput impedance (1 GΩ) allow measurements even if the contact impedance of the electrodes to the ground is very large, which is the case for capacitive coupling. The equipment was tested at several sites (Mudler, 2021), was investigated with reciprocity tests (Sugand et al., 2022) and has demonstrated its principal feasibility up to frequencies of approx. 200 kHz.

The data are normally taken along profiles with a conventional dipole-dipole configuration, and processed with a 2-D inversion code (AarhusInv), described in Mudler et al. (2019). The 2-D inversion uses a parameterization of the complex electrical permittivity in the following form:

$$\varepsilon_r^* = \varepsilon_{HF} + \frac{\varepsilon_{DC} - \varepsilon_{HF}}{1 + (i\omega\tau)^c} + \frac{1}{i\omega\varepsilon_0\rho_{DC}}$$

(1)

The parameterization is a modified Cole-Cole type model and describes the frequency behaviour with five parameters: the DC resistivity ρ_{DC}, the high-and low-frequency limits of permittivity ε_{HF}, ε_{DC}, the relaxation time τ and frequency exponent c.

In order to calculate the complex electrical conductivity of frozen ground, i.e. ice-containing material, we use the two-phase model suggested by Zorin and Ageev (2017):

$$\tilde{\sigma}_b^k(\omega) = (1 - \alpha)\, \tilde{\sigma}_m^k(\omega) + \alpha\, \tilde{\sigma}_i^k(\omega)$$

(2)

Here, σ_b is the bulk electrical conductivity, σ_m is the complex conductivity of the matrix (i.e. the mixture of the non-ice phases) σ_i is the conductivity of ice, and α is ice content. Parameter k characterises the geometry of the mixture. The complex conductivity of ice is well known and may be described by a Debye type model, a relaxation with relaxation exponent $c=1$. In order to estimate ice content α from a 2-D inversion result, we devised an inversion scheme that fits 5 free parameters included in eq. (2) to the spectra obtained at each cell, defined by eq. (1).

Results. Figure 1 shows sample data sets recorded with the Chameleon II at a permafrost site in the Yakutsk region/Siberia. The data were recorded with a Schlumberger configuration with two different spacings and correspondingly different penetration depths. The long spacing is assumed to penetrate into the frozen layer. The distinct phase minimum at 2 kHz (right panel) corresponds to the frozen layer and is caused by the characteristic spectral behaviour of ice. The short spacing data do not show this peak and reflect the thawed layer above the permafrost.
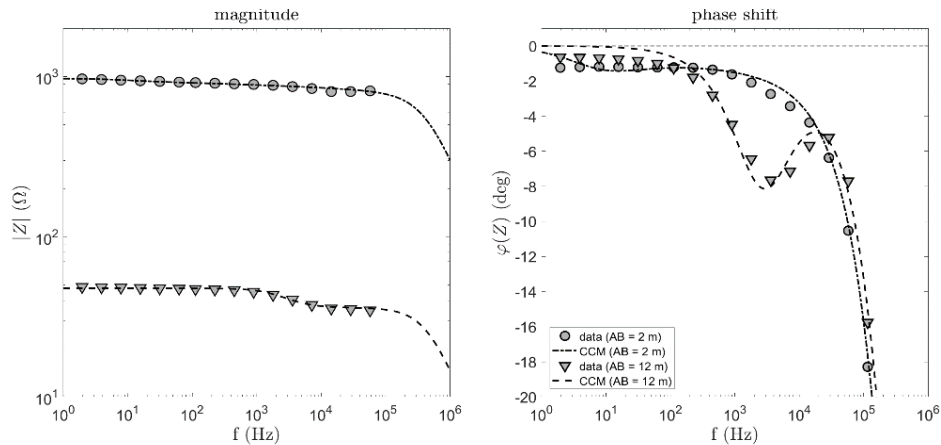
Figure 1: Spectral data recorded with the HFIP equipment (from Mudler et al., 2022). Impedance magnitude (left) and phase shift (right) measured with a Schlumberger configuration with AB=2m and AB=12m. The lines indicate a data fit obtained with eq. (1)

Data were recorded along a 50 m long profile in the Yakutsk region in Siberia using the dipole-dipole configuration. The 2-D inversion result obtained with AarhusInv was used to estimate ice content with the procedure explained above. The result is shown in figure 2. The main feature is an approx. 2m thick layer with non-zero ice content (yellowish colours), corresponding to the known permafrost layer. The near-surface zone corresponds to the active layer which is seasonally thawed. The zone with zero ice content below the frozen layer corresponds to a known feature called talik, which is unfrozen material likely caused by heat transport by groundwater flow. Quantitatively, the ice content estimates agree within 10% with results obtained from ice core measurements taken at well 3/18.
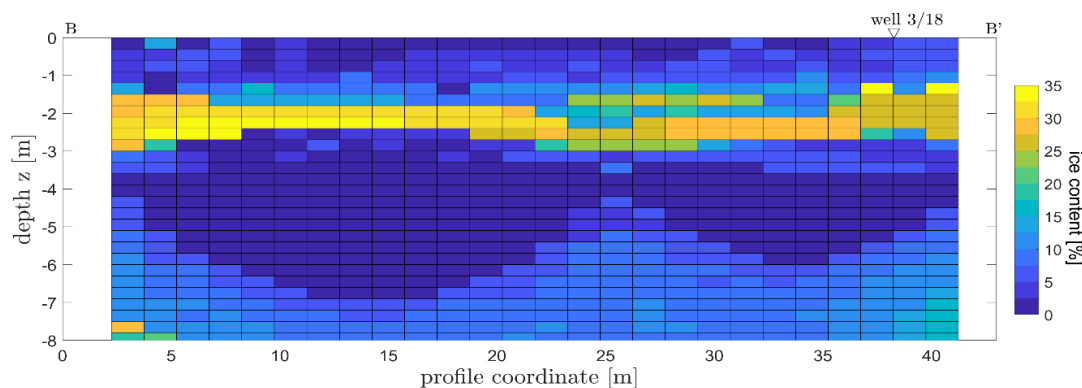
Figure 2: 2-D section of ice content estimated from HFIP data at a permafrost profile in the Yakutsk region, Siberia (from Mudler et al., 2022)

Conclusions. We have demonstrated that ice content estimation with HFIP can be a useful alternative to the conventional combination of DC resistivity with seismic refraction tomography. With the Chameleon II equipment, sufficient data quality can be achieved up to the required frequencies of approx. 200 kHz. The method can differentiate frozen from unfrozen ground and is sufficiently sensitive to provide quantitative ice content estimates with reasonable accuracy.

References

Martin, L. C. P., Nitzbon, J., Aas, K. S., Etzelmüller, B., Kristiansen, H., and Westermann, S., 2019. Stability conditions of peat plateaus and palsas in northern Norway. Journal of Geophysical Research: Earth Surface, 124, 705–719.

Mollaret, C., Wagner, F.M., Hilbich, C., Scapozza, C. and Hauck, C. 2020. Petrophysical Joint Inversion Applied to Alpine Permafrost Field Sites to Image Subsurface Ice, Water, Air, and Rock Contents. Front. Earth Sci. 8:85.

Mudler, J., Hördt, A., Przyklenk, A., Fiandaca, A., Maurya, P.K. and Hauck, C., 2019. Two-dimensional inversion of wideband spectral data from the capacitively-coupled resistivity method - first applications in periglacial environments. The Cryosphere, 13, 2439-2456.

Mudler, J., Hördt, A., Kreith, D., Bazhin, K., Lebedeva, L. and Radic, T., 2022. Broadband Spectral Induced Polarization for the detection of Permafrost and an approach to ice content estimation – A Case study from Yakutia, Russia, The Cryosphere, *submitted.*

Mudler, J., 2021. Kapazitive Geoelektrik und Hochfrequente Spektrale Induzierte Polarisation zur Detektion und Charakterisierung eishaltigen Untergrundes. PhD thesis, TU Braunschweig.

Pellet, C., Hilbich, C., Marmy, A., Hauck, C., 2016. Soil moisture data for the validation of permafrost models using direct and indirect measurement approaches at three alpine sites, *Frontiers in Earth Science*, 3.

Sugand M., Hördt A., Hoppenbrock J., Mudler J., 2022. Reciprocity performance of high-frequency induced polarisation field system, Chameleon II. Annual mtg. German Geoph. Soc., abstract.

Zorin, N. and Ageev, D., 2017. Electrical properties of two-component mixtures and their application to high-frequency IP exploration of permafrost, Near Surface Geophysics, 15, 603 – 613.

P5 - Multi-Frequency excitation speeds up SIP measurement.

T. Radić

Radic Research, Company, Berlin, Germany

Presenter: T. Radić (radic@radic-research.de)   **Student:** No
Web page: www.radic-research.de ; **Preferred presentation:** Poster

Abstract: The multi-frequency excitation allows to determine the complete complex-valued resistivity spectrum of a rock with only one single IP measurement. Using a real measurement, we show that only 34 seconds are required for the selected frequency range (0.03 Hz - 256 kHz). This is the theoretical maximum speed for both frequency and time domain measurements.

Introduction. Spectral IP measurements are usually performed sequentially. This has led to the unfounded prejudice that frequency domain measurements are in principle slower than time domain measurements. Sequential frequency domain measurements were originally introduced to achieve sufficient measurement accuracy even at great exploration depths where time domain measurements failed. The idea: narrowband excitation facilitates the separation of useful and interfering signals. However, if the S/N ratio is high enough, then multi-frequency excitation can also be considered.
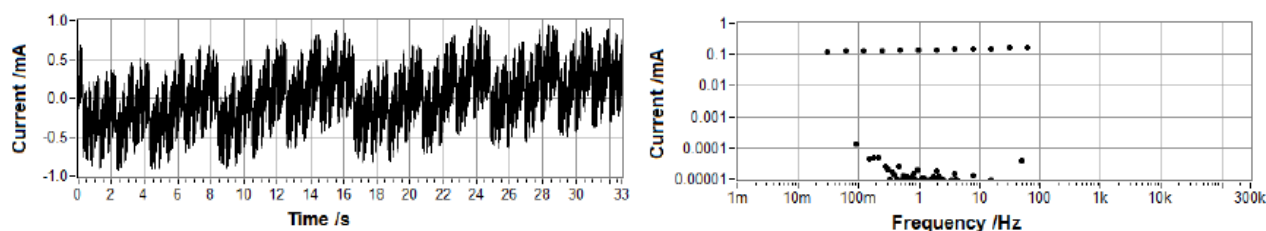
Figure 1. Multi-frequency excitation with 12 frequencies. Left: Time series, Right: Spectrum.

Multi-Frequency Excitation. With single-frequency excitation, a sinusoidal current is fed into the ground and correlated with the resulting voltage signal, which is also sinusoidal. The resulting complex-valued transfer function Z, multiplied by the geometry factor, provides the apparent resistivity for the selected frequency. Further measurements with other frequencies then provide the entire resistivity spectrum. In the case of multi-frequency excitation, on the other hand, some or all frequencies are fed in simultaneously (Fig. 1). The resulting multi-frequency voltage signal can be evaluated using the same algorithms that were used to evaluate the single-frequency measurements. The numerical filters for suppressing drift or technical interference frequencies are also available without modification. In addition, the use of the Reference Noise Cancelation technique (Radić, 2011), which suppresses spatially coherent interference signals, can be combined. If the local noise varies with the frequency, it is possible to individually adjust the amplitudes of the superimposed frequencies.
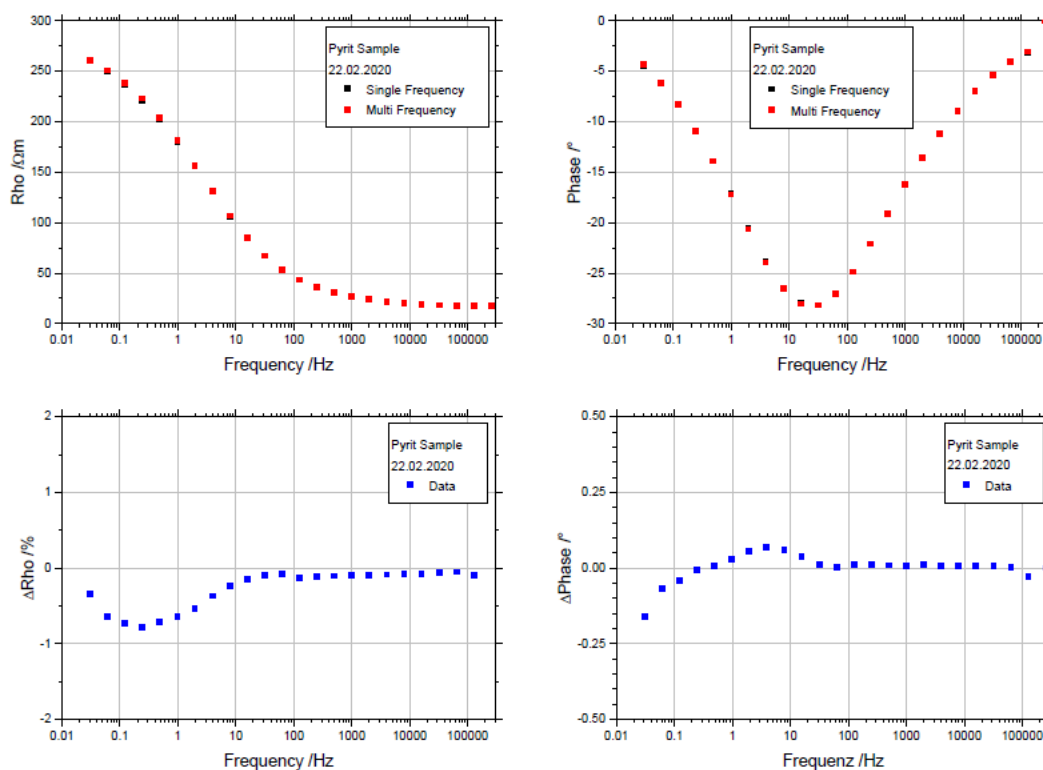
Figure 2. Comparison of the resistivity spectra measured on a pyrite sample single-frequency (black) and multi-frequency (red). Upper row: Amplitude and phase of the resistivity. Lower row: Relative amplitude ratio and absolute phase difference between spectra.

Case Example. Figure 2 compares the results of a conventional, single-frequency measurement with those of a multi-frequency IP measurement. The test material pyrite was in a 200 ml measuring cell. The multi-frequency measurement was performed in two steps of 12 frequencies each. The duration of a multi-frequency measurement is always determined by the lowest frequency used. In this case the lowest frequency was 0.03 Hz and only one period was measured. This measurement thus took 33 seconds. Added to this was the duration of the high-frequency measurement: <1 second. Single and multi-frequency measurement results strongly agree. Small systematic differences, primarily below 10 Hz, were due to the sample material itself. This shows a constant drift of its electrical properties. The hardly noticeable scatter of measured values indicates that the statistical errors are very small.

Conclusions. The first practical tests showed that the measurement progress can be significantly increased by a multi-frequency excitation. We will implement this option in all future field and laboratory measuring instruments. Users of our measuring instruments will then have the possibility to optimally balance measuring accuracy and measuring progress on site.

References

Radić, T. (2011). Improving the IP data quality on field and lab scale by use of the geoelectric reference technique. In: Proceedings of the 2nd International Workshop on Induced Polarization, 31.10-2.11.2011, Golden, USA.

Radić, T. (2022). Effective measurement of both fast and very slow temporal impedance changes. In: Proceedings of the 6th International Workshop on Induced Polarization, 27.-30. June 2022, Annecy, France.

P6 – New hardware for measurement of fast and slow temporal changes of spectral resistivity.

T. Radić

Radic Research, Company, Berlin, Germany

Presenter: T. Radić (radic@radic-research.de)   **Student:**   No
Web page: www.radic-research.de ; **Preferred presentation:**   Poster

Abstract: The measurement of very fast as well as very slow changes in electrical resistivity pose a great challenge for conventional IP measuring devices. We have developed hardware (SIP-COMPACT-S) for small-scale SIP measurements that offers novel technical solutions to both challenges.

Introduction. Conventional SIP instruments are sometimes too slow to capture very fast impedance variations. Even very slow changes can only be captured ineffectively. This is due, among other things, to the high personnel effort required for operation over weeks and months. The multi-frequency excitation allows more than twice the measurement speed. The autonomous operation, on the other hand, allows the detection of very slow changes over a period of up to one year.

Fast SIP measurements. Usually, a SIP measurement is performed sequentially, i.e. frequency by frequency. The new hardware now allows all measurement frequencies to be combined into one measurement signal by superimposition, if required. In this way, the entire impedance spectrum can be acquired in a single measurement process. Thanks to these innovations, the SIP measurement can be accelerated to the maximum possible extent. The achievable temporal resolution is limited only by the duration of one period, the lowest frequency used. In order to also enable continuous measurement, the measured time series are Fourier transformed already during their registration. Gaps caused by signal processing overhead can thus be completely avoided.
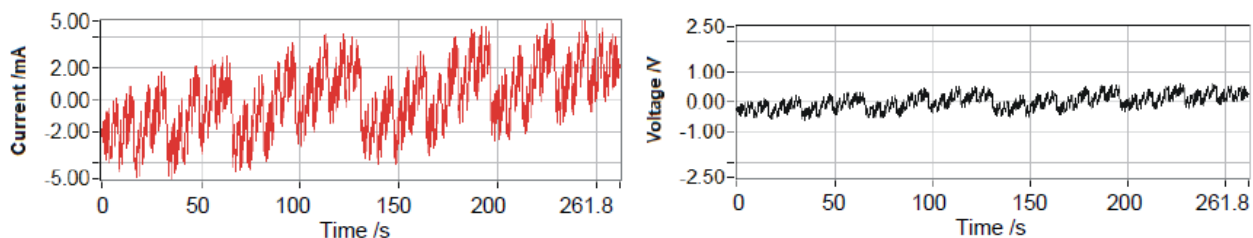
Fig.1: Exemplary representation of a superimposed excitation current (red), as well as the resulting voltage signal (black). Up to 24 frequencies can be superimposed.

Autonomous SIP long-term measurements

The implemented autonomous measurement operation simplifies the performance of long-term measurements, since neither a control computer nor an operator is required for this. Before the start, the desired measurement times and parameters of the spectral measurement are transferred via

WiFi from the notebook to the measuring instrument. Then the autonomous measurement mode starts. Between the individual spectral measurements, the measuring instrument goes into a very energy-saving "sleep". The already measured data can be read out at any time via WiFi from the fail-safe SD card.
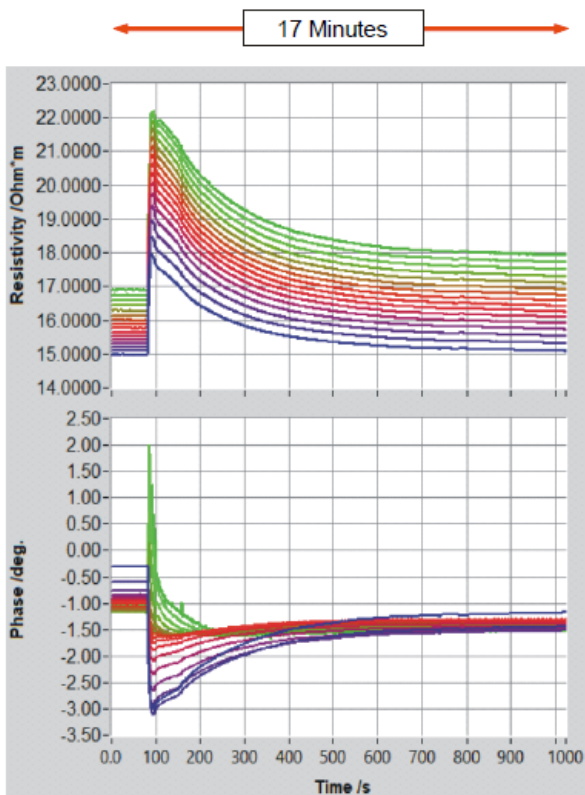
Fig. 2: Impedance spectra measured in fast mode. At 80 seconds, the 10-second sprinkling starts.
Repetition rate: 1.03 Seconds
Multi-Frequency meas.: 0.97 Hz - 32 kHz
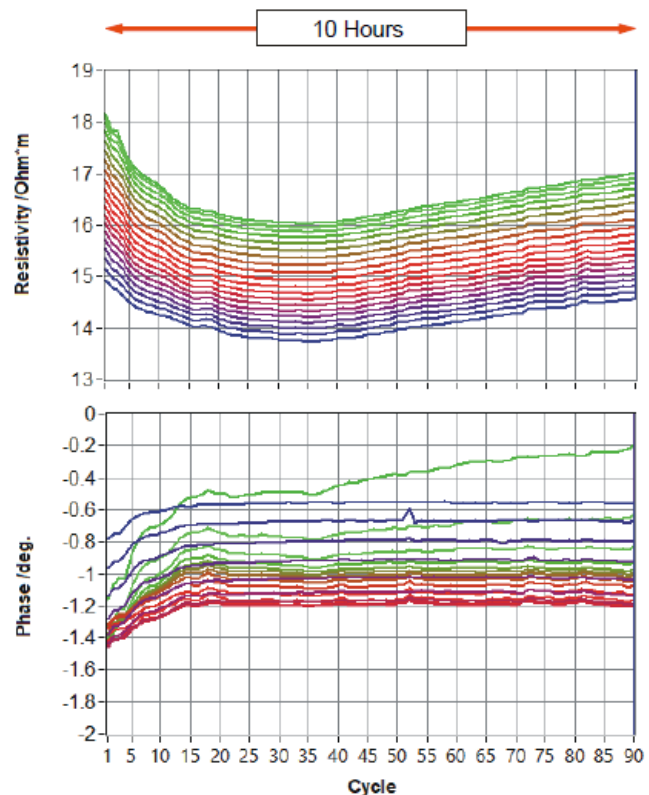
Fig. 3: Impedance spectra measured in autonomous mode. The measurement immediately followed the end of the fast measurement.
Repetition rate: 400 Seconds
Frequency range: 0.061 Hz - 32 kHz

Case Example Lawn (Luebars, Berlin)

On a lawn, the effects of irrigation on the electrical resistivity of the top soil layers should be recorded. For this a dipole-dipole configuration with an electrode spacing of 10 cm was used. The field measurement was divided into 4 time periods:

1. Fast multi-frequency measurement of the resistivity spectrum of the undisturbed lawn soil for 80 seconds.
2. Sprinkling of the lawn in the vicinity of the measuring arrangement for approx. 10 seconds. The fast SIP measurement was not interrupted during this time.
3. Continue fast SIP measurement for another ~16 minutes.
4. This is immediately followed by a 10-hour autonomous measurement.

Conclusions

The comprehensive recording of the effects of 10 second irrigation requires the highest possible measurement progress in the initial phase - which was achieved thanks to the new multi-frequency excitation. As the measurement progresses, the resistivity changes more and more slowly. Here, the autonomous measurement technique proved to be an efficient method of recording them.

Reference

Radić, T. (2022): Multi-Frequency excitation speeds up SIP measurement. In: Proceedings of the 6nd International Workshop on Induced Polarization, 27.-30. June 2022, Annecy, France.

P7 - Anisotropy of induced polarization response- sulfide ore samples

S. Ahmadi[1], A. Coperey[2], A. Ghorbani[1,3], and A. Revil[2]

(1) Yazd University, Department of Mining and Metallurgical Engineering, Yazd, Iran
(2) Univ. Grenoble Alpes, Univ. Savoie Mont-Blanc, CNRS, UMR CNRS 5204, EDYTEM, 73370 Le Bourget du Lac, France
(3) Naga Geophysics, Technolac, 73370 Le Bourget du Lac, France

Presenter: A. Ghorbani (aghorbani@yazd.ac.ir) **Student y/n:** No
Web page: NA   **Preferred presentation oral/poster:** Poster

Abstract. Induced polarization (IP) is a way to determine some of the economic sulfide ores. Two IP parameters, chargeability and phase angle, represent the metallic ores volume and weight content, respectively. The dependency of these parameters on the direction of external electric field injection can affect the content of the metallic ores estimated by the IP. So, in this paper, the chargeability and phase angle anisotropy were studied using the laboratory measurement of the complex conductivity in the frequency range of 10 mHz to 45 kHz, parallel and perpendicular to the bedding on the low to high-grade samples of Pb-Zn mine Koushk, central Iran. The chargeability for the Koushk samples was determined by a double Cole-Cole fit. The results showed that the phase magnitude and the frequency of its peak are different in two directions for all samples. There is no considerable difference between the chargeability in the two directions for the samples.

Introduction

The anisotropy property of the in-phase, quadrature, and complex conductivity was investigated by researchers, like, Siegesmund et al. (1991), Winchen et al. (2009), Revil et al. (2013), Woodruff et al. (2014), Al-Hazaimay (2015), Kenkel and Kemna (2017), and Woodruff et al. (2017). Also, the anisotropy of the phase angle was shown by Zisser and Nover (2009), Zisser et al. (2010), and Kenkel et al. (2012). These studies were conducted on porous media without metallic particles. Börner et al. (2018) and Abdulsamad et al. (2019) observed the anisotropy of the complex conductivity in the media containing graphite plates. In these studies, the anisotropy was attributed to the texture and the preferential orientation of laminated minerals, such as clay, graphite, etc. This anisotropy affects some macroscopic petrophysical properties of the media (e.g., Revil et al., 2013).

The anisotropy of the complex conductivity and phase angle in media with metallic particles was displayed by De Witt (1979) and Wong and Strangway (1981). And after those, based on our knowledge, there is no published study on the anisotropy property of the phase angle and especially, the chargeability in the presence of metallic grains. The phase angle and chargeability are respectively, related to volume content (Revil et al., 2015) and weight content (e.g., Nelson and Van Voorhis, 1983) of the metallic particles. So, studying the anisotropy of IP parameters is useful for a better understanding of the factors affecting the estimation of the metallic content in the porous media. Hence, in the present study, we investigated the anisotropy of the phase angle and chargeability by conducting the complex conductivity on eight samples of mine Koushk, central Iran parallel, and perpendicular to the bedding.

Results and discussion

The samples are ten mineralized clay-rich relatively low porosity dark rocks of the zinc-lead deposit of Koushk, central Iran (Figure 1). The Koushk samples have low to high values (9 to 61 weight percent) of metallic minerals, including pyrite, sphalerite, and Galena. In low-grade samples, like one cylindrical sample with 9 percent ores, the metallic minerals are dispersed into a variscite background. And, in the high-grade samples, e.g., one with 57 percent ores, metallic minerals are located between the layers of the background of illitic clay and have formed a layered structure to them that is observed in microscopic (based on mineralogy studies) and macroscopic scale. The complex conductivity was conducted on these samples, in the frequency range of 10 mHz to 45 kHz in two directions. The electrode configuration was designed so that the current passes the sample parallel to the bedding plane of clay and metallic minerals in one direction, and perpendicular to it in the other. All the Koushk samples are cubic, except one that is cylindrical. The complex conductivity measurement was carried on the later sample in four directions, like what is explained in Woodruff et al. (2014). Cole-Cole parameters were computed by a double Cole-Cole fit (Cole-Cole equation in conductivity form).

The chargeabilities are almost the same whether the applying external electric field is parallel to the bedding or perpendicular to it (Figures 2). While the in-phase and quadrature conductivities, as well as the phase angle magnitude, the frequency of its peak (and as a result the corresponding time constant), and the shape of the phase angle spectrum, is different in parallel and perpendicular to the bedding (Figures 2). We attribute this behavior to the structure of the samples. So that in parallel to the bedding, the layered structure of the metallic and clay minerals increases the conductive paths for the external electric current and decreases the polarizable interfaces compared to the perpendicular to the bedding. Therefore, the IP response parallel to the bedding is smaller than the one perpendicular to it (see, for instance, Nelson and Van Voorhis, 1983).
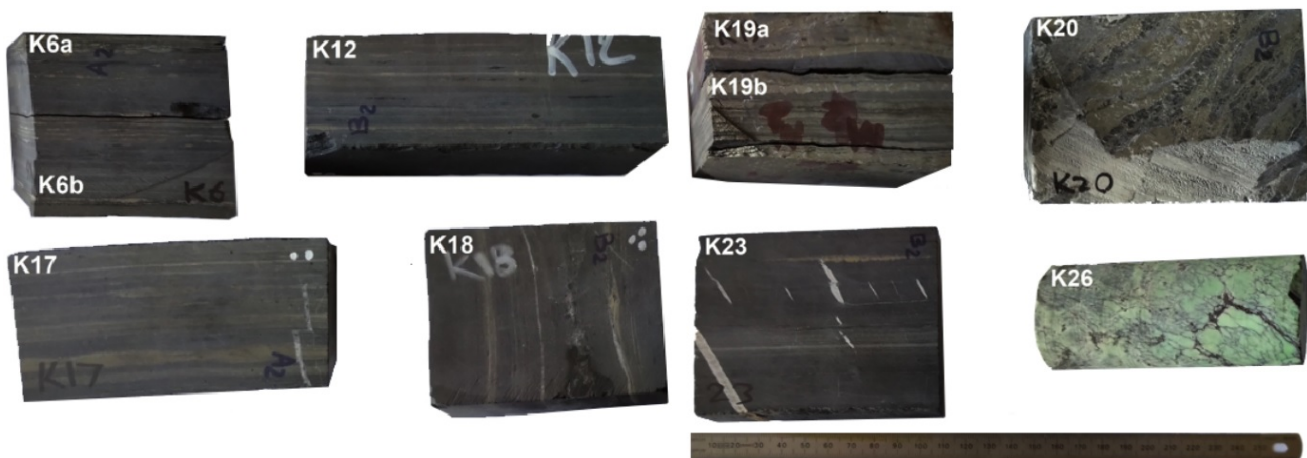
Figure 1. Ten mineralized clay-rich relatively low porosity dark rocks of the zinc-lead deposit of Koushk, central Iran.
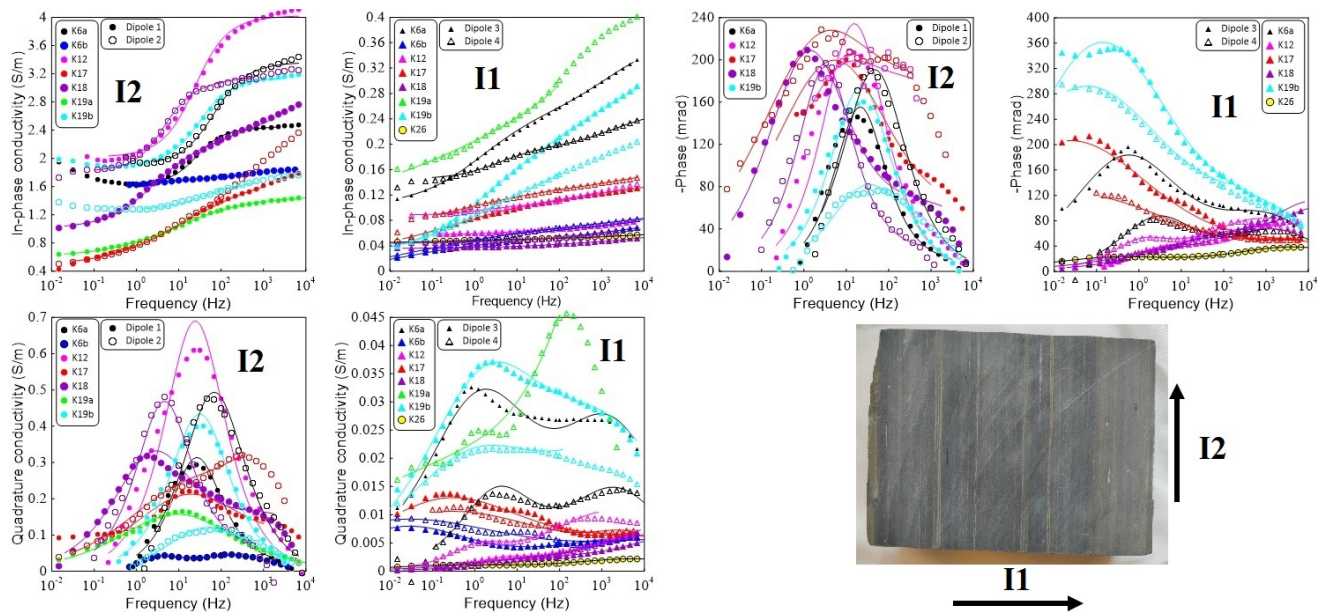
Figure 2. Complex conductivity measurements on the ore samples, Zn-Pb mine Koushk, central Iran.

Conclusions. The measurements were conducted parallel and perpendicular to the bedding of the metallic and clay minerals for the samples of Koushk. The differences between the phase angle magnitude, the frequency of its peak, and the shape of its spectrum for all samples emphasize that the phase angle has the anisotropy property. These observations appeal that the structure can have an influence on the amount of IP response. This effect must be encountered for the estimation of the metallic ores based on the IP responses. However, this property was not observed for the chargeability. We attribute this behavior to the relation between the chargeability and the volume content of the metallic minerals.

References

Abdulsamad, F., Revil, A., Ghorbani, A., Toy, V., Kirilova, M., Coperey, A., Duvillard, P. A., Ménard, G. & Ravanel, L. (2019). Complex Conductivity of Graphitic Schists and Sandstones. Journal of Geophysical Research: Solid Earth, 124(8), 8223-8249. https://doi.org/10.1029/2019JB017628.

Al-Hazaimay, S. (2015). Using the anisotropy of electrical properties for the characterization of sedimentological structures and preferential flow processes. Forschungszentrum Jülich GmbH Zentralbibliothek, Verlag Jülich, ISBN: 978-3-95806-090-6.

Börner, J. H., Girault, F., Bhattarai, M., Adhikari, L. B., Deldicque, D., Perrier, F., & Spitzer, K. (2018). Anomalous complex electrical conductivity of a graphitic black schist from the Himalayas of central Nepal.

Geophysical Research Letters, 45(9), 3984-3993. https://doi.org/10.1029/2018GL077178.

De Witt, G. W. (1979). Parameter Studies of Induced Polarization Spectra. Master's Thesis, University of Utah, Salt Lake City, UT, USA.

Kenkel, J., & Kemna, A. (2017). Sensitivity of 2-D complex resistivity measurements to subsurface anisotropy. Geophysical Journal International, 208(2), 1043-1057. https://doi.org/10.1093/gji/ggw353.

Kenkel, J., Hördt, A., & Kemna, A. (2012). 2D modelling of induced polarization data with anisotropic complex conductivities.

Near Surface Geophysics, 10(6), 533-544. https://doi.org/10.3997/1873-0604.2012050.

Nelson, P. H., & Van Voorhis, G. D. (1983). Estimation of sulfide content from induced polarization data. Geophysics, 48(1), 62-75. https://doi.org/10.1190/1.1441408.

Revil, A., Florsch, N., & Mao, D. (2015). Induced polarization response of porous media with metallic particles- Part 1: A theory for disseminated semiconductors. Geophysics, 80(5), D525-D538. https://doi.org/10.1190/GEO2014-0577.1.

Revil, A., Woodruff, W. F., Torres-Verdín, C., & Prasad, M. (2013). Complex conductivity tensor of anisotropic hydrocarbon-bearing shales and mudrocks. Geophysics, 78(6). https://doi.org/10.1190/GEO2013-0100.1.

Siegesmund, S., Vollbrecht, A., & Nover, G. (1991). Anisotropy of compressional wave velocities, complex electrical resistivity, and magnetic susceptibility of mylonites from the deeper crust and their relation to the rock fabric. Earth and Planetary Science Letters, 105(1-3), 247-259. https://doi.org/10.1016/0012-821X(91)90134-4.

Winchen, T., Kemna, A., Vereecken, H., & Huisman, J. A. (2009). Characterization of bimodal facies distributions using effective anisotropic complex resistivity: A 2D numerical study based on Cole-Cole models.Geophysics, 74(3), A19-A22. https://doi.org/10.1190/1.3113986.

Wong, J., & Strangway, D. W. (1981). Induced polarization in disseminated sulfide ores containing elongated mineralization. Geophysics, 46(9), 1258–1268. https://doi.org/10.1190/1.1441264.

Woodruff, W. F., Lewan, M. D., Revil, A., & Torres-Verdín, C. (2017). Complex electrical conductivity changes associated with hydrous pyrolysis maturation of the Woodford Shale. Geophysics, 82(2), D85–D106. https://doi.org/10.1190/GEO2016-0279.1.

Woodruff, W. F., Revil, A., & Torres-Verdín, C. (2014). Laboratory determination of the complex conductivity tensor of unconventional anisotropic shales. Geophysics, 79(5), E183–E200. https://doi.org/10.1190/GEO2013-0367.1.

Zisser, N., & Nover, G. (2009). Anisotropy of permeability and complex resistivity of tight sandstones subjected to hydrostatic pressure. Journal of Applied Geophysics, 68(3), 356-370. https://doi.org/10.1016/j.jappgeo.2009.02.010.

Zisser, N., Kemna, A., & Nover, G. (2010). Relationship between low-frequency electrical properties and hydraulic permeability of low-permeability sandstones. Geophysics, 75(3), E131-E141. https://doi.org/10.1190/1.3413260.

P8 – Electromagnetic coupling in time and frequency domains induced polarization- a review

A. Ghorbani[1,2] and P. Vaudelet[2]

(1) Yazd University, Department of Mining and Metallurgical Engineering, Yazd, Iran
(2) Naga geophysics : Naga Geophysics, Technolac, 73370 Le Bourget du Lac, France

Presenter: A. Ghorbani (ah.ghorbani@yahoo.fr) **Student y/n:** No
Web page: NA **Preferred presentation oral/poster:** poster

Abstract. Induced polarization (IP) method is used in mining and environmental exploration. In recent years, the demand for the exploration of deep induced polarization has increased. In deep induced polarization measurements, the noise due to EM coupling affects the data even in the time domain in the absence of a current source signal. As a result, it is necessary to better understand the effect of EM coupling on IP data in both of time and frequency domains. In this study, we show the induction polarization response and EM coupling for a homogeneous half space, in time and frequency domains. we review the researchs done to remove the EM coupling effect. The result shows that EM coupling effect is important in both of time- and frequency domain IP.

Introduction

Undesired electromagnetic (EM) coupling in induced polarization (IP) measurements between the grounded wire pairs for current and potential measured circuits is result of capacitive coupling between the electrically conductive shield of the cable and the electrically conductive environment surrounding the electrode cables and the conductive ground. Depending on the electrical properties of the ground and the measured transfer impedances, EM coupling will create transient voltages, like induced polarization (IP) effects that are not due to electrical polarization. In the present study, we calculate the mutual impedance of a complex resistive half space, in both of frequency- and time domain IP measurements. This is followed by a review of some coupling removal methods.

In most IP studies, in order to reduce the EM coupling effects, the current frequency is limited to less than 100 Hz. In time domain IP measurements, a delay time on decay curve is used to remove the transient voltages associated with the high frequency part of spectrum. A number of studies remove/reduce EM coupling using practical methods as Dahlin and Leroux (2012); Schmutz et al. (2014); Zhao et al. (2015). A number of studies present EM coupling in the frequency domain and e.g., Millett (1967), Hohmann (1973), Dey and Morrison (1973), Hallof (1974), Wynn and Zonge (1975), Pelton et al. (1978), Coggon (1984), Wang et al. (1985), Tripp et al. (1990), Routh and Oldenburg (2001), Ingeman-Nielsen and Baumgartner (2006).

Less study has been done on EM coupling in the time domain. Dey and Morrison (1973) using fast Fourier transform, calculate time domain coupling curves for the dipole-dipole configuration over a homogeneous half-space and a suite of multi-layer cases. Trofimenkoff et al. (1982) derived late-time coupling formulation for dipole-dipole and Schlumberger configurations on a half-space, based on the exact expression for parallel wire coupling. Johnson (1990) modelled the measured voltage decay as a superposition of two Cole-Cole transients, one for the IP component and one for the EM-coupling component. Fullagar et al. (2000) used the EM half-space response that best fits the observed data is

subtracted to yield a de-coupled IP decay. Their procedure has been implemented for dipole-dipole arrays. Ji-Shan et al. (2008) concludes that for the routine charging and discharging time of IP method, the course of EM coupling for middle-grads and dipole-dipole configurations are less than 10^{-2} s. Mocitaiba et al. (2017) analysis the decay voltage in the time domain and shows that the contribution of the EM coupling to the chargeability has to be taken into account if the induction number is higher than a critical value. For a half space, this value corresponds to the case when the resistivity of the ground is equal or lower than 10 m, especially if the Dipole length of a Dipole-Dipole array is larger than 50 m and the separation between the current and the potential Dipoles is larger than twice the Dipole length.

EM coupling for Dipole-Dipole array on a Half space

a. Frequency domain. We used CR1Dmod (Ingeman-Nielsen and Baumgartner 2006) to calculate the mutual impedance of half space in frequency domain for Dipole-Dipole array. The complex resistivity of half space is modelled using Cole-Cole model (Pelton et al., 1978). Figure 1a shows the real and the imaginary part of resistivities spectra for the resistive half space (ρ=1 Ωm, dash lines) and for the complex resistive half space (Cole-Cole parameters: ρ=1 Ωm, chargeability m=0.1, time constant τ=0.01 sec and exponent c=0.5, lines). Dipole-Dipole electrode spacings, *a*, are 100, 300 and 600 m. Dipole-Dipole *n* is considered constant and 6 for three cases. The real and the imaginary part of Cole-Cole half space is also shown for resistive and complex resistive half spaces. For a resistive half space, increasing the electrode spacing *a*, the real and the imaginary part of the mutual impedances don't vary but shift to lower frequencies. For a complex resistive half space with the same resistivity, the real and the imaginary part of the mutual impedances change very slowly with changing *a*. as shown in Figure 1a, Cole-Cole parameters to be able to extract from the difference between the mutual impedance of pure resistive half space and the mutual impedance of complex resistive half space.

b.Time domain. Discrete Fourier transform (DFT) is used to transfer the mutual impedance calculated above to the time domain decay voltages. The result is also recalculate using Fast Fourier Transform (FFT). Figure 1b shows the decay curves for the same Dipole-Dipole arrays and the same half spaces. As shown in Figure 1b, the difference between the pure resistive half space and the complex resistive half space with the same resistivity is small. This result shows that the de-coupling method represented by Fullagar et al. (2000) can be critical. EM coupling affect strongly the decay curve when electrode spacing increase. When *a* is large, Siegel chargeability (Seigel, 1959) is 50% (Eadie, 1981). Figure 1c shows the partial chargeabilities as a function of middle time of windows. The partial chargeability is calculated considering 1) Cole-Cole mode with 20 windows and 2) arithmetic windows mode (windows width are equal to 80 msec). however, when electrode spacing is large, both of early-time and late times are affected by EM coupling. Table 1 shows the integrated chargeability for the case represented above.

Conclusion. Time domain and frequency domain courses of the mutual impedance is calculated for both of the pure resistive and the complex resistive homogenous half space. We also reviewed the research works in EM coupling removal, especially in time domain. The result shows that EM coupling effect is important in both of time- and frequency domain IP.
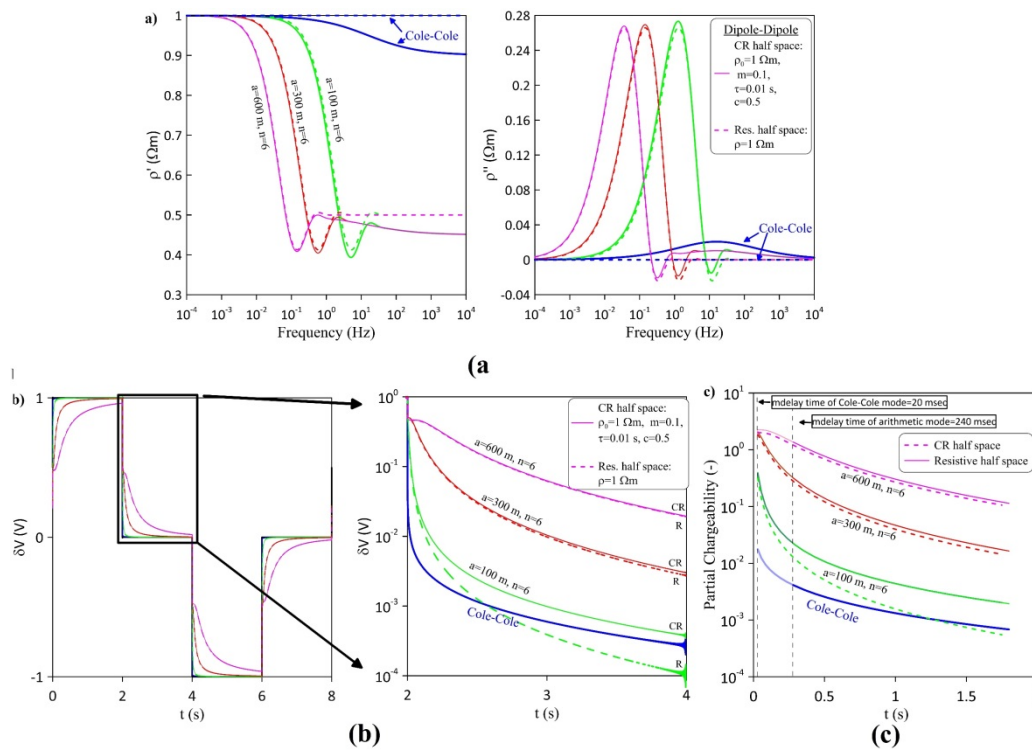
Figure 1. a) The real and the imaginary part of the mutual impedance as a function of frequency, b) The decay curves of the mutual impedances and c) The partial chargeability curves. Array is Dipole-Dipole with a=100, 300 and 600 m and n=6. Dash lines show the result of a pure resistive half space (ρ=1 Ωm) and lines show the result for the complex resistive half space. Complex resistivity of half space is Pelton (1978) equation: ρ_0=1 Ωm, m=0.1, τ=0.01 sec and c=0.5 (blue line). The partial chargeability is calculated for Cole-Cole mode (20 windows and delay time 20 msec) and arithmetic mode (20 windows with equal width 80 msec and delay time 240 msec).

Table 1. The integrated chargeability for the example of Figure 1.

	Pure resistive half space (ρ=1 Ωm)		Complex resistive half space (ρ_0=1 Ωm, m=0.1, τ=0.01s, c=0.5)	
	Arithmetic mode	Cole-Cole mode	Arithmetic mode	Cole-Cole mode
TD Cole-Cole	0	0	1.6	2.4
DD: n=6, a=100 m	2.8	11.8	6.3	18.0
DD: n=6, a=300 m	66.3	162.0	76.9	185.1
DD: n=6, a=600 m	376.3	542.7	425.3	612.4

References

Coggon, J.H. (1984). New three-point formulas for inductive coupling removal in induced polarization. Geophysics, 49, 307-309.

Dahlin, T., & Leroux, V. (2012). Improvement in time-domain induced polarization data quality with multi-electrode systems by separating current and potential cables. Near surface Geophysics, 10(6), 545-565.

Dey, A., & Morrison, H.F. (1973). Electromagnetic coupling in frequency and time-domain induced polarization surveys over a multilayered earth. Geophysics, 38, 380-405.

Eadie, E.T. (1981). Detection of hydrocarbon accumulation by surface electrical methods - a feasibility study. Research in Applied Geophysics #9, Geophysics Laboratory, Univ. of Toronto.

Fullagar, P.K., Zhou, B., & Bourne, B. (2000). Electromagnetic coupling removal from time domain IP data. Exploration Geophysics, 31, 134-139.

Hallof, P.G. (1974). The IP phase measurement and inductive coupling. Geophysics, 39, 650-665.

Hohmann, G.W. (1973). Electromagnetic coupling between grounded wires at the surface of a two-layer Earth. Geophysics, 38, 854-863.

Ingeman-Nielsen, T., & Baumgartner, F. (2006). CR1Dmod: a Matlab program to model 1D complex resistivity effects in electrical and EM surveys. Computers & Geosciences, 32, 1411–1419.

Ji-Shan, HE., Bin, X., Li-Zhi, B., & Yun-Chun, Y. (2008). Time characteristics of EM coupling in Induced Polarization. Chinese Journal of Geophysics, 51(3), 645-653.

Johnson, I.M. (1990). Spectral IP parameters derived from time domain measurements, in Fink, J.B., Sternberg, B.K., McAlister, E.O., Wieduwilt, W.G. and Ward, S.H., Eds., Induced Polarization - Applications and Case Histories: Society of Exploration Geophysicists, 57-78.

Millet, F.B. Jr. (1967). Electromagnetic coupling of collinear dipoles on a uniform half-space. In: Hansen D.A., Heinrichs W.E., Holmer R.C., MacDougall R.E., Rogers G.R., Sumner J.S. and Ward S.H. (Eds), Mining Geophysics, Volume II, Theory. Society of Exploration Geophysicists, Tulsa, OK, 401-419, DOI: 10.1190/1.9781560802716.ch2e.

Mocitaiba, L.S.R., Sampaio, E.E.S., & de Lima, O.A.L. (2017). Effect of coupling noise on the interpretation of results of electromagnetic horizontal sounding and modeling. Stud. Geophys. Geod., 61, Doi: 10.1007/s11200-015-0348-5.

Pelton, W.H., et al. (1978). Mineral discrimination and removal of EM coupling with multi-frequency IP. Geophysics, 43, 588-609.

Routh, P.S., & Oldenburg, D.W. (2001). Electromagnetic coupling in frequency-domain induced polarization data: a method for removal. Geophysics Journal International, 145, 59-76.

Schmutz, M., Ghorbani, A., Vaudelet, P., & Blondel, A. (2014). Cable arrangement to reduce electromagnetic coupling effects in spectral-induced polarization studies. Geophysics, 79(2).

Seigel, H.O. (1959). Mathematical formulation and type curves for induced polarization. Geophysics, 24, 547-565.

Tripp, A.C., et al. (1990). Induced-polarization spectral interpretation including electromagnetic coupling data - a field example, in Fink, J.B., Sternberg, B.K., McAlister, E.O., Wieduwilt, W.G., and Ward, S.H., Eds., Induced Polarization - Applications and Case Histories: Society of Exploration Geophysicists, 179-198.

Trofimenkoff, et al. (1982). Electromagnetic coupling between parallel lines on a uniform earth. IEEE Trans. Geoscience and Remote Sensing, GE-20, 197-200.

Wang, J. et al. (1985). Fundamental characteristics of an approximate correction method for electromagnetic coupling in frequency-domain induced polarization. Geophysics, 50(2), 235-241.

Wynn, J.C. & Zonge, K.L. (1975). EM coupling - its intrinsic value, its removal, and the cultural coupling problem. Geophysics, 40, 831-850.

Zhao, Y., Zimmermann, E., Huisman, J.A., Treichel, A., Wolters, B., Van Waasen, S., & Kemna, A., 2015, Phase correction of electromagnetic coupling effects in cross-borehole EIT measurements, Measurement Science and Technology, 26.

P9 - On a new method for the determination of Relaxation Time Distributions

A. Maineult[1] and N. Florsch[1,2]

(1) Sorbonne Université, CNRS, EPHE UMR 7619 METIS, France
(2) Sorbonne Université, UMI 209 UMMISCO, France

Presenter: A. Maineult (alexis.maineult@sorbonne-universite.fr) **Student y/n:** No
Web page: NA   **Preferred presentation oral/poster:** poster

Abstract. In this work, we assume that a Relaxation Time Distribution (RTD) can be approximated by a spline, which has the advantage to be a "smooth" function. Searching for the RTD is equivalent to determining the ordinates of the nodes defining the spline.

Introduction: the problem. To estimate the characteristic relaxation times of the polarization phenomena producing an IP response σ^*, it is useful to use the following decomposition (e.g., Florsch et al. 2014):

$$\sigma^* = \sigma_\infty + \left(\sigma_0 - \sigma_\infty\right) \int_0^{+\infty} \frac{G(\tau)}{1 + 2i\pi f\tau}\,d\tau \quad (1)$$

where σ_∞ (resp σ_0) is the real part of the conductivity at high (resp. low) frequencies, f is the frequency, and G is the distribution of the relaxation times. The objective is to determine the distribution G which explains the observed spectra σ^*. But two difficulties arise: a) formulation (1) does not take into account the increase of the phase at frequencies above 1000 Hz, and b) we cannot determine separately the term (σ_0 - σ_∞) and the right amplitude of G. As a consequence, we propose to use the following formulation:

$$\sigma^* = \sigma_\infty + M \int_0^{+\infty} \frac{G_n(\tau)}{1 + 2i\pi f\tau}\,d\tau + 2i\pi fC \quad (2)$$

where M is a real number and C a capacitance, both to be determined, and G_n is the normalized distribution we are looking for.

The solution. We propose to use a cubic spline for G_n. It is therefore perfectly defined by the abscissae and ordinates of its nodes, and has the advantage of being continuous and derivable twice. As a first step, we take one point per decade for the abscissae, and determine the ordinates as well as σ_∞, M and C using the Simulated Annealing (SA) method (by modifying the code by Maineult (2016)). As a second step, we take two points per decade and run again the SA procedure, starting from the solution determined in Step 1. For Step 2, we also try to add a regularization term on the first derivative, and another on the second derivative.

Applications. We validated our code by testing it on the distribution associated to the Cole-Cole model, and as expected we retrieved the right G_n (not shown here). We also considered a real IP spectra, obtained on an artificial sample of illite saturated with a 0.01 M NaCl solution (Mendieta et al., 2021). In this case, the validation is obtained by comparing the obtained G_n to the distribution produced by another code using a different approach (Florsch et al., 2014). The results are shown in Figure 1: both codes produce similar curves, provided that a regularization is used to avoid oscillations during refinement.

Conclusions. We developed a simple way to determine the RTD, with a minimal regularization procedure. It has also the advantage to estimate the capacitive term which disturbs the spectra at high frequencies.
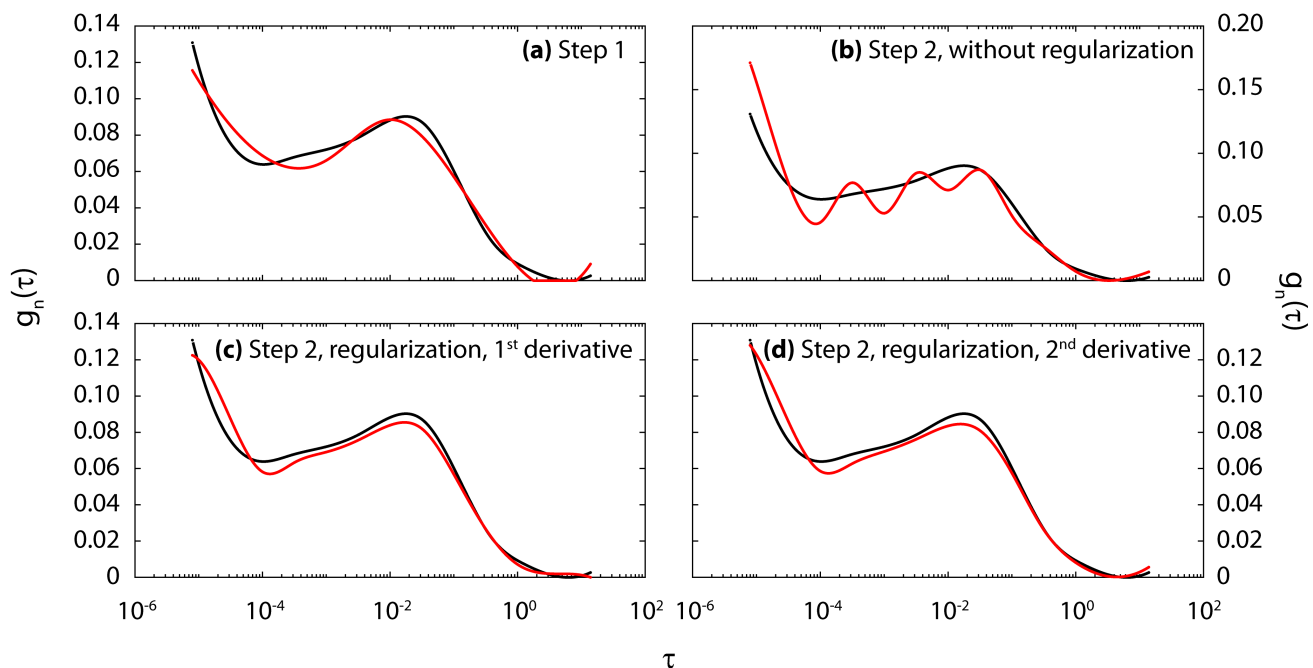
Figure 1. RTD obtained by our procedure (in red), and by Florsch et al.'s code (in black), for an artificial illite sample saturated with 0.01 M NaCl solution.

References

Florsch, N., Revil, A. & Camerlyck, C. (2014). Inversion of generalized relaxation time distributions with optimized damping parameter. Journal of Applied Geophysics, 109, 119132.

Maineult, A. (2016). Estimation of the electrical potential distribution along metallic casing from surface self-potential profile. Journal of Applied Geophysics, 129, 6678.

Mendieta, A., Leroy, P., Jougnot, D. & Maineult A. (2021). Spectral induced polarization characterization of non-consolidated clay samples for varying salinities – an experimental study. Journal of Geophysical Research Solid Earth, 126(4), e2020JB021125.

P10 - Comparative analysis on IP data obtained in LNAPL contamination sites of different concentrations

B. Kim[1*], H. Yu[2], S. Y. Song[2], I. S. Joung[2], A. Cho[2], J. Jeong[2], J. S. Son[3], M. J. Nam[2,4**]

(1) DGR/CIM, BRGM, France
(2) Department of Energy and Mineral Resources Engineering, Sejong University, South Korea
(3) KIGAM, South Korea
(4) Department of Energy Resources and Geosystems Engineering, Sejong University, South Korea
* formerly, Sejong University, South Korea
** Corresponding author, nmj1203@gmail.com/nmj1203@sejong.ac.kr

Presenter: B. Kim (bkim@brgm.fr) **Student y/n:** y (post-doc)
Web page: NA   **Preferred presentation oral/poster:** Poster

Abstract. Comparative analyses were made on induced polarization (IP) data obtained in two-different LNAPL contaminated sites, which have different pollution concentration. The first site shows relatively low TPH concentration with a maximum value of 1180 mg/L, while the second severely high concentration TPH a maximum value of 10,000 mg/L. Complex resistivity (CR) surveys were also performed for both sites using the same instrument, a transmitter of ZT-10 and a receiver of GDP-26 (Zonge) at the same source frequencies of 0.125, 1, and 8 Hz, together with direct current (DC) resistivity surveys with the same geometries of the CR ones. For the interpretation of the field data, 2D inversion was performed using commercial software (DC2Dpro for DC resistivity data and DC2DproCR for CR data), while 3D inversion using in-house algorithms.

For the first site, recovered resistivity sections located geological bedrock structures even though delineation of the contaminated region was not vogue. Phase sections recovered from CR data show strong IP anomalies, some of which matched well with high TPH value points. Contrastingly, to the first site, conductive zones in resistivity sections for the second site matched with high TPH regions while phases become close to zero values near the high TPH regions. Considering the fact that IP effects increased moderately with increasing contamination concentration but decreased above the saturation concentration (Orozco et al., 2012; Johansson et al., 2015), we can make discussion on IP effects of LNAPL as an extension of the previous studies. This study is supported by SEM project no.2018002440005.

References

Orozco, A. F., Kemna, A., Oberdörster, C., Zschornack, L., Leven, C., Dietrich, P., & Weiss, H. (2012). Delineation of subsurface hydrocarbon contamination at a former hydrogenation plant using spectral induced polarization imaging. Journal of contaminant hydrology, 136, 131-144. https://doi.org/10.1016/j.jconhyd.2012.06.001.

Johansson, S., Fiandaca, G., & Dahlin, T. (2015). Influence of non-aqueous phase liquid configuration on induced polarization parameters: Conceptual models applied to a time-domain field case study. Journal of Applied Geophysics, 123, 295-309. https://doi.org/10.1016/j.jappgeo.2015.08.010.

P11 - Analysis on fitting time domain decaying curves from time domain induced polarization inversion for NAPL synthetic models

J. Jeong[1], B. Kim[2*], D. Caesary[1], Y. S. Mun[3], and M. J. Nam[1, 4**]

(1) Department of Energy and Mineral Resources Engineering, Sejong University, South Korea
(2) DGR/CIM, BRGM, France
(3) DevBox Inc.
(4) Department of Energy Resources and Geosystems Engineering, Sejong University, South Korea

* Formerly, Sejong University, South Korea
** Corresponding author, nmj1203@gmail.com/nmj1203@sejong.ac.kr

Presenter: Juyeon Jeong (juhaappyy@gmail.com) Student **y/n:** y
Web page: NA   **Preferred presentation oral/poster:** Poster

Abstract. Among various induced polarization (IP) methods, Time-domain (TD) IP is the most commonly used ones thanks to the effectiveness of the survey, while spectral IP (SIP) using many different-frequency sources is the most time consuming but can provide with Cole-Cole parameters. For the analysis on Cole-Cole parameters or the dispersion characteristics of complex resistivity (CR), SIP measurements have been conducted in laboratory scale experiments. Theoretically, the dispersion curves of CR with respect to source frequencies in SIP should be identically correspond to the decaying curves of time gates measurements of TD IP when identical sources are used. However, limited ranges of measurement time and number of source frequencies results in dissimilarities between SIP and TD IP. Despite the dissimilarities, studies have been made to mutually interpret between TD IP and SIP data while the modern instruments have been advanced measurable sampling rates.

In this study, we conducted numerical experiments to estimate Cole-Cole parameters by fitting time decaying curves of inverted TD IP time-channel decaying curve data. The Cole-Cole model parameters from TD IP decay curves are compared with SIP-based estimation of Cole-Cole parameters for the same anomalies. To make more realistic synthetic models, we digitized and fitted SIP dispersion curves measured in various experimental studies for NAPL contaminated samples especially before and after biodegradation. After numerically simulating TD IP decaying curve for the NAPL contaminated models, TD IP inversion was performed for the synthetic decaying curve to estimate Cole-Cole parameters through fitting the inverted decaying curve for each inversion block. After repeating the process for SIP, we compare estimated Cole-Cole parameters with the TD IP estimation in order to analyze how precisely Cole-Cole parameters can be recovered by making not only TD IP but also SIP surveys. This study is supported by SEM project no.2018002440005.

P12 - Geophysical mapping of aquifer properties in infrastructure projects using DCIP and MRS

T. Martin[1], M. A. Kass[2], D. Grombacher[2], G. Fiandaca[3], C. Butron[4], M. Griffiths[2], M. Østbjerg Vang[2], S. Rejkjaer[1], A. Mendoza[1] & T. Dahlin[1]

(1) Lund University, Engineering Geology, Lund, Sweden
(2) Aarhus University, Geoscience Department, Hydrogeophysics Group Aarhus, Denmark
(3) University Milano, Department on Earth Sciences "Ardito Desio", Milano, Italy
(4) Trafikverket – Swedish Transport Administration, Sweden

Presenter: T. Martin (tina.martin@tg.lth.se)   **Student y/n:** No
Web page: NA   **Preferred presentation oral/poster:** poster

Abstract. The derivation of hydrological properties from IP results is a big research topic and target of many investigations. In contrast to just punctual information from selected drilling points, it would enable the mapping of large areas which is crucial for many applications as (e.g.,) groundwater detection and protection, for environmental purposes and for infrastructure projects. So far, the link between IP and permeability resp. hydraulic conductivity has been mainly shown in laboratory investigation. In our study we use DCIP at different field sites and compare the data with the existent hydraulic information won from slug tests or grain size analysis. We also combine DCIP with the magnetic resonance sounding (MRS) since it enables us to get the water content along the profiles and to compare MRS and DCIP with the known hydraulic properties. Our first results reveal a good comparability, depending on the site conditions. Nevertheless, the data processing and interpretation is still ongoing.

Introduction

Information about the groundwater is crucial in order to protect groundwater resources and to avoid structural and environmental problems in infrastructure projects. To determine the hydrogeological properties in an aquifer, usually drillings followed by hydraulic tests are conducted which are reliable but expensive and, in most cases, only give point-scale information. The use of geophysical methods can overcome this problem and help to minimize drillings and therefore provide continuous information while also saving resources, time and budget. It is known that the Induced Polarization (here referred to as DCIP - Direct Current resistivity and time-domain Induced Polarization) can give information about the permeability and thus about the hydraulic conductivity (Revil et al. 2012, Weller et al. 2015). In addition, MRS (Magnetic Resonance Sounding) can provide information about the water content and pore size characteristics and therewith information related to the intrinsic permeability and the hydraulic conductivity (Schirov et al. 1991). By combining both methods and use them in a two- or three-dimensional approach, a more elaborated interpretation of the underground is possible. To evaluate these methods and to test different site scenarios, we have applied these methods to three different test sites in Sweden that were chosen based on their different geological setting and their electromagnetic noise level.

Test sites and Measurements

Test site 1 is located in the very South of Sweden (Svedala) and characterized by sandy and clayey material, with available hydraulic conductivity test data. Here, several DCIP profiles were measured using the ABEM Terrameter LS2. At this site also 10 MRS soundings were conducted with

the Apsu system (Larsen et al. 2020). The subsurface conditions of test site 2, locate close to Mariestad, consists mainly of glacial clay in varying thicknesses but also an esker structure is present. The electromagnetic noise level was higher compared to test site 1 and mainly caused by houses nearby, buried pipes, power lines and electrical fences. Several DCIP profiles and MRS soundings were performed at test site 2 with the same instrumentation. The third test site is close to Hässleholm and was chosen due to their very low noise level and their esker, sandy moraine, and postglacial sand occurrence. At this site the MRS and DCIP profiles were taken on the same profiles and the interpretation will be supported by drillings and slug tests, determining the hydrological properties along these profiles.

The data processing and inversion is done subsequently. For the DCIP data, a processing after Olsson et al 2016 (e.g., de-noising, drift correction, spike removal, etc.) was carried out before it was auto processed and hand checked to remove outliers and negative data points. The inversion was conducted based on the inversion routine from Fiandaca et al 2021 with a direct inversion for the hydraulic conductivity. The MRS data were acquired using a steady-state acquisition scheme (Grombacher et al. 2021) and follow a stepwise processing procedure which includes despiking, Wiener filtering with remote reference noise coils, Larmor frequency estimation, and removal of power line signal. Data were subsequently inverted for water content and relaxation parameters related to grain size distribution.

Results and Discussion

In general, the DCIP data quality is good at all test sites. Depending on the expected underground material (sand, clay, esker) the resistivity changes in the different layers. The chargeability values are usually quite small at all profiles. In **Figure 3**, an example of an DCIP profile in Mariestad on a very clayey site can be seen. The conductivities on top are characterized by high values whereas in depth the conductivity decreases. That can be related to the clay lying above the sand moraine. The known hydraulic conductivity value from that profile (in the middle of the profile) was $2*10^{-5}$ m/s and is in good agreement with the inverted K-value ($10^{-4} - 10^{-5}$ m/s). The MRS data reveal mostly low water content at test site 1 with some occasional higher contents at the western part. At test site 2 elevated noise was present which affected the MRS data quality considerably. At test site 3, high-quality data were acquired coincident with the DCIP data with high lateral resolution along the 4 lines.
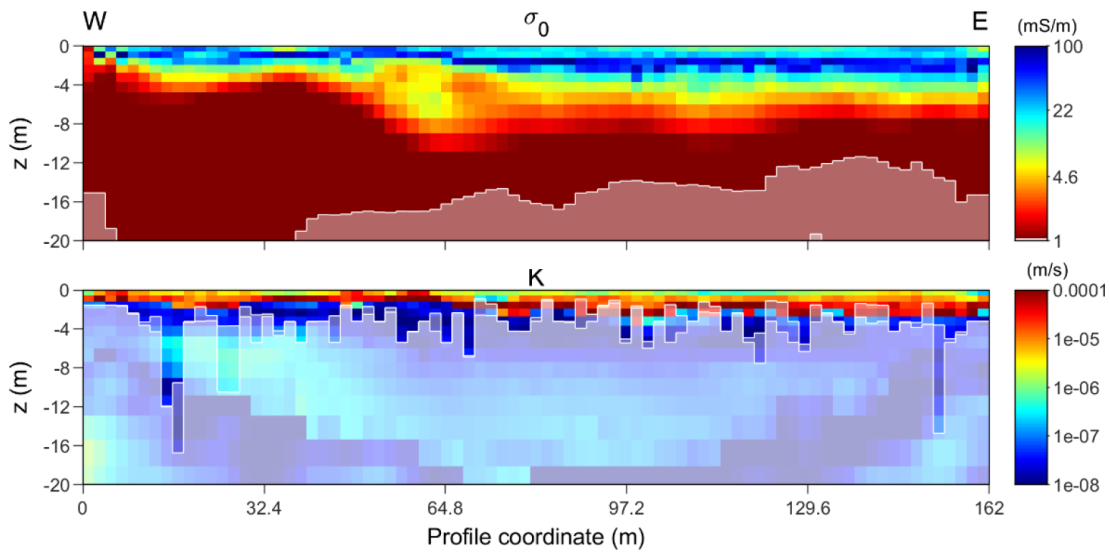
Figure 3. DCIP Inversion results for one profile at the second test site in Mariestad. The inversion is inverting for the electrical conductivity (s_0) with a known fluid conductivity (s_w) of 140 mS/cm.
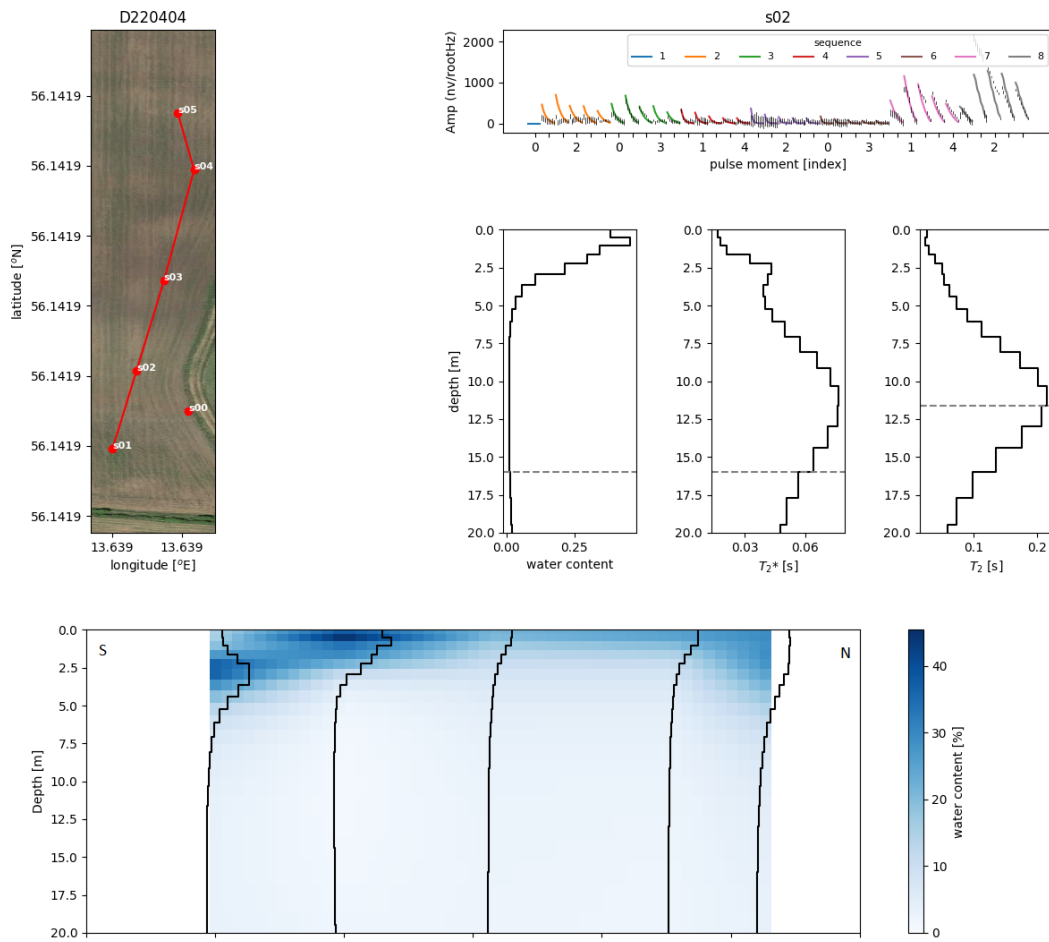
Figure 4. MRS inversion results for one line of soundings at Site 3: Hässleholm. The top left panel shows a map of the sounding centres, while the top right sets show the data fit and inverted models for site S02. Dashed line indicates a conservative depth of investigation estimation. The bottom panel shows a transect of water content from south to north along the line.

Conclusions

So far, the DCIP measurement at all test sites shows some layered underground structure with varying resistivities. The IP signals response is quite small but for some profiles significant. The MRS data quality depends a lot on the test site. While the Mariestad site had too high noise level for accurate interpretation, at Hässleholm it provided excellent data quality and laterally varying water content levels as high as 40+% in some locations. The first correlation of the DCIP measurements with the known hydraulic conductivity values are promising but a deeper analysis and interpretation is needed. The next steps in the project are to finalize the processing and inversion and to interpret the results from both methods. Subsequently, the data will be compared then with the available hydrogeological information based on slug or pump tests. For that, also drillings with the hydraulic profiling tool (HPT) and further slug test will be conducted. In addition, laboratory measurements are planned on samples, taken from the three test sites.

References

Fiandaca G., Meldgaard Madsen L., Olmo M., Römhild L., Maurya P.K., 2021. Inversion of hydraulic conductivity from Induced Polarisation, Part A: methodology and verification. Near Surface Geoscience 2021-27th European Meeting of Environmental and Engineering Geophysics, 1-4.

Grombacher, D., Liu, L., Griffiths, M.P., Vang, M.Ø., & Larsen, J.J. (2021). Steady-state surface NMR for mapping of groundwater, Geophysical Research Letters, 48(23), 9p.

Larsen, J.J., Liu, L., Grombacher, D., Osterman, G., & Auken, E. (2020). Apsu—A new compact surface nuclear magnetic resonance system for groundwater investigation, Geophysics, 85(2), JM1-JM11.

Maurya P.K., Balbarini N., Møller I., Rønde V., Christiansen A.V., Bjerg P.L., Auken E., Fiandaca G., 2018. Subsurface imaging of water electrical conductivity, hydraulic permeability and lithology at contaminated sites by induced polarization, Geophys. J. Int, 213, 770-785. DOI: 10.1093/gji/ggy018

Olsson P.-I., Fiandaca G., Larsen J.J., Dahlin T. & Auken E., 2016. Doubling the spectrum of time-domain induced polarization by harmonic de-noising, drift correction, spike removal, tapered gating and data uncertainty estimation, Geophys. J. Int., 207 (2), 774-784. 10.1093/gji/ggw260

Revil, A., Koch, K., & Holliger, K. (2012). Is it the grain size or the characteristic pore size that controls the induced polarization relaxation time of clean sands and sandstones? Water Resources Research, 48(5).

Schirov M., Legchenko, A., & Creer, G. (1991). A new direct non-invasive groundwater detection technology for Australia. Exploration Geophysics, 22(2), 333-338.

Weller, A., Slater, L., Binley, A., Nordsiek, S., & Xu, S. (2015). Permeability prediction based on induced polarization: Insights from measurements on sandstone and unconsolidated samples spanning a wide permeability range. Geophysics, 80(2), D161–D173.

P13 - Spectral induced polarization response of lake-bottom sediments

R.Glebe[1], J. Hoppenbrock[1], J. Buckel[1], A. Hördt[1], L. Pérez[2], P. Hoelzmann[3], M.Bücker[1]

(1) TU Braunschweig, Institute of Geophysics and extraterrestrial Physics, Braunschweig
(2) TU Braunschweig, Institute of Geosystems and Bioindication, Braunschweig
(3) FU Berlin, Institute for Geographical Sciences, Berlin

Presenter: R. Glebe (ruth.glebe@tu-braunschweig.de) **Student y/n:** Yes
Web page: https://www.tu-braunschweig.de/igep **Preferred presentation oral/poster:** Poster

Abstract. Geoelectrical measurements can complement standard lake-bottom sediment exploration techniques, such as seismics. In order to improve the inversion of geoelectrical data from lakes, it is useful to constrain the range of resistivity in the lake water and within the sediment layer. While the resistivity of the water column can be measured easily, such a-priori information on electrical properties of lake-bed sediments is often not available. The laboratory work included the analysis of 21 sediment samples from six karst lakes in southern Mexico. We measured the spectral induced polarization (SIP) response (resistivity and phase) and determined Cole-Cole-parameters from the measured spectra. Geochemical (main elements, organic and inorganic carbon) and mineralogical analyses were conducted as well. Our key finding is that resistivity and phase of the investigated lake-sediment samples increase with increasing content of organic matter.

Introduction

Geoelectrical measurements can be used to characterize thickness and composition of lake-bottom sediments (Bücker et al., 2021). They are especially useful, when other methods, such as seismic measurements do not work as well, for example, in case of gas-rich sediments or a highly reflective lake bed. To improve the interpretation of geoelectrical data in terms of sediment thickness, it can be useful to constrain sediment resistivity during the inversion process (Hoppenbrock et al., 2021); The exploration of lake-bottom sediments is important, for example for paleolimnological research. Findings from the sediment can be used for climate reconstruction, e.g., the sedimentation rate can be an indicator for climate change.

Study area and Methods

In order to provide sensible constraints for the inversion of geoelectrical data, 21 sediment samples were collected at different locations across six karst lakes, using an Ekman-grab. All six lakes are situated in the Lacandon Forest in the State of Chiapas, Mexico. In the laboratory, resistivity and phase of the samples were measured in the frequency range between 1 mHz and 240 kHz, using the Chameleon I equipment (Radic Research). Organic and inorganic carbon content were measured, using the loss-on-ignition method. Furthermore, the sediment composition was analysed, using portable energy-dispersive X-ray fluorescence spectrometry (p-ED-XRF), X-ray powder diffraction

(XRD) and ICP-OES element analyses of the carbonate and aqua-regia fraction, to obtain, e.g., contents of elements such as C, N, and metals, as well as mineral fraction of, e.g., kaolinite or calcite.
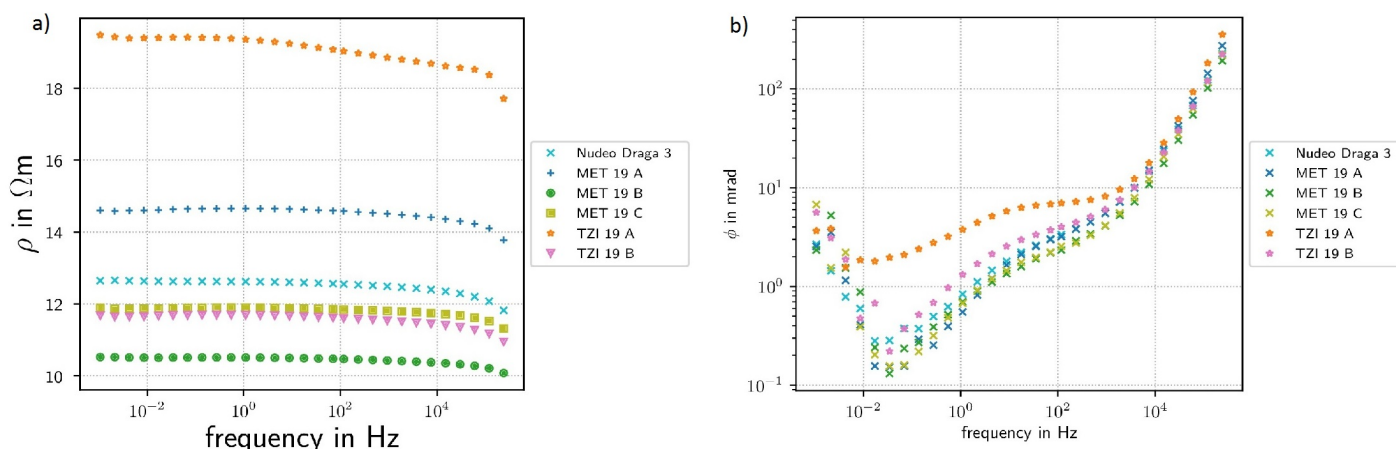
Figure 1. Complex resistivity spectra of six samples from lakes Metzabok (MET) and Tzibaná (TZI) in the Lacandon Forest in Chiapas, Mexico. **a.** Resistivity magnitude **b.** Resistivity phase. A phase peak appears around 10 Hz.

Results and Interpretation

The resistivity of the studied sediment samples was found to range between 5 and 22 Ωm, the phase (at frequencies between 0.01 Hz and 100 Hz) between 0.05 mrad and 11 mrad. The critical phase (maximum phase at a small peak, which is located around 10 Hz) increases with increasing organic content, which is higher at locations close to the shorelines. Towards the central parts of the lakes, the total organic carbon decreases, which is reflected in a decrease of both, the critical phase and the resistivity of the samples.
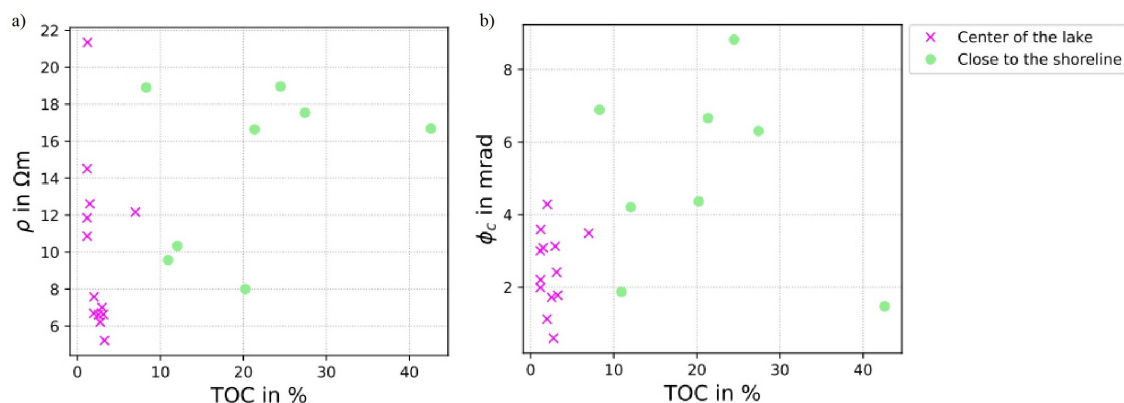
Figure 2. Variation of a) resistivity and b) critical phase with the total organic carbon (TOC). Colours indicate, whether the samples were taken close to the shoreline (green) or in the distal parts of the lake (magenta). Samples were taken at depths between 0.5 m and 40 m.

Conclusions

Both, resistivity and phase, clearly increase with the content of organic matter. As the studied lakes are located in a karst region, the content of inorganic carbon is generally high. The clear relation between organic carbon content and resistivity and phase might be used to define suitable positions for sediment core recovery, or when seeking peat. The low but measurable polarization response of the lake sediments in the study area has also already been used to discriminate between the pure sedimentary infill of lakes and the underlying fractured and sediment-filled karst bedrock below the lake bottom (Bücker et al., 2021).

References

Bücker, M., Flores Orozco, A.., Gallistl, J., Steiner, M., Aigner, L., Hoppenbrock, J., et.al. (2021). Integrated land and water-borne geophysical surveys shed light on the sudden drying of large karst lakes in southern Mexico. Solid Earth, 12, 439-461. https://doi.org/10.5194/se-12-439-2021.

Hoppenbrock, J., Bücker, M., Gallistl, J., Flores Orozco, A., de la Paz, C.P., García García, C.E., et.al. (2021). Evaluation of Lake Sediment Thickness from Water-Borne Electrical Resistivity Tomography Data. *Sensors*, *21*, 8053. https://doi.org/10.3390/s21238053.

P14 - Characterization of surface conductivity of clays

V. Emelianov[1], Z. Zhang[2], K. Titov[1], M. Halisch[3], A. Weller[2]

(1) St. Petersburg State University, Institute of Earth Sciences, Department of Geophysics, 199034 St. Petersburg, Russia
(2) Technische Universität Clausthal, Institut für Geophysik, 38678 Clausthal-Zellerfeld, Germany
(3) Leibniz-Institut für Angewandte Geophysik, 30655 Hannover, Germany

Presenter: Z. Zhang (zeyu.zhang.1@tu-clausthal.de) **Student y/n:** Yes
Web Page: NA **Preferred presentation oral/poster:** poster

Abstract. Clay minerals are extensively used in a wide range of applications. They are a key component in the production of ceramics, concrete, drilling fluids, molding sands, paints, and paper. Furthermore, clay formations can be used as radioactive waste repository. However, the hydrodynamic regime within such kind of storage should be considered due to possible interactions with groundwater. Electrical resistivity tomography can be used as one of the monitoring methods. A conclusive interpretation of field data requires reliable knowledge on the electrical properties of clays that are gained in laboratory experiments. The main purpose of this study is the investigation of the electrical properties of clay samples with a special focus on the contribution of surface conductivity. The influence of water content on complex conductivity values for four clay powder samples was investigated by the spectral induced polarization method. Experiments were conducted with kaolinite, illite, bentonite clays, and a breccia containing saponite (~ 90%). We also employed density, cation exchange capacity and specific surface area measurements to characterize the samples.

The measured complex conductivity spectra indicate a decrease of the real part of electrical conductivity with rising water content for the illite, bentonite and saponite breccia samples. The electrical conductivity of kaolinite does not show any significant changes with water content. Kaolinite indicates an iso-conductivity situation with similar conductivities of the solid and liquid phases, whereas the total conductivity of the other three samples is dominated by the contribution of surface conductivity. The imaginary part of electrical conductivity increases with water content. Moreover, we observed an increasing porosity and decreasing surface conductivity with increasing water content. Finally, the ratio between imaginary conductivity and surface conductivity increased with increasing water content (i.e. with a decrease of clay content).

P15 - Temperature dependence of SIP ice signatures of partially frozen rocks based on Cole-Cole model parameterization

J. K. Limbrock and A. Kemna

Institute of Geosciences, Geophysics Section, University of Bonn, 53115 Bonn, Germany

Presenter: J. K. Limbrock (limbrock@geo.uni-bonn.de) **Student y/n:** Yes
Web page: www.geo.uni-bonn.de   **Preferred presentation oral/poster:** Poster

Abstract. Spectral induced polarization was measured on 6 solid rock samples and 2 loose sediment samples from alpine permafrost sites with different texture and mineralogy in a frequency range of 10 mHz to 45 kHz during controlled freeze-thaw cycles (+20°C to -40°C). The measured spectra were fitted with a permittivity-based, multi-term Cole-Cole model with the high-frequency polarization response interpreted as ice relaxation. To investigate the influence of the temperature-dependent SIP ice signature on the total SIP response, the corresponding Cole-Cole model parameters of ice were modified systematically and the new total SIP response was calculated. The SIP responses of the different samples exhibit the same qualitative, well-known temperature-dependent relaxation behavior of ice at high frequencies with variations in shape and strength, for different textures and mineralogy. The study of the influence of the Cole-Cole ice parameters shows that frequency shifts of the phase peak can not only be interpreted as changes in relaxation time, and changes in the amplitude of the phase peak can not only be attributed to changes in the strength of the polarization response.

Introduction

Due to climate change, mountain permafrost is thawing globally with an associated increase in geological risks, like landslides or rock falls (e.g., Ravanel and Deline, 2008). Since the electrical properties of rocks and soil are sensitive to the phase change of liquid to frozen water, geoelectrical methods are increasingly being used for non-invasive characterization and monitoring of permafrost sites. Here, electrical resistivity tomography (ERT) is most commonly applied, using resistivity as a proxy for various quantities, such as temperature or ice content (e.g., Hauck et al., 2011; Krautblatter et al., 2010). However, it is still challenging to distinguish between air and ice in the pore space of the rock based on resistivity alone due to their similarly low electrical conductivity. Meanwhile, geoelectrical methods that utilize electrical polarization effects to characterize permafrost are also being explored. For example, the application of the spectral induced polarization (SIP) method, which measures the complex, frequency-dependent impedance, can reduce ambiguities in the interpretation of subsurface conduction properties, considering the SIP signature of ice. These measurements seem to be suitable for the quantification of ice content (and thus the differentiation of ice, rock, and air), and for the improved thermal characterization of alpine permafrost sites (e.g., Grimm and Stillman, 2015; Maierhofer et al., 2022). However, to improve the interpretation of SIP measurements, it is necessary to understand the electrical conduction and polarization properties as a function of

temperature, ice content, texture, and mineralogy under frozen and partially frozen conditions in more detail.

Background

The complex dielectric permittivity, $\varepsilon^* = \varepsilon' + i\,\varepsilon''$ (with $i = \sqrt{-1}$), is a measure of the electrical polarizability of a material in an external electric field. A simple model to describe its frequency dependence is the so-called Cole-Cole model (Cole and Cole, 1941). Here given as a multi-term model

$$\varepsilon^* = \varepsilon_\infty + \sum_k \frac{\Delta\varepsilon_k}{1+(i\omega\tau_k)^{c_k}}, \tag{1}$$

with $\Delta\varepsilon = \varepsilon_0 - \varepsilon_\infty$, low-frequency asymptote ε_0, high-frequency asymptote ε_∞, angular frequency ω, time constant τ, and Cole-Cole exponent c. Adding the DC electrical conductivity σ_{DC}, the resulting total complex resistivity $\rho^* = |\rho^*|\,e^{i\phi}$ is given as

$$\rho^* = \left(\sigma_{DC} + i\omega\,\varepsilon_v \left[\varepsilon_\infty + \sum_k \frac{\Delta\varepsilon_k}{1+(i\omega\tau_k)^{c_k}}\right]\right)^{-1}, \tag{2}$$

which is equivalent to the Cole-Cole model parameterization used by Stillman et al. (2010) to describe the low-frequency electrical properties of ice-silicate mixtures. Here, ε^* denotes the relative permittivity, and ε_v is the permittivity of vacuum.

Methods

In the study presented here, the electrical impedance was measured continuously using SIP in the frequency range of 10 mHz to 45 kHz during controlled freeze-thaw cycles (+20°C to -40°C to +20°C). These measurements were performed on cylindrical samples of 10 cm length and 3 cm diameter of five solid rock samples from different alpine permafrost sites, with different mineralogical compositions and textures (Zugspitze: limestone, Schilthorn: mica schist, Lapires: gneiss, Sonnblick: granite, Cervinia: amphibolite) plus on one sandstone sample with higher porosity (Röttbacher sandstone). After saturating the samples with water whose fluid conductivity is close to field conditions, the samples were sealed in a shrinking tube and placed in a climate chamber where they were cooled down from +20°C to -40°C by successively changing the temperature in steps between 0.2°C and 4°C with a duration of 120 to 180 minutes for each temperature step. This was found to be sufficient for the given size and thermal properties of the samples to reach thermal equilibrium. Afterwards, the samples were heated up again following the same temperature procedure. For potential measurements, we used ring electrodes made out of tinned copper with a distance of 3 cm. For the loose sediment samples, the samples were saturated with a water content comparable to field conditions and placed in a cylindrical container with a total length of 18 cm, a diameter of 4 cm and a potential electrode separation of 6 cm. Due to the increased sample size, the duration of each temperature step was increased by 60 minutes.

For each spectrum, we used a non-linear least-squares solver of the SciPy Python package to fit $\ln(|\rho^*|)$ and $\ln(-\phi)$ simultaneously and to determine the Cole-Cole parameters of up to three Cole-Cole relaxation terms, as well as σ_{DC} following Eq. (2). To get a better understanding of the temperature-dependent behavior of these Cole-Cole parameters and to investigate their influence on the resulting temperature-dependent SIP spectra, the Cole-Cole parameters associated with the

relaxation of ice $\Delta\varepsilon_{ice}$ and τ_{ice} were systematically changed by factors of 10 and 0.1 and the overall model response was inspected.

Results

In Figure 5, we observe that the impedance phase spectra, which is a measure of the polarization (relative to conduction), exhibit the same qualitative, well-known temperature-dependent relaxation behavior of ice (Auty and Cole, 1952) at higher frequencies (1 kHz - 45 kHz), with variations in shape and strength for different rock texture and mineralogy. At lower frequencies (1 Hz - 1 kHz), a polarization with a weak frequency dependence is observed in the unfrozen state of the samples. We interpret this response as membrane polarization, which likewise depends on the texture as well as on the mineralogy of the respective sample. This polarization response partially vanishes for the frozen state. The same behavior can be observed for the solid rock samples as well as for the loose sediment samples. Overall, the investigated SIP spectra do not only show a dependence on texture and mineralogy, but mainly depend on the presence of ice in the sample as well as the change in temperature.
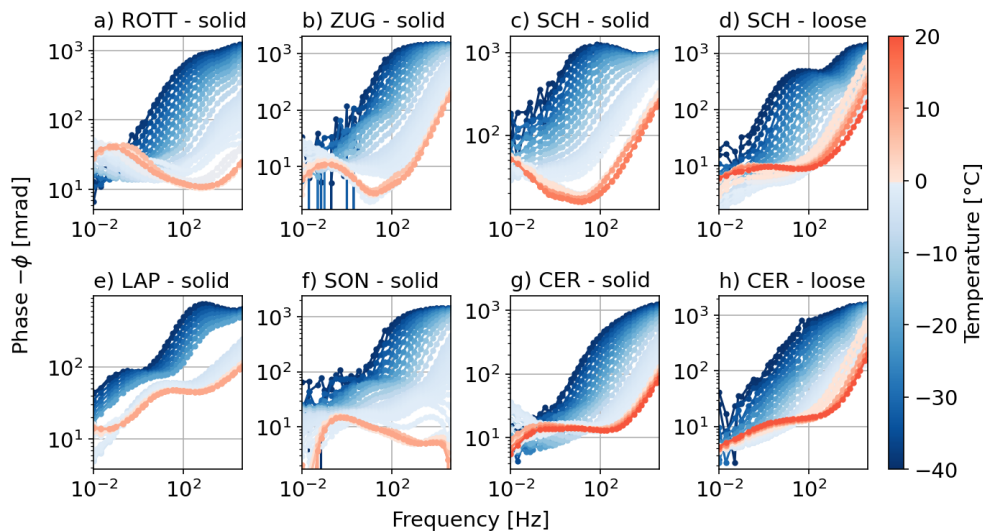
Figure 5. Temperature-dependent resistivity phase spectra of six solid rock samples (a-c and e-g) and two loose sediment samples (d and h) during thawing for temperatures from $-40°C$ to $+20°C$. At each temperature step, SIP measurements were conducted after thermal equilibrium had re-established.

The (partially) frozen state SIP data from all samples could be well fitted by a Cole-Cole model with up to three dispersion terms. As an example, the data of the Schilthorn solid rock sample at -20°C and the fitted Cole-Cole model response, here with two dispersion terms, are shown in Figure 6 (a): One low-frequency term and one high-frequency term with $\tau = 3.4 \cdot 10^{-4}s$, which is close to the expected relaxation time of ice at that temperature (e.g., Auty and Cole, 1952).

For the relative changes of τ_{ice} by the factors of 10 and 0.1 (Figure 6 (b)), we cannot only observe the expected frequency shift of the peak frequency of the resistivity phase, but also a clear change in the absolute value of the phase peak. For the same relative changes of $\Delta\varepsilon_{ice}$, we mostly observe a frequency shift of the phase peak to lower frequencies for larger $\Delta\varepsilon_{ice}$ and to higher

frequencies for smaller $\Delta\varepsilon_{ice}$ (Figure 6 (c)). A clear change in the absolute value of the peak frequency is not visible.

Conclusions

The results of this study show that low-frequency electrical properties measured via SIP give direct access to the polarization response of the ice in the pores of (partially) frozen rocks. The observed SIP responses of the (partially) frozen rocks are dominated by the SIP ice signatures and their temperature dependence. In contrast, the lithology of the rocks seems to have less influence. Fitting a Cole-Cole model with an appropriate parameterization to the measured SIP data, a separation of the different polarization responses is possible, which indicates the possibility of a thermal characterization, as well as a determination of the ice content, of permafrost rocks using SIP. However, the presented results also show that caution is required when interpreting corresponding SIP phase spectra, as a relative change in the phase peak frequency can be caused by a change in τ but also by a change of $\Delta\varepsilon$ only. Likewise, a relative change in τ can also cause a change in the phase peak amplitude, which is usually interpreted as a change in the strength of the polarization.
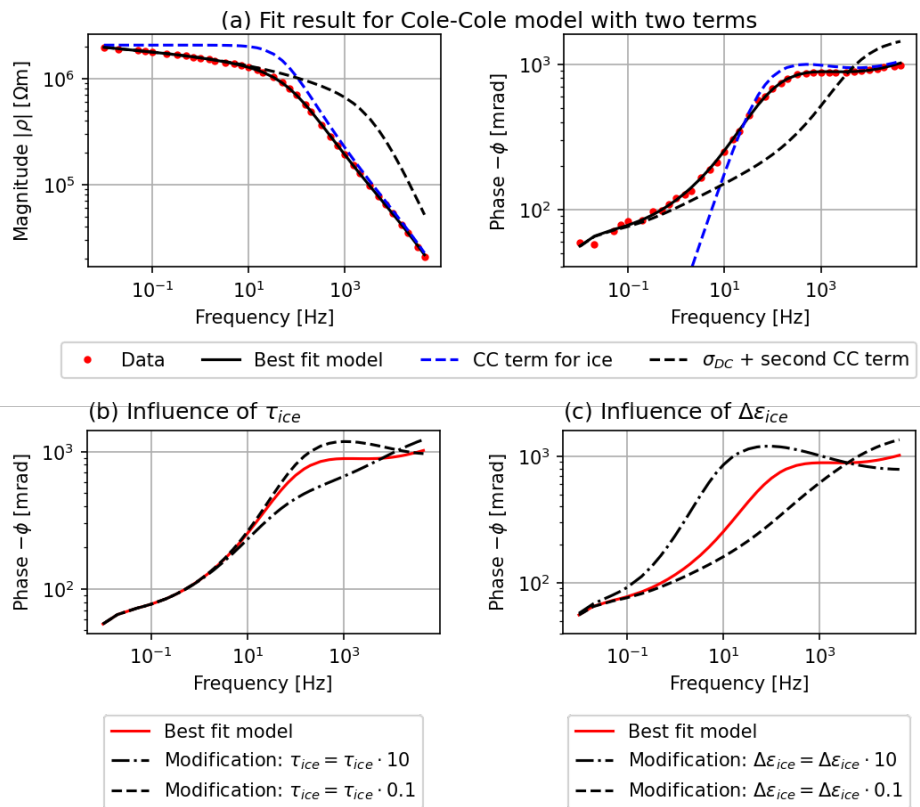
Figure 6. (a) SIP data (red dots) and corresponding fit result (black solid line) of Cole-Cole model with two dispersion terms after Eq. (*2*) for Schilthorn solid rock sample at $-20°C$ during thawing. Blue dashed line indicates the Cole-Cole term interpreted as ice polarization, black dashed line shows the residual components of the Cole-Cole fit. **(b)** Influence of relative changes in τ_{ice} on the total model response. **(c)** Influence of relative changes in $\Delta\varepsilon_{ice}$ on the total model response.

References

Auty, R. P., & Cole, R. H. (1952). Dielectric properties of ice and solid D2O. J. Chem. Phys. 20, 1309 1314, https://doi.org/10.1063/1.1700726.

Cole, K.S., & Cole, R.H. (1941). Dispersion and absorption in dielectrics I. Alternating current characteristics. Journal of Chemical Physics 9, 341–351, https://doi.org/10.1063/1.1750906.

Grimm, R. E., & Stillman, D. E. (2015): Field test of detection and characterisation of subsurface ice using broadband spectral induced polarisation, Permafr. Periglac. Process., 26, 28–38, https://doi.org/10.1002/ppp.1833.

Hauck, C., Böttcher, M., & Maurer, H. (2011): A new model for estimating subsurface ice content based on combined electrical and seismic data sets, The Cryosphere, 5, 453–468, https://doi.org/10.5194/tc-5-453-2011.

Krautblatter, M., Verleysdonk, S., Flores Orozco, A., & Kemna, A. (2010): Temperature-calibrated imaging of seasonal changes in permafrost rock walls by quantitative electrical resistivity tomogra- phy (Zugspitze, German/Austrian Alps), J. Geophys. Res., 115, F02003, https://doi.org/10.1029/2008JF001209.

Maierhofer, T., Hauck, C., Hilbich, C., Kemna, A., & Flores-Orozco, A. (2022): Spectral induced polarization imaging to investigate an ice-rich mountain permafrost site in Switzerland, The Cryosphere, 16, 1903–1925, https://doi.org/10.5194/tc-16-1903-2022.

Ravanel, L., & Deline, P. (2008). The West Face of Les Drus (Mont Blanc massif): slope instability in a high Alpine steep rock wall since the end of the Little Ice Age. Géomorphologie 4:261 272.

Stillman, D. E., Grimm, R. E., & Dec, S. F. (2010). Low-frequency electrical properties of ice silicate mixtures. Journal of Physical Chemistry B, 114(18), 6065 6073, https://doi.org/:10.1021/jp9070778.

P16 - Complex conductivity response of diffusion driven calcite precipitation in sandstone

A. M. Mansfeld and A. Kemna

Institute of Geosciences, Geophysics Section, University of Bonn, Meckenheimer Allee 176, Bonn, 53115, Germany.

Presenter: A. M. Mansfeld (mansfeld@geo.uni-bonn.de) **Student y/n:** Yes
Web page: NA **Preferred presentation oral/poster:** Poster

Abstract: Interactions between mineral phases and pore fluids in the subsurface inevitably lead to mineral precipitation reactions and dissolution. One mineral often involved in these naturally occurring processes is calcite due to its strong relationship between solubility and the pH value. Calcite is commonly used in many geotechnical engineering applications. However, information on the progress of such a reaction, or a direct quantification of the precipitated material, is difficult or costly to obtain. The spectral induced polarization (SIP) method provides the potential not only to localize the precipitate in the subsurface non-invasively, but also to quantify the amount and location within the pore space. The real part of the measured complex electrical conductivity holds information on the salinity of the pore fluids present in the subsurface and allows the estimation of solute concentrations. Through the imaginary part of the complex conductivity changes stemming from newly formed minerals can be detected, given its sensitivity to the pore space geometry and fluid-mineral interactions.

In this study we performed multiple laboratory experiments on mixing-induced precipitation in rocks monitored with SIP measurements. The setup consists of two fluid reservoirs that are connected via a quartz-rich sandstone sample, creating a reaction zone in the pore space. As reactant, 0.2 molal $NaHCO_3$ and 0.1 molal $CaCl_2$ solutions were used, the mixing of which resulted in $CaCO_3$ formation. The experimental results show a distinguished complex conductivity evolution associated with the precipitation of calcite throughout the sample. We observe two features in the spectral response: One early low-frequency phenomenon associated with the pH value changes, and a second higher-frequency one, that can be connected to $CaCO_3$ growth. These results show not only the potential for precipitation monitoring in deeper subsurface applications, but also potential for a multipurpose investigation of both chemical environment and pore space geometry in one measurement.

Introduction:

The precipitation of minerals is a naturally occurring process, where two or more dissolved substances mix, chemically react and form a new substance with a lower solubility than the reagents. Calcite precipitation, one of the most prevalent examples for these types of reaction, is used in many geotechnical and geoengineering processes, such as soil stabilization or pH-value moderation. However, this process can also lead to karstification or the unwanted clogging of pore spaces or drainage systems. Though interest in this topic is high, common methods to investigate and monitor such systems are often invasive and expensive. In the past years, several studies investigating the complex conductivity response to induced calcite precipitation have been performed. Here, the reaction process resulting in the precipitation of calcite (Microbiologically induced calcium carbonate precipitation (MICP) and anorganic processes) as well as the type of media (from glass beads to sand-clay mixtures), was varied (Wu et al., 2010, 2011; Zhang et al., 2012; Izumoto et al., 2020). All these studies show the potential of the SIP method to detect and monitor calcite precipitation, but also

yielded differing results, thus showing that there is no uniform signature of these processes. This could be due to a multitude of reasons since the SIP signature of such a process is sensitive to temperature, pH value, ambient salinity, pore space geometry (and its changes due to the precipitation) (e.g., Börner, 1992; Hördt et al., 2007; Revil and Florsch, 2010; Weller et al., 2010 a,b, 2013), the location of the precipitate (on macroscale), and the background signature of the porous medium itself.

In this study we follow an alternative approach. Instead of unconsolidated materials, consolidated sandstone samples were chosen, relating more closely to the geological scenarios of interest. The reactants were introduced into the system solely via diffusion, thus minimizing material advection, which in turn reduces streaming potentials and alignment of the reactive zone alongside the hydraulic flow profile. Additionally, consolidated samples inhibit dynamic deformation of the pore space. Further details on the experimental setup will be provided in the following sections.

Methods: Experiments were performed on Obernkirchen sandstone, a relatively homogeneous medium grained quartz-rich sandstone type with up to 5 wt.% of clay minerals, and were carried out over a varying duration of 10-32 days. The experiment was conducted in a SIP-sample holder developed at the Leibniz-Institut für Angewandte Geophysik (LIAG). The sample holder features two Pt-net electrodes for current injection and two non-polarizable ring electrodes for potential measurements. SIP measurements were conducted with a ZEL-SIP04-V02 system by the Central Institute for Electronics (ZEA-2), Forschungszentrum Jülich GmbH. The sample holder provides two tanks for fluid reservoirs filled with a 0.1 Mol/kg $CaCl_2$ solution on one side and a 0.2 Mol/kg $NaHCO_3$ solution on the other. Mixing of these two fluids results in the following reaction:

$$2\ NaHCO_3(aq) + CaCl_2(aq) \leftrightarrow H_2O + CO_2 + CaCO_3 + 2\ NaCl.$$
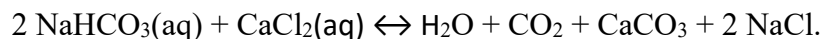
Samples were presaturated with a 1 Mol/m³ KCl solution to minimize leaching of clay minerals. Estimates of the precipitated masses of calcites, changes in the pH value and fluid electrical conductivity were gathered via modeling with PHREEQC 3 (Parkhurst and Appelo, 2013).

Results & Discussion: The results of the spectral measurements for the 32-day experiment are shown in the figures (Figs. 1, 2). While the real part conductivity (σ') data shows very little variation over the measured frequency range, they are indicative of the occurring diffusion process and the temperature (Fig. 1). A relatively stable real part conductivity of 450 µS/cm is reached after ca. 7 days. Following changes depend on the room temperature. In the imaginary part, several phenomena occurring over the duration of the experiment can be identified. First is the expected overall increase in imaginary conductivity (σ'') due to the higher electrolyte concentration, which is most notable over the first hours of the experiment. Then we observe a decrease in σ'', being especially pronounced in the lower-frequency spectra around 0.1 Hz (about 0.25 µS/cm). This behavior changes again after three days, where a secondary higher-frequency peak starts to develop with a maximum around 20-40 Hz. During the following days, σ'' increases over the whole frequency range again and the second peak slightly shifts towards lower frequencies. However, on day 24 the maximum is shifted to around 100 Hz spontaneously and becomes much more visible, while the lower-frequency values decrease slightly. After this last shift σ'' continues to rise over the whole frequency range until the end of the experiment. At the end of the experiment σ'' has increased between 50% (~ 0.37 µS/cm) at low frequencies and up to 75% (~ 0.75 µS/cm) at high frequencies. PHREEQC modeling results suggest that the pH value in the sample increases for the first 16 hours of the experiment. The end of this period coincides with the predicted beginning of the calcite precipitation. Following this onset of the chemical reaction, the pH values drop significantly for 14 hours and then decrease further

until day 15, at which then in turn it increases slightly until the end of the experiment. This behavior is similar to the one observed in the low frequencies. The higher-frequency peak developed a bit later than the 16-hour mark, but continues to grow for the rest of the experiment. Results from similar studies also suggest a higher-frequency feature associated with calcite precipitation (Wu et al., 2010; Izumoto et al., 2020). However, MICP studies by Saneiyan et al. (2018) suggest a low-frequency calcite peak in a similar frequency range to our observed low-frequency peak. The differences in the position of the peaks could be due to the available pore space or the slightly differing pore fluid chemistry.
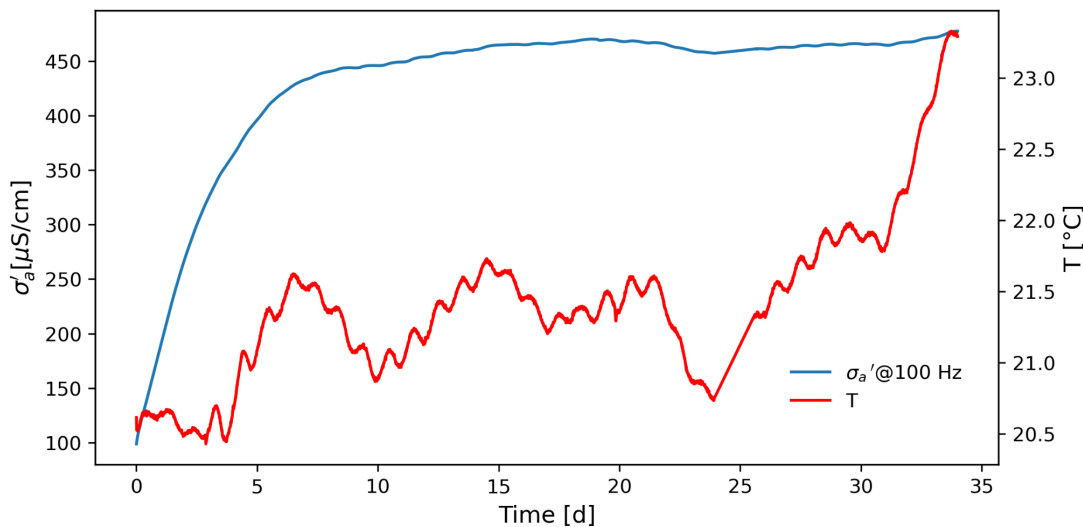
Figure 1: Temporal evolution of σ' at 100 Hz, temperature was tracked in a water vet next to the sample to simulate the average temperature in the sample holder.
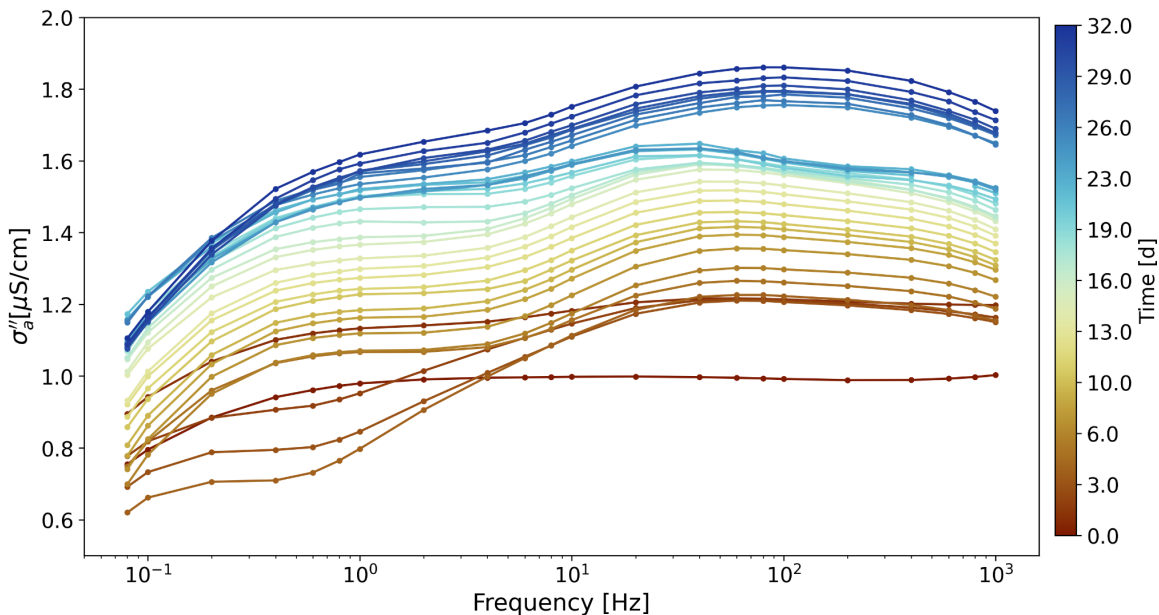
Figure 2: Daily sampled development of σ'' over 32 days. Spectral data were collected in 12-minute intervals. Note: Significant changes in the spectral response on days 3, 7 and 25 did not occur gradually over the days but within the 12-minute timeframes.

Conclusions: Over the course of the experiments multiple relaxation phenomena corresponding to the chemical processes occurring in the sample were observed. This study shows that even in

confined pore spaces and without high hydraulic gradients the precipitation of calcite results in significant changes in SIP response of the rock samples. Thus, even when applied to a more complex scenario, mineralization processes can be monitored with the SIP method. Our experimental results show a distinguished complex conductivity evolution associated with the precipitation of calcite throughout the sample. We observe two features in the spectral response: One low-frequency phenomenon observable early on, which we associate with the pH value changes, and one higher-frequency one that can be connected to $CaCO_3$ growth. These results show not only the potential for precipitation monitoring in deeper subsurface application, but also the potential for a multipurpose investigation of both chemical environment and pore space geometry in one measurement. The experimental data of this study are only in partial agreement with previous studies, proving that more research is required, for a complete understanding of the connection between the complex conductivity and calcite precipitation. Further more rigorous studies will show whether existing quantitative models can be applied to the considered case or adaptations need to be introduced based on sample and reaction mechanism.

References

Börner, F. (1992). Complex conductivity measurements of reservoir properties. Advances in Core Evaluation III (Reservoir Management). Gordon and Breach Science Publishers, London.

Hördt, A., Blaschek, R., Kemna, A., & Zisser, N. (2007). Hydraulic conductivity estimation from induced polarisation data at the field scale – the Krauthausen case history: J. Appl. Geophys., 62, 33-46.

Izumoto, S., Huisman, J. A., Wu, Y., & Vereecken, H. (2020). Effect of solute concentration on the spectral induced polarization response of calcite precipitation. Geophysical Journal International, 220(2), 1187-1196.

Parkhurst, D. L., Appelo, C. A. J. (2013). Description of input and examples for PHREEQC version 3-a computer program for speciation, batch-reaction, one-dimensional transport, and inverse geochemical calculations. US Geological Survey Techniques and Methods, 6(A43), 497.

Revil, A., & Florsch, N. (2010). Determination of permeability from spectral induced polarization in granular media. Geophysical Journal International ,181(3),1480-1498.

Saneiyan, S., Ntarlagiannis, D., Werkema Jr, D. D., & Ustra, A. (2018). Geophysical methods for monitoring soil stabilization processes. Journal of Applied Geophysics, 148, 234-244.

Weller, A., Slater, L., Nordsiek, S., & Ntarlagiannis, D. (2010 a). On the estimation of specific surface per unit pore volume from induced polarization: A robust empirical relation fits multiple data sets. Geophysics, 75(4), WA105-WA112.

Weller, A., Nordsiek, S., & Debschütz, W. (2010 b). Estimating permeability of sandstone samples by nuclear magnetic resonance and spectral-induced polarization. Geophysics, 75(6), E215-E226.

Weller, A., Slater, L., & Nordsiek, S. (2013). On the relationship between induced polarization and surface conductivity: Implications for petrophysical interpretation of electrical measurements. Geophysics, 78(5), D315-D325.

Wu, Y., Hubbard, S., Williams, K. H., & Ajo-Franklin, J. (2010). On the complex conductivity signatures of calcite precipitation. Journal of Geophysical Research: Biogeosciences, 115(G2).

Wu, Y., Ajo-Franklin, J. B., Spycher, N., Hubbard, S. S., Zhang, G., Williams, K. H., Taylor, J., Fujita, Y. & Smith, R. (2011). Geophysical monitoring and reactive transport modeling of ureolytically-driven calcium carbonate precipitation. Geochemical Transactions, 12(1), 1-20.

Zhang, C., Slater, L., Redden, G., Fujita, Y., Johnson, T., & Fox, D. (2012). Spectral induced polarization signatures of hydroxide adsorption and mineral precipitation in porous media. Environmental Science & Technology, 46(8), 4357-4364.

P17 - Measurement of dried seafloor massive sulphides

M. Lührs and A. Hördt

Institute for Geophysics and Extraterrestrial Physics, TU Braunschweig, Mendelssohnstr. 3, 38106 Braunschweig, Germany

Presenter: M. Lührs (m.luehrs@tu-braunschweig.de) **Student:** Yes
Web page: NA   **Preferred presentation:** Poster

Abstract. We carried out spectral induced polarization measurements on a set of dried seafloor massive sulphide samples and compared the results with those obtained with the same samples fully saturated with NaCl solution. We find that the conductivity and polarizability (measured by phase shift and imaginary conductivity) are generally high for both dried and saturated samples. The high polarizability of dried samples is a significant observation, because most of the existing theories to explain the polarization of mineralized rock assume a pore space filled with an electrolyte. We also found that the frequently used agar gel is unsuitable to couple the dried samples to the electrodes, because it releases water into the sample. Coupling with modelling clay is a feasible alternative, because no fluid is absorbed by the sample when it is incorporated into the sample holder.

Introduction

Existing theories to explain the spectral behaviour of mineralized rock generally assume an electrolyte in the pore space (Wong 1979). Spagnoli et al. (2016) carried out various measurements on seafloor massive sulphides. The measurements on the saturated samples showed a strong polarizability with high conductivity at the same time. For many samples, the electrical conductivities were even higher that what would be expected from Archie's lay if the conduction mechanism would be purely electrolytic. Therefore, it is likely that conduction is carried by connected semiconductors in the massive sulphides. This observation raises the question whether the polarizability might also be controlled by the conductors alone, without the need of a bulk electrolyte. To investigate this hypothesis, we focus on measuring dry samples in this study.

When measuring dry samples, the coupling of the samples to the electrodes becomes an issue. Agar gel, which is often used for coupling, has the disadvantage that the water is not bound in it. Agar is available as granules and is heated with water and dissolved in it. When it cools down, the agar gels. However, since the water diffuses from the gel into the sample, the originally dry sample is now filled with the fluid to an unknown and possibly non-negligible extent.

Material and Methods

The samples already examined by Spagnoli et al. (2016) are measured, whereby only the polarizable samples are of interest (sample numbers 11-36). A measuring cell with cylindrical cross-section is used, where the current electrodes are located at the ends of the cell and the potential electrodes are concentric ring electrodes. The space between the electrodes and the sample must be filled with a medium to ensure the flow of current through the sample.

The samples are saturated with NaCl solution with a conductivity of 5 S/m. After the measurement, the samples are dried for several days in a vacuum drying oven. If the sample is to be measured in the dried state, it is installed in the same cell, but without first undergoing the saturation procedure. The volume of the measuring cell is then filled with the coupling material. Modelling clay was chosen for this work because it has a high conductivity and is easy to shape. For comparison, we also used the conventional coupling with agar. To find out how well the fluid remains in the coupling material, the samples are weighed before installation and after removal. The mass difference of the sample before the saturation process and in the saturated state before installation is also used for comparison.

Results

Weighing the samples shows that a large proportion of the pore space is filled with fluid when agar is used. Thus, the mass increase is on average about 63 % of the increase at normal saturation. The use of modelling clay shows significantly lower mass increases. Compared to saturation with electrolyte, the mass increase is only 8 %. It must also be taken into account that a residue of the modelling clay always remains on the sample surface after measurement. After weighing, the residual modelling clay is removed with water. Due to the favourable properties of modelling clay, only measurements of samples coupled with modelling clay and saturated samples will be compared in the following.

Figure 1 shows the spectra of sample 21 as an example. Even the dried sample exhibits small resistivities, indicating that the current is carried by connected conductive minerals in the sample. Both phase shift (panel B) and imaginary conductivity (panel C) which may be considered measures of polarizability, remain large even if the sample is dried.
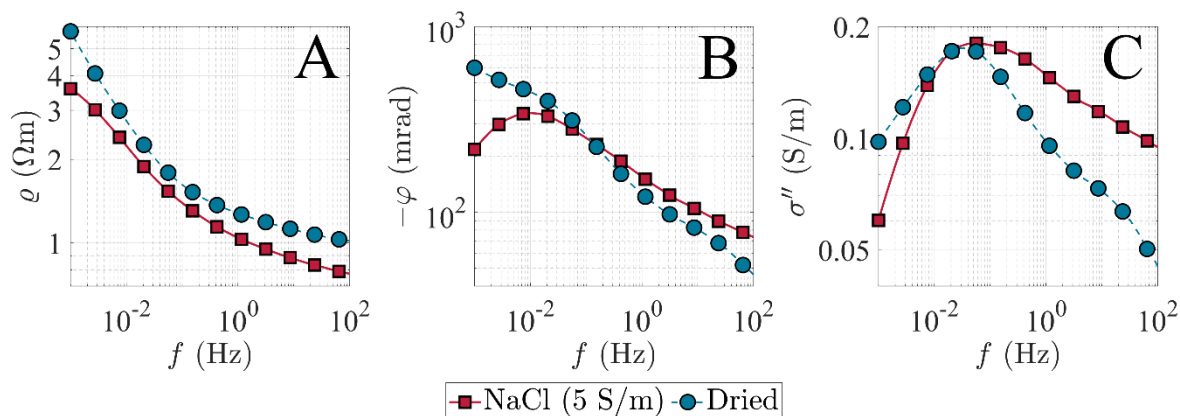
Figure 1. Spectra of sample 21 (Cu-Zn rich). The red squares show the measurements on the sample saturated with 5 S/m NaCl solution, the blue circles the dry sample coupled with modelling clay (figure from Lührs et al. 2022).

In figure 2A, the resistivities at the lowest frequency are displayed for saturated and dried samples. The samples are sorted and marked according to the main components as in Spagnoli et al. (2016). In general, resistivities are low (<100 Ωm) even after drying.

Figure 2B and C show the phase maxima and the imaginary part at the frequency of the phase maximum. While the phase shift increases for most samples by drying, the imaginary part normally

decreases. However, the decrease of imaginary conductivity is generally small (less than one order of magnitude), and for a few samples, even an increase can be observed.
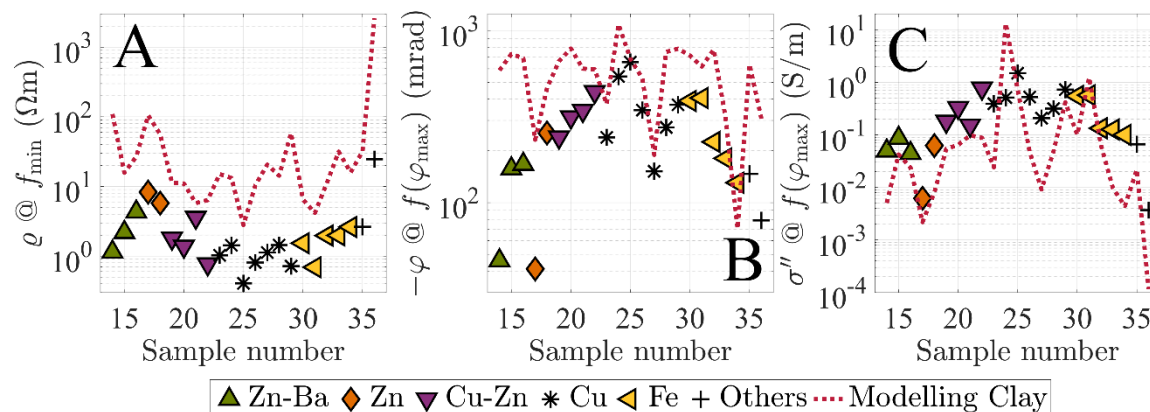
Figure 2. Comparison of measurements at saturation with 5 S/m NaCl solution and coupling of dry samples with modelling clay. A: Resistivity at lowest frequency as approximation to the DC value. B: Phase maximum C: Imaginary part of the conductivity at the frequency of the phase maximum. (figure from Lührs et al. 2022).

Conclusion

The agar gel often used for coupling of samples to the electrodes has the disadvantage that the water in it is not strongly bound and enters the pore space of the sample. For this reason, the samples were coupled with modelling clay. The modelling clay has good electrical conductivity, does not polarize and loses less fluid than agar. We conclude that modelling clay is a well-suited material for carrying out measurements on dry samples.

The measurements on the 26 samples show that even dried samples have low resistivity and high polarizability. Additional experiments on the polarization behaviour of the samples after different time spans of drying in the vacuum oven were carried out on selected samples. Even after several days in the vacuum oven, the samples were still strongly polarizable. We conclude that it is difficult to destroy polarization of massive sulphide samples by drying. Therefore, a bulk electrolyte in the pore space is not be necessary to generate a significant polarization. The development of new theories might be required to explain the behaviour of massively mineralized rock.

References

Lührs, M., Hördt, A. (2022). Measuring Induced Polarization on dry seafloor massive sulphides. *in prep.*

Spagnoli, G, Hannington, M., Bairlein, K., Hördt, A., Jegen, M., Petersen, S., Laurila, T. (2016). Geo-Marine Letters, 36.3, 235-245. https://doi.org/10.1007/s00367-016-0439-5.

Wong, J. (1979). An electrochemical model of the induced polarization phenomenon in disseminated sulfide ores. Geophysics, 44, 1245-1265. https://doi.org/10.1190/1.1441005.

P18 - Estimating spectra of embedded ore samples

M. Lührs and A. Hördt

Institute for Geophysics and Extraterrestrial Physics, TU Braunschweig, Mendelssohnstr. 3, 38106 Braunschweig, Germany

Presenter: M. Lührs (m.luehrs@tu-braunschweig.de) **Student:** Yes

Web page: NA   **Preferred presentation:** Poster

Abstract. In Spectral Induced Polarization (SIP) measurements, the phase shift between current and voltage is measured in addition to the frequency-dependent apparent resistivity. If a SIP measurement is carried out in the laboratory, the sample is usually installed in a suitable measuring cell. However, if the starting material is not to be destroyed, it is not possible to obtain a sample that fits the measuring cell and an alternative procedure is required. In this study, we embed seafloor massive sulphide samples in quartz sand and investigate the estimation of the sample's spectra. For this purpose, we use a frequency-independent, real dilution factor obtained from numerical simulations. With the help of this factor, we succeed in estimating 73 % of the samples with a deviation less than 50 % from the reference.

Introduction

The behaviour of embedded polarizable bodies is studied by Guptasarma (1984). He describes how the apparent spectra of resistivity ρ and phase shift φ are composed of the spectra of target and surrounding material. In this study, the theory of Guptasarma (1984) is used to infer the spectra of the embedded sample from the apparent spectra.

To test the new method, cylindrical samples, for which the electrical properties can be determined in both ways, are measured. The samples are 30 seafloor massive sulphides, which have already been studied by Spagnoli et al. (2016). The samples are mainly rich in Fe, Cu and Zn and originate from various hydrothermal deposits (Spagnoli et al. 2016). The samples are first saturated with 100 mS/m NaCl solution and measured in suitable cylindrical measuring cells. The measurements serve as a reference for the subsequently performed measurements on embedded samples. Samples and the quartz sand used are saturated with the same fluid and installed in a larger measuring cell.

Theory

In his work, Guptasarma (1984) suggests a procedure to determine the resulting spectra from the spectra of an embedded target and the surrounding material by means of numerical simulations. For this purpose he introduces the so called dilution factor $\tilde{B}$:

$$\tilde{B} = \frac{\partial \ln \rho_a}{\partial \ln \rho_i} \tag{1}$$

The dilution factor is complex and frequency-dependent and enables the calculation of the phase shift and the slope of the resistivity spectrum through the following equations:

$$\varphi_a = \left(1 - \text{Re}[\tilde{B}]\right)\varphi_o + \text{Re}[\tilde{B}]\varphi_i \tag{2}$$

$$\frac{d \ln|\rho_a|}{d \ln \omega} = \left(1 - \text{Re}[\tilde{B}]\right)\frac{d \ln|\rho_o|}{d \ln \omega} + \text{Re}[\tilde{B}]\frac{d \ln|\rho_i|}{d \ln \omega} \tag{3}$$

In his work Guptasarma (1984) denotes the equations as Approximation III.

As a real and constant approximation for $\tilde{B}$, Guptasarma (1984) describes the possibility of forming the geometric mean for the dilution factor of resistivities at $\omega = 0$ and $\omega \to \infty$. The dilution factor determined in this way is referred to as B in the following.

The quartz sand used has no IP effect, so the equations 2 and 3 become:

$$\varphi_a = B\varphi_i \tag{4}$$

$$\frac{d\ln|\rho_a|}{d\ln\omega} = B\frac{d\ln|\rho_i|}{d\ln\omega} \tag{5}$$

In order to calculate the spectra of an embedded sample from the apparent spectra, the equations 4 and 5 only have to be rearranged and there is only a multiplication with the reciprocal value of B for the phase and a recursive relationship for the resistivity:

$$\varphi_i = \frac{1}{B}\varphi_a \tag{6}$$

$$\rho_i(\omega_{n+1}) = \exp\left(\ln\rho_i(\omega_n) + \frac{1}{B}(\ln\rho_a(\omega_{n+1}) - \ln\rho_a(\omega_n))\right) \tag{7}$$

Thus, only the phase spectrum of the embedded sample is required for the determination of the phase; for the resistivity an initial value is required and is determined with numerical simulations.

Estimation of the spectra

The procedure is illustrated in figure 1. A numerical simulation with COMSOL Multiphysics © yields a resistivity ρ_a for each resistivity contrast, whereby a separate simulation is carried out for each sample geometry. In a first step, the resistivity ρ_i of the sample is determined from the measured apparent resistivity ρ_a (figure 1A). In a second step, the dilution factor is determined with another set of numerical simulation based on eq. 1 (figure 1B). From the measurement on the embedded sample, the resistivities at 10^{-3} Hz and 10^2 Hz are chosen as an approximation for the value at DC and infinite frequency. An alternative, but less accurate method to estimate the dilution factor is from the relative volume of the sample, which is illustrated as a blue dashed line in figure 1B.
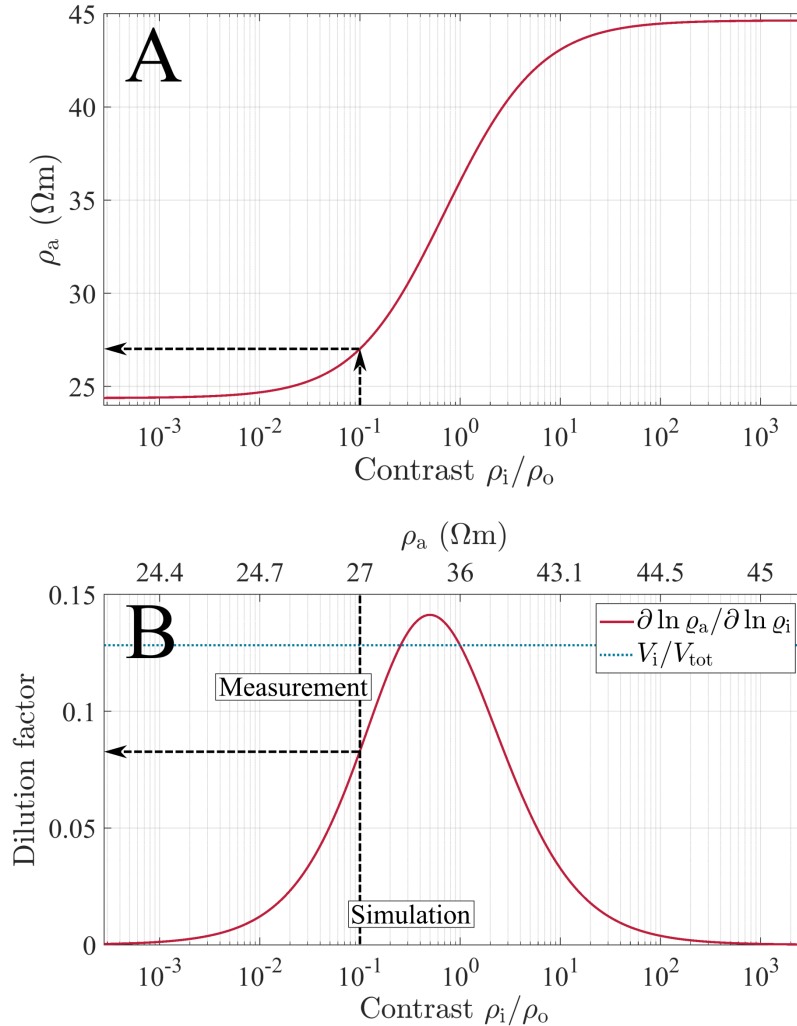
Figure 1. A: Simulation results for a sample with resistivity ρ_i embedded in a surrounding medium with resistivity ρ_o. B: Numerical simulation of dilution factor vs. resistivity contrast. From the measured resistivity of an embedded sample ρ_a (here 27 Ωm) the dilution factor B can be determined (figure from Lührs et al. 2022).

The determined dilution factors can be applied to the spectra of the embedded samples using the equations 6 and 7. The estimation is carried out with the dilution factor from the simulation as well as with the relative volume as a further approximation. Figure 2 shows the maximum phase shifts of the estimated spectra, plotted against the phase of the reference measurement.

Of the 30 samples, eight have more than ±30 % deviation of the maximum phase when the dilution factor obtained by simulation is applied (figure 2A). In total, 22 samples can be estimated with <50 % deviation. On average, the total deviation from the reference measurements is 37 %. If the relative volume is used to estimate the phase, nine samples show >±30 % deviation of the maximum phase shift (figure 2C). Overall, the deviation of the estimation with the relative volume is 38 %.
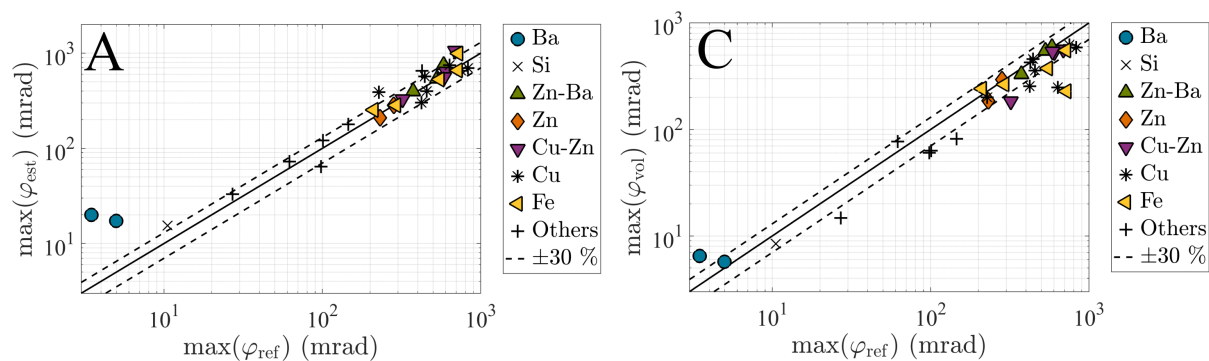
Figure 2. Overview of the deviations of the estimated maximum phase shift from the reference measurements (black line). The dashed line marks an interval of 30 % deviation. A: Estimation by the simulated dilution factor. B: Estimation by the relative volume of the sample (figure from Lührs et al. 2022).

Conclusion

With the theory based on Guptasarma (1984), the spectra of resistivity and phase of a in quartz sand embedded sample can be estimated by calculating the dilution factor. It can be determined by means of numerical simulations and was applied to the spectra of 30 seafloor massive sulphide samples. A total of 22 samples can be estimated with a deviation <50 %. On average, the deviation is 37%. In addition, the relative volume was used as an approximation for the dilution factor, which leads to an overall deviation of 38 % on average. Considering that ore samples are generally heterogeneous and their electrical properties show considerable scatter even between similar samples, our method seems feasible to estimate to estimate electrical spectra of handpieces of seafloor massive sulphides.

References

Guptasarma, D. (1984). True and apparent spectra of buried polarizable targets. Geophysics, 49(2), 171–176. https://doi.org/10.1190/1.1441648.

Lührs, M., Hördt, A. (2022). Estimation of electrical spectra of embedded samples. *in prep.*

Spagnoli, G, Hannington, M., Bairlein, K., Hördt, A., Jegen, M., Petersen, S., Laurila, T. (2016). Geo-Marine Letters, 36.3, 235-245. https://doi.org/10.1007/s00367-016-0439-5.

P19 - Sensing of winter wheat root systems at the field scale using spectral electrical impedance tomography

V. Michels, M. Weigand, and A. Kemna

Institute for Geosciences, Geophysics Section, University of Bonn, Meckenheimer Allee 176, 53115 Bonn, Germany

Presenter: V. Michels (michels@geo.uni-bonn.de) **Student y/n:** Yes
Web page: NA   **Preferred presentation oral/poster:** Poster

Abstract. Spectral electrical impedance tomography (sEIT) is used as a non-invasive tool to monitor root growth and root activity dynamics at the field scale. The main goal of the experiment is to provide information about the spatial extent and physiological state of the investigated crop root system. A multichannel impedance measurement system has successfully been operated at the field scale over a whole growing season of winter wheat and is achieving a high temporal resolution through continuously running measurements. The retrieved data are analyzed with respect to the seasonal and daily timescales using a measure of the spectral dispersion strength of the observed polarization in the Hz to kHz range as an indicator for the presence of active roots. For simplicity, we refer to this measure as electrical root index (ERI). The seasonal analysis shows that the approach produces spatially resolved images for the different timesteps that are following the expected root growth pattern of the sown winter wheat varieties. The investigation of the diurnal timescale reveals a 24 hour cyclic trend of the ERI that closely follows the photosynthetic active radiation, suggesting that the considered ERI parameter is sensitive to the photosynthetic activity of the plants. The monitoring results thus provide evidence for the potential of sEIT as a functional imaging technique of crop root systems at the field scale.

Introduction

Spectral electrical impedance tomography (sEIT) is a geoelectrical, non-invasive imaging method that is used in geophysical applications to derive information about the subsurface from the retrieved complex electrical resistivity and its frequency dependence. The measurements can be used to gain insight into the conductive properties of the material, but, more importantly, are additionally able to capture polarization processes in response to the injected electric current. Past research at the laboratory scale indicates that this polarization does not only take place at grain-solute interfaces, but also at the root-soil contact and at root cell membrane walls, and therefore holds potential to investigate the spatial extent and activity of the root system (e.g., Weigand et al., 2019; Ehosioke et al., 2020). Although still challenging, recent methodological advances (Weigand et al., 2022) have shown the applicability of sEIT in monitoring mode at the field scale. In this work, an sEIT monitoring system is deployed in a winter wheat field to monitor the root system over a growing period from March to August. The aim is to establish the method as a tool to characterize the spatial extent and physiological state of crop root systems at the plot scale. Every two hours, surveys over a frequency range from 0.1 Hz to 10 kHz were conducted in a measurement profile with 40 stainless-steel electrodes and a total length of 9.75 m, delivering the high temporal resolution necessary for the investigation of plant activity related processes.

Methodology

The observed electrical polarization, as measured by the imaginary component of the complex conductivity (σ''), contains contributions on the account of both the root system and the soil, with the latter being dependent on soil texture, mineralogy, and water content. This makes the interpretation of σ'', or temporal changes therein, in terms of solely the root response a challenging task, in particular over a growing period during which soil moisture can strongly vary. However, previous studies have shown that the polarization of root biomatter is mainly taking place in the kHz range (e.g., Ozier-Lafontaine and Bajazet, 2005; Ehosioke et al., 2018; Peruzzo et al., 2021). It therefore can be expected that the combined soil-root response exhibits a stronger increase of imaginary conductivity with frequency compared to the soil response alone. Based on this, one can formulate the ratio between high (1 kHz) and low (1 Hz) frequency values of the imaginary conductivity as a rough indicator for the presence of root biomass in the investigated area. This ratio is introduced as the *electrical root index* (ERI):

$$ERI = \frac{\sigma''_{1kHz}}{\sigma''_{1Hz}}.$$

Although this simple approach is limited when the background soil spectra change significantly (e.g. due to strong changes in the soil water content or salinity), it allows a first interpretation of the root-soil-continuum in a root monitoring context for moderate background changes.

Using the ERI, the collected data are analyzed at two timescales, namely the overall seasonal evolution and the daily dynamics, as pictured in Figure 1. Selected timesteps over the season are inverted using the complex conductivity inversion code CRTomo (Kemna, 2000) to capture the spatial evolution of the root system over the growing period. The daily dynamics are investigated by looking into the short-term variations of the ERI for selected measurement configurations over several days and performing cross-wavelet transforms of the data with different environmental quantities (soil temperature, photosynthetic active radiation, conductivity magnitude).

Results

Inverting the set of 4-point impedance measurements yields complex conductivity distributions of the subsurface for different timesteps and frequencies during the season that can be converted to images of the ERI (Figure 1a). The resulting spatial distribution of the ERI over the growing period shows an overall increase near the surface that follows the expected rooting pattern of the winter wheat.

a) Seasonal scale
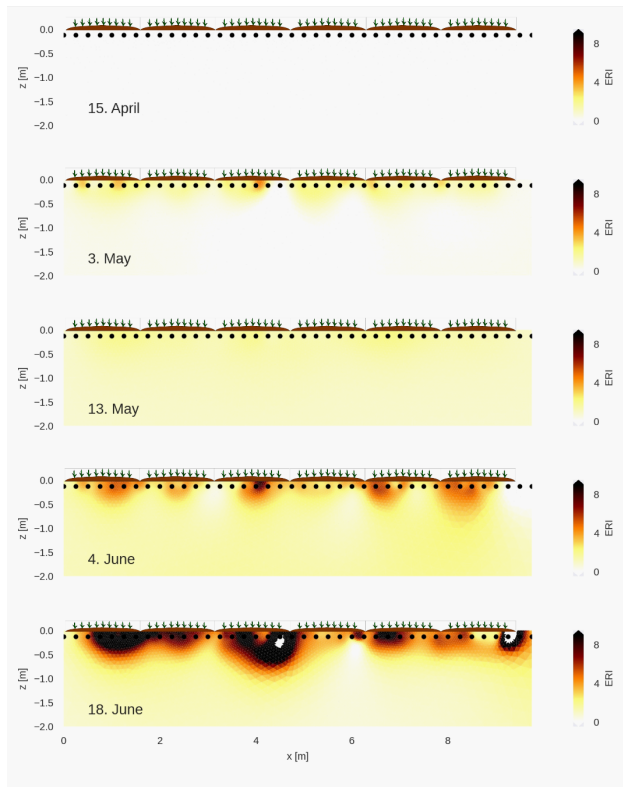
b) Diurnal scale
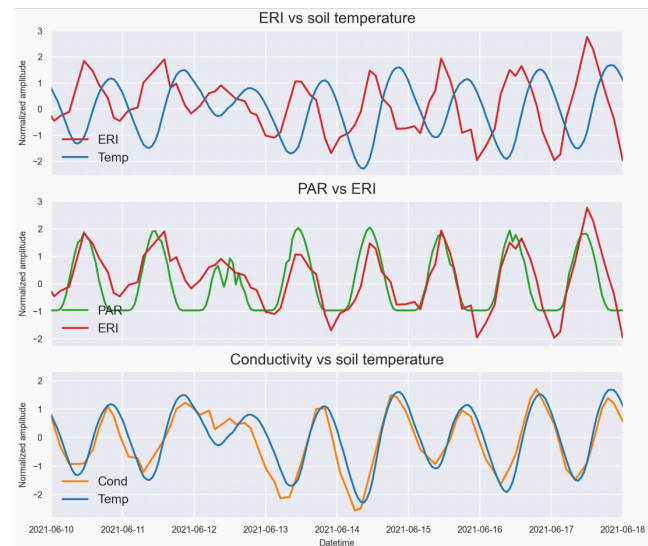
Figure 1. a) Seasonal evolution of the electrical root index. Pictured are five timesteps over the duration from April to June. b) Diurnal variations in the measured apparent ERI (normalized) for an exemplary measurement configuration, plotted against the soil temperature at 20 cm depth (upper) and the photosynthetic active radiation (middle). The lower plot shows the variations in the apparent conductivity magnitude against the soil temperature at 20 cm depth.

Investigating the daily dynamics, the analysis for a shorter timeframe of several days reveals that the ERI follows a cyclic 24 hour pattern (red line in Figure 1b). It is out of phase with the soil temperature variation, ruling out temperature variations as an explanation for the ERI behavior. However, it can be observed that the ERI does closely follow the photosynthetic active radiation (PAR) variations, indicating a correlation to the plant photosynthetic activity. The in-phase behavior between ERI and PAR is also confirmed by the cross-wavelet transform.

Conclusions

The deployed sEIT measurement system was successfully operated over several months at the field scale and it was possible to produce two-dimensional image series of the ERI for this period. The spatial distribution of the ERI in these images follows the expected rooting pattern of the sown winter wheat varieties. Looking into the daily variations, a 24 hour cyclic pattern of the ERI was observed that follows the photosynthetic active radiation. This correlation suggests that root activity related processes alter the polarization strength of the root system and can be measured with the sEIT method.

References

Ehosioke, S., Garré, S., Kremer, T., Rao, S., Kemna, A., Huisman, J.A., Javaux, M., & Nguyen, F. (2018). A new method for characterizing the complex electrical properties of root segments. ISSR International Symposium: Exposing the hidden half.

Ehosioke, S., Nguyen, F., Rao, S., Kremer, T., Placencia-Gomez, E., Huisman, J.A., Kemna, A., Javaux, M., & Garré, S. (2020). Sensing the electrical properties of roots: A review. Vadose Zone J., 19, 1539-1663. https://doi.org/10.1002/vzj2.20082.

Kemna, A. (2000). Tomographic inversion of complex resistivity: Theory and application. PhD thesis, Ruhr-University of Bochum.

Ozier-Lafontaine, H., & Bajazet, T. (2005). Analysis of Root Growth by Impedance Spectroscopy (EIS). Plant Soil, 277, 299-313. https://doi.org/10.1007/s11104-005-7531-3.

Peruzzo, L., Liu, X., Chou, C., Blancaflor, E., Zhao, H., Ma, X., Mary, B., Iván, V., Weigand, M., & Wu, Y. (2021). Three-channel electrical impedance spectroscopy for field-scale root phenotyping. The Plant Phenome Journal, 4(1), 2578-2703. https://doi.org/10.1002/ppj2.20021.

Weigand, M., & Kemna, A. (2019). Imaging and functional characterization of crop root systems using spectroscopic electrical impedance measurements. Plant Soil, 435, 201-224. https://doi.org/10.1007/s11104-018-3867-3.

Weigand, M., Zimmermann, E., Michels, V., Huisman. J.A., & Kemna, A. (2022). Design and operation of a long-term monitoring system for spectral electrical impedance tomography (sEIT). Geosci. Instrum. Method. Data Syst. Discuss [preprint]. https://doi.org/10.5194/gi-2021-36.

P20 - 3D Cole Cole Inversion of time domain induced polarization data

H. Langenbach and B. Tezkan

University of Cologne, Institute of Geophysics and Meteorology, Germany

Abstract. A 3D Cole Cole inversion algorithm for time-domain Induced Polarisation (IP) data is developed. The efficiency of the algorithm is demonstrated using synthetic data and field data measured in Krauthausen near Julich in Germany. The calculated 3D time-domain IP model is based on the time-dependence of the resistivity. The IP model considers chargeability, relaxation time and frequency exponent. The electrical field at each time point is inverted independently using a DC inversion code, based on the finite difference method and uses the reciprocity principle for calculating the sensitivity. In time-domain, the exact solution of the IP effect can be realised by calculating the electrical field values in frequency-domain, which are afterwards transformed into the time-domain. In the applied algorithm, an approximate solution is utilised where the forward problem is solved directly in the time-domain. Thereby, every time point is calculated independently from and parallel to each other. Neumann and Dirichlet boundary conditions are used and the linear set of equations is solved by a preconditioned method of conjugate gradients. Three types of regularisation are implemented: minimum gradient support, Occam L1 and L2 norm. First, the last time point of all transients is inverted resulting in a resistivity model. The resulting model of the previous time point is used as a starting model for the inversion of all time points. Afterwards, the estimated time-dependent resistivity for each cell is independently fitted using a half space IP model.

9 parallel time-domain IP profiles were measured in Krauthausen using the Terrameter LS by ABEM. A gradient array with an electrode spacing of 2.5 m was used to measure transients of up to 6 s. For pre-processing, a new routine was developed. After filtering, each time series is cut into transients. These transients are stacked and the standard deviation is calculated for every time point. After pre-processing, the data quality conforms to the high requirements of the inversion algorithm. The inversion of the field data with the newly developed 3D algorithm results in a satisfying 3D IP model for the survey area. A two layer resistivity model is estimated, where the second layer is partly interrupted. In comparison with former measurements and the geology, the obtained results are satisfying.

P21 - The evaluation of HIRIP data to investigate a large scale graphite anomaly in the Bavarian Forest/Germany

S. Schiebel[1], W. Mörbe[1], P. Yogeshwar[1], B. Tezkan[1], T. Günther[2] and M. Tauchnitz[3]

(1) Insitute of Geophysics and Meteorology, University of Cologne, Germany
(2) Leibniz Institute for Applied Geophysics, Hannover, Germany
(3) Terratec Geophysical Services GmbH & Co.KG, Heitersheim

Abstract. In the framework of the DESMEX2 (Deep Electromagnetic Sounding for Mineral Exploration, Becken, 2019) project funded by the BMBF a newly semi-airborne system was tested over a large-scale graphite deposit in the Bavarian Forest/Germany. Since strong IP effects of the target can overlay the measured EM-signal, Terratec Geophysical Services applied its own developed HIRIP survey system on two profiles to determine the IP influence. The HIRIP survey system (Tauchnitz et al. 2019) consists of simultaneous measurements of DCR and IP data, where the current and voltage electrode are separated to send a high-powered current into the subsurface . For measuring IP data in time domain, the voltage decay is measured within 20 time gates and the received decay curves are fitted with a Debye model to determine the initial chargeability m_0 in mV/V. Latter is used for the determination of the IP model. The evaluation of HIRIP data is based on the Gauß-Newton inversion method implemented in pyGIMLI (Günther & Rücker, 2012; Rücker et al., 2017), using the two-step inversion of Oldenburg & Li (1994). The forward response of HIRIP data is calculated on a 3D prism mesh and its inversion works on a 2D triangular mesh. Due to the survey conditions, the remote poles are in close distance to their profiles and are considered in the calculation of the geometry factor and in the inversion. Data measured for large offsets cannot be fitted properly and they had to be removed, therefore deep structures could not be resolved.

P22 - Numerical modelling of Stern-layer polarization in dense packings

J. Wentzki and D. Bücker

Institute of Geophysics and Extraterrestrial Physics, TU Braunschweig, Braunschweig, Germany

Presenter: M. Bücker (m.buecker@tu-braunschweig.de) **Student y/n:** No
Web page: https://www.tu-braunschweig.de/igep   **Preferred presentation oral/poster:** Poster

Abstract. We present a fine-element modelling approach, which allows simulating the complex-conductivity response of dense packings of grains. In our model, a simple, polarizable Stern layer covers the grains, which are immersed in an electrolyte solution. The interaction with charges in the electrolyte outside the Stern layer is taken into account by an effective boundary condition. This removes the need to discretize the field-induced diffuse layer, which builds up in response the polarization of the Stern layer. We first test our new model against analytical and earlier 2D rotationally symmetric finite-element models and then use it to study the influence of pairs and larger conglomerates of spherical grains. Our key findings are that (i) the Stern-layer polarization is generally reduced by the interaction with close neighbors and that (ii) an additional smaller polarization appears at frequencies slightly higher than the critical frequency of a single sphere.

Introduction

Finite-element models exist for induced polarization, which can be used to numerically calculate the conduction and polarization processes in the electrical double layer at the mineral surface of individual grains. The models we have used so far are based on 2D or 2D rotationally symmetric geometries (Bücker et al., 2019), which severely limits the ability to simulate realistic granular media. Even simple geometries of few spheres arranged next to each other (and not aligned with the external electric field) cannot be implemented in such a 2D geometry. A simple 1:1 translation of 2D models into 3D models is also not feasible. This is due to the need to fully discretize the diffuse part of the electric double layer, the thickness of which is mostly orders of magnitude smaller than the grain diameter. Thus, a 3D grid becomes too large even for a single spherical particle.

Effective boundary condition and new 3D model

To further develop our previous numerical model for the Stern-layer polarization (and the corresponding feedback with the charge carriers in the diffuse layer) into a full 3D model, we implement effective boundary conditions, which are based on the model by Lyklema et al. (1983). These boundary conditions take the diffuse layer into account without the need to actually

discretizing the latter. The new 3D model gives us the ability to simulate complex geometries for the first time, allowing us to achieve a significant approximation of computable models to real materials.

Model validation and first results

We test the output of our new model against the response of a single sphere computed with the analytical model by Lyklema et al. (1983) for the Stern-layer polarization of a single sphere as well as with our existing 2D-rotiational symmetric model (Bücker et al., 2019). The agreement between the three models is good over the entire modeled spectrum.

We also examine the polarization responses of both regular sphere packings (modeled on the solid-state structures SC, BCC, FCC, and the densest sphere packing) and irregular, randomly generated packings. The results show a varying decrease of the polarization response of the packings compared to the response of spheres without any interaction with neighboring spheres. In addition, we observe the appearance of a polarization at slightly higher frequencies compared to the main relaxation related to the mean diameter of the spherical grains.

Conclusions

We have developed and tested a new numerical model for Stern-layer polarization, which can be applied to much more complex geometrical models than before. As Stern-layer polarization is often argued to be the dominating process causing the low-frequency IP response of granular media, our new numerical model represents an important step towards the modelling of more complex and realistic geometrical configurations of solid matrix and fluid-filled pore space.

References

Bücker, M., Flores-Orozco, A., Undorf, S., and Kemna, A., 2019. On the Role of Stern- and Diffuse-Layer Polarization Mechanisms in Porous Media. Journal of Geophysical Research: Solid Earth, 124, 5656-5677.

Lyklema, J., Dukhin, S. S., and Shilov, V. N., 1983. The relaxation of the double layer around colloidal particles and the low-frequency dielectric dispersion: Part I. Theoretical considerations. Journal of Electroanalytical Chemistry and Interfacial Electrochemistry, 143, 1-21.

P23 - Multi-geophysical approach to characterize fracturation and characterize the transport properties of carbonate rocks

A. N. Yacouba[1], C. Mallet[1], J. Deparis[2], and D. Jougnot[3]

(1) Université d'Orléans, CNRS, BRGM, ISTO, UMR 7327, F-45071, Orléans, France
(2) BRGM, Orléans, France
(3) Sorbonne Université, CNRS, EPHE, UMR 7619 METIS, F-75005 Paris, France

Presenter: A. N. Yacouba (abdoul-nasser.yacouba-amani@univ-orleans.fr) **Student y/n:** Yes
Web page: NA   **Preferred presentation oral/poster:** Poster

Introduction

In a context of energy transition and overexploitation of water resources, studying the critical zone appears to be a major preoccupation. In order to address these scientific questions, the *Observatoire des transferts dans la Zone Non-Saturée* (OZNS - Observatory of transfers in the Vadose Zone) of Beauce (Orleans, France) has been designed in order to characterize Beauce limestone and monitor the aquifer pollution. In the same time, the site ensures its perfect evaluation thanks to several geoscience methods (geology, geophysics, hydrogeology, hydrology, etc.). The lacustrine Beauce limestone, main reservoir of the Beauce aquifer in the region (Lorain, 1973), is located between 10 and 20 m deep and presents important heterogeneous facies (microporosity, cracks, fractures, karstification). Its characterization requires multi-method and multi-scale (field and laboratory) studies. The presented project focuses on a laboratory study based on a multi-geophysical approach using samples coming from the O-ZNS site. The main objective is to carry out a characterization of the petrophysical and the transport/transfer properties of the Beauce limestone by combining ultrasound acoustic method (Bourbié, Coussy, & Zinszner, 1987) and complex resistivity (SIP and/or TDIP) method (Chelidze & Gueguen, 1999) (Craig & Peter, 1998). Major challenges to tackle: the complementarity of these both geophysical parameters knowing that each of them having different petrophysical sensitivity and resolution.

Material and methods

Four blocks (4-6 Kg from O-ZNS site) of different depth have been selected based on well logs analysis carried out on 4 well datasets acquired on the O-ZNS site, which made it possible to identify several facies of the Beauce limestone. In these blocks, samples have been cored considering two different diameters:

- samples of 4 cm in diameter with a length varying around 10 cm
- samples of 2.5 in diameter with a length less than 5 cm.

Samples of 4 cm-diameter (2 per facies) will be used to carry out a complete characterization including petrophysical measurement such as porosity (triple weighing, mercury porosimeter), and permeability (water and air permeability), and geophysical measurements coupling acoustic, SIP and TDR measurements. The ultrasound acoustic measurements will be carried out in dry and saturated conditions with longitudinal (P waves) and transverse (S waves) piezoelectric transducers (PZT) at different frequencies ranging from 1 MHz to 50 KHz.

The SIP measurements will be carried out with the SIP-LAB-IV apparatus using a 4-electrode configuration [fig. 1, (Cosenza & Ghorbani, 2007)] where the potential electrodes are non-polarizable Ag/AgCl electrocardiograms (ECG) and the current electrodes are made of carbon films. The other samples (2.5 cm-diameter) will be used for a further petro-acoustic study where the frequency effect as a function of heterogeneities will be looked for.

Expected results

The expected results are the following:

- a new or an updated petrophysical model of Beauce limestones
- a relationship between the petrophysical model and the geophysical parameters (acoustic velocities, complex resistivity, dielectric permittivity) at laboratory scale for Beauce limestone
- Relationship between the microstructure and the petrophysical model
- An understanding of the frequency effect on the acoustic limitations to characterize different heterogeneity sizes and a comparison to electrical frequency effects
- Extrapolation to field scale of the developed petrophysical model
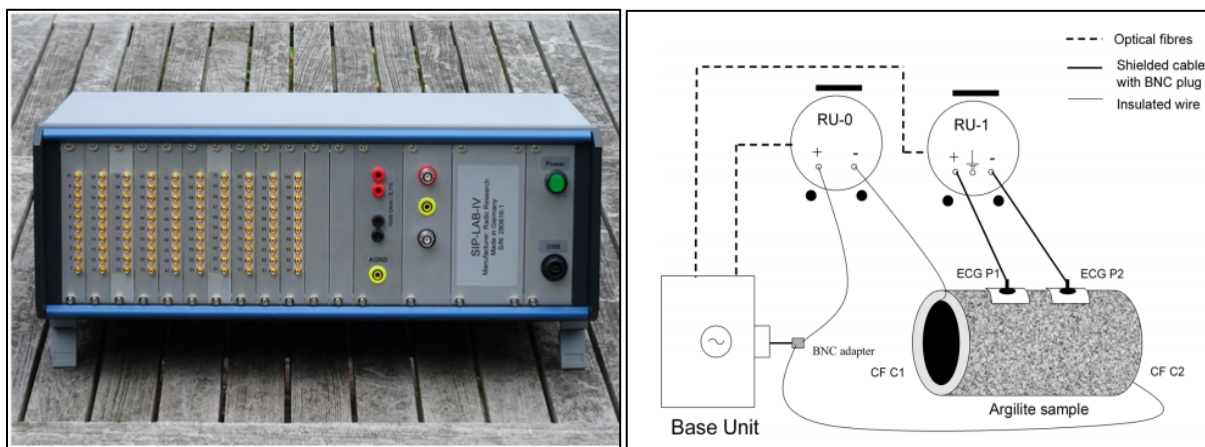
Figure 1: picture of the SIP-LAB-IV apparatus (left). Schematic presentation of the 4 electrodes configuration after P. Cosenza and al. (right): RU-0: Remote Unit 0 (or Transmitter); RU-1: Remote Unit 1 (or Receiver). ECG P1 and ECG P2: electrocardiogram Ag/AgCl electrodes as potential electrodes; CF C1 and CF C2: Carbon films as current electrodes.

References

Bourbié, T., Coussy, O., Zinszner, B. (1987). *Acoustics of porous media.* Houston: Technip.
Chelidze, T. L., Gueguen, Y. (1999). Electrical spectroscopy of porous rocks: a review-II. Experimental results and interpretation. *Geophys. J. Int., 137*, 16-34.
Cosenza, P., Ghorbani, A. (2007). Effects of Drying on the Low-Frequency Electrical Properties. *Pure appl. geophys.*, 1-24.
Craig, B., Peter, B. (1998). Time-domain Reflectometry (TDR) in Geotechnics: A review. *American Society of Testing and Materiels*.
Lorain, J. M. (1973). *La géologie du calcaire de Beauce. Bulletin de Liaison des Laboratoires des Ponts et Chaussées.* Blois.

P24 - Past metallurgic sites and deposits characterization using complex conductivity measurements

P. Kessouri[1], C. Ryckebusch[1], J. Deparis[1], A. Fernandez Visentini[1], J. Gance[2], D. Caterina[3], I. Isunza Manrique[3], F. Nguyen[3]

(1) BRGM, 3 av. Claude Guillemin, 45100 Orléans, France
(2) IRIS Instrument, 1 Av. Buffon, 45100 Orléans, France
(3) University of Liège, place du 20 Août 7, 4000 Liège, Belgium

Presenter: P. Kessouri (p.kessouri@brgm.fr) **Student y/n:** No
Web page: NA   **Preferred presentation oral/poster:** poster

Abstract. This study is part of a North West Europe (NWE) Interreg project called NWE-REGENERATIS that aims at the regeneration of past metallurgic sites and deposits through innovative circularity for raw materials. The example of the Pompey field site is used to present the interest in using TDIP field measurements to characterize metallurgical past deposits. Several paths are explored to convert resistivity and chargeability TDIP tomographies into quantitative interpretation of metallic element concentrations: (1) extraction of frequency data from TDIP field measurements; and (2) upscaling of lab results through numerical simulations.

Introduction

This study is part of a North West Europe (NWE) Interreg project called NWE-REGENERATIS (NWE-REGENERATIon of Past Metallurgical Sites and Deposits through innovative circularity for raw materials) that aims at the regeneration of past metallurgic sites and deposits through innovative circularity for raw materials. Metal foundry sites account for a significant proportion of potentially contaminated sites in the European Union. While recent wastes from sites still in operation are commonly recovered, this is not the case for old aggregated materials with a high content of ferrous (and other) metals, white and black slag, etc., which are considered to be sources of pollution and are costly to manage or dispose of. The NWE-REGENERATIS project transforms this situation into an opportunity: large volumes of resources (metals, materials and land) from former metallurgical sites and dumps can be recovered by urban mining techniques. NWE-REGENERATIS combines innovative geophysical characterization of sites with efficient material recovery processes, a harmonized inventory structure and the use of artificial intelligence algorithms (development of an open source 4D Smart Tool called SMARTIX), for resource recovery from metallurgical sites. Its final goal is to design and implement a new model, which enables the reintegration of raw materials and land in the regional economy.

Time domain induced polarization is applied on the pilot test sites of the project. It is a geophysical method known to be sensitive to the presence of various metallic particles disseminated in the soil layers (e.g. Bücker et al., 2018; Revil et al., 2015; Wong, 1979). If qualitative interpretation of the measured TDIP parameters (i.e. resistivity and chargeability) are widespread, quantitative interpretation in terms of concentrations of different metallic particles is yet to be developed. Several paths are explored in this study to reach this goal: (1) extraction of frequency data from TDIP field measurements; and (2) upscaling through numerical simulations.

In situ characterization of a past metallurgical site: the example of Pompey (France)

Pompey (France) has been chosen as one of the three pilot test sites for the NWE-REGENERATIS methodology. It is a former tailing pond, part of the past metallurgic site of Pompey-Frouard-Custine. It hosted various activities for iron-based alloys production, including special manganese steel. The last blast furnace of the iron and steel complex was stopped in 1986. Over time, a forest ecosystem, including diversified deciduous vegetation, more or less dense depending on the area, developed on the former tailing pond. The geological substratum consists of the Lias marl formations, which are covered by alluvium from the two rivers, composed of coarse siliceous materials (sands, gravel and pebbles) at the base, and finer materials (sands, silts and clays) on first 1 to 3 m depth. These alluvial formations were locally exploited and backfilled with metallurgical site deposits (e.g. waste rock, iron and steel by-products).

Several qualitative observations can be made on the TDIP results:

- 3 pseudo-horizontal layers are observed on the entire surface of the pond, in terms of electrical resistivity: (1) one resistant (**R4** in Figure 2) at the surface (between 2 and 3 m thick); (2) one conductive in the center (**C3** in Figure 1), with a thickness ranging from 4 (northern part) to 10 m southern part) ; (3) one with a medium resistivity at the base (**R3** in Figure 1) (between 8 and 9 m deep), that can be interpreted as the natural terrain (quaternary alluvium). Other more localized layers can also be identified (i.e. R1 or R2 in Figure 1), but their interpretation will not be developed here.
- For the conductive layer **C3**, a distinction can be made between the SSE and NNW parts of the ERT profiles (see Figure 2). These variations could correspond to the presence of 2 different settling pounds (not mentioned in the historical documents) with two different variations in the composition of the deposited material (observed on historical aerial photos).
- Chargeability anomalies, especially localized in the first resistant layer (e.g. layer R1 in figure 1), are potentially linked to all-comers household and construction wastes, including large metallic pieces.
- The chargeability of the intermediate layer could be mitigated by the high conductivity of this layer. The metal factor might be a better parameter to reveal pronounced anomalies in the conductive intermediate layer interpreted as the main tailing material layer.
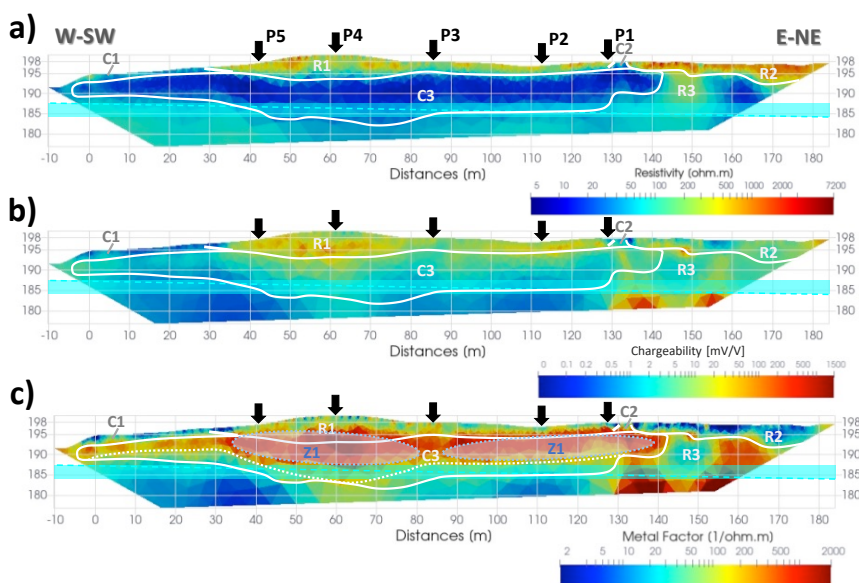
Figure 1. Example of a tomography results measured at Pompey (France). The parameters presented are: a) the inverted electrical resistivity, b) the inverted chargeability, c) the estimated metal factor. The black arrow and line represent the position of the profiles measured perpendicular to the shown profile. The turquoise rectangle and associated dotted line corresponds to the known range of the water level. White lines correspond to interpreted limits of electrical resistivity layers named Cn or Rn, depending on their resistive or conductive relative nature. Dotted white lines correspond to the limits interpreted from the metal factor variations. Light blue circles highlight zones of particular interest called Z1, with the highest MF values.

New developments to extract frequency data from TDIP file measurements

6 TDIP profiles were measured in Pompey. On one of the profile, IP data were acquired in several ways: (1) in 50 % duty cycle with an acquisition time of 2 s ; and (2) in full cycle with an acquisition time of (1.1) 2 s ; (1.2) 1 s ; (1.3) 500 ms and (1.4) 250 ms. This measurement with different time windows (different frequencies) gives us access to SIP processing and interpretation, not only at the fundamental frequency, but also at the first four odd harmonics. These new frequency interpretations of the TDIP data allows us to better understand the polarization processes occurring at the field scale. Indeed they can be compared to lab measurements run on samples from the site as well _____ lab. The upscaling of these relationships is thus facil
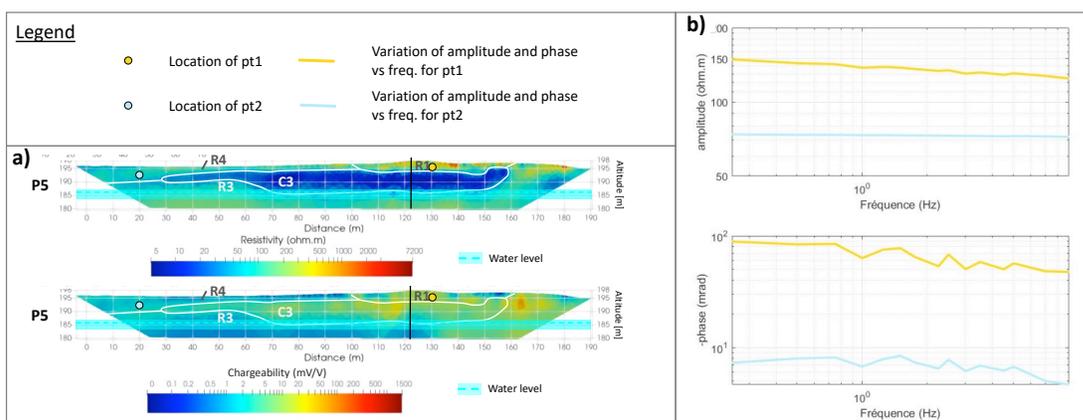
Figure 2: a) resistivity and chargeability tomography results measured at Pompey (France) with the location of 2 points that present different frequency signatures; b) amplitude and phase of the resistivity versus frequency for 2 selected points of the 2D profile (pt1 and pt2).

Towards quantitative interpretation of TDIP measurements

In order to interpret the TDIP results in terms of concentration of metallic particles, known petrophysical relationships (e.g. Revil et al., 2015a; Wong, 1979) and geochemical measurements obtained at the lab scale need to be interpreted at the field scale. Indeed, the geophysical properties estimated by the field-scale study are impacted by factors such as complex averaging of heterogeneity at the survey scale, and also artifacts introduced through data inversion. With the data from Pompey, we propose to use a Bayesian framework for inferring field-scale metallic particles concentrations. This work is ongoing.

Conclusions

The interest of using TDIP measurements to characterize metallurgical past deposits has been shown through an example at the Pompey pilot site. The combination of resistivity and chargeability data shows potential to estimate the volume of metallic compounds that could be re-used within the tailing pond. To reach a more quantitative interpretation in terms of concentrations of different metallic particles, several approaches are explored. The extraction of frequency data from TDIP measurements shows promising results to delineate areas with different frequency signatures. The upscaling approach through numerical simulations is yet to be completed, but seems to present interesting outgrowth. To go even further, these geophysical characterizations will be part of the entry parameters in the artificial intelligence software SMARTIX that will provide a fully integrated response to resource recovery potential of the studied field site.

References

Bücker, M., Flores Orozco, A., Kemna, A., 2018. Electro-chemical polarization around metallic particles – Part 1: The role of diffuse-layer and volume-diffusion relaxation. GEOPHYSICS 1–53. https://doi.org/10.1190/geo2017-0401.1

Revil, A., Abdel Aal, G.Z., Atekwana, E.A., Mao, D., Florsch, N., 2015a. Induced polarization response of porous media with metallic particles — Part 2: Comparison with a broad database of experimental data. Geophysics 80, 552–551. https://doi.org/10.1190/GEO2014-0578.1

Revil, A., Florsch, N., Mao, D., 2015b. Induced polarization response of porous media with metallic particles — Part 1: A theory for disseminated semiconductors. Geophysics 80, 525–538. https://doi.org/10.1190/GEO2014-0577.1

Wong, J., 1979. An electrochemical model of the induced-polarization phenomenon in disseminated sulfide ores. Geophysics 44.

P 25- Understanding landslide triggering processes with induced polarization - Case studies in New Caledonia

S. Barde Cabusson[1], P. Vaudelet[1], A. Revil[2] and P-A. Duvillard[13]

(1) NAGA Geophysics, Le Bourget-du-Lac, France
(2) Univ. Grenoble Alpes, Univ. Savoie Mont-Blanc, CNRS, UMR CNRS 5204, EDYTEM, 73370 Le Bourget du Lac, France
(3) STYX 4D, Le Bourget-du-Lac, France

Presenter: S. Barde Cabusson (stephanie.barde-cabusson@naga-geophyiscs.com)
Web page: www.naga-geophysics.com   **Preferred presentation oral/poster:** Poster

Abstract. Understanding and diagnosing the triggering process of landslides is a major issue for the implementation of preventive measures. Over the past decade, great progress has been made in the induced polarization geophysical method, from field acquisition to the understanding of the underlying petrophysical mechanisms. Today, these advances provide access to essential parameters for the study of landslides, such as water and clay contents as well as permeability. The possibility of imaging these parameters in the underground with a non-intrusive method all over a risky site allows us to develop a new alert tool based on this technique.

Introduction

Hazard anticipation is fundamental to minimize risk. Traditionally, a geomorphological analysis makes it possible to map the potential for landslides, depending on the issues, in order to identify which sites need to be monitored. There are many existing tools, such as LIDAR, interferometry or optic, to survey a ground movement (Jaboyedoff et al., 2012, 2019). The challenge is to develop an approach to alert before the critical limit is reached. The most important risk is related to clay-rich landslides because they lead to rapid movements. Their mechanisms depend on the water content, which, when a critical threshold is exceeded, generating partial or complete liquefaction. Recently, somes studies demonstrated that an approach using seismic noise monitoring can detect this threshold (e.g. Le Breton et al., 2021). Our ambition is to propose a method to follow the water content evolution in order to alert before the mechanism is engaged. In this way, we take advantage of the past decade's progress in induced polarization to characterize and diagnose landslides.

Method

Time-domain induced polarization datasets were acquired on landslide sites in New Caledonia. Petrophysical measurements on samples from the sites validate a recent mechanistic fundamental mechanistic model called the dynamic Stern layer model. This model was applied to interpret the conductivity and normalized chargeability tomograms obtained in the field. Thus a procedure was developed to image the water content, the cation exchange capacity, and the permeability distribution at the test sites.

Case studies

At the beginning of 2021, New Caledonia was subjected to bad weather in the context of a climatic episode 'La Nina' with an increase in rainfall causing many landslides. We show here two cases on peridotite laterites, the first one concern a slide of the mine waste slopes and the second on natural environment.
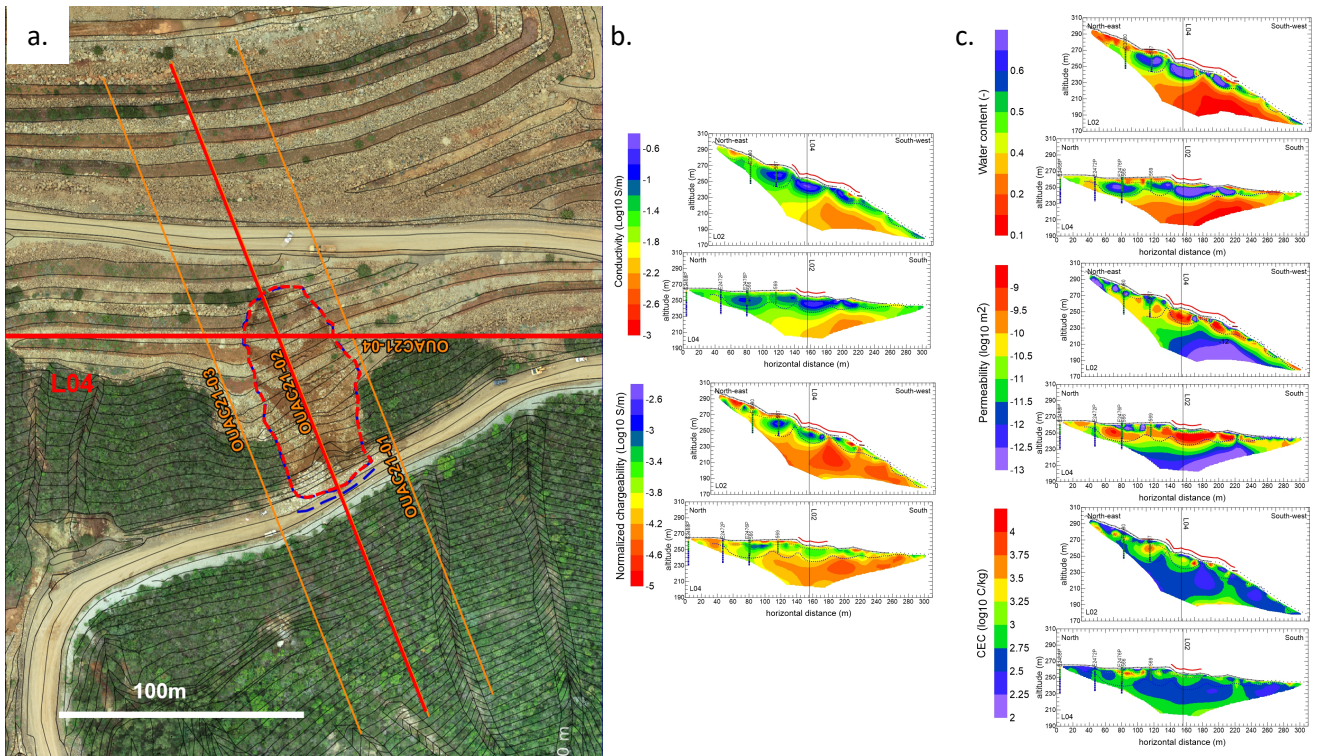
Figure 7. Case study #1 – a landslide on mining exploitation. a. Localization of measurements b. Geoelectrical tomograms (conductivity and normalized chargeability) c. Hydrogeological parameters from the petrophysical modelling.
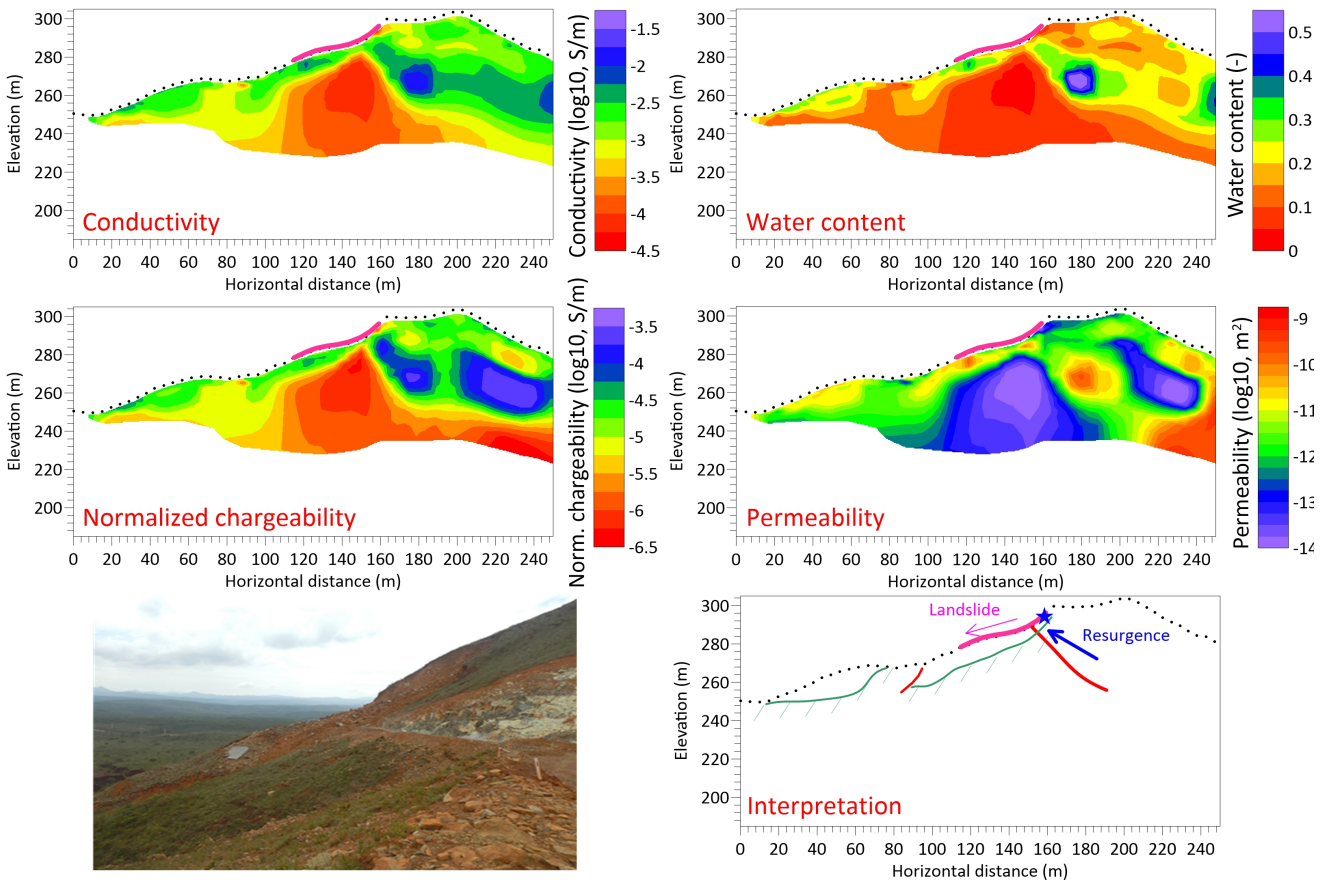
Figure 8. Case study #2 – Geoelectrical tomograms (conductivity and normalized chargeability) and hydrogeological parameters from the petrophysical modelling, with interpretations

Conclusions

The comprehension of petrophysical models allows to interpret induced polarization from the field with a quantitative approach to determine water content, permeability and CEC (associated with the clay content). These parameters are necessary for the understanding of the triggering mechanisms of landslides. Induced polarization appears as a promising non-intrusive geophysical imaging method to monitor crucial change in the soil in order to alert one step ahead. In the future, a 4D approach will be developed to propose a tool for the monitoring sites associated with such geohazards.

References

Jaboyedoff, M., Oppikofer, T., Abellán, A., Derron, M.-H., Loye, A., Metzger, R., et al. (2012). Use of LIDAR in landslide investigations: a review. Nat. Hazards 61. 5–28.

Jaboyedoff, M., Del Gaudio, V., Derron, M.H., Grandjean, G. and Jongmans, D., (2019). Characterizing and monitoring landslide processes using remote sensing and geophysics. Engineering Geology, 259, p.105167.

Le Breton, M., Bontemps, N., Guillemot, A., Baillet, L., & Larose, É. (2021). Landslide monitoring using seismic ambient noise correlation: challenges and applications. Earth-Science Reviews, 103518.

Soueid Ahmed, A., & Revil, A. (2018a). 3-D time-domain induced polarization tomography: a new approach based on a source current density formulation. Geophysical Journal International, 213(1), 244-260.

Soueid Ahmed, A., Revil, A., Jardani, A., & Chen, R. (2018b). 3D geostatistical inversion of induced polarization data and its application to coal seam fires. Geophysics, 83(3), 1–59.

Revil A., Soueid Ahmed A., Coperey A., Ravanel L., Sharma R., Panwar N. (2020) Induced polarization as a tool to characterize shallow landslides. Journal of Hydrology, 589, 125369.

Part 3. Field excursion

The Aiguille du Midi

A pilot site for the investigation of rock wall permafrost

1. Caracteristics *(from Magnin et al., 2015)*

The AdM lies on the NW side of the Mont Blanc Massif (Fig. 1). Its summit (45.88_ N, 6.89_ E) consists of three granite peaks (Piton Nord, Piton Central, and Piton Sud) and culminates at 3842 m a.s.l. The steep and partly glaciated north and west faces of the AdM tower more than 1000m above the Glacier des Pélerins and Glacier des Bossons, while its south face rises just 250m above the Glacier du Géant (i.e. the accumulation zone of the Mer de Glace). This part of the Mont Blanc Massif is formed by an inclusion-rich, porphyritic granite and is bounded by a wide shear zone. A main, N 40_ E fault network intersected by a secondary network determines the distribution of the main granite spurs and gullies (Leloup et al., 2005). The highest parts of the peak tend to be steep, contain few large fractures, and, in places, are characterized by vertical foliation bands and small fissures. The lower parts are less steep and more fractured. In the present paper we use the abbreviation AdM to refer only to the upper section of the Piton Central, between 3740 and 3842ma.s.l. where most of the instruments are installed. A tourist cable car runs from Chamonix to the Piton Nord. Galleries and an elevator allow visitors to gain the viewing platform on top of the Piton Central, from where there is a 360_ panorama of the Mont Blanc Massif. We chose the AdM as a monitoring site for the following scientific and logistical reasons: (i) permafrost is extremely likely due to the AdM's high altitude and the presence of cold-based hanging glaciers on its north face; (ii) the morphology of the peak offers a range of aspects, slope angles and fracture densities that are representative of many other rock walls in the massif; (iii) the easy access by cable car from Chamonix and the availability of services (e.g. electricity) at the summit station. Monitoring equipment was installed as part of the PERMAdataROC (2006–2008) and PermaNET (2008–2011) projects, funded by the European Union and run jointly by EDYTEM Lab (France), ARPA VdA (Italy), and the Universities of Zurich (Switzerland), Bonn and Munich (Germany). As such, it complements other rock wall observation sites – for example, those within the Swiss Permafrost Monitoring Network (PERMOS). Data from the monitoring equipment on the AdM were completed by data from ARPA VdA's weather stations, which measured air temperature and relative humidity, incoming and outgoing shortwave and longwave solar radiation, wind speed, and wind direction on the south and north faces between 2006 and 2010. Electrical Resistivity Tomography (ERT) and Induced Polarization (IP) have been measured since 2008 in conjunction with the universities of Bonn and Munich. High-resolution (cm scale) triangulated irregular networks (TIN) of rock walls and galleries of the AdM were obtained from terrestrial laser scanning. In July 2012, six crack-meters equipped with wireless sensors were installed in major fractures in the Piton Central and Piton Nord in order to complement existing studies of cleft dilatations and shearing movements in rock wall permafrost, to check the stability of the AdM and to test an early warning system. Finally, two GPR surveys were performed along vertical transects in 2013 and 2014. Not all of these data were used in the present study but they will contribute to future research.

2. Rock temperature monitoring

The present study is based on rock surface temperatures taken at the top of the AdM (between 3815 and 3825ma.s.l.; Fig. 2) since 2005 by a network of mini-loggers (GeoPrecision PT1000 sensors, accuracy _0.1 _C) installed by the University of Zurich and ARPA VdA. Two loggers were installed in snow-free locations on each face of the AdM (Table 1). The south face has an additional logger (S3) installed just above a small ledge on which snow accumulates in winter, covering the logger. The loggers record the temperature every hour at depths of 0.03, 0.30 and 0.55 m, in line with the method described by Gruber et al. (2003). In September 2009, three boreholes were drilled in the lower section of the Piton Central, at between 3738 and 3753ma.s.l. In order to minimize possible thermal disturbances caused by air ventilation in the galleries and heating from staff rooms, the boreholes were drilled several tens of metres below the galleries running through the AdM. The criteria used to decide the exact location of each borehole were the aspect, fracturing, roughness and angle of the rock wall (Fig. 2). Each borehole was drilled perpendicular to the rock surface and to a depth of 11 m. Borehole depths were constrained by the drilling equipment and the funding available. The boreholes on the northeast (BH_E) and south (BH_S) faces were drilled in fractured rock walls that slope at 65 and 55°, respectively. Even on rock walls at these angles, snow can accumulate on the micro-reliefs in the face. The borehole on the northwest face (BH_N) was drilled in a vertical, unfractured wall. The only place that snow can accumulate on this wall is on small ledges such as the one above which BH_N was drilled. The boreholes were drilled between 14 and 27 September 2009 by a team of five people (two mountain guides, plus three members of the EDYTEM Lab) who had to contend with very variable weather and challenging logistics. For each borehole it was necessary to: (i) install a safety line for the workers, (ii) set up a rope system to carry the equipment from the galleries to the drill site, (iii) install a work platform for the three drillers, (iv) anchor a base on which to fix a rack way, (v) drill the hole using a 380VWeka Diamond-Core DK 22 electric drill, (vi) insert into the hole a polyethylene PE100 tube (outer diameter: 40 mm; inner diameter: 29 mm) sealed at its bottom, and (vii) remove the work platform. In addition to the difficult environment and harsh weather, the drilling work was complicated by the heterogeneity and hardness of the granite, which took a heavy toll on the equipment (11 diamond heads worn out or broken, a dozen steel tubes damaged, and a motor broken). At first we tried to drill 46mm diameter boreholes but we had to increase the diameter to 66mm so we could use a more robust pipe string. Cooling required 1 to 3m3 of water per day, which was carried up from Chamonix in 1m3 tanks via the cable car. Space between the drill hole and the casing was not filled. The three boreholes were fitted with 10 m length Stump thermistor chains, each with 15 nodes (YSI 44031 sensors, accuracy _0.1 _C) arranged along a 6mm fiberglass rod. Following calibration at 0 _C in an ice-water basin, the sensors were inserted in BH_S and BH_N in December 2009 and in BH_E in April 2010 (Fig. 3). In order to prevent heat convection, each sensor was separated from the others on the chain by insulating foam. The boreholes were closed at the top, but the chains can be removed to check for thermistor drift. Rock temperatures at depths between 0.3 and 10m are recorded every 3 hours (Table 1). Because BH_S is shallower than 10 m, the thermistor chain protrudes from the rock surface by 36 cm. Temperature comparisons between BH_S and BH_N/BH_E were carried out at the closest equivalent depths (e.g. temperatures at a depth of 2.64m in BH_S were compared with temperatures at a depth of 2.5m in BH_E and BH_N).
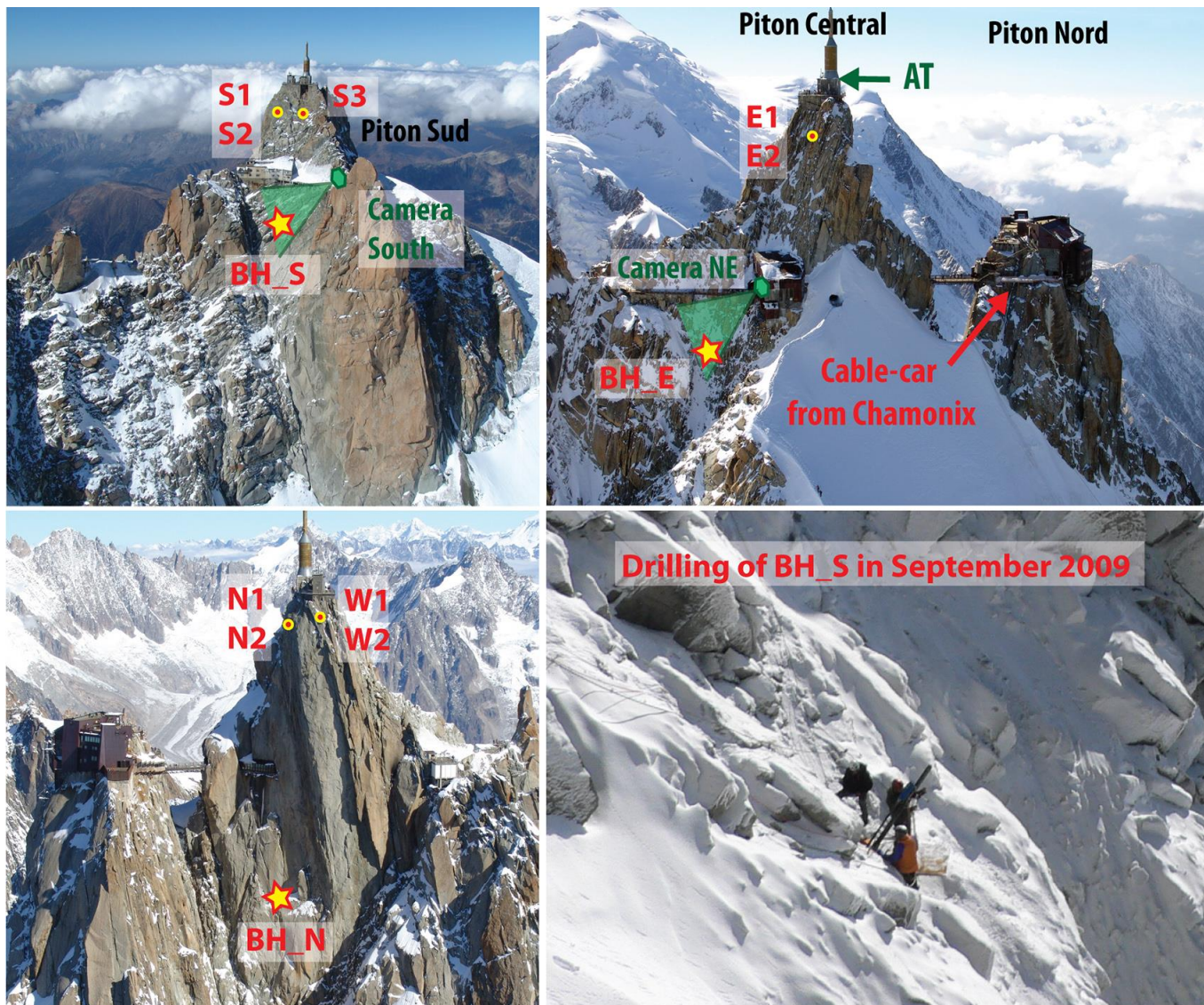
Figure 1. Temperature boreholes and surface sensors locations

Table 1. Instrument positions. BH: borehole thermistor chains, X1 and X2: rock surface temperature loggers, AT: air temperature. Estimated snow accumulation: from automatic cameras and probes for BH_S and BH_E (winter 2012 and 2013), from field observation for S3 and BH_N.

Site Code	Elevation [m a.s.l]	Aspect [°]	Slope [°]	Sensor depths [m]	Estimated snow accumulation [m]
BH_S	3753	135	55	0.14, 0.34, 0.74, 1.04, 1.34, 1.64, 2.14, 2.64, 3.64, 4.64, 6.64, 8.64, 9.64	> 0.8
BH_N	3738	345	90	0.3, 0.5, 0.7, 0.9, 1.1, 1.4, 1.7, 2, 2.5, 3, 4, 5, 7, 9, 10	> 1.0
BH_E	3745	50	65	0.3, 0.5, 0.7, 0.9, 1.1, 1.4, 1.7, 2, 2.5, 3, 4, 5, 7, 9, 10	< 0.6
W1	3825	270	80	0.1	0
S1	3820	140	74	0.1	0
N1	3820	354	84	0.1	0
E1	3823	124	60	0.1	0
N2	3820	334	80	0.03, 0.1, 0.3, 0.55	0
E2	3820	118	60	0.03, 0.1, 0.3, 0.55	0
S2	3815	160	85	0.03, 0.1, 0.3, 0.55	0
W2	3825	270	85	0.03, 0.1, 0.3, 0.55	0
S3	3820	158	70	0.03, 0.1, 0.3, 0.55	0.5 to 1.0
AT	3845	0	0		0

Figure 2. Temperature evolution at 10 m depth and Tz (Temperature-depth) profiles (non-published). Blue = BH_N, Yellow = BH_E, red = BH_S for hydrological years (1st Oct – 30th Sept)
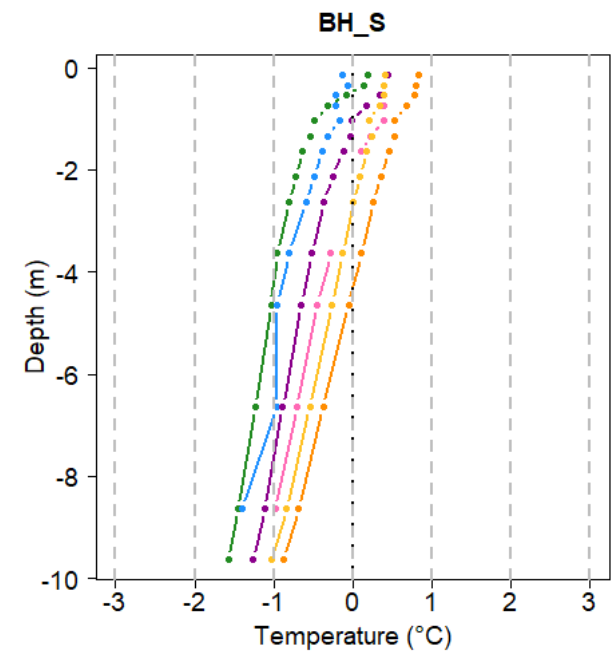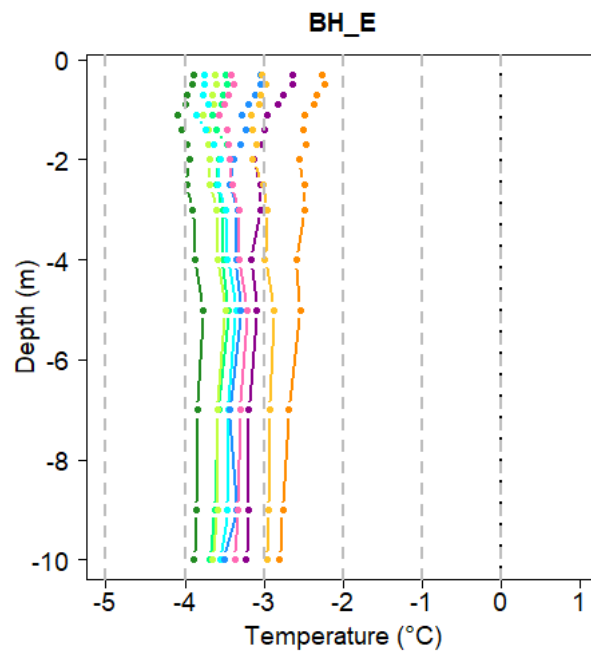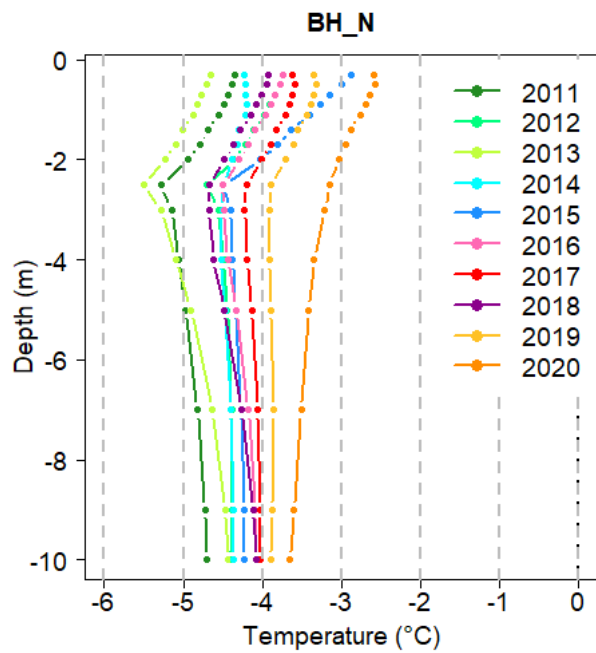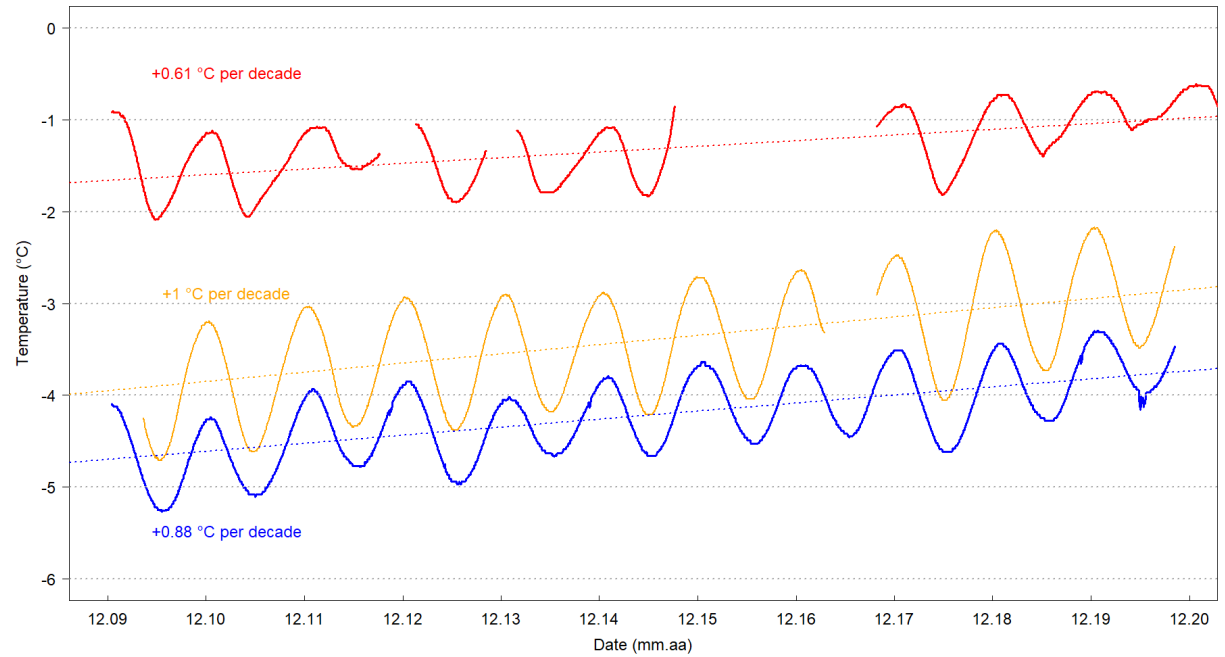
Figure 3. Maximum activer layer depth registered in the boreholes
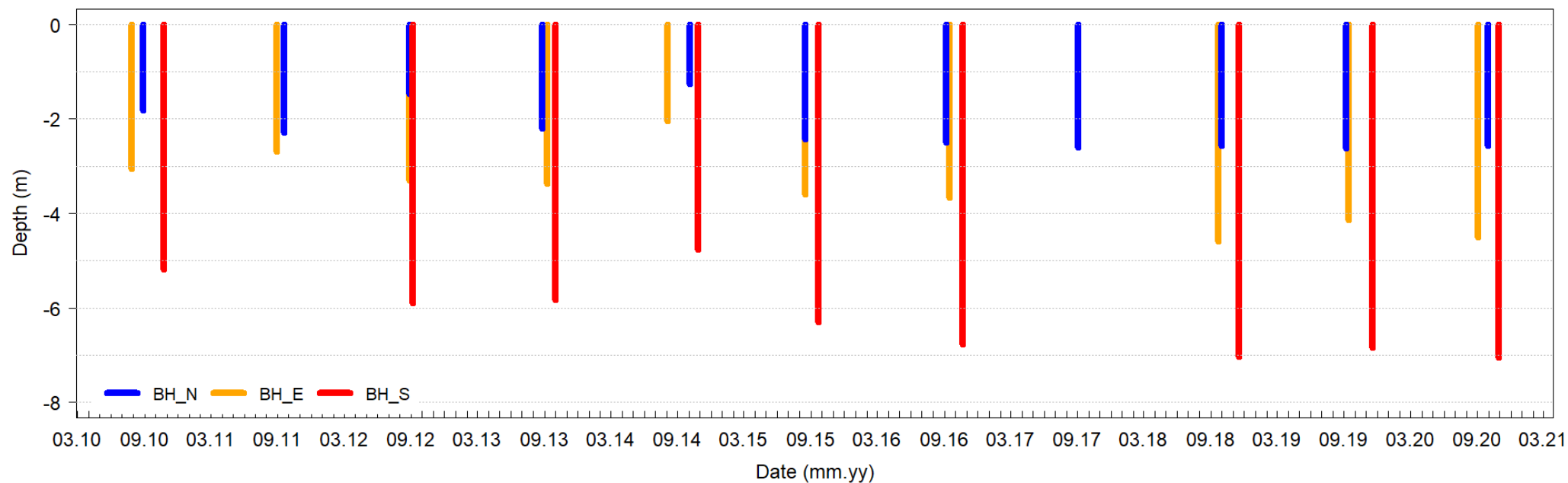
Air temperature records (annual means, °C) ➔ hydro years

	2011	2012	2013	2014	2015	2016	2017	2018	2019	2020
AdM (3842 m)	-7.43	-7.33	-7.78	-7.41	-6.72	-6.86	-6.88	-7.19	-6.82	NA
Chamonix (1042 m)	7.07	6.57	6.37	7.06	7.77	7.16	7.2	7.35	7.33	8.15
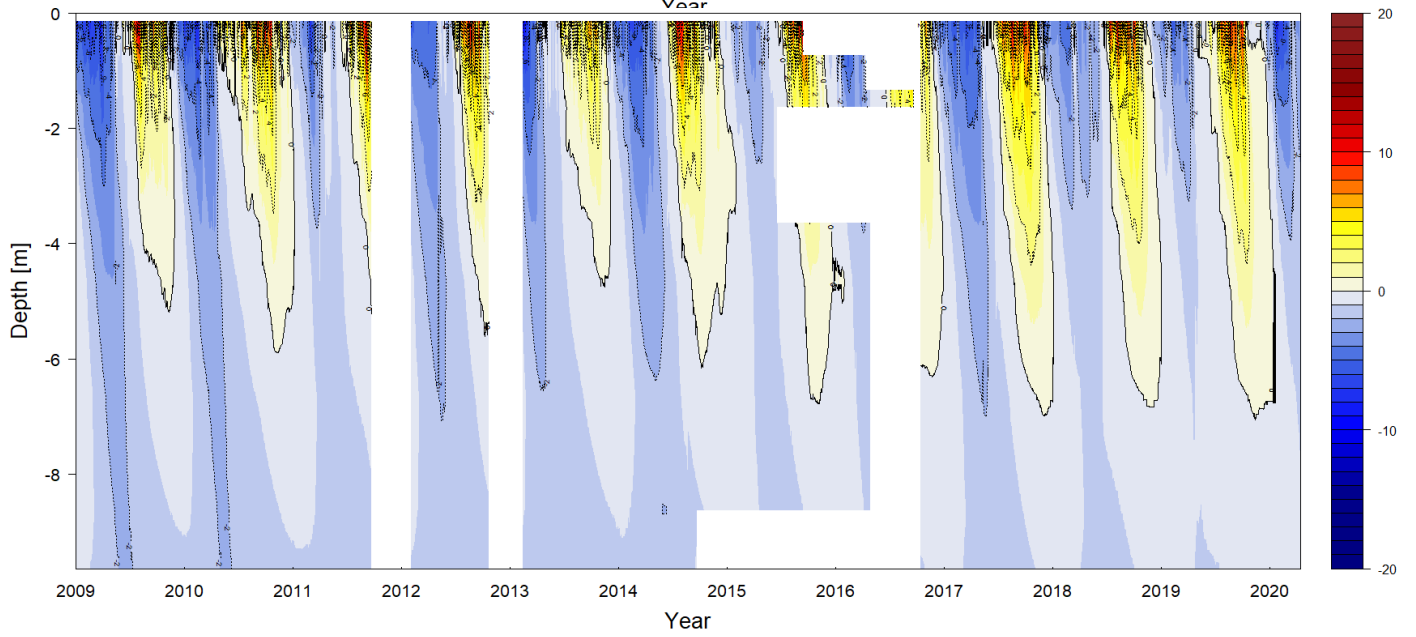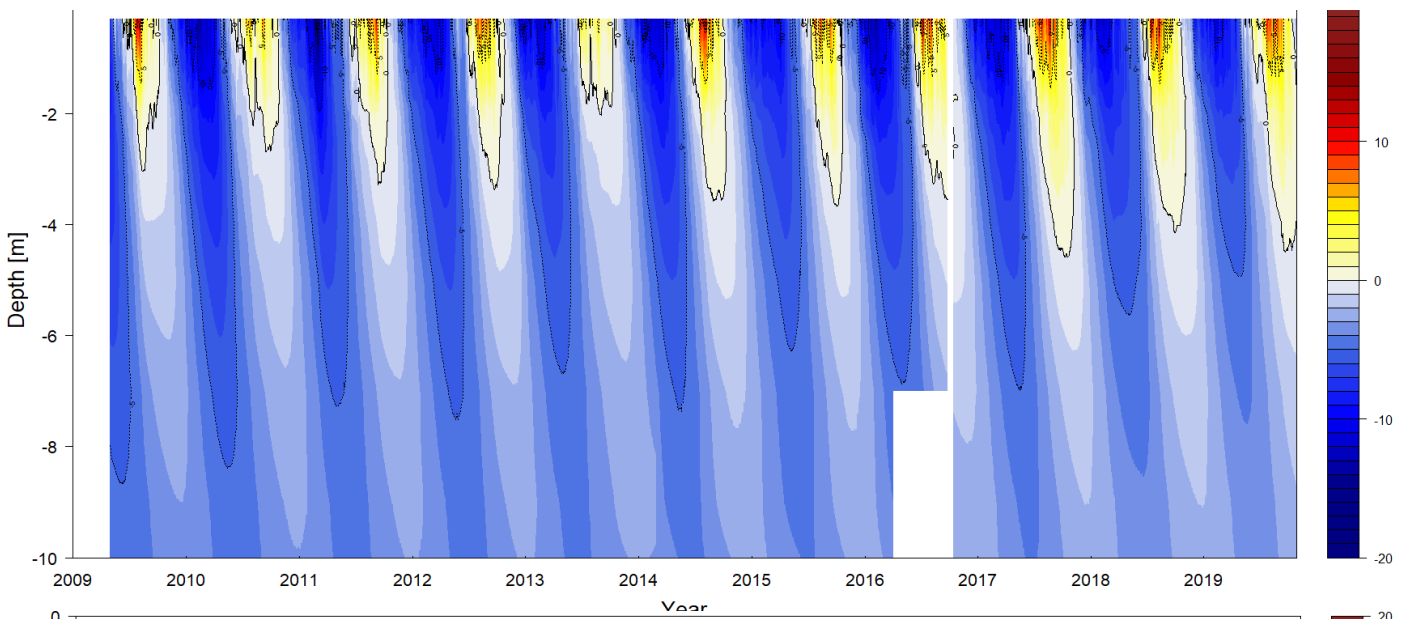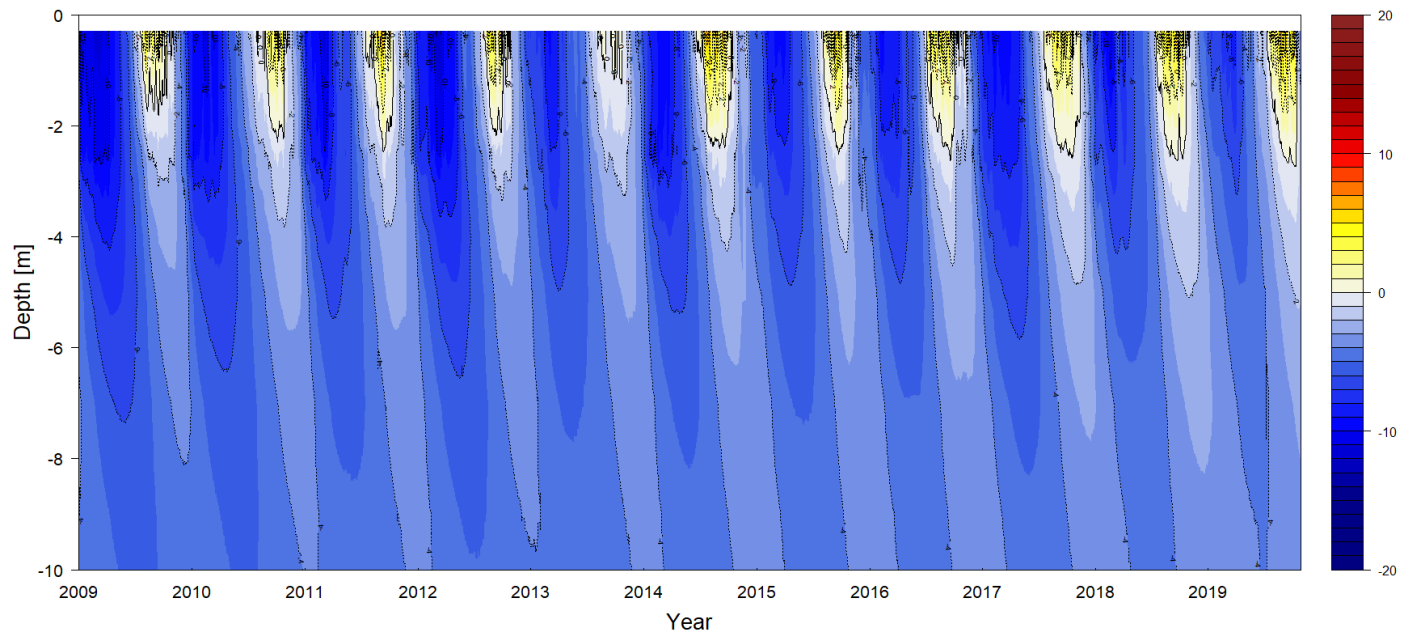
Figure 4. Daily temperature evolution in the three boreholes (from top to bottom : BH_N, BH_E , BH_S)

3. Effects of snow (Magnin et al., 2017a)

Figure 5. The Aiguille du Midi site and monitoring network used in this study. PC: Piton Central; PN: Piton Nord; PS: Piton Sud; CS: camera on the South face; CE: camera on the NE face; BH_S, BH_N and BH_E: boreholes on the S, NW, and NE faces, respectively; MFWS: Météo France weather station; SWS: automatic weather station on the South face; S1: surface logger on the South face.
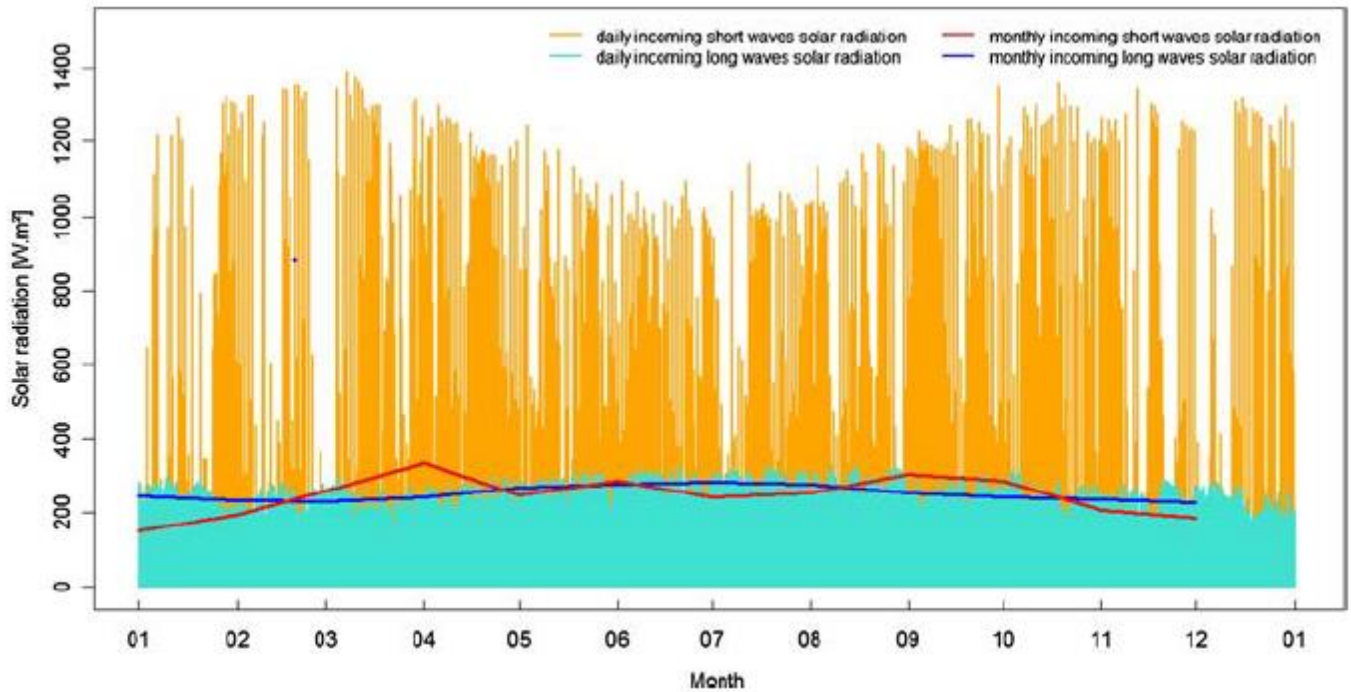
Figure 6. Daily incoming short-wave (orange) and long-wave (turquoise) solar radiation and monthly averages (red and blue) measured at the Aiguille du Midi south face in 2007.

⇨ These data were used to Run CryoGRID 3 (among others). Then the model was run with various snow fall scenarios to test the sensitivity of permafrost to this unknown paramater. The heat conduction model is run with thermal paramaters calibrated with the Bh8S temperature data.

⇨ Results are shown on Figure 7 which shows that permafrost subsists only because of snow in spring and early autumn, and summe snow also favors its presence. When snow only falls in winter, permafrost doesn't exist any more.
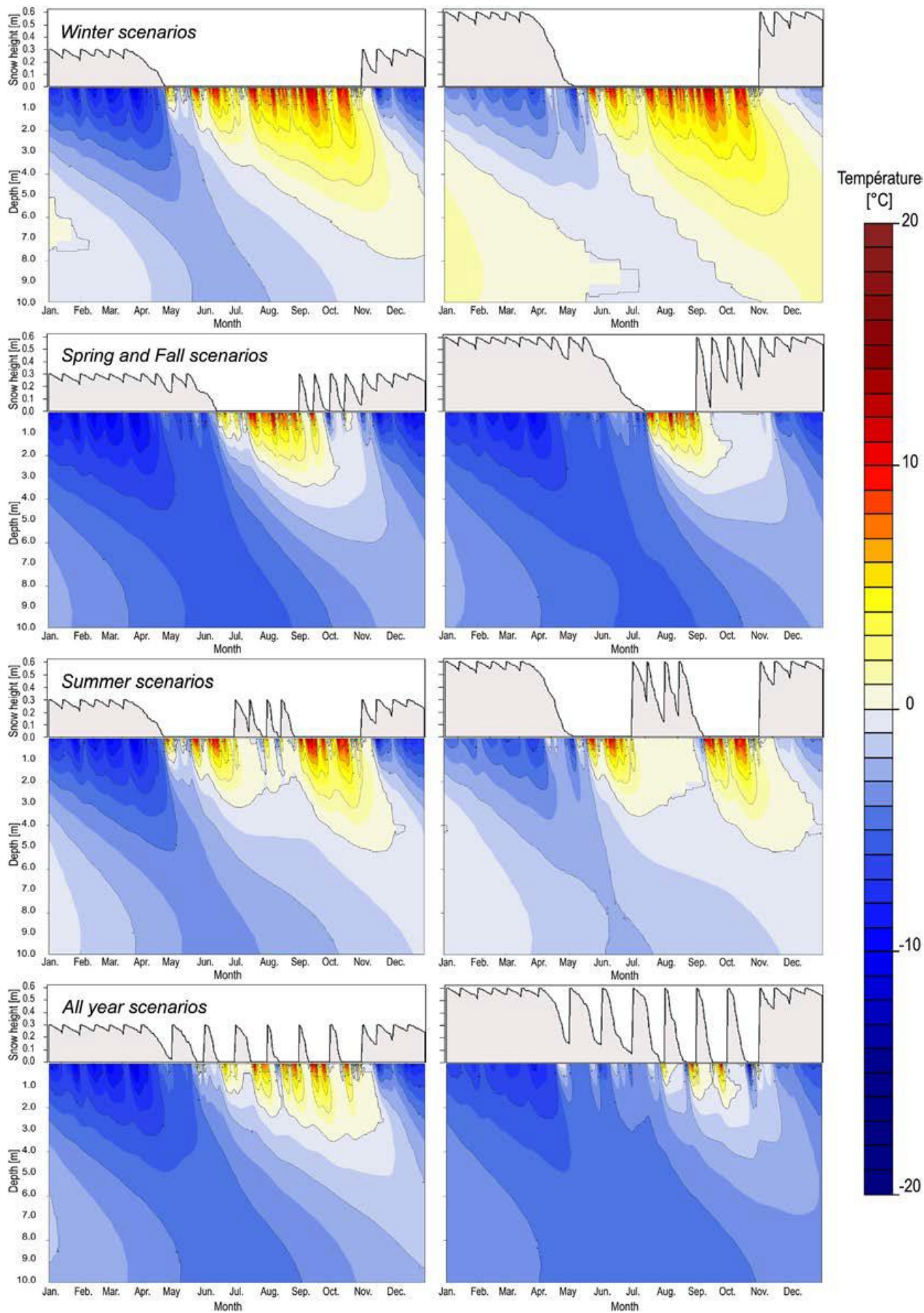
Figure 7. Results of Cryogrid3 runs with various snow fall scenarios

4. Permafrost evolution in the Central Pillar (Magnin et al., 2017b)
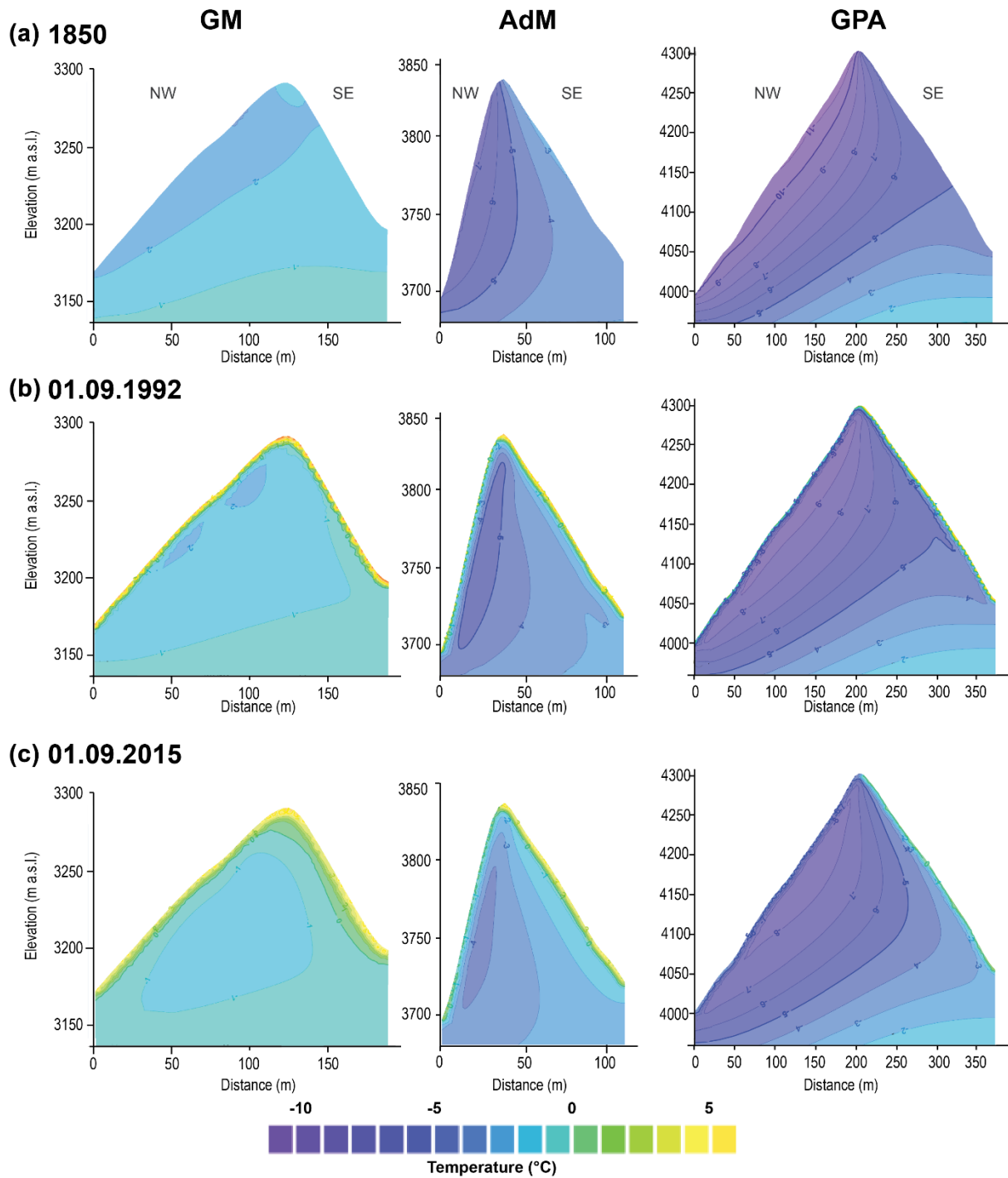
Figure 8. Past evolution of permafrost for 3 sites of the Mont Blanc massif, including the Aiguille du Midi (surface temperature forced with air temperature anomaly/day-to-day change, and heat transfer simulated with heat conduction and latent heat exchanges in a homogeneous and isotropic rock mass)
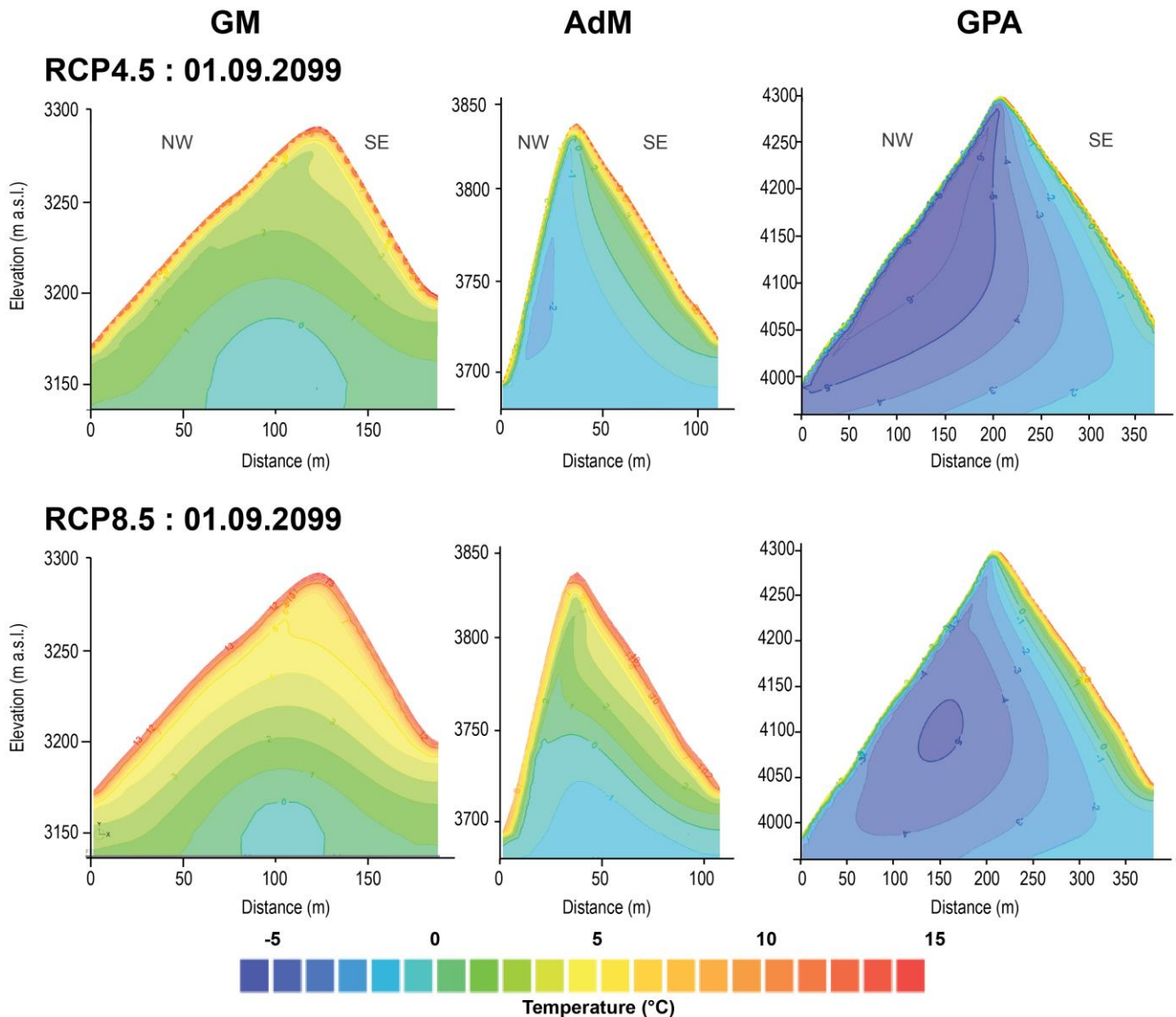
Figure 9. Future evolution according to various RCP.

Ref

Magnin, F., Deline, P., Ravanel, L., Noetzli, J., and Pogliotti, P.: Thermal characteristics of permafrost in the steep alpine rock walls of the Aiguille du Midi (Mont Blanc Massif, 3842 m a.s.l), 9, 109–121, https://doi.org/10.5194/tc-9-109-2015, 2015.

Magnin, F., Westermann, S., Pogliotti, P., Ravanel, L., Deline, P., and Malet, E.: Snow control on active layer thickness in steep alpine rock walls (Aiguille du Midi, 3842ma.s.l., Mont Blanc massif), CATENA, 149, 648–662, https://doi.org/10.1016/j.catena.2016.06.006, 2017a.

Magnin, F., Josnin, J.-Y., Ravanel, L., Pergaud, J., Pohl, B., and Deline, P.: Modelling rock wall permafrost degradation in the Mont Blanc massif from the LIA to the end of the 21st century, 11, 1813–1834, https://doi.org/10.5194/tc-11-1813-2017, 2017b.

NW face ERT

Borehole